THE UNIVERSITY
of EDINBURGH

Rare radiative and semileptonic B meson decays

James Gratrex

Doctor of Philosophy
The University of Edinburgh
October 2018

Lay Summary

The discovery of the Higgs boson at the Large Hadron Collider at CERN, confirming the predictions of the Standard Model, has marked the end of a chapter in particle physics. To date, the Standard Model remains our best description of how the most fundamental particles in our Universe interact with each other. No matter how successful the Standard Model has been, though, it is also known to be incomplete. There are many puzzles that it cannot fully explain, such as the existence of Dark Matter, or the true nature of Gravity.

Various attempts to extend the Standard Model in order to explain these mysteries exist, all of which ultimately lead to the prediction of new particles, or changes to the behaviour of existing particles. It is these new particles that the Large Hadron Collider is hoping to discover, but, so far, no such particles have been seen.

Recently, however, some signs have emerged that certain rare particle decay processes, involving particles known as B mesons, have behaviours that seem to differ from what theoretical calculations predicted. These may be promising hints of New Physics, but they are not yet significant enough to be called a definite discovery. One of the reasons for this is that the decay processes themselves are still not perfectly understood, even within the Standard Model. Making predictions for such processes is difficult, as mesons are complicated objects.

This thesis aims to contribute to the understanding of these decay processes, and their associated experimental results, in two related ways. The first part presents a new method that helps to explain the origin of the structure in experimental measurements of such decays. This is exploited to show how generic new effects might interfere with and change the expected results within the Standard Model. More importantly, it will be shown how these effects can be isolated from the "normal" predictions of such decays, and thereby assessed separately.

In the second part, some new calculations are presented for a set of important inputs in the theoretical prediction of B meson decay processes, where the B meson decays to a particular class of mesons known as vector mesons. These results update and extend previous calculations in the literature. It will be shown how to exploit the patterns appearing in these calculations to make it possible to isolate New Physics effects appearing in experimental measurements.

Abstract

Recent results at the LHCb and B-factory experiments have suggested that rare processes in $B \to V\gamma$ and $B \to V\ell\bar{\ell}$ decays, where V is a vector meson, show some deviation from Standard Model predictions. Although these anomalies are not yet at the level to constitute a formal discovery, they are certainly suggestive of potential New Physics effects in flavour-changing neutral currents. However, explanations within the Standard Model cannot yet be ruled out.

This thesis contributes to the understanding of such anomalies in two ways. Firstly, the angular distribution of the $B \to K_J(\to K\pi)\ell_1\bar{\ell}_2$ decay is derived, for the full dimension-six effective weak Hamiltonian, using a generalisation of the helicity formalism to effective theories mediating $b \to s\ell_1\bar{\ell}_2$ transitions. This approach sheds light on the origin of the underlying structure, and in the process extends the general angular distribution to decays in which the two leptons in the final state, $\ell_1\bar{\ell}_2$, are not necessarily identical.

An additional benefit of the derivation of the angular distribution presented in this manner is that it lends itself to a moments analysis of the decay. It is shown how the angular distribution changes in the presence of new operators, predicted to be vanishingly small in the Standard Model. Such operators could be sizeable in the presence of New Physics, but using a moments analysis enables the contribution of such operators to be assessed.

Secondly, an analysis is presented of the three-particle vector and axial meson distribution amplitudes. It is shown that the distribution amplitudes of both particles are, up to QCD corrections, nearly identical. These results are applied to a new calculation of the long-distance charm loop contribution to radiative $B \to V\gamma$ decays, and it is shown that the approximate symmetry can be exploited to provide an improved theoretical control in the search for New Physics contributions to right-handed currents in radiative decays.

Declaration

I declare that this thesis was composed by myself, that the work contained herein is my own except where explicitly stated otherwise in the text, and that this work has not been submitted for any other degree or professional qualification except as specified.

Parts of this work have been published in [34, 36, 37].

(*James Gratrex, October 2018*)

Acknowledgements

Before I thank anyone else, I want to say how thankful I am to my family, for their support throughout my life. It has been, to say the least, a hard journey getting here, and I would never have been able to make it without them. Thanks to my Dad, who may have given up teaching me maths himself but never stopped encouraging me when I came to learning it. I especially want to say a huge "thank you" to my Mum and my brother Paul, who both went to a great deal of trouble to proofread the thesis, and at short notice, even though particle physics isn't exactly their day job.

To my friends as well, I'd like to say thanks for helping me along the journey. To Laura and Mairi, in particular, for their patience in listening to my struggles and moaning; to James Cockburn, for being a fine office mate, and to Julia and Joel for taking up the mantle; to Gustav, Joshua, Andries, and Rafa for helping me understand various technical points, always happy to answer my questions; and many people I'm bound to have missed out but who nevertheless made a huge difference.

I am grateful to my supervisor, Dr. Roman Zwicky, for his role in getting me across the finish line, and for providing such interesting material to work on in the first place.

Also, I wish to thank my friends and mentors in my undergraduate and high-school days, especially Emily and Beth. I do not think I would even have started this thesis without their help and encouragement. And thanks to all those I met along the way, and gave me a lift when I needed one.

Finally, this thesis marks the end of a journey that began when I was twelve, having read the late Professor Stephen Hawking's book *The Universe in a Nutshell*, and then and there deciding that studying physics was what I wanted to do with my life. It seems appropriate to thank him, especially as his death came only shortly before completion of this thesis. I am sure I am not the only PhD student of my generation, and many to come, who will be similarly grateful to Prof. Hawking.

Contents

List of Figures

List of Tables

Chapter 1

Introduction

The announcement of the discovery of the Higgs boson at the Large Hadron Collider (LHC) in July 2012 is a triumph of modern science [1, 2]. The Higgs boson was a central prediction of the Standard Model (SM), developed mainly during the 1960s and '70s [3–6], and confirmation of its existence, at the most complex experiment humanity has ever undertaken, marks the end of a chapter in Particle Physics.

But as one chapter ends, another begins. Almost every thesis on Particle Physics written in the last thirty years will inevitably draw attention to the deficiencies of the SM. To put it simply, the SM is not, and cannot be, the end of the journey, as many questions remain unanswered, many gaps remain unfilled, and many puzzles remain unsolved. For example, the Brout-Englert-Higgs mechanism [7–10] successfully explains how particles can acquire masses, when symmetry arguments otherwise forbid massive particles from existing. It cannot, however, account for the observed hierarchy of masses within the fermions. The current "answer" within the SM is to insert this hierarchy "by hand", arbitarily tuning the values of input parameters to produce the observed mass scales. Such a resolution is hardly satisfying.

Another of the myriad questions that remain unanswered in the SM is the problem of matter-antimatter asymmetry. Paul Dirac, in the late 1920s, famously predicted the existence of antimatter as a by-product of his attempts to describe the behaviour of the electron [11, 12], and it did not take long for this theoretical prediction to be verified by experiment [13]. Antimatter particles are, in a certain sense, the mirror images of "normal" matter particles, differing only in their

charge and parity. But perfect mirror-image antimatter would behave in exactly the same way as matter, and, luckily for life, this is not observed. For physicists, though, this inevitably leaves another puzzle. How is the matter-antimatter symmetry broken?

This time, the answer is already partially known, and a feature of the SM known as the CKM matrix contains a parameter that leads to matter and antimatter having subtly different behaviour. This is known as CP violation. Still, a problem remains: CP violation is necessary for the formation of the universe as it exists today [14], but the only source of CP violation contained in the SM is insufficient to account for the observed matter-antimatter asymmetry.

So it goes on, the SM providing a remarkably accurate description of most particle phenomena observed so far, but falling short of a complete explanation. These deficiencies have naturally inspired physicists to search for new theories that resolve such shortcomings. The most well-known of these new models is Supersymmetry, which predicts an additional relationship between the two classes of fundamental particle, fermions and bosons; but Supersymmetry is far from the only new avenue that theory has explored in the last few decades.[1]

Ultimately, all new models must, if they are worth proposing, make testable predictions. In practice, this means that one or more new particles, beyond those contained within the SM, can be expected to exist. Following the launch of the LHC in 2008, it was hoped that it would not take long for these anticipated new particles to be observed. Yet, so far, such new particles as the LHC has discovered can all be understood within the SM. While these discoveries are still exciting – they include the Higgs boson itself, as well as exotic particles such as pentaquarks [16], which had long been expected to exist – the absence of any genuine signal of New Physics means that the questions attached to the SM remain unresolved. Run II of the LHC, with collisions at double the energy of the earlier Run I, has begun only recently, and it is not impossible that results from the latest set of experiments will change this assessment.

On the other hand, even if no New Physics is directly observed, there remains the difficult issue of understanding the predictions of the SM itself. The SM explains the physics of ordinary matter by introducing the elementary particles known as quarks, which combine together to create the baryons and mesons that are

[1] See [15] for a readable introduction to various scenarios of physics beyond the SM, as well as a more complete discussion of problems with the SM.

actually what is observed in experiments. The transition in theory between quarks and hadrons is difficult to capture completely, but understanding the relationship between the two is fundamental to making proper theoretical predictions.

One sector of particle physics where this interplay is particularly important is B physics [17, 18]. B mesons are particles that contain at least one bottom (b) quark, the second-heaviest quark in nature observed behind the top (t) quark. The mass of the b quark sits in between two other mass scales within the SM: the weak scale, defined by the masses of the heaviest particles in the SM (W, Z and Higgs bosons along with the t quark); and the Quantum Chromodynamics (QCD) scale, relevant for defining the relationship between quarks and hadrons. This scale separation allows both weak and short-distance QCD physics, where they enter decay processes of B mesons, to be handled perturbatively. Although some non-perturbative physics inevitably remains, related to the full internal structure of hadrons, this can be separated from the perturbative physics and dealt with separately. B physics therefore provides a natural laboratory for testing most of the features of the SM.

Recently, the predictions of theory and results of experiment have diverged in a number of B physics decays [19–25]. This tension could arise either because the theoretical predictions are, for some reason, incorrect [26], or because the SM is incomplete after all [27]. At present, these anomalies, which appear in multiple separate decay channels and have even been observed by separate experimental groups, are neither fully understood nor properly confirmed, and remain at a level below the "5σ" gold standard of a confirmed discovery [28].

The anomalies mentioned above appear specifically in decays mediated by $b \to s$ and $b \to d$ transitions. As will be made clear later, these processes are expected to be particularly rare within the SM, as they can only proceed by loop processes. Separately, there has also been evidence of anomalies in tree-level processes, such as $B \to D\ell\nu_\ell$ and $B \to D^*\ell\nu_\ell$, where the D mesons contain a charm quark [29–32]. However, it is the loop decay anomalies that provide more interest, because such processes are expected to be particularly sensitive to New Physics (NP) effects, which may enter at tree level and so dominate the SM contribution.

Whether these anomalies persist and reach the 5σ standard, or ultimately vanish, it is still clear that they warrant further investigation. This thesis aims to play a part in this investigation, and does so in two ways: firstly, by describing and applying a systematic technique to understanding the angular distributions of

$B \to K_J(\to K\pi)\ell_1\bar{\ell}_2$ decays; and secondly, by fresh computations of parameters in the distribution amplitudes (DAs) of vector mesons, showing explicitly the relations to similar results for axial mesons. This will be applied to a study of long-distance (LD) contributions to right-handed currents (RHC) in $B \to (V, A)\gamma$ decays.

The remainder of the thesis is organised as follows:

Background

- In chapter 2, the effective theory for weak decays is introduced, defining the necessary operators and explaining the calculation techniques required. Attention is also paid to the properties of CP violation, which will be applied to define useful observables when searching for right-handed currents. Material in this chapter relates primarily to the first part of the thesis.

- In chapter 3, the DAs are introduced, by first discussing the language of conformal symmetry in which they are defined. The DAs enter calculations of hadronic matrix elements, and it is shown how these calculations are performed using the method of Light-Cone Sum Rules (LCSR). The Borel transformation, an often-used technique in sum rules calculations, is also introduced and discussed, with attention paid to competing considerations when choosing Borel parameters. This chapter finally introduces the notation for DAs to be applied to the thesis. Material in this chapter relates primarily to the second part of the main thesis.

Part One

- In chapter 4, the angular distribution of decays of the general form $B \to K_J(\to K\pi)\ell_1\bar{\ell}_2$ is presented in the context of a generalised helicity formalism. Although related techniques have appeared in other contexts since the seminal paper of Jacob and Wick [33], this represents the first systematic application of the technique in this context. Applications of the method, in particular the implications for experimental studies using a moments analysis, are discussed. In addition, this chapter provides the link between the angular conventions for this decay in the theory and

experimental communities, which, prior to the release of [34], had not been satisfactorally related to each other. Further material relevant to this chapter is presented in appendix C.

- Chapter 5 illustrates the benefits of the approach of chapter 4 by considering extensions to the angular distribution. These are presented in the context of higher-dimensional, derivative operators, and how they enter the angular distribution of the $B \to K_2(1430)(\to K\pi)\ell_1\bar{\ell}_2$ decay. The potential impact of QED corrections, and how they might be distinguished from NP scenarios, is also discussed.

Part Two

- In chapter 6, the calculation of the parameters for three-particle DAs is presented, demonstrating explicitly the relationships between vector and axial meson DAs, which have previously been un-noticed, or not completely exploited. The contribution of the three-gluon condensate is also included for the first time, and fresh determinations of the numerical values of the first few parameters in these DAs are given. Technical details of the calculation, relevant for an extension to twist-4 DAs, are outlined, with preliminary twist-4 results in appendix D. An alternative technique for computing the leading contribution to the DA parameters, the diagonal sum rules approach, is discussed in appendix E.

- Chapter 7 presents a computation of long-distance contributions to $B \to V\gamma$ decays in a fully exclusive LCSR approach. The same calculation was presented in [35], but certain disagreements are noted and commented on, while explicit formulas not presented in [35] are given in appendix F. The fresh determinations of the DA parameters, in chapter 6, allows for an updated evaluation of these results, along with an extension to the axial meson processes. It is shown how the calculation of LD contributions can be used to improve the search for right-handed currents. This relies on exploiting the relationship between vector and axial mesons elaborated upon in chapter 6, along with the related paper [36] and proceedings [37].

- The thesis ends with conclusions, and a discussion of future extensions, in chapter 8.

- Alongside the appendices mentioned above, appendix A provides further

details on conventions used in the thesis, along with useful results of integrals; and appendix B gives the numerical inputs used in this thesis, as well as comments on competing estimates for the values of condensates entering the sum rules results of chapter 6.

Chapter 2

Effective theory of weak decays

This chapter discusses various topics and techniques relevant to the material presented later in the thesis, with a particular emphasis on the origin of the effective theory of weak decays.

2.1 The flavour sector of the Standard Model

Since its development in the 1960s [3–10], the SM has remained at the forefront of theoretical physics, and is to date the best description of nature available. The particle content – three generations of quarks and leptons, the strong (g), weak ($W^{\pm}$, Z), and electromagnetic (γ) gauge bosons, and the Higgs boson – represents all matter so far observed in collider experiments.

More concretely, the SM tells us how these particles interact, by combining the theories of QCD, Quantum Electrodynamics (QED) and the weak interaction. The gauge group of the SM, $SU(3)_C \times SU(2)_L \times U(1)_Y$, determines the behaviour of these interactions, while Yukawa couplings between the Higgs field and fermions ultimately give rise to bare quark and lepton masses. Neglecting the terms specific to leptons, all this is captured by the Lagrangian

$$\mathcal{L} = -\frac{1}{4} F^a_{\mu\nu} F^{a\mu\nu} + \sum_f \left(i\bar{Q}^f_L \not{D}_L Q^f_L + i\bar{u}^f_R \not{D}_R u^f_R + i\bar{d}^f_R \not{D}_R d^f_R \right)$$

$$+ (D_\mu \varphi)^\dagger (D^\mu \varphi) + \mu^2 \varphi^\dagger \varphi - \lambda (\varphi^\dagger \varphi)^2 - \sum_{a,b} \bar{Q}_L^a \left(Y_{ab}^u \tilde{\varphi} u_R^b + Y_{ab}^d \varphi d_R^b \right) + \text{h.c.} \tag{2.1}$$

with the left-handed $SU(2)$ doublets $Q_L^f = (u_L^f, d_L^f)$ and the right-handed singlets u_R, d_R describing the quark content; φ is the Higgs field, also in an $SU(2)$ doublet (with $\tilde{\varphi}$ the Higgs field in the anti-fundamental representation of $SU(2)$). The fields $F^{a\mu\nu}$ implicitly contain all gauge bosons for the group, and split into three parts for each part of the SM symmetry. The covariant derivative D_μ transforms according to the relevant representation in the SM gauge group of the field on which it acts, and is defined by[1]

$$D_\mu = \partial_\mu - i g_s G_\mu - i e Y B_\mu - i g_2 W_\mu \,. \tag{2.2}$$

The form of the Lagrangian (2.1) strictly applies only above the scale of electroweak symmetry breaking, $\nu_{\text{VEV}} \approx 246$ GeV, which is generated by the non-trival vacuum behaviour of the Higgs potential $V_H = -\mu^2 \varphi^\dagger \varphi + \lambda (\varphi^\dagger \varphi)^2$. Below this scale, the Lagrangian is rewritten to account for this effect. In particular, the Higgs field can be replaced (in unitary gauge) by $\varphi \to h + \nu_{\text{VEV}}$, with the principal consequence that the Higgs, $W^\pm$ and Z bosons, and quarks and leptons all acquire a mass. It is important to stress that the gauge symmetry $SU(2)_L \times U(1)_Y$ forbids the inclusion of explicit mass terms in the Lagrangian, and such terms can only be generated by this spontaneous symmetry breaking. For the up-type quarks (and charged leptons), the mass terms take the form $\nu_{\text{VEV}} Y_{ab}^u \bar{u}_L^a u_R^b$, and similarly for the down-type quarks [40, 41].

The two matrices $Y_{ab}^{u,d}$ that arise are known as Yukawa matrices, and represent the relationship between the weak and mass eigenstates of the quark sector. Up to a redefinition in quark phases, they can be written as

$$Y^{u,d} = U^{u,d} \Sigma^{u,d} \,, \tag{2.3}$$

where Σ are diagonal matrices whose entries are proportional to the observed quark masses. The matrices $U^{u,d}$ represent the fact that, in general, there is no requirement for the mass and weak eigenstates to be the same. Transformation to the mass basis of quarks then modifies, for example, the charged-current

[1] The signs in the covariant derivative are a choice of convention. The negative sign is standard in the literature, and is used by, for example, [38, 39], but occasionally the opposite sign convention is used.

contribution to the form

$$W_\mu \bar{u}^i_L \gamma^\mu d^i_L \to W_\mu \bar{u'}^i_L \gamma^\mu d'^j_L (U^{\dagger u} U^d)_{ij} \,, \tag{2.4}$$

where the new matrix $U^{\dagger u}U^d \equiv V_{CKM}$ represents the potential for mass and weak eigenstates to mix into each other, and is known as the Cabibbo-Kobayashi-Maskawa (CKM) matrix [42, 43]. This is a 3×3 unitary matrix, which has four degrees of freedom, of which one is a phase, with the remaining three interpretable as angles [44]. The other five degrees of freedom possible in a unitary matrix can be absorbed as phase rotations over the quark flavours. The phase degree of freedom is responsible for the phenomenon of CP violation, which will be discussed in more detail in section 2.2. Various ways of parametrising the matrix exist; this thesis will make use of the Wolfenstein parametrisation [45, 46]

$$V = \begin{pmatrix} V_{ud} & V_{us} & V_{ub} \\ V_{cd} & V_{cs} & V_{cb} \\ V_{td} & V_{ts} & V_{tb} \end{pmatrix} = \begin{pmatrix} 1 - \frac{1}{2}\lambda^2 & \lambda & A\lambda^3 (\rho - i\eta) \\ -\lambda & 1 - \frac{1}{2}\lambda^2 & A\lambda^2 \\ A\lambda^3 (1 - \rho - i\eta) & -A\lambda^2 & 1 \end{pmatrix}, \tag{2.5}$$

which is an expansion in $\lambda \approx 0.23$ accurate to $\mathcal{O}(\lambda^4)$.[2] The Wolfenstein parametrisation has the advantage that it reveals some structures to the CKM matrix. Most notably, it can be seen that there is a clear hierarchy of magnitudes of $|V_{ab}|$, such that transitions are favoured between quarks of the same generation, and generally suppressed otherwise. To date, the origin of this structure is an open question [47]. In addition, the presence of the CP violating parameter η is crucial, as CP violation provides one of three conditions required for baryogenesis in the early universe [14], but its value is too small to be sufficient on its own to explain the necessary matter-antimatter asymmetries [48].

Note that the CKM matrix only couples to the charged currents of the weak interaction. The *neutral* currents, mediated by the γ and Z bosons, do see the mass and weak eigenstates of the quark flavours as identical. This has the consequence that flavour-changing neutral currents (FCNCs) cannot occur at tree level in the SM. As a result, they are suppressed by at least loop factors, and FCNC processes can therefore be expected to be small. Examples of FCNCs include the $b \to s$ and $b \to d$ transitions, which can generate such decay channels as $B \to K^* \ell\bar{\ell}$ or $B \to \rho \ell\bar{\ell}$ respectively.

[2] See appendix B for more discussion about the CKM matrix and its modern values.

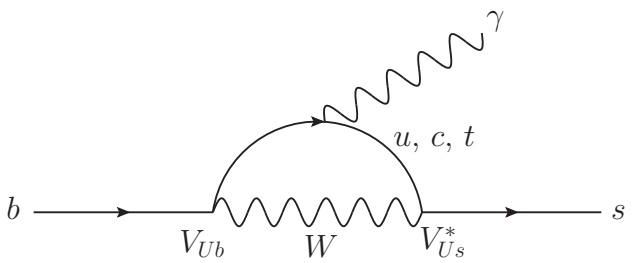

Figure 2.1 *A typical loop diagram mediating flavour-changing neutral currents in the SM. The CKM matrices indicated at either vertex form the product $V^*_{Us}V_{Ub}$, which, when summed over all possible quarks $U = u, c, t$ running through the loop, gives zero. This would lead to all flavour-changing processes vanishing via the GIM mechanism, were it not for the non-equal quark masses.*

In fact, there is a further suppression of FCNCs implied by the structure of the CKM matrix. Because it is unitary, and because any quark flavour can appear in the loop, processes exemplified by the diagram in figure 2.1 lead, as long as the quark masses are equal, to amplitudes proportional to $V^*_{ub}V_{us} + V^*_{cb}V_{cs} + V^*_{tb}V_{ts}$, and unitarity implies that this sum is exactly zero. This is known as the Glashow-Iliopolous-Maiani (GIM) mechanism [49], and only the non-equal masses of quarks means that FCNC processes occur at all.

These considerations mean that FCNC decays are expected to be rare within the SM, but on the other hand it also follows that they could be particularly sensitive to NP effects, which could be significant if such NP enters as a tree-level FCNC process. Models do exist in which this occurs; in an example of relevance to this thesis, models that contain leptoquarks could enter $b \to s$ processes including lepton emissions [50]. In section 2.5, the properties of such transitions will be explored more thoroughly.

The lepton sector of the SM has the same structure as the quark sector, but the absence of right-handed neutrinos simplifies the discussion somewhat, as it is possible to simultaneously diagonalise the weak and mass eigenstates of leptons. The phenomenon of neutrino oscillations [51, 52] implies that neutrinos do, in fact, have (very small) masses. Much of the discussion in this section can therefore, in principle, be applied to leptons, by introducing the Pontecorvo-Maki-Nakagawa-Sakata (PMNS) matrix [53, 54], which is the leptonic equivalent of the CKM matrix (2.5). The PMNS matrix, however, has a very different hierarchical structure from the CKM matrix, and it is also far from clear that the neutrino sector should simply be a copy of the quark sector. One alternative is to generate

a mass for the neutrinos through introducing the Weinberg operator [55, 56]

$$\mathcal{L}_W = \sum_{a,b} \frac{Y_W^{ab}}{\Lambda} \left(\bar{\ell}_a \varepsilon H^*\right) \left(\ell_b^c \varepsilon H^*\right) + h.c.\,, \tag{2.6}$$

where ε is the totally antisymmetric Levi-Civita symbol of rank two, ℓ^c is the charge-conjugated lepton doublet, and Λ is the scale at which this operator, not present in the usual SM, becomes significant. Introducing this new operator in fact generates Majorana-type masses for the neutrinos, and is therefore distinct from merely duplicating the quark sector. In addition, this operator would provide a mechanism for lepton-number violating decay processes. One recent review [57] explores various models related to the question of neutrino masses and CP violation in leptons. For the purposes of this thesis, however, neutrinos are taken to be massless, and only the quark sector will be of interest.

2.2 CP violation

In the previous section, it was noted that the imaginary contribution to the CKM matrix implies that weak decays exhibit CP violation. This section outlines some of the consequences of this property, as well as outlining the underlying theory. Useful reviews of CP violation can be found in, for example, [38, 58].

The charge C and parity P are discrete transformations that can act on quantum states to invert the charge of a particle or its spatial direction respectively. The third discrete symmetry of time-reversal, T, combines with these to make the CPT transformation, under which any physical process is invariant, a result known as the CPT theorem. This states that, as long as a quantum field theory is Lorentz-invariant, local, and hermitian, then there is no difference between two physical processes related by a CPT transformation. The CPT theorem is also related to the fundamental distinction between bosons and fermions, as fermions under $(CPT)^2$ gain an extra sign, whereas bosons do not (a result known as the spin-statistics theorem [59]).

On the other hand, although the combination CPT is always respected as a symmetry under these conditions, it is not necessarily true that individual symmetries hold. Of particular interest is the combination CP (or, equivalently, T), which relates particles to their antiparticles. To see this, consider a situation where, initially, CP symmetry holds over a particle decay process $a \to b$ (and the

equivalent antiparticle process $\bar{a} \to \bar{b}$). By definition, this implies that

$$\mathcal{A}_{a\to b} = \bar{\mathcal{A}}_{\bar{a}\to\bar{b}}\,, \tag{2.7}$$

where $\mathcal{A}$, $\bar{\mathcal{A}}$ are the relevant amplitudes, summed over all possible transitions of $a \to b$. In the case where there are two such intermediate processes, one could also write

$$\begin{aligned}\mathcal{A}_{a\to b} &= |\mathcal{A}_1|e^{i\theta_1} + |\mathcal{A}_2|e^{i\theta_2}\,,\\ \bar{\mathcal{A}}_{\bar{a}\to\bar{b}} &= |\mathcal{A}_1|e^{i\theta_1} + |\mathcal{A}_2|e^{i\theta_2}\,,\end{aligned} \tag{2.8}$$

where the amplitudes of the subprocesses have been split into their magnitudes and phases, and CP-conserving phases θ_i do not change sign: $\bar{\mathcal{A}}_{\bar{a}\to\bar{b}} \neq \mathcal{A}^*_{a\to b}$. Not all phases conserve CP, however. In the equations above, these can be included by adding a CP-violating phase ϕ_i to each intermediate process

$$\begin{aligned}\mathcal{A}_{a\to b} &= |\mathcal{A}_1|e^{i\theta_1}e^{i\phi_1} + |\mathcal{A}_2|e^{i\theta_2}e^{i\phi_2}\,,\\ \bar{\mathcal{A}}_{\bar{a}\to\bar{b}} &= |\mathcal{A}_1|e^{i\theta_1}e^{-i\phi_1} + |\mathcal{A}_2|e^{i\theta_2}e^{-i\phi_2}\,,\end{aligned} \tag{2.9}$$

so that

$$|\bar{\mathcal{A}}|^2 - |\mathcal{A}|^2 = 4|\mathcal{A}_1||\mathcal{A}_2|\sin(\theta_2-\theta_1)\sin(\phi_2-\phi_1)\,, \tag{2.10}$$

and, as long as the two intermediate processes generate a non-zero phase difference $\phi_2 - \phi_1$ (which is almost certainly true by virtue of the intermediate processes being different), then it follows automatically that particle and anti-particle processes do not proceed at the same rate. This phenomenon is the most basic illustration of CP violation, but it has profound consequences.

In the SM, under CP, the weak charged currents go as

$$W^+_\mu \bar{u}'^i_L \gamma^\mu d'^{\,j}_L (U^{\dagger u}U^d)_{ij} \xrightarrow[CP]{} W^-_\mu \bar{d}'^j_L \gamma^\mu u'^{\,i}_L (U^{\dagger u}U^d)^*_{ji}\,, \tag{2.11}$$

which demonstrates that if the CKM matrix has a non-zero phase then it does indeed provide a source of CP violation, as such a phase behaves as ϕ_i does in equation (2.9).

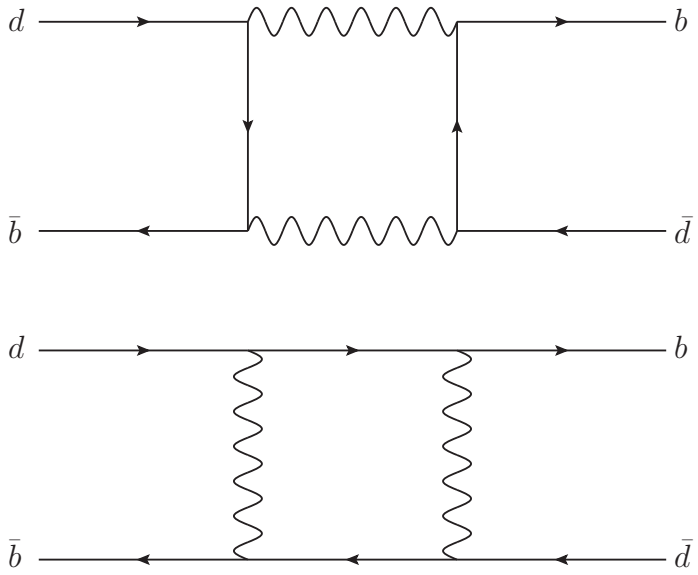

Figure 2.2 *Box diagrams contributing to B^0-$\bar{B}^0$ mixing. Both processes are needed to generate CP violation, through interference effects between the two amplitudes.*

2.2.1 Time-dependent CP violation

Another explicit demonstration of the importance of CP violation is in the mixing of two states related by a CP transformation. Historically, the K^0-$\bar{K}^0$ system was one of the first experimental verifications of the CP violation (and the even stronger property of weak interactions, that they violate the P symmetry), but, as the focus of this thesis is B physics, the discussion below is presented in the context of B^0-$\bar{B}^0$ mixing.

The time-dependent wavefunction for a B^0-$\bar{B}^0$ system is given by [58, 60]

$$|\Psi(t)\rangle = a(t)\left|B^0\right\rangle + b(t)\left|\bar{B}^0\right\rangle , \tag{2.12}$$

and a general Hamiltonian can be written, in the $|B^0\rangle$-$\left|\bar{B}^0\right\rangle$ basis,

$$\mathcal{H} = \mathbf{M} - \frac{i}{2}\mathbf{\Gamma} = \begin{pmatrix} M_{11} & M_{12} \\ M_{21} & M_{22} \end{pmatrix} - \frac{i}{2}\begin{pmatrix} \Gamma_{11} & \Gamma_{12} \\ \Gamma_{21} & \Gamma_{22} \end{pmatrix} \tag{2.13}$$

where $\mathbf{M}$ and $\mathbf{\Gamma}$ are Hermitian matrices, and the system is confined to two states for simplicity. CPT invariance implies that $M_{11} = M_{22}$ and $\Gamma_{11} = \Gamma_{22}$, but

otherwise at this point the matrix elements are arbitrary (and all are possibly complex). Physically, the matrix $\mathbf{M}$ carries information about the masses and mass mixing, and $\mathbf{\Gamma}$ carries information about the decay rates. The eigenstates of $\mathcal{H}$ are then defined by

$$\begin{aligned} |B_{1,2}\rangle &= p\left|B^0\right\rangle \pm q\left|\bar{B}^0\right\rangle , \\ \frac{q}{p} &= \sqrt{\frac{M_{12}^* - \frac{i}{2}\Gamma_{12}^*}{M_{12} - \frac{i}{2}\Gamma_{12}}} . \end{aligned} \tag{2.14}$$

In the B^0-$\bar{B}^0$ system, Γ_{12}, which represents the B^0-$\bar{B}^0$ width difference, is usually assumed to be negligible, in which case $\frac{q}{p}$ reduces to simply a measure of the B^0-$\bar{B}^0$ mixing angle:

$$\frac{q}{p} = \left|\frac{q}{p}\right| e^{-i\phi_{\text{mix}}} , \quad \left|\frac{q}{p}\right| \simeq 1 . \tag{2.15}$$

Note also that the states $|B_{1,2}\rangle$, in the case where the mixing angle is zero, are CP eigenstates with opposite sign: $CP\,|B_{1,2}\rangle = \pm\,|B_{1,2}\rangle$.[3] The time evolution of the observed B^0-$\bar{B}^0$ states is then given by

$$\begin{aligned} \left|B^0(t)\right\rangle &= f_+(t)\left|B^0\right\rangle + \frac{q}{p} f_-(t)\left|\bar{B}^0\right\rangle , \\ \left|\bar{B}^0(t)\right\rangle &= f_+(t)\left|\bar{B}^0\right\rangle + \frac{p}{q} f_-(t)\left|B^0\right\rangle , \end{aligned} \tag{2.16}$$

where

$$f_\pm(t) = \frac{1}{2} e^{-iM_1 t} e^{-\frac{1}{2}\Gamma_1 t}\left(1 \pm e^{-i\Delta M t} e^{-\frac{1}{2}\Delta\Gamma t}\right) , \tag{2.17}$$

with $\Delta M = M_2 - M_1$ and $\Delta\Gamma = \Gamma_2 - \Gamma_1$.

This can now be applied to decay processes with some final state $|f\rangle$ accessible (either directly or indirectly) by both the B^0 and $\bar{B}^0$, which is to say that the $B^0 \to f$ decay can also proceed via mixing into $B \to \bar{B}^0 \to f$. The combination

$$A_{CP}(t) = \frac{\Gamma(\bar{B} \to f) - \Gamma(B \to f)}{\Gamma(\bar{B} \to f) + \Gamma(B \to f)} \neq 0 \tag{2.18}$$

is then a measure of CP violation. In terms of the variables defined in the time-

[3] Briefly returning to the Kaon system, the fact that the $K_{1,2}$ are CP eigenstates is historically important because, initially, it was assumed that $K_{1,2}$ were identical respectively to $K_{S,L}$, where $K_{S,L}$ are defined by their principal decay chains: $K_S \to \pi\pi$ and $K_L \to \pi\pi\pi$. The final states have CP eigenvalues ± 1, matching those of the $K_{1,2}$, so assuming that CP is a good symmetry, $K_L \to \pi\pi$ is impossible. K_L has a much longer lifetime owing to the smaller available phase space of the 3-π decay. In fact, $K_L \to \pi\pi$ decays are occasionally observed, owing to the correct relation $K_L = K_2 + \varepsilon K_1$, where ε is the CP-violating parameter.

evolution functions $f_\pm(t)$, the time-dependent decay rates $\Gamma(\bar{B}(B) \to f)$ are

$$\Gamma(\bar{B}(B) \to f) = \mathcal{B}_0 e^{-\Gamma t} \left(\cosh(\frac{\Delta\Gamma}{2}t) - H \sinh(\frac{\Delta\Gamma}{2}t) \mp C \cos(\Delta M t) \pm S \sin(\Delta M t) \right) , \tag{2.19}$$

so that A_{CP} can also be written

$$A_{CP}(t) = \frac{S \sin \Delta M t - C \cos \Delta M t}{\cosh \frac{\Delta\Gamma}{2}t - H \sinh \frac{\Delta\Gamma}{2}t} , \tag{2.20}$$

where S, C and H are functions dependent on the specific Hamiltonian, and S and C are respectively measures of indirect and direct CP violation. The particular form above relies on the assumption $|q/p| \simeq 1$, which is true (up to negligible corrections) in the B^0-$\bar{B}^0$ system. This observable will be later used in a more explicit set of scenarios in Chapter 7.

2.3 Renormalisation

It is almost inevitable that calculations in Quantum Field Theory (QFT) will run into divergent terms. This can be understood as a consequence of various limiting behaviours to the theory; in general, it cannot be expected that a QFT is valid at arbitrary (very high or very low) energy scales. The two main classes of divergence are the high-energy ultraviolet (UV) and low-energy infrared (IR) cases. Whilst these divergences arise naturally from calculations, they also have a physical interpretation. UV divergences can be thought of as arising from the mistaken assumption that the theory being considered is valid at all distance scales, whereas in fact a more complete theory may be required to understand the physics at ultra-short distances. On the other hand, IR divergences can be associated with the presence of massless particles in a theory: since massless particles can have arbitrarily low energies, it is possible for an infinite number of them to be produced but with a finite total energy.

One way of dealing with such issues is simply to impose a cut-off scale, excluding either very low or very high energies from the integrals under consideration. However, doing so immediately breaks Lorentz symmetry, as well as any gauge symmetries of the theory, and therefore cut-off regularisation techniques are often applied only when there is a well-motivated physical interpretation for the specific value of that cut-off scale. In section 2.4, when the effective theory of weak

interactions is introduced in more detail, the cut-off scale is naturally associated to the mass of the W boson.

Regardless of the technique, the divergences must still be dealt with in a systematic way in order to make meaningful predictions. If divergent terms were not removed systematically, then, in principle, a calculation could lead to any answer. Moreover, while there is some freedom to remove divergences from the theory, in order to do so one needs at least as many free parameters as there are distinct divergences.

The technical resolution of these issues is known as renormalisation, and was actively researched in the 1950s and '60s [61, 62] before the seminal paper of 't Hooft and Veltman, introducing dimensional regularisation, resolved the issue of how to include renormalisation in gauge theories [63]. The general result of any renormalisation procedure is that the couplings of a theory acquire a dependence on a regularisation parameter ε. Then the initial, "bare", coupling, denoted C_0, can be written

$$C_0(\varepsilon) = \mu^{-n\varepsilon} Z_C(g(\mu), \varepsilon) C(\mu) \tag{2.21}$$

where $g(\mu)$ is the gauge coupling, dependent on the energy scale μ, and $d = 4 - 2\varepsilon$ defines the deviation ε from the usual number of dimensions. The parameter n is fixed by measuring the natural dimension of the coupling. Z_C is the renormalisation constant, which depends on the scale μ only implicitly, and is dimensionless. The equation above can be extended naturally to theories with multiple couplings C_0 by promoting $Z_C(g(\mu), \varepsilon)$ to a matrix, and so one consequence of renormalisation is that couplings can mix under Renormalisation Group (RG) evolution.

Since the bare coupling C_0 does not depend on the scale μ, it follows that differentiating the right-hand side of (2.21) with respect to μ gives 0. Considering the two cases where C_0 is an arbitrary coupling, and C_0 is the gauge coupling itself, then this leads to the equations

$$\begin{aligned} \frac{dc}{d\ln\mu} \equiv \mu\frac{dC}{d\mu} &= C(\gamma_C(g) + n\varepsilon)\,, \\ \frac{dg}{d\ln\mu} \equiv \mu\frac{dg}{d\mu} &= -g(\beta(g) + \varepsilon)\,, \end{aligned} \tag{2.22}$$

where $\beta(g)$ is the β-function, and whose calculation in QCD was one of the most celebrated results of renormalisation theory [64, 65]. $\gamma_C(g)$ is the anomalous dimension of the coupling C, and both β and γ arise from the dependence of Z_C

on g.

Unfortunately, the equations (2.22) cannot be solved except via a perturbative approach, expanding in powers of the coupling g. The β function of QCD, for example, is defined by

$$\beta(\alpha_s) = -\beta_0 \frac{\alpha_s^2}{4\pi} - \beta_1 \frac{\alpha_s^3}{8\pi^2} - \beta_2 \frac{\alpha_s^4}{128\pi^3} + \dots \,, \tag{2.23}$$

where $\alpha_s = g_s^2/(4\pi)$. The β_i are constants whose values have been determined only for the first few terms, depending on the number of loops $i+1$ in the diagrams. The β function was recently computed to five-loop accuracy in 2017 [66], although for the purposes of this thesis running of the QCD coupling constant is restricted to three loops at most [67].

As for general couplings C, the equation (2.22) is usually rewritten to be in terms of the gauge coupling

$$\alpha \frac{dC}{d\alpha} = -\frac{\gamma_C}{2\beta} C \,, \tag{2.24}$$

which can be solved at leading order to give

$$C(\mu) = \left(\frac{\alpha(\mu)}{\alpha(\mu_0)} \right)^{-\frac{\gamma_C^{(0)}}{2\beta_0}} C(\mu_0) \,, \tag{2.25}$$

where μ_0 is the reference scale and $\gamma_c^{(0)}$ is the leading contribution to the anomalous dimension.

In the case of multiple relevant couplings, the equations above are promoted to matrix equations governed by the anomalous dimension matrix γ_{ij}, and the solution (2.25) becomes, at leading order,

$$C_i(\mu) = \sum_{j,k} V_{ij}^{-1} \left(\frac{\alpha(\mu)}{\alpha(\mu_0)} \right)^{-\frac{\gamma_{D,j}^{(0)}}{2\beta_0}} V_{jk} C_k(\mu_0) \tag{2.26}$$

where V is the matrix that diagonalises γ_{ij}.

Again, analytic solutions such as (2.26) can only be obtained at leading order in perturbation theory. At higher orders, the solutions to (2.24) or its matrix equivalent must be solved numerically. For the coefficients relevant to the physics discussed in this thesis, the procedure is well-described in the appendices of [68], as well as in a comprehensive review in [39].

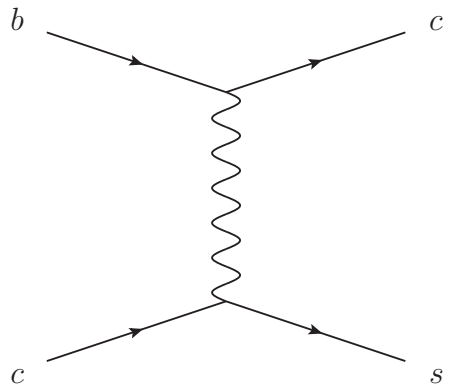

Figure 2.3 *Tree-level Feynman diagram for the $b \to \bar{c}cs$ transition, which leads to the amplitude in* (2.27).

2.4 Effective Hamiltonian at tree-level and the Wilson coefficients $C_{1,2}$

The principal decays of interest to this thesis are those mediated by a $b \to (d, s)\gamma$ or $b \to (d, s)\ell\bar{\ell}$ transition. In both cases, the leading contributions are one-loop diagrams, owing to the absence of tree-level FCNCs in the SM, as discussed in the introductory section. However, the typical energy scale of B decays is of the same order as the B meson mass itself, 5 GeV, which is far removed from the weak scale, defined by $m_W \sim 80$ GeV. This can be exploited to develop an *effective* theory, where the heavy particles are removed from the theory ("integrated out") and the residual operators define a new Hamiltonian, valid only at the energy scales of interest.[4]

This process can be made more formal by requiring that the effective theory consists of all possible operators $\mathcal{O}_i$ below a certain mass dimension that are consistent with the symmetries of the full theory. These operators are associated with Wilson coefficients C_i, whose value is fixed such that the full theory is recovered up to corrections in inverse powers of the heavy mass scale. It is important to stress that these coefficients are related to the short-distance (SD) physics, and so they are universal for all processes described by the effective theory [39]. For the weak sector, this suffices to define the full operator set, although the coefficients C_i are affected by QCD interactions, and so the theory must be renormalised according to the procedure sketched out in section 2.3. To illustrate

[4]Historically, the effective weak theory was developed first by Fermi, and only later was the full weak theory understood.

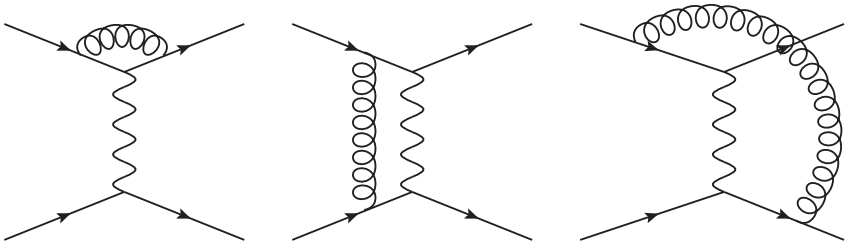

Figure 2.4 *QCD corrections to tree-level weak decay, used in computing the Wilson coefficients $C_{1,2}$. Three more diagrams, related to the ones drawn above by a reflection, are not shown.*

this more completely, consider the leading contribution to effective weak theory, which arises from $b \to c\bar{c}s$ processes and is represented in the diagram in figure 2.3. The discussion in this section is also heavily based on that in [39].[5] The amplitude in the complete theory is (in unitary gauge)

$$iA = -\frac{g_w^2}{8m_W^2} V_{cs}^* V_{cb} \frac{1}{k^2 - m_W^2} \Big(m_W^2 \eta_{\mu\nu} - k_\mu k_\nu \Big) \bar{s}_i \gamma^\mu (1-\gamma_5) c_i \bar{c}_j \gamma^\nu (1-\gamma_5) b_j \,, \quad (2.27)$$

which, on expansion around low momentum exchange $|k_\mu| << m_W$, can be reduced to

$$iA = \frac{G_F}{\sqrt{2}} V_{cs}^* V_{cb} \left(\bar{s}c\right)_{V-A} \left(\bar{c}d\right)_{V-A} + \mathcal{O}\left(\frac{k^2}{m_W^2}\right) \,, \quad (2.28)$$

where $\left(\bar{s}c\right)_{V-A} = \bar{s}\gamma_\mu(1-\gamma_5)c$. This amplitude, which can be defined independently of the external physics,[6] can be used to define the first effective operator $\mathcal{O}_2 = \left(\bar{s}c\right)_{V-A} \left(\bar{c}d\right)_{V-A}$, where the subscript two arises for historical reasons. The new coefficient G_F is Fermi's constant, and has the value

$$G_F = \frac{g_w^2}{2\sqrt{2}m_W^2} = 1.166 \times 10^{-5} \text{ GeV}^{-2} \,, \quad (2.29)$$

and defines the scale of low-energy weak interactions.

The operator $\mathcal{O}_2$ is sufficient to capture the behaviour of weak effective theory at tree level, but it is also possible to write down a second operator $\mathcal{O}_1 = \left(\bar{s}_i c_j\right)_{V-A} \left(\bar{c}_j b_i\right)_{V-A}$, which is related to $\mathcal{O}_2$ under a colour reordering. Thus,

[5] For a true $b \to s$ transition, the $c\bar{c}$ pair must close to form a loop, and this will form the leading contribution to the Wilson coefficient C_7, but, as C_2 will enter into the long-distance charm loop calculations discussed in chapter 7, it is pertinent to illustrate the matching procedure on this simplest example.

[6] The technical definition of this amplitude is an "amputated Green's function" [39].

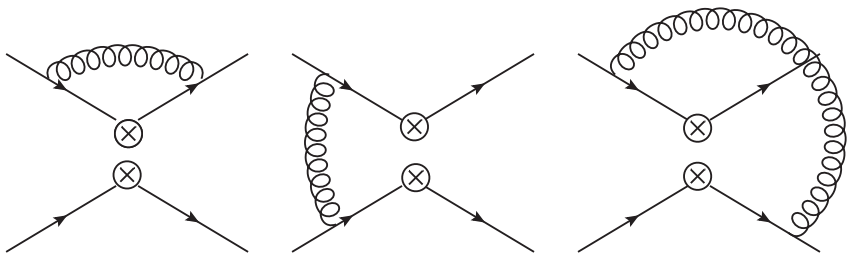

Figure 2.5 *QCD corrections to the effective theory, with effective operators indicated by a cross. Three more diagrams, related to the ones drawn above by a reflection, are not shown. The separation of the vertex into two parts is useful for tracking the colour structure through the vertex (which is different for the operators $\mathcal{O}_{1,2}$), but is a non-standard representation.*

a more complete tree-level weak effective Hamiltonian is

$$\mathcal{H}_{\text{eff}}^{(\text{tree})} = \frac{G_F}{\sqrt{2}} V_{cs}^* V_{cb} \left(C_1 \mathcal{O}_1 + C_2 \mathcal{O}_2 \right) , \tag{2.30}$$

This is generated through QCD corrections to the tree-level theory, and, as such corrections can be sizeable, it is therefore important to consider this operator and to fix the coefficients $C_{1,2}$ including these corrections. This is achieved by comparing the results of the one-loop diagrams in the full theory, illustrated in figure 2.4, with those arising from the effective theory, illustrated in figure 2.5.

On performing these computations, it can be found that the matrix Z_C, defined in (2.21), has the value [39]

$$Z_{ij} = \delta_{ij} + \frac{\alpha_s}{4\pi\epsilon} \begin{pmatrix} 3/N_C & -3 \\ -3 & 3/N_C \end{pmatrix} , \tag{2.31}$$

in terms of which the anomalous dimension matrix is given by

$$\gamma_{ij}^{(0)} = Z^{-1} \frac{d}{d \ln \mu} Z = \frac{\alpha_s}{4\pi} \begin{pmatrix} 6/N_C & -6 \\ -6 & 6/N_C \end{pmatrix} . \tag{2.32}$$

Without RG improvement, the one-loop matching above would lead to

$$C_1 = -3 \frac{\alpha_s}{4\pi} \ln \left(\frac{m_W^2}{\mu^2} \right),$$

$$C_2 = 1 + \frac{3}{N_C}\frac{\alpha_s}{4\pi}\ln\left(\frac{m_W^2}{\mu^2}\right), \tag{2.33}$$

but it can be seen that, as the energy scale μ moves away from m_W, the resulting logarithms are too significant for the expressions above to be truly perturbative; at $\mu = 1$ GeV, the correction to C_2 is well over 30%, at which level higher-order terms might well also be significant, so that a one-loop calculation is no longer trustworthy. This is a further motivation for the more rigorous approach via the RG equations, which have the effect of resumming the large logarithms $\alpha_s^n \ln(m_W^2/\mu^2)^n$ to all orders n.

Applying the equations (2.25) and (2.26) gives the RG-improved *Leading Logarithmic* behaviour of the Wilson coefficients as [39]

$$C_{1,2} = \frac{1}{2}\left(\left(\frac{\alpha_s(\mu)}{\alpha_s(m_W)}\right)^{\frac{\gamma_1^{(0)}}{2\beta_0}} \pm \left(\frac{\alpha_s(\mu)}{\alpha_s(m_W)}\right)^{\frac{\gamma_2^{(0)}}{2\beta_0}}\right) C_1(m_W)\,, \tag{2.34}$$

where $\gamma_{1,2}^{(0)} = 6 \mp 6/N_C$, and N_C is the number of colours.

The procedure can be extended to the full operator set relevant for $b \to s\ell\ell$ transitions, and leads ultimately to the effective Hamiltonian to be introduced in the next section, although the resulting RG behaviour of the Wilson coefficients is much more complicated in this case.

2.5 Effective Hamiltonian for $b \to (s,d)\gamma$ and $b \to (s,d)\ell\bar{\ell}$ decays

The tree-level effective Hamiltonian (2.30) is not sufficient to describe the decays of interest to this thesis, as the FCNC transitions only appear at loop level. These can, however, be generated by several types of operator. The full operator set relevant to such decays is defined by the effective Hamiltonian [35, 39, 70, 71]

$$H_{\text{eff}}^{b\to D} = \frac{4G_F}{\sqrt{2}}\left(\sum_{i=1}^{2}\left(\lambda_u^D C_i \mathcal{O}_i^u + \lambda_c^D C_i \mathcal{O}_i^c\right) - \lambda_t \sum_{3}^{10} C_i \mathcal{O}_i\right), \tag{2.35}$$

where $\lambda_U^D = V_{UD}^* V_{Ub}$ is a useful shorthand form for the product of two CKM matrix elements that arises from the two weak vertices at either end of the loop,

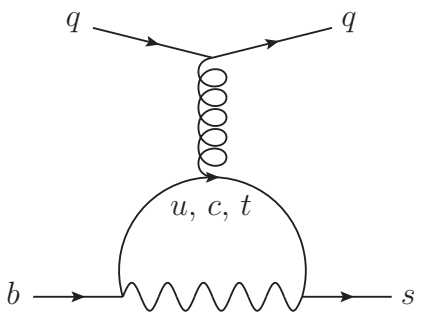

Figure 2.6 *A typical diagram contributing to the operators $\mathcal{O}_{3\text{-}6}$ (2.37). This diagram topology is known as a penguin diagram; such topologies are ubiquitous in FCNC decays. In $b \to (d,s)\gamma/\ell\bar{\ell}$ decays, these diagrams only contribute at loop level or through the definition of effective Wilson coefficients $C^{eff}_{7,V,A}$, but are still important subleading contributions to these processes, such as in weak annihilation [69].*

with $D = d, s$ depending on the transition in question. The operators $\mathcal{O}_i$ can be split into five categories: the current-current operators (already defined in the previous section)

$$\begin{aligned}\mathcal{O}_1^U &= \left(\bar{D}_{L,i}\gamma_\mu U_j\right)\left(\bar{U}_{L,j}\gamma^\mu b_i\right) ,\\ \mathcal{O}_2^U &= \left(\bar{D}_L\gamma_\mu U_L\right)\left(\bar{U}_L\gamma^\mu b\right) ,\end{aligned} \tag{2.36}$$

the QCD penguins (figure 2.6)

$$\begin{aligned}\mathcal{O}_3 &= \left(\bar{D}_L\gamma_\mu b\right)\sum_q\left(\bar{q}_L\gamma^\mu q\right) ,\\ \mathcal{O}_4 &= \left(\bar{D}_{L,i}\gamma_\mu b_j\right)\sum_q\left(\bar{q}_{L,j}\gamma^\mu q_i\right) ,\\ \mathcal{O}_5 &= \left(\bar{D}_L\gamma_\mu b\right)\sum_q\left(\bar{q}_R\gamma^\mu q\right) ,\\ \mathcal{O}_6 &= \left(\bar{D}_{L,i}\gamma_\mu b_j\right)\sum_q\left(\bar{q}_{R,j}\gamma^\mu q_i\right) ,\end{aligned} \tag{2.37}$$

the chromoelectric and chromomagnetic penguins (figure 2.7)

$$\begin{aligned}\mathcal{O}_7 &= \frac{-em_b}{16\pi^2}\bar{D}_L\sigma_{\mu\nu}bF^{\mu\nu} ,\\ \mathcal{O}_8 &= \frac{-g_s m_b}{16\pi^2}\bar{D}_L\sigma_{\mu\nu}bG^{\mu\nu} ,\end{aligned} \tag{2.38}$$

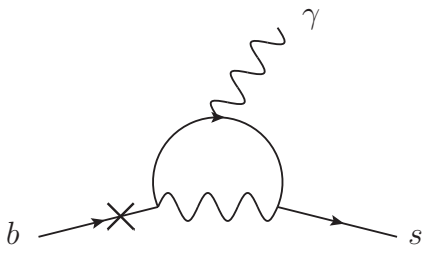

Figure 2.7 *Diagram contributing to the magnetic operators $\mathcal{O}_{7,8}$ (2.38). The cross represents a mass insertion on the b quark propagator. $\mathcal{O}_7$ has been shown, as it is more relevant to the thesis; the diagram for $\mathcal{O}_8$ follows on replacing the photon with a gluon. In $b \to (d,s)\gamma$ processes, $\mathcal{O}_8$ still contributes through loop effects, while both diagrams can play a role in $b \to (d,s)\ell\bar{\ell}$ through mixing, or a redefinition of the Wilson coefficient C_V. The effect of $\mathcal{O}_8$ has been computed in [72, 73] using two different techniques.*

and the semileptonic operators (figure 2.8)

$$\begin{aligned} \mathcal{O}_9 \equiv \mathcal{O}_V &= \frac{\alpha}{4\pi}\left(\bar{D}_L\gamma_\mu b\right)\bar{\ell}\gamma^\mu\ell\,, \\ \mathcal{O}_{10} \equiv \mathcal{O}_A &= \frac{\alpha}{4\pi}\left(\bar{D}_L\gamma_\mu b\right)\bar{\ell}\gamma^\mu\gamma_5\ell\,, \end{aligned} \tag{2.39}$$

where the notation $\mathcal{O}_{9,10}$ for these last two operators is standard in the literature, but they will typically be denoted $\mathcal{O}_{V,A}$ from now on. The subscripts i, j refer to colour sums (which, when they are not explicitly indicated, can be taken to be over the quarks inside the same brackets), while $\bar{q}_{L,R} = \bar{q}(1 \pm \gamma_5)/2$ is the left-(right-)handed antiquark. The Wilson coefficients for this Hamiltonian exhibit a clear hierarchy, with $C_{3\text{-}6}$ much smaller than the remainder. In $b \to D\ell\bar{\ell}$ decays, these coefficients also enter only at next-to-leading order, and their effects are therefore included via an absorption into effective coefficients $C^{\text{eff}}_{7,8,V}$ ($C_{10} \equiv C_A$ does not mix with any of the other coefficients, and is in fact constant), defined for example in [68].

It is also important to make clear that there are two bases for the effective Hamiltonian (2.35). The basis quoted above is based on that in [39], but most calculations of the Wilson coefficients are performed in the basis of [74], which was developed to ease the necessary loop calculations for computing the anomalous dimension. The relevant anomalous dimensions and three-loop matching for all coefficients are available from [75–77]. Finally, the signs of the operators above, in particular $\mathcal{O}_{7,8}$, are sensitive to the convention for the covariant derivative. Those above are based on the sign convention established by equation (2.2), whereas, for example, [71] employs the opposite sign convention.

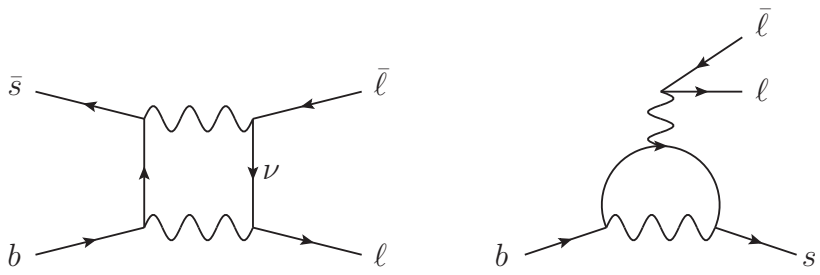

Figure 2.8 *Diagrams featuring in the computation of the operators $\mathcal{O}_{V,A}$ (2.39). Both the box and penguin diagrams contribute to both operators.*

The operators above form a complete set within the SM for the decays of interest, but it is important to note that the current-current and QCD penguins only contribute to the $b \to (d,s)\gamma$ and $b \to (d,s)\ell\bar{\ell}$ decays through their mixing under the RG evolution of the Wilson coefficients [78]. The operator $\mathcal{O}_2$ is nevertheless important for the charm loop calculations in chapter 7. The magnetic operators $\mathcal{O}_{7,8}$ come with parity-flipped equivalents that, within the standard model, can be written

$$\begin{aligned}\mathcal{O}'_7 &= \frac{-em_D}{16\pi^2}\bar{D}_R\sigma_{\mu\nu}bF^{\mu\nu}\,,\\ \mathcal{O}'_8 &= \frac{-g_s m_D}{16\pi^2}\bar{D}_R\sigma_{\mu\nu}bG^{\mu\nu}\,,\end{aligned} \tag{2.40}$$

with $m_D = m_{d,s}$ much smaller than m_b, such that the right-handed contributions to $b \to D\gamma$ are heavily suppressed within the SM.

In chapter 4 and the results in appendix C, the further operators $\mathcal{O}_{S,P,\mathcal{T}}$ are included, which could arise in certain NP scenarios [79, 80], and are given below for completeness:

$$\begin{aligned}\mathcal{O}_S &= \left(\bar{D}_L b\right)\bar{\ell}\ell\,,\\ \mathcal{O}_P &= \left(\bar{D}_L b\right)\bar{\ell}\gamma_5\ell\,,\\ \mathcal{O}_\mathcal{T} &= \left(\bar{D}_L\sigma_{\mu\nu}b\right)\bar{\ell}\sigma^{\mu\nu}\ell\,,\end{aligned} \tag{2.41}$$

to which can also be added the parity-flipped equivalents $\mathcal{O}'_{S,P,V,A,\mathcal{T}} = \mathcal{O}_{S,P,V,A,\mathcal{T}}|_{L\to R}$. The further operator $\mathcal{O}_{\mathcal{T}'} = \left(\bar{D}_L\sigma_{\mu\nu}b\right)\bar{\ell}\sigma^{\mu\nu}\gamma_5\ell$ is not required, owing to the relation $\sigma^{\mu\nu}\gamma_5 = -\frac{i}{2}\epsilon^{\mu\nu\rho\tau}\sigma_{\rho\tau}$. The Hamiltonian used in chapters 4 and 5 is then given more compactly by ($c_H = -\frac{4G_F}{\sqrt{2}}\frac{\alpha}{4\pi}V^*_{ts}V_{tb}$)

$$H^{\text{eff}} = c_H \sum_{i=V,A,S,P,\mathcal{T}} \left(C_i O_i + C'_i O'_i\right)\,. \tag{2.42}$$

Chapter 3

Distribution amplitudes

This chapter focuses on the structure of distribution amplitudes of vector and axial mesons, as well as questions related to their calculation.

3.1 Conformal symmetry

Before moving on to defining the properties of matrix elements arising from the effective Hamiltonian (2.35), it is worth giving an overview of the theory of conformal symmetry, as this will soon be used to define the relevant objects of interest to this thesis, namely the meson DAs. These can be derived by exploiting the properties of conformal symmetry, which is an inherent property of massless QCD at tree level.[1] This section largely follows the more detailed discussion found in [81], which also provides many useful references. The direct application to the processes considered in this thesis was established at the end of the 1990s, chiefly by [82, 83].

The Poincaré group, which consists of Lorentz transformations and translations, can be further extended by the inclusion of transformations under which the light-cone $\mathrm{d}s^2 = 0$ is invariant, or, equivalently, transformations that change the scale of the metric $g'_{\mu\nu}(x') = \omega(x) g_{\mu\nu}(x)$. There are five such transformations: the

[1] Clearly, the physical quark masses therefore break the conformal symmetry immediately, but this does not affect the validity of the conformal expansion when applied to DAs, see p.35 of [81].

dilatation $x_\mu \to \lambda x_\mu$ (for λ real), and the four *special conformal transformations*

$$x_\mu \to x'_\mu = \frac{x_\mu + x^2 a_\mu}{1 + 2a\cdot x + a^2 x^2}\,, \tag{3.1}$$

where a_μ is some arbitrary vector. Taken together, these transformations add five generators $\mathbf{D}, \mathbf{K}_\mu$ to the usual Poincaré algebra (four translations $\mathbf{P}_\mu$ and six Lorentz transformations $\mathbf{M}_{\mu\nu}$).

The action of these generators on an arbitrary fundamental field $\Phi(x)$ is then given by

$$\begin{aligned}
\delta_P^\mu \Phi(x) &\equiv i[\mathbf{P}^\mu, \Phi(x)] = \partial^\mu \Phi(x)\,,\\
\delta_M^{\mu\nu} \Phi(x) &\equiv i[\mathbf{M}^{\mu\nu}, \Phi(x)] = (x^\mu \partial^\nu - x^\nu \partial^\mu - \Sigma^{\mu\nu})\,\Phi(x)\,,\\
\delta_D \Phi(x) &\equiv i[\mathbf{D}, \Phi(x)] = (x\cdot\partial + \ell)\,\Phi(x)\,,\\
\delta_K^\mu \Phi(x) &\equiv i[\mathbf{K}^\mu, \Phi(x)] = \left(2x^\mu x\cdot\partial - x^2\partial^\mu + 2\ell x^\mu - 2x_\nu \Sigma^{\mu\nu}\right)\Phi(x)\,,
\end{aligned} \tag{3.2}$$

where ℓ is the *scaling dimension*, which specifies the action of the dilatation operator, while $\Sigma^{\mu\nu}$ is the generator of spin rotations for the field $\Phi(x)$. For scalar fields $\varphi(x)$, Dirac (spin-$\frac{1}{2}$) fields $\psi(x)$, and vector fields $A^\mu(x)$, the action of $\Sigma^{\mu\nu}$ is given by

$$\begin{aligned}
\Sigma^{\mu\nu}\varphi(x) &= 0\,,\\
\Sigma^{\mu\nu}\psi(x) &= \frac{i}{2}\sigma^{\mu\nu}\psi(x)\,,\\
\Sigma^{\mu\nu}A^\tau(x) &= g^{\nu\tau}A^\mu(x) - g^{\mu\tau}A^\nu(x)\,.
\end{aligned} \tag{3.3}$$

Because the conformal group leaves the light cone invariant, particles moving along (or, more generally, close to) the light cone can be usefully described in the language of conformal symmetry. It therefore makes sense to consider the subalgebra that acts on the light cone, and to work in the light-cone basis of Minkowski space. An arbitrary four-vector is decomposed in this basis as

$$\begin{aligned}
&A^\mu = (A_+, A_-, A_\perp^\mu)\,,\\
&A_+ = A^\mu \frac{p^\mu}{p\cdot z}\,, \quad A_- = A_\mu \frac{z^\mu}{p\cdot z}\,, \quad A_\perp^\mu = g_\perp^{\mu\nu} A_\nu\,,
\end{aligned} \tag{3.4}$$

where $p^2 = z^2 = 0$ are null vectors pointing along the light cone, and

$$g_\perp^{\mu\nu} = g^{\mu\nu} - \frac{1}{p\cdot z}\left(p^\mu z^\nu + z^\mu p^\nu\right) . \tag{3.5}$$

In this convention, p_μ is a light-like momentum vector and z_μ a light-like position vector, which helps to connect the general theory to the physics it will be applied to. Fields travelling along the light cone are assigned a definite spin value s, expressed by the condition $\Sigma_{+-}\Phi(\alpha z) = s\Phi(\alpha z)$, where α is some real parameter. With these restrictions, the remaining symmetries are described by four generators, which can be written as

$$\begin{aligned} \mathbf{L}_+ = \mathbf{L}_1 + i\mathbf{L}_2 = -i\mathbf{P}_+ , \quad \mathbf{L}_- = \mathbf{L}_1 - i\mathbf{L}_2 = \frac{i}{2}\mathbf{K}_- , \\ \mathbf{L}_0 = \frac{i}{2}\left(\mathbf{D} + \mathbf{M}_{+-}\right) , \qquad \mathbf{E} = \frac{i}{2}\left(\mathbf{D} - \mathbf{M}_{+-}\right) , \end{aligned} \tag{3.6}$$

where the $\mathbf{L}_{\pm,0}$ generate the algebra of $SL(2,\mathbb{R})$, and $\mathbf{E}$ commutes with the other generators. This last operator also defines the *collinear twist*, t, of a field, through its action

$$[\mathbf{E}, \Phi(\alpha)] = \frac{1}{2}(\ell - s)\Phi(\alpha) \equiv \frac{1}{2}t\Phi(\alpha) . \tag{3.7}$$

The resulting group is known as the collinear conformal group. The states $\Phi(\alpha z)$ are eigenstates of the quadratic Casimir operator:

$$L^2\Phi(\alpha z) = \sum_{i=0,1,2} [\mathbf{L}_i, [\mathbf{L}_i, \Phi(\alpha z)]] = j(j-1)\Phi(\alpha z) , \tag{3.8}$$

which provides a definition of the conformal spin j. The operator $\mathbf{L}_-$ has the important property that $\mathbf{L}_-\Phi(0) = 0$, which means that $\Phi(0)$ is the lowest state in the conformal space. Higher states can be built up by a repeated application of the raising operator $\mathbf{L}_+$ to $\Phi(0)$.

In order to apply this algebra to the physics of hadrons, it is important to connect the general fields $\Phi(\alpha z)$ to operators representing QCD processes. To this end, consider a non-local quark bilinear $\bar{q}(z)\Gamma s(-z)$, which can arise as the leading two-particle representation of a meson state. On defining the spin-projection operators [70]

$$\Pi_+ = \frac{\not{p}\not{z}}{2p\cdot z} , \quad \Pi_- = \frac{\not{z}\not{p}}{2p\cdot z} , \tag{3.9}$$

with $\Pi_+ + \Pi_- = 1$, it is possible to project onto specific spins of the quark fields. Using the definition of the spin operator $\Sigma^{\mu\nu}$ (3.3), it follows that the

projections $\Pi_\pm\psi = \psi_\pm$ have spins $s = \pm\frac{1}{2}$, and the conformal spins are $j = 1$, $j = \frac{1}{2}$ respectively. It is usual to order operators by their twist value instead, so the bilinear $\bar{q}\Gamma s$ can be split into twist-2, twist-3 and twist-4 components:

$$\begin{aligned} &\text{twist-2}: && \bar{q}_+\Gamma s_+ \,, \\ &\text{twist-3}: && \bar{q}_+\Gamma s_- + \bar{q}_-\Gamma s_+ \,, \\ &\text{twist-4}: && \bar{q}_-\Gamma s_- \,. \end{aligned} \tag{3.10}$$

This connects general *local* quark fields to conformal fields. However, in practice the hadron representations of interest are non-local operators. Returning to the general case, a product of two conformal fields $\mathcal{O}_n(\alpha_1, \alpha_2) = \Phi_1(\alpha_1 z)\Phi_2(\alpha_2 z)$ can also be expanded about the origin:

$$\mathcal{O}_n(0) = \mathcal{P}_n^{j_1,j_2}(\partial_{\alpha_1}, \partial_{\alpha_2})\ \Phi_1(\alpha_1 z)\Phi_2(\alpha_2 z)|_{\alpha_1=\alpha_2=0}\ , \tag{3.11}$$

where the $\mathcal{P}_n$ are homogeneous polynomials of degree n. It is possible to show (p.13 of [81]) that these polynomials take the form

$$\mathcal{P}_n^{j_1,j_2}(x, y) = (x + y)^n P_n^{(2j_1-1,2j_2-1)}\left(\frac{y - x}{y + x}\right)\ , \tag{3.12}$$

where the $P_n^{(a,b)}(x)$ are Jacobi polynomials. A similar relation exists for the important three-particle case, although there the relevant basis functions for the conformal expansion are Appell polynomials [84].

The final connection to QCD physics is made by considering, for example, the matrix element

$$\langle 0|\bar{q}(z)\Gamma s(-z)|M(p)\rangle = i f_M^\Gamma \int_0^1 du\, e^{ip\cdot z(2u-1)} F(u, \mu)\,, \tag{3.13}$$

where f_M^Γ is the meson decay constant (whose value depends also on the specific matrix element, indicated here by the superscript Γ), $F(u, \mu)$ is a DA, and μ is a renormalisation scale, which enters into the complete definition of the DA. In the twist-2 case, the form of the DA, denoted $\phi_M(u, \mu)$, can be extracted by using the polynomials (3.12), which for leading twist-2 reduce to the Gegenbauer polynomials $C_n^{3/2}(2u - 1)$. Hence, the moments of the DA are given by

$$\int_0^1 du\, C_n^{3/2}(2u - 1)\phi_M(u, \mu) = \langle\!\langle \mathbb{Q}_n^{t=2} \rangle\!\rangle\,, \tag{3.14}$$

where $\langle\langle \mathbb{Q}_n^{t=2} \rangle\rangle$ is the reduced matrix element of the operator $\mathbb{Q}_n^{t=2}$, which in turn is given by

$$\mathbb{Q}_n^{t=2}(0) = (i\partial_+)^n \left(\bar{q}(0)\Gamma_+ C_n^{3/2}\left(\frac{\overleftrightarrow{D}_+}{\partial_+}\right) s(0) \right) , \tag{3.15}$$

where the derivatives are defined by $\partial_+ = \overleftarrow{D} + \overrightarrow{D}$ and $\overleftrightarrow{D}_+ = \overrightarrow{D} - \overleftarrow{D}$.

The Gegenbauer polynomials $C_n^{3/2}(2u-1)$ are mutually orthogonal with respect to the weight function $6u(1-u) \equiv 6u\bar{u}$:

$$\int_0^1 du\, 6u\bar{u} C_m^{3/2}(2u-1) C_n^{3/2}(2u-1) = \delta_{mn} \frac{3(n+1)(n+2)}{2(2n+3)} , \tag{3.16}$$

from which it follows that the DA itself can be expanded in this basis. $\bar{u} \equiv 1-u$ is a shorthand that will be used for the remainder of the thesis. As a consequence, the DA can be written

$$\phi_M(u,\mu) = 6u\bar{u} \sum_{n=0}^{\infty} a_n(\mu) C_n^{3/2}(2u-1) , \tag{3.17}$$

where the $a_n(\mu)$ are the hadronic parameters that ultimately define the behaviour of the DA. The moments $a_n(\mu)$ are, in principle, scale-dependent, but obey well-defined RG evolution equations [81, 85]. In the two-particle case, all such moments are multiplicatively renormalisable – that is, they do not mix into each other – although this behaviour does not necessarily hold for higher-twist DAs. In future, the DA (3.17) will be normalised such that $\int_0^1 du\, \phi(u,\mu) = 1$, which is equivalent to fixing the zeroth moment $a_0 = 1$.

Finally, the asymptotic DA is defined as the limit when all moments $a_n = 0$ for $n \neq 0$, which can be interpreted as the limit when all constituent particles in the multiparticle state are "at rest", or have their lowest possible conformal spin. The general asymptotic DA for an n-particle state with conformal spins $j_{1,\ldots,n}$, is given by

$$\phi_{\text{as.}}(u_i) = \frac{\Gamma(2j_1 + 2j_2 + \cdots + 2j_n)}{\Gamma(2j_1)\Gamma(2j_2)\ldots\Gamma(2j_n)} u_1^{2j_1-1} u_2^{2j_2-1} \ldots u_n^{2j_n-1} . \tag{3.18}$$

Section 3.4 collects the definitions of the DAs to be used in this thesis.

3.2 QCD and light-cone sum rules

The effective Hamiltonian defined in (2.35) is sufficient to describe all FCNCs, but there still arises a problem when it comes to calculations. The amplitude for a general process $i \to f$, where i and f are the initial and final states respectively, can be described by matrix elements $\langle f|\mathcal{H}|i\rangle$, which for the effective Hamiltonian (2.35) leads to the definition of the amplitude

$$i\mathcal{A} \sim \sum_{i=1}^{10} C_i(\mu)\, \langle f|\mathcal{O}_i(\mu)|i\rangle \ , \tag{3.19}$$

where the explicit RG dependence of both the Wilson coefficients and the matrix elements has been indicated. Unfortunately, the initial and final states for the decays of interest both include mesons, and these are bound states that cannot be accurately described. Put another way, although the $C_i(\mu)$ can be computed perturbatively, the matrix elements are complicated non-perturbative objects and relate to long-distance properties of the decay.

This difficulty can be circumvented in a number of ways, one of the most important of which is Lattice QCD,[2] but the techniques exploited in this thesis are based on the sum rules formalism, developed in [88, 89], and extended to non-local Light-Cone Sum Rules (LCSR) in [90, 91]. The essence of these techniques is to replace the hadronic matrix elements by correlation functions, by replacing states $|M\rangle$ by suitable interpolating currents, which can be built up in terms of the bare quark and gluon fields defined in the SM. The resulting matrix elements can then be calculated using standard techniques, but the important extra feature is that non-perturbative effects can be classified in terms of non-vanishing vacuum expectation values, such as the quark condensate $\langle\bar{q}q\rangle$ and the gluon condensate $\langle G^2\rangle$.[3] These objects capture the non-trivial interactions with the QCD vacuum. In particular, the quark condensate $\langle\bar{q}q\rangle$ has been studied since 1968, and is related to the spontaneous chiral symmetry breaking of QCD. The Gell-Mann–Oakes–Renner relation [93]

$$\frac{m_\pi^2 f_\pi^2}{2(m_u + m_d)} = -\langle\bar{q}q\rangle \tag{3.20}$$

relates the mass of the pion to the breaking of chiral symmetry (note that the

[2] Developed by Wilson in [86]; for a review see [87].

[3] This is formally known as the Operator Product Expansion (OPE) [92].

chiral symmetry must be broken by *both* non-zero quark masses and a non-trivial vacuum condensate $\langle \bar{q}q \rangle$ in order to generate pion masses through this mechanism). Here, f_π is the pion decay constant; in the normalisation above, it has the value of approximately 130 MeV, but other conventions exist in which the pion decay constant is either $\sqrt{2}f_\pi \sim 184$ MeV [94] or $F_\pi = f_\pi/\sqrt{2} \sim 93$ MeV [38].

Having defined the vacuum condensates, the matrix elements can then be expressed as a power series expansion in terms of these condensates. Alongside the contribution from perturbation theory, this provides a means of estimating the size of the relevant matrix elements. Unfortunately, there are still problems with this approach: there is an infinite set of non-trivial vacuum condensates, and there is no guarantee that the coefficients of higher-dimensional condensates will converge. A second problem is that the condensates themselves must be evaluated with non-perturbative techniques. As discussed in more detail in appendix B, even the leading condensates still come attached to sizeable uncertainties.

Still, when combined with the formalism developed in section 3.1, the problem of evaluating the complicated matrix elements $\langle f|\mathcal{O}_i(\mu)|i\rangle$ can be reduced to one of determining hadronic parameters.

As an illustration of the LCSR method, consider its application to the $B \to \pi e \bar{\nu}$ transition [95, 96]. The matrix element of interest is

$$\langle \pi(p)|\bar{u}\gamma_\mu b|B(p_B)\rangle = (p_B + p)_\mu f_+(q^2) + q_\mu f_-(q^2)\,, \tag{3.21}$$

where $q^2 = (p_B - p)^2$ is the momentum transfer, and $f_\pm(q^2)$ are the $B \to \pi$ form factors. LCSR are most valid in the low-q^2 region (which is to say, on or near to the light cone). In this region, $f_+(q^2)$ is the dominant contribution to the $B \to \pi e \bar{\nu}$ branching ratio, making it the form factor most accessible in a LCSR calculation.

The first step in calculating this is to consider the correlation function

$$\begin{aligned}\Pi_\mu(q^2, p_B^2) &= (p_B + p)_\mu \Pi_+(q^2) + q_\mu \Pi_-(q^2) \\ &= i \int d^4x e^{-ip_B \cdot x} \langle \pi(p)|\mathcal{T}\{\bar{u}(0)\gamma_\mu b(0)\bar{b}(x)i\gamma_5 d(x)\}|0\rangle\end{aligned} \tag{3.22}$$

where the B meson has been replaced by the interpolating current $\bar{b}(x)i\gamma_5 d(x)$. Allowing the b-quark to propagate, and performing a spin projection using the

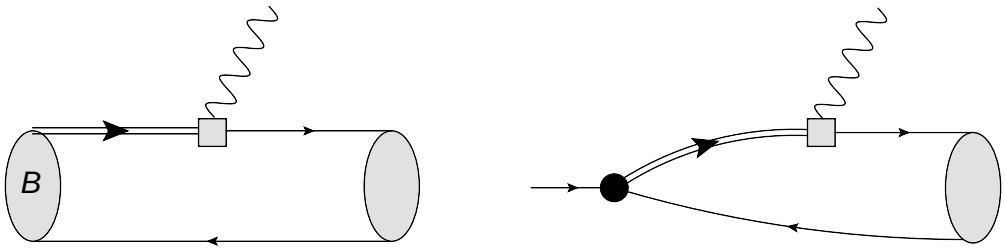

Figure 3.1 *Diagrammatic interpretation of* (3.22)*, with the B-meson replaced by an interpolating current. The pion is on the right, and, in a representation used throughout this thesis, the b quark is indicated by a double line.*

decomposition (A.19), results in

$$\begin{aligned}\Pi_\mu(q^2,p_B^2) &= -\frac{1}{4}\int d^4x \frac{d^4k}{(2\pi)^4}\frac{e^{i(k-p_B)\cdot x}}{k^2-m_b^2}\langle\pi(p)|\bar{u}(0)\gamma^\tau\gamma_5 d(x)|0\rangle \mathrm{Tr}[\gamma_\tau\gamma_5\gamma_\mu(\not{k}+m_b)\gamma_5] \\ &= m_b\int d^4x \frac{d^4k}{(2\pi)^4}\frac{e^{i(k-p_B)\cdot x}}{k^2-m_b^2}\langle\pi(p)|\bar{u}(0)\gamma_\mu\gamma_5 d(x)|0\rangle. \end{aligned} \tag{3.23}$$

This leaves behind the pion-to-vacuum matrix element; using the techniques in section 3.1, this can be defined in terms of the leading twist-2 pion distribution amplitude (3.17):

$$\langle\pi(p)|\bar{u}(0)\gamma_\mu\gamma_5 d(x)|0\rangle = -if_\pi p_\mu\int_0^1 du e^{i\bar{u}p\cdot x}\varphi_\pi(u,\mu)\,, \tag{3.24}$$

where, in this normalisation, $f_\pi \approx 130$ MeV, as in (3.20) [97]. The physical interpretation of the parameter u is that it is the momentum fraction carried by the u quark. Using this definition, and performing the x- and k-integrals, leaves

$$\begin{aligned}\Pi_\mu(q^2,p_B^2) &= f_\pi m_b p_\mu\int_0^1 du\frac{\varphi_\pi(u,\mu)}{m_b^2-up_B^2-\bar{u}q^2} \\ \implies \Pi_+(q^2,p_B^2) &= \frac{1}{2}f_\pi m_b\int_0^1 du\frac{\varphi_\pi(u,\mu)}{m_b^2-up_B^2-\bar{u}q^2}\,, \end{aligned} \tag{3.25}$$

where the second line follows from comparison with the decomposition given in (3.21), and matching the coefficients of p_μ.

Before moving on to the second aspect of form-factor calculations, quark-hadron duality – outlined in more detail below – it is worth stressing that the computation presented in (3.23) is merely the leading contribution, and can be extended in multiple ways. Firstly, the propagation of the b-quark can include higher-order

QCD corrections. The necessary expression of the modified quark propagator to account for these corrections is given in equation (A.33), while an alternative form will be used in chapter 7 for the related expansion of the charm quark propagator. Expanding the b-quark propagator in this way leads to additional loop and radiative corrections, and also necessitates an understanding of three-particle distribution amplitudes for the final-state meson. The three-particle distribution amplitudes in the vector-meson case form the topic of chapter 6.

A second source is to include higher-twist corrections to the two-particle correlation function $\langle \pi(p)|\bar{u}(0)\gamma_\mu\gamma_5 d(x)|0\rangle$. These go beyond the purview of this thesis, and the interested reader is referred to [98], as well as [99] for the similar expansions of vector meson DAs up to twist-5.

Bearing in mind these limitations, the computation (3.25) can be regarded as the leading computation. On its own, though, this is still not enough to compute the form factor of interest $f_+(q^2)$. The next step is to consider $\Pi_+(q^2, p_B^2)$ from the point of view of hadrons: comparing (3.21) and (3.22) will then lead to an expression for the form factor. In terms of hadrons, the leading contribution will be due to a pole at the B meson resonance, which means that

$$\Pi_+(q^2, p_B^2) = \frac{m_B^2 f_B}{m_b} \frac{f_+(q^2)}{m_B^2 - p_B^2} + \dots , \tag{3.26}$$

where f_B is defined, in analogy with f_π, in terms of a B-to-vacuum transition: $m_B^2 f_B = m_b \langle 0|\bar{q} i\gamma_5 b|B\rangle$. The assumption that allows the two expressions to be related is that of quark-hadron duality: in a given region, the results of calculating processes in terms of quarks will coincide with those defined in terms of hadrons [100, 101]. This duality is clearly necessary in order to make any further progress, but careful attention must be paid to the "$+\dots$" in (3.26). These represent contributions from higher resonances, and in principle there is a continuum of such resonances.

The more formal statement of the duality above is that

$$\Pi_+(q^2, p_B^2) = \int_{m_b^2}^{\infty} \frac{ds}{s - p_B^2} \rho(q^2, s) - \int_{s_0^B}^{\infty} \frac{ds}{s - p_B^2} \rho(q^2, s) \, , \tag{3.27}$$

where the parameter s_0^B represents the width of the interval in which duality applies, or, equivalently, the continuum threshold [95]. The function $\rho(q^2, s)$ is the spectral density, and, from comparing with (3.25), can be expressed in terms of the DA $\varphi_\pi(u, \mu)$, which has the usual asymptotic form for a two-particle twist-

2 DA of $\varphi_\pi(u,\mu) = 6u\bar{u}$ (3.18). Note that (3.27) is a consequence of Cauchy's integral theorem, which states that

$$f(p^2) = \frac{1}{2\pi i}\oint_\Gamma ds \frac{f(s)}{s-p^2}\,, \tag{3.28}$$

for analytic functions $f(p^2)$, where Γ is a closed contour in the complex plane that separates the pole at $s = p^2$ from all other discontinuities of $f(s)$. If $f(s)$ falls off sufficiently quickly as $|s| \to \infty$, then the contour can be extended to ∞ and be expressed only in terms of the discontinuities of $f(s)$, i.e.

$$f(p^2) = \frac{1}{\pi}\int ds \frac{\text{Disc.}f(s)}{s-p^2}\,, \tag{3.29}$$

which will also be used in the context of the charm loop calculations of chapter 7. Here, though, it allows the left-hand side of (3.27) to be written in terms of the continuum of states, which manifests itself as a branch cut in the complex plane of $\Pi(q^2, s)$.

Explicitly, then, the form factor $f_+(q^2)$ can be expressed as

$$\frac{m_B^2 f_B}{f_\pi m_b^2}\frac{f_+(q^2)}{m_B^2 - p_B^2} + \cdots = \frac{1}{2}\int_{u_0}^1 du \frac{\varphi_\pi(u,\mu)}{m_b^2 - up_B^2 - \bar{u}q^2}\,, \tag{3.30}$$

but the presence of further contributions to the left-hand side means, as stressed earlier, that this first result is unreliable. The situation can be improved by means of the Borel transformation, which will be discussed in more detail in the following section, but in this case amounts to a further (exponential) suppression of any higher resonances on the left-hand side. Using the results in appendix A.5, the final, leading order, result for $f_+(q^2)$ becomes

$$\frac{m_B^2 f_B}{m_b^2 f_\pi} e^{(m_b^2 - m_B^2)/M^2} f_+(q^2) = \frac{1}{2}\int_{u_0}^1 du \frac{\varphi_\pi(u,\mu)}{u} e^{-\bar{u}(m_b^2 - q^2)/(uM^2)}\,, \tag{3.31}$$

where

$$u_0 = \frac{m_b^2 - q^2}{s_0 - q^2}\,, \tag{3.32}$$

which follows from the continuum subtraction in (3.27). The DA $\varphi_\pi(u,\mu)$ has the form in (3.17), with the further restriction that, owing to G-parity,[4] the odd-

[4] G-parity, defined by the operator $\mathcal{G} = \mathcal{C}e^{-i\pi T_2}$, where C is charge conjugation, and T_2 is the isospin rotation about the 2-axis, provides the extension of charge conjugation to particle multiplets. It can be interpreted as a quark-antiquark exchange. The odd-numbered moments a_n in (3.17) are G-parity odd, and therefore in mesons with identical quarks (the u and d quarks

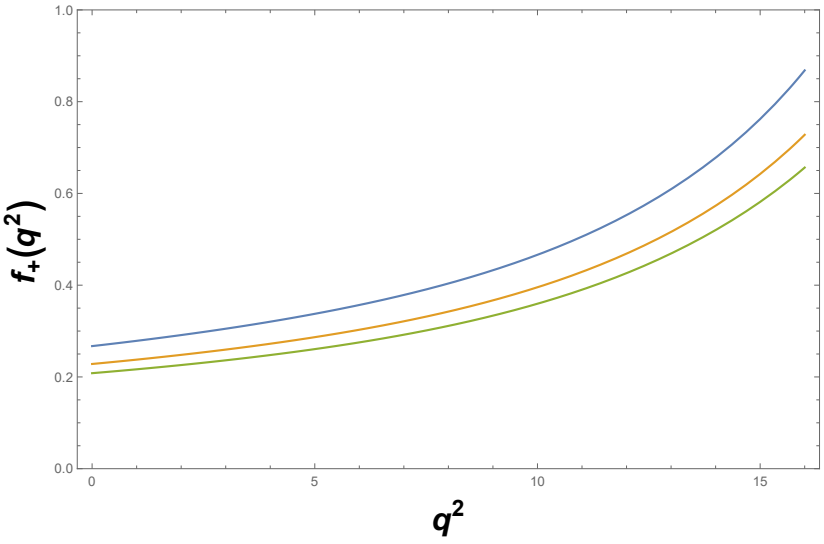

Figure 3.2 *Characteristic behaviour of the pion form factor* $f_+(q^2)$ (3.31)*, where the Borel mass scale* M^2 *has been given three different values* $M^2_{\hat{\mathcal{B}}} = 5\ GeV^2$ *(top line),* $M^2_{\hat{\mathcal{B}}} = 6.5\ GeV^2$ *(middle line), and* $M^2_{\hat{\mathcal{B}}} = 8\ GeV^2$ *(bottom line). In this computation* $\varphi_\pi(u,\mu) \to 6u\bar{u}$ *has been used, so that the results are independent of the renormalisation scale* μ*. The predicted value of* $f_+(0) \simeq 0.20$ *above is somewhat lower than that obtained from the more complete calculation in [95], but the characteristic behaviour implied by the model* (3.33) *is clearly illustrated.*

numbered Gegenbauer moments are identically zero.

This tree-level version of the sum rule is not accurate enough, but leads to the results in figure 3.2. Further corrections, from higher-twist DAs and radiative corrections, are also rather important, but the qualitative behaviour is the main feature of note in this leading calculation. Form factors can typically be modelled by the form

$$F(q^2) = \frac{F(0)}{1 - q^2/m_R^2} + \dots \tag{3.33}$$

which reflects the resonant behaviour, and this is also shown by the result in 3.2, even for the leading calculation (3.31). This simple expression is, on its own, insufficient to capture the full behaviour of form factors, as indicated by the dots. In many cases extra q^2 poles, or a further quartic term in the denominator, will be needed [99, 102], but nevertheless (3.33) is the archetypal model for the q^2 dependence of form factors, and it is instructive to see how this is captured by an LCSR calculation in the simplest case.

also being equivalent under G-parity) these moments vanish [70].

3.3 Borel transformation

The sum rule derived for the form factor $f_+(q^2)$ in the previous section relied on the Borel transformation to improve the convergence. The Borel transformation is defined as

$$f_{\hat{\mathcal{B}}}(M^2_{\hat{\mathcal{B}}}) = \hat{\mathcal{B}} f(Q^2) = \lim_{Q^2\to\infty, n\to\infty} \frac{(Q^2)^{n+2}}{n!}\left(-\frac{d}{dQ^2}\right)^{n+1} f(Q^2)\,, \tag{3.34}$$

where $Q^2 = -p^2$ is a Euclidean momentum and $Q^2/n = M^2_{\hat{\mathcal{B}}}$ defines the Borel mass. The immediate advantage of using a Borel transformation in sum rules calculations follows from the properties

$$\begin{aligned} \hat{\mathcal{B}}(p^2)^n &= 0\,, \\ \hat{\mathcal{B}}\frac{1}{m^2-p^2} &= e^{-m^2/M^2_{\hat{\mathcal{B}}}}\,, \\ \hat{\mathcal{B}}\frac{1}{(p^2)^a} &= \frac{1}{a!(M^2_{\hat{\mathcal{B}}})^{a-1}}\,, \end{aligned} \tag{3.35}$$

which implies that any uncalculated polynomial terms vanish under Borel transformations, while poles appearing from higher resonances in the meson spectrum are exponentially suppressed. Both of these properties therefore help to improve the validity of the sum rules by removing or suppressing terms that were neglected in the left-hand side of (3.31). The trade-off is that this introduces a new, arbitrary parameter $M^2_{\hat{\mathcal{B}}}$, which has no physical meaning. The Borel-improved sum rules then can only have meaning in a region where the dependence of (3.31) on $M^2_{\hat{\mathcal{B}}}$ is minimal.

On the right-hand side, in terms of the OPE, a typical sum rules calculation leads to contributions from vacuum condensates, here denoted schematically by $\langle\mathcal{Q}_{(d)}\rangle$, where d is the mass dimension of the condensate:

$$\Pi(Q^2) = \Pi_{PT}(Q^2) + \sum_d \frac{c_d}{(Q^2)^{d-n}}\langle\mathcal{Q}_{(d)}\rangle\,, \tag{3.36}$$

where the correlation function $\Pi(Q^2)$ has a mass dimension n, and $\Pi_{PT}(Q^2)$ is the perturbative contribution to the correlation function (along with any polynomial terms). The Borel-improved version of this sum rule ensures that the polynomial terms vanish, but will introduce only a factorial suppression of the condensates, according to the third line of (3.35). In practice, therefore, the sum in (3.36) must

be truncated at some mass dimension d. This introduces yet another uncertainty into the method: there is no guarantee that the coefficients c_d will be sufficiently small to be completely negligible, but on the other hand condensates of higher mass dimension can be increasingly difficult to calculate to any degree of certainty. But then, since the point of this computation is to evaluate the non-perturbative effects, it would be pointless to suppress these terms altogether by taking $M^2_{\hat{\mathcal{B}}} \to \infty$.

A further practical difficulty emerges when considering the sum rules for a particle for which it is known that there is a lower resonance in the spectrum, as well as the continuum lying above the meson of interest. This can be a problem when calculating the sum rules for axial mesons, such as the a_1, which are contaminated by the presence of the pion. The way to circumvent this difficulty is to ensure that the left-hand side of (3.36) scales with the meson mass, since $m_\pi^2 e^{-m_\pi^2} \ll m_{a_1}^2 e^{-m_{a_1}^2}$, whereas $e^{-m_\pi^2} > e^{-m_{a_1}^2}$. If this does not occur by definition of the correlation function, then it is legitimate to introduce this scale by taking instead the Borel transformation of $Q^2\Pi(Q^2)$ instead. This exploits the relation

$$\frac{Q^2}{m^2+Q^2} = \frac{Q^2+m^2}{m^2+Q^2} - \frac{m^2}{m^2+Q^2} = 1 - \frac{m^2}{m^2+Q^2}\,, \tag{3.37}$$

and then the residual polynomials so created by these manipulations vanish under Borel transformation.

The trade-off for this is to reduce the suppression of higher condensates on the right-hand side, but this is often a price worth paying; for typical values of $m^2_{\hat{\mathcal{B}}} \sim 2$ GeV, the exponential $e^{-m_\pi^2/m^2_{\hat{\mathcal{B}}}}$ is about twice the size of $e^{-m_{a_1}^2/m^2_{\hat{\mathcal{B}}}}$, but $m_\pi^2 e^{-m_\pi^2/m^2_{\hat{\mathcal{B}}}}$ is no more than 5% of $m_{a_1}^2 e^{-m_{a_1}^2/m^2_{\hat{\mathcal{B}}}}$, which is a clear improvement. Not sufficiently suppressing higher condensates, however, increases the potential uncertainty due to their contribution.

The net effect of all these competing considerations is that there is a limit to the accuracy attainable through any sum rules calculation. Despite this, the method has been shown to work in practice, and an uncertainty in the region of even 30% can be easily tolerated.

The rule of thumb adopted in Borel-improved sum rule calculations in this thesis is to insist that the Borel scale is fixed such that the contribution to the final result from the condensates of highest dimension is between $\sim 10\%$ and $\sim 30\%$ of the total value; this will define the "Borel window". This rule also amounts to

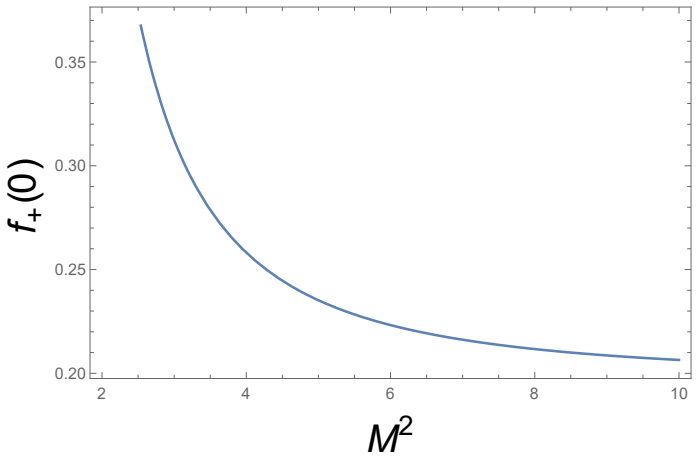

Figure 3.3 *Scaling of $f_+(0)$ (3.31) with increasing Borel mass, for central values of the parameters. Again, the numerical estimate of the form factor is not the feature of interest, and instead the qualitative behaviour is the main point. It can be seen that for values of the Borel mass that are too low, the sum rule estimate is unstable; on the other hand, choosing a Borel window that is too high risks suppressing the non-perturbative behaviour altogether. This leads to a typical range for sum rules of this kind of process in the range 5 $GeV^2 \lesssim M^2_{\hat{\mathcal{B}}} \lesssim$ 10 GeV^2 [95].*

requiring that the variation of the extracted value of any sum rule be only weakly dependent on the Borel parameter $M^2_{\hat{\mathcal{B}}}$ in a given range. Figure 3.3 illustrates this idea by plotting the dependence of $f_+(0)$ (3.31) on Borel mass, where the Borel window is taken to be around 5 to 10 GeV^2. The Borel window will, however, vary depending on the specific computation. In the calculations for vector meson sum rules, in chapter 6, the typical scale of Borel mass will be rather lower, as the appropriate scale is somewhat influenced by the mass of the relevant meson.

Useful results for the Borel transformation of different functions are given in appendix A.5.

3.4 Definitions of distribution amplitudes for vector and axial mesons

This section collects the definitions of the DAs used in this thesis, establishing the notation of chapters 6 and 7. Throughout this section, and the work in chapter 6, the two quark flavours are distinguished for clarity. The three classes of meson under consideration are the vector mesons, $J^{PC} = 1^{--}$, and two axial meson

nonets, the $J^{PC} = 1^{++}$ and 1^{+-} nonets. In spectroscopic notation, these are denoted $^3P_1$ and $^1P_1$ respectively, although results will primarily focus on the $^3P_1$ nonet.

Definitions of the DAs can also be found in [82, 83, 85, 99, 103, 104], with differing notation developed as the field has progressed. The notation below is somewhat inspired by that used in the earlier works of [82, 83], but relations to the more modern notation are provided in table 3.1. The reason for this reversion is that relations between vector and axial meson DAs can be made more transparent when the DAs are labelled in terms of the current that generates them. Thus, for three-particle DAs especially, those generated by vector, axial, and tensor currents will be denoted $\mathcal{V}, \mathcal{A}, \mathcal{T}$ respectively for vector mesons, and $\tilde{\mathcal{V}}, \tilde{\mathcal{A}}, \tilde{\mathcal{T}}$ respectively for axial mesons.

The two-particle twist-2 matrix elements for vector mesons are defined as

$$\begin{aligned}\langle 0|\bar{q}(z)\gamma_\mu s(0)|K^*(\eta,p)\rangle &= f^{\parallel}_{K^*} m_{K^*}\eta_\mu \int_0^1 du e^{-i\bar{u}p\cdot z}\phi^{\parallel}_{2;K^*}(u,\mu)\,,\\ \langle 0|\bar{q}(z)\sigma_{\mu\nu} s(0)|K^*(\eta,p)\rangle &= i f^{\perp}_{K^*}\eta_{[\mu}p_{\nu]}\int_0^1 du e^{-i\bar{u}p\cdot z}\phi^{\perp}_{2;K^*}(u,\mu)\,,\end{aligned} \tag{3.38}$$

where η is the polarisation vector. Terms of higher twist are neglected for simplicity. The twist-2 DAs have the usual conformal expansion in terms of Gegenbauer polynomials

$$\phi^{\parallel,\perp}_{2;V}(u,\mu) = 6u\bar{u}\left(1+\sum_{n=1}^{\infty} a^{\parallel,\perp}_{n;V}(\mu)C_n^{3/2}(2u-1)\right)\,, \tag{3.39}$$

where μ is the RG scale. All results will be only for the first few moments, as beyond $n = 2$ in the conformal expansion the contributions from higher condensates become increasingly significant and the sum rules approach becomes unreliable at lower order. Definitions for higher-twist two-particle DAs can be found in, for example, [82, 99, 103]. The equivalent twist-2 matrix elements for axial mesons are defined by [104]

$$\begin{aligned}\langle 0|\bar{q}(z)\gamma_\mu\gamma_5 s(0)|K_{1A}(\eta,p)\rangle &= f^{\parallel}_{K^*} m_{K_{1A}}\eta_\mu \int_0^1 du e^{-i\bar{u}p\cdot z}\phi^{\parallel}_{2;K_{1A}}(u,\mu)\,,\\ \langle 0|\bar{q}(z)\sigma_{\mu\nu}\gamma_5 s(0)|K_{1A}(\eta,p)\rangle &= i f^{\perp}_{K_{1B}}\eta_{[\mu}p_{\nu]}\int_0^1 du e^{-i\bar{u}p\cdot z}\phi^{\perp}_{2;K_{1B}}(u,\mu)\,,\end{aligned} \tag{3.40}$$

where, owing to G-parity, $\phi^{\parallel}_{2;K_{1A}}$ ($^3P_1$) has vanishing odd moments in the limit of

equal quarks, and $\phi^{\perp}_{2;K_{1A}}$ has vanishing *even* moments. The opposite is true for the K_{1B} ($^1P_1$) state.

The matrix elements for the three-particle DAs are defined as

$$\begin{aligned}
\langle 0|\left(J^V(z,vz,0)\right)^{\alpha\beta\mu}|K^*(\eta,p)\rangle &= \eta_\perp^{[\alpha}p^{\beta]}p^\mu f^\parallel_{K^*}m_{K^*}\mathcal{V}(v,p\cdot z)\,,\\
\langle 0|\left(J^A(z,vz,0)\right)^{\alpha\beta\mu}|K^*(\eta,p)\rangle &= \eta_\perp^{[\alpha}p^{\beta]}p^\mu f^\parallel_{K^*}m_{K^*}\mathcal{A}(v,p\cdot z)\,,\\
\langle 0|\left(J^S(z,vz,0)\right)^{\alpha\beta}|K^*(\eta,p)\rangle &= i\eta_\perp^{[\alpha}p^{\beta]}f^\perp_{K^*}m^2_{K^*}\mathcal{S}(v,p\cdot z)\,,\\
\langle 0|\left(J^P(z,vz,0)\right)^{\alpha\beta}|K^*(\eta,p)\rangle &= i\eta_\perp^{[\alpha}p^{\beta]}f^\perp_{K^*}m^2_{K^*}\mathcal{P}(v,p\cdot z)\,,\\
\langle 0|\left(J^T(z,vz,0)\right)^{\alpha\beta\mu\nu}|K^*(\eta,p)\rangle &= f^\perp_{K^*}m^2_{K^*}\Big(\mathcal{L}^{\alpha\beta\mu\nu}_{\mathcal{T}}\mathcal{T}(v,p\cdot z)+\mathcal{L}^{\alpha\beta\mu\nu}_{\mathcal{T}_4^{(1)}}\mathcal{T}_4^{(1)}(v,p\cdot z)\\
&\quad+\mathcal{L}^{\alpha\beta\mu\nu}_{\mathcal{T}_4^{(2)}}\mathcal{T}_4^{(2)}(v,p\cdot z)+\mathcal{L}^{\alpha\beta\mu\nu}_{\mathcal{T}_4^{(3)}}\mathcal{T}_4^{(3)}(v,p\cdot z)\\
&\quad+\mathcal{L}^{\alpha\beta\mu\nu}_{\mathcal{T}_4^{(4)}}\mathcal{T}_4^{(4)}(v,p\cdot z)\Big)\,,
\end{aligned}\tag{3.41}$$

where $J^\chi = \bar q(z)\mathcal{G}^{\alpha\beta}(vz)\chi s(0)$, with $\mathcal{G}^{\alpha\beta}(vz)\chi$ determined by the current of interest, according to the definitions in tables 3.1 and 3.2. Each three-particle DA is further specified by

$$\Phi(v,p\cdot z)=\int\mathcal{D}\underline{\alpha}e^{-ip\cdot z(\alpha_2+v\alpha_3)}\Phi(\underline{\alpha},\mu)\,,\tag{3.42}$$

where $\mathcal{D}\underline{\alpha}=d\alpha_1d\alpha_2d\alpha_3\delta\left(1-\sum_{i=1}^3\alpha_i\right)$. In analogy with the variable u of two-particle DAs, the three α_i can be interpreted as the momentum fractions for the three particles in the meson: specifically, $(\alpha_1,\alpha_2,\alpha_3)$ are the momentum fractions of the s quark, q quark, and gluon respectively. The delta function then imposes conservation of momentum on these partons. The further variable $v\in[0,1]$ determines the spatial separation along the light cone direction z between the s quark and gluon.

The $\mathcal{L}_\mathcal{T}$ are Lorentz structures given specifically by[5]

$$\begin{aligned}
\mathcal{L}_\mathcal{T}&=\frac{\eta\cdot z}{2p\cdot z}\left(p^\alpha p^\mu g_\perp^{\beta\nu}-p^\beta p^\mu g_\perp^{\alpha\nu}-(\mu\leftrightarrow\nu)\right)\,,\\
\mathcal{L}_{\mathcal{T}_4^{(1)}}&=\eta_\perp^\alpha p^\mu g_\perp^{\beta\mu}-\eta_\perp^\beta p^\mu g_\perp^{\alpha\mu}-(\mu\leftrightarrow\nu)\,,\\
\mathcal{L}_{\mathcal{T}_4^{(2)}}&=p^\alpha\eta_\perp^\mu g_\perp^{\beta\mu}-p^\beta\eta_\perp^\mu g_\perp^{\alpha\mu}-(\mu\leftrightarrow\nu)\,,\\
\mathcal{L}_{\mathcal{T}_4^{(3)}}&=\frac{1}{p\cdot z}\left(p^\alpha z^\beta p^\mu\eta_\perp^\nu-p^\beta z^\alpha p^\mu\eta_\perp^\nu-(\mu\leftrightarrow\nu)\right)\,,
\end{aligned}$$

[5]Owing to the conventions for indices in this thesis, this expression appears to differ from that given in equation (4.1) of [103], but the two are identical up to a relabelling of indices.

DA	twist	chirality	$\mathcal{G}^{\alpha\beta}\,\chi$	Γ^χ
$\mathcal{V} \equiv \Phi^{\parallel}_{3[\rho]}$	3	even	$G^{\alpha\beta} i\gamma^\mu$	$\gamma^{\alpha'}$
$\mathcal{A} \equiv \tilde{\Phi}^{\parallel}_{3[\rho]}$	3	even	$\tilde{G}^{\alpha\beta}\gamma^\mu\gamma_5$	
$\mathcal{T}_3 \equiv \Phi^{\perp}_{3[\rho]}$	3	odd	$G^{\alpha\beta}\sigma^{\mu\nu}$	$\sigma^{\alpha'\beta'}$
$\mathcal{T}_4^{(1)} \equiv \Phi^{\perp(1)}_{4[\rho]}$	4	odd		
$\mathcal{T}_4^{(2)} \equiv \Phi^{\perp(2)}_{4[\rho]}$	4	odd		
$\mathcal{T}_4^{(3)} \equiv \Phi^{\perp(3)}_{4[\rho]}$	4	odd		
$\mathcal{T}_4^{(4)} \equiv \Phi^{\perp(4)}_{4[\rho]}$	4	odd		
$\mathcal{S} \equiv \Psi^{\perp}_{4[\rho]}$	4	odd	$G^{\alpha\beta}\mathbf{1}$	$\sigma^{\alpha'\beta'}$
$\mathcal{P} \equiv \tilde{\Psi}^{\perp}_{4[\rho]}$	4	odd	$\tilde{G}^{\alpha\beta} i\gamma_5$	

Table 3.1 *The currents of interest, labelled by the gluon field type and Dirac structure of the current and the corresponding distribution amplitude. This thesis uses the labels $\mathcal{S}, \mathcal{P}$, etc., to distinguish each current and DA more simply. The leftmost column indicates the conversion to the standard literature definitions for these DAs [85, 103]. The right-hand column represents the vertex used in the non-diagonal sum rules, to be computed in chapter 6.*

$$\mathcal{L}_{\mathcal{T}_4^{(4)}} = \frac{1}{p\cdot z}\left(p^\alpha \eta_\perp^\beta p^\mu z^\nu - p^\beta \eta_\perp^\alpha p^\mu z^\nu - (\mu \leftrightarrow \nu)\right) . \tag{3.43}$$

For axial mesons, the definitions follow by replacing the currents in (3.41) above by the equivalent definitions in table 3.2, leading to the DAs $\tilde{\mathcal{V}}$, and so on. The properties of these DAs for the ${}^3P_1$ mesons are shown in the same table; those for ${}^1P_1$ mesons are outlined in [104].

The DAs $\mathcal{V}$, $\mathcal{A}$, $\mathcal{T}_3$, $\mathcal{T}_4^{(1)}$, $\mathcal{T}_4^{(3)}$ above all have a well-defined conformal expansion, which can be written in the basis of Appell polynomials [84]

$$\Phi\left(j_1, j_2, j_3, \underline{\alpha}\right) = \Phi^{(0)}(j_1, j_2, j_3, \underline{\alpha}) \sum_{k,l=0}^{\infty} \omega_{kl}^{(j_1,j_2,j_3)} \mathcal{J}_{kl}\left(2(j_1+j_2+j_3)-1, 2j_2, 2j_3, \alpha_1, \alpha_2\right) , \tag{3.44}$$

where

$$\Phi^{(0)}(j_1, j_2, j_3, \underline{\alpha}) = \frac{\Gamma\left(2(j_1+j_2+j_3)\right)}{\Gamma\left(2j_1\right)\Gamma\left(2j_2\right)\Gamma\left(2j_3\right)} \alpha_1^{2j_1-1}\alpha_2^{2j_2-1}\alpha_3^{2j_3-1} \tag{3.45}$$

DA	twist	chirality	$\mathcal{G}^{\alpha\beta}\,\chi$	Γ^{χ}
$\tilde{\mathcal{V}} \equiv \Phi^{\parallel}_{3[\tilde{\rho}]}$	3	odd	$\tilde{G}^{\alpha\beta}\gamma^{\mu}$	$\gamma^{\alpha'}\gamma_5$
$\tilde{\mathcal{A}} \equiv \tilde{\Phi}^{\parallel}_{3[\tilde{\rho}]}$	3	odd	$G^{\alpha\beta}i\gamma^{\mu}\gamma_5$	
$\tilde{\mathcal{T}}_3 \equiv \Phi^{\perp}_{3[\tilde{\rho}]}$	3	even	$(-i)\tilde{G}^{\alpha\beta}\sigma^{\mu\nu}$	$\sigma^{\alpha'\beta'}$
$\tilde{\mathcal{T}}_4^{(1)} \equiv \Phi^{\perp(1)}_{4[\tilde{\rho}]}$	4	even		
$\tilde{\mathcal{T}}_4^{(2)} \equiv \Phi^{\perp(2)}_{4[\tilde{\rho}]}$	4	even		
$\tilde{\mathcal{T}}_4^{(3)} \equiv \Phi^{\perp(3)}_{4[\tilde{\rho}]}$	4	even		
$\tilde{\mathcal{T}}_4^{(4)} \equiv \Phi^{\perp(4)}_{4[\tilde{\rho}]}$	4	even		
$\tilde{\mathcal{S}} \equiv \Psi^{\perp}_{4[\rho]}$	4	even	$\tilde{G}^{\alpha\beta}i\mathbf{1}$	$\sigma^{\alpha'\beta'}\gamma_5$
$\tilde{\mathcal{P}} \equiv \tilde{\Psi}^{\perp}_{4[\rho]}$	4	even	$G^{\alpha\beta}\gamma_5$	

Table 3.2 *The equivalent definitions to those in table 3.1 for ${}^3P_1$ mesons, using $\tilde{\rho} \equiv a_1$ as a template.*

is the asymptotic DA, and explicit expressions are

$$\begin{aligned}
\Phi^{(1,1,3/2)}(\underline{\alpha}) &= 360\alpha_1\alpha_2\alpha_3^2\left(\omega_{0,0}^{(1,1,3/2)} + \omega_{1,0}^{(1,1,3/2)}\left(\alpha_3 - \frac{3}{2}\alpha_1\right) + \omega_{0,1}^{(1,1,3/2)}\left(\alpha_3 - \frac{3}{2}\alpha_2\right)\right), \\
\Phi^{(1/2,1,3/2)}(\underline{\alpha}) &= 60\alpha_2\alpha_3^2\left(\omega_{0,0}^{(1/2,1,3/2)} + \omega_{1,0}^{(1/2,1,3/2)}\left(\alpha_3 - 3\alpha_1\right) + \omega_{0,1}^{(1/2,1,3/2)}\left(\alpha_3 - \frac{3}{2}\alpha_2\right)\right), \\
\Phi^{(1,1/2,3/2)}(\underline{\alpha}) &= 60\alpha_1\alpha_3^2\left(\omega_{0,0}^{(1,1/2,3/2)} + \omega_{1,0}^{(1,1/2,3/2)}\left(\alpha_3 - \frac{3}{2}\alpha_1\right) + \omega_{0,1}^{(1,1/2,3/2)}\left(\alpha_3 - 3\alpha_2\right)\right), \\
\Phi^{(1,1,1)}(\underline{\alpha}) &= 120\alpha_1\alpha_2\alpha_3\left(\omega_{0,0}^{(1,1,1)} + \omega_{1,0}^{(1,1,1)}\left(\alpha_3 - \alpha_1\right) + \omega_{0,1}^{(1,1,1)}\left(\alpha_3 - \alpha_2\right)\right).
\end{aligned} \tag{3.46}$$

$\Phi^{(1,1,3/2)}(\underline{\alpha})$ is the expansion for all twist-3 three-particle DAs, while the others are important only for twist-4 expressions. For the twist-3 DAs, it is more convenient to work in the basis [81, 104]

$$\Phi\left(j_1, j_2, j_3, \underline{\alpha}\right) = \Phi^{(0)}(j_1, j_2, j_3, \underline{\alpha}) \sum_{N=0}^{\infty}\sum_{n\leq N} \upsilon_{N,n} Y_{Nn}^{(12)3}\left(\alpha_1, \alpha_2, \alpha_3\right) \tag{3.47}$$

$$Y_{Nn}^{(12)3}\left(\alpha_1, \alpha_2, \alpha_3\right) = \frac{(-1)^N}{2}\left(1-\alpha_3\right)^n P_{N-n}^{(2j_3-1,2j-1)}\left(1-2\alpha_3\right) P_n^{(2j_1-1,2j_2-1)}\left(\frac{\alpha_2-\alpha_1}{1-\alpha_3}\right), \tag{3.48}$$

where the $P_n^{(a,b)}(x)$ are Jacobi polynomials. This basis is orthogonal, but can only be applied to DAs for which the conformal spins of the quarks are identical, a

fact that appears to have been overlooked, or at least not emphasised, in previous literature. When extending to twist-4 DAs, it will therefore be essential to work in the basis of Appell polynomials. The relationship between the two bases can be also expressed in terms of the parameters:

$$\begin{aligned} \omega_{0,0}^{(1,1,3/2)} &= \upsilon_{0,0}\,, \\ \frac{1}{2}\left(\omega_{0,1}^{(1,1,3/2)} + \omega_{1,0}^{(1,1,3/2)}\right) &= \upsilon_{1,0}\,, \\ \frac{3}{4}\left(\omega_{0,1}^{(1,1,3/2)} - \omega_{1,0}^{(1,1,3/2)}\right) &= \upsilon_{1,1}\,. \end{aligned} \tag{3.49}$$

In future applications, this series expansion will be restricted to the first three terms, where hereafter (using the $\mathcal{V}$ DA as a template)

$$\upsilon_{0,0} = \mathcal{V}_{(0)V}\,, \quad \upsilon_{1,1} = \mathcal{V}_{(1)V}\,, \quad \upsilon_{1,0} = \mathcal{V}_{(2)V}\,. \tag{3.50}$$

The relation of the first three parameters in the notation of this thesis to the standard literature notation [85] is as follows:

$$\begin{aligned} \mathcal{V}_{(0)V} &= \kappa_{3V}^{\parallel}\,, & \mathcal{V}_{(1)V} &= \omega_{3V}^{\parallel}\,, & \mathcal{V}_{(2)V} &= \lambda_{3V}^{\parallel}\,, \\ \mathcal{A}_{(0)V} &= \zeta_{3V}^{\parallel}\,, & \mathcal{A}_{(1)V} &= \tilde{\lambda}_{3V}^{\parallel}\,, & \mathcal{A}_{(2)V} &= \tilde{\omega}_{3V}^{\parallel}\,, \\ \mathcal{T}_{(0)V} &= \kappa_{3V}^{\perp}\,, & \mathcal{T}_{(1)V} &= \omega_{3V}^{\perp}\,, & \mathcal{T}_{(2)V} &= \lambda_{3V}^{\perp}\,. \end{aligned} \tag{3.51}$$

The DAs $\mathcal{S}$, $\mathcal{P}$, $\mathcal{T}_4^{(2)}$, $\mathcal{T}_4^{(4)}$ do not have a well-defined conformal expansion by themselves, and instead one must define auxiliary functions

$$\begin{aligned} \mathcal{F}_1^{\uparrow\downarrow} &= \mathcal{S} + \mathcal{T}_4^{(4)}\,, \\ \mathcal{F}_1^{\downarrow\uparrow} &= \mathcal{S} - \mathcal{T}_4^{(4)}\,, \\ \mathcal{F}_2^{\uparrow\downarrow} &= \mathcal{P} - \mathcal{T}_4^{(2)}\,, \\ \mathcal{F}_2^{\downarrow\uparrow} &= \mathcal{P} + \mathcal{T}_4^{(2)}\,, \end{aligned} \tag{3.52}$$

which *do* have an explicit conformal expansion [103], making use of the functions $\Phi^{(1/2,1,3/2)}(\underline{\alpha})$ and $\Phi^{(1,1/2,3/2)}(\underline{\alpha})$ in equation (3.46).

This thesis focuses on applications of the methods above to the twist-3 case, with some results for twist-4 DAs presented in appendix D, but it is hoped that the more general notation developed above will be useful for extensions of the work presented in chapters 6 and 7.

Chapter 4

Generalised helicity formalism and the $B \to K^*(\to K\pi)\ell\bar{\ell}$ decay

In the 1990s, the B factories at Belle and BaBar began gathering data related to B meson production and decay properties. Almost inevitably, in anticipation of the results and continuing through the full programs of these experiments, theoretical predictions associated to relevant decay processes were developed and enhanced.

The research programme investigating decays specifically of the type $B \to K^{(*)}\ell\bar{\ell}$ can be said to have begun at the end of the 1980s [105, 106]. The earliest studies were restricted to the decay rate, before moving to consider the angular distribution without the subsequent decay of $K^* \to K\pi$ [107], and finally with the full four-body final state in [108]. After mass corrections from the final-state leptons were added [109, 110], studies of this process were extended to include the full dimension-six operator basis, including scalar and tensor structures [78, 111–113].

The $B \to K^*\ell^+\ell^-$ decay was first observed in 2003 by both the Belle [114] and BaBar [115] Collaborations, although it was not until later that more detailed measurements were made [116, 117]. Once the LHC began operations, the LHCb experiment also started to study the decay, and in 2013 announced the first signs of a possible deviation from the SM prediction in the observable known as P_5' [20]. This has prompted further experimental measurements of these observables, both by the LHCb and other experiments [22, 24, 25, 118]. ATLAS and CMS have also released results on the angular distribution [119, 120]; the ATLAS result supports

the P_5' anomaly, whereas the CMS result appears more consistent with the SM prediction [121]. Currently, the tension between experimental measurements and theoretical prediction is not significant enough to declare a certain discovery (of either *bona fide* NP or some previously unanticipated effect within the SM), but it is usually held that the tension is approaching the level of 5σ [27, 122]. The latest status of decays of this type is summarised in [123], which also provides many other useful references.

This chapter presents a generalisation of the helicity formalism to effective field theories of rare decays of the type $B \to K_{J_K}(\to K\pi)\bar{\ell}_1\ell_2$, and illustrates its application by deriving the full angular distributions for $\bar{B} \to \bar{K}\ell_1\bar{\ell}_2$ and $\bar{B} \to \bar{K}^*(\to \bar{K}\pi)\ell_1\bar{\ell}_2$ for the complete dimension-six effective Hamiltonian, including with non-equal lepton masses. With the inclusion of non-equal lepton mass terms, the principal results of this chapter can be regarded as a completion of the theoretical description of the full angular distribution of this decay, following the work described above. The method was also discussed in chapter 8 of [124].

This chapter is based on work previously published in [34].

4.1 Introduction to the helicity formalism

The helicity formalism, introduced in 1959 [33], presents an alternative method to compute the structure of angular distributions for a given decay. The formalism relies on conservation of total angular momentum of a system, and on the invariance of the helicity, $\lambda = \mathbf{s}\cdot\hat{\mathbf{p}}$, under Lorentz transformations centred on the direction of momentum. This section introduces some of the key concepts of the formalism; for a more complete review, see, for example, [125–127].

The base unit of the helicity formalism is a one-to-two particle decay chain $A \to B_1B_2$. In the rest frame of the initial particle A, the state of that particle can be written $|J_AM_A\rangle$, and, for a decay governed by the operator $\hat{O}$, the matrix element of interest is

$$\begin{aligned}\mathcal{M}_{A\to B_1B_2} &= \langle \mathbf{p}_1,\lambda_1,\mathbf{p}_2,\lambda_2|\hat{O}|J_AM_A\rangle \\ &= \langle \theta,\phi,\lambda_1,\lambda_2|\hat{O}|J_AM_A\rangle\,, \end{aligned} \tag{4.1}$$

where in the rest frame of A, the two decay products are produced back-to-back along some axis defined by the angles θ,ϕ. The final-state $|\mathbf{p}_1,\lambda_1,\mathbf{p}_2,\lambda_2\rangle$ is a

plane-wave state, but it does not have a definite angular momentum j. To move to the helicity formalism, the final state above is projected over states $|j, m, \lambda_1, \lambda_2\rangle$ with definite helicities m, so that

$$\begin{aligned}\mathcal{M}_{A\to B_1B_2} &= \sum_{j,m}\langle\theta,\phi,\lambda_1,\lambda_2|j,m,\lambda_1,\lambda_2\rangle\langle j,m,\lambda_1,\lambda_2|\hat{O}|J_AM_A\rangle \\ &= \sqrt{\frac{2J_A+1}{4\pi}}D^{J_A}_{M_A,\lambda_1-\lambda_2}(\phi,\theta,-\phi)\,\mathcal{A}_{\lambda_1\lambda_2}\,, \end{aligned} \tag{4.2}$$

which splits the amplitude into two separate parts: the Wigner functions, $D^{J_A}_{M_A,\lambda_1-\lambda_2}(\phi,\theta,-\phi)$, describing the angular structure; and the helicity amplitude (HA) $\mathcal{A}_{\lambda_1\lambda_2}$, containing all physical information about the decay.

The Wigner functions provide a representation of $SO(3)$ of dimension $(2J+1)$, as seen through the action of the rotation operator on the state $|jm\rangle$,

$$R(\alpha,\beta,\gamma)|jm\rangle = \sum_{m'=-j}^{j} D^{j}_{m',m}(\alpha,\beta,\gamma)\,|jm\rangle\,, \tag{4.3}$$

with Euler angles (α,β,γ). The final angular distribution is given by the square of the matrix element, summed over external helicities.

The Wigner functions obey many useful properties, fulfilling in particular the orthogonality relations

$$\int \bar{D}^{j}_{m,n}(\alpha,\beta,\gamma)\,D^{l}_{p,q}(\alpha,\beta,\gamma)\,d\alpha d\cos\beta d\gamma = \frac{8\pi^2}{2j+1}\delta_{jl}\delta_{mp}\delta_{nq}\,, \tag{4.4}$$

along with the general representation

$$\begin{aligned} D^{j}_{m,n}(\alpha,\beta,\gamma) &= e^{-im\alpha}d^{j}_{m,n}(\beta)\,e^{-in\gamma}\,, \\ \bar{D}^{j}_{m,n}(\alpha,\beta,\gamma) &= e^{im\alpha}d^{j}_{m,n}(\beta)\,e^{in\gamma}\,, \end{aligned} \tag{4.5}$$

where the $d^{j}_{m,n}(\beta)$, the little-d functions, are standard, and can be found tabulated in many places in the literature, e.g [128].

A striking feature of the helicity formalism can be seen when considering sequential decay chains; in the simplest example, in the decay chain $A \to B_2(\to$

$C_4C_5)B_3$, the matrix element becomes [125]

$$\mathcal{M}_{A\to B_2(\to C_4C_5)B_3} = \sqrt{\frac{2J_A+1}{4\pi}\frac{2J_2+1}{4\pi}}\sum_{\lambda_2} D^{J_A}_{M_A,\lambda_2-\lambda_3}(\Omega_A)\,\mathcal{A}_{\lambda_2\lambda_3} D^{J_2}_{M_2,\lambda_4-\lambda_5}(\Omega_2)\,\mathcal{B}_{\lambda_4\lambda_5}\,, \tag{4.6}$$

which is to say that the amplitude becomes a product over two decay chains, coherently summed over the helicity states of the internal particle B_2. The angles $\Omega_A = (\theta_A, \phi_A)$ and $\Omega_2 = (\theta_2, \phi_2)$ are defined in the rest frames of particles A and B_2 respectively. This procedure can be applied arbitrarily often to describe increasingly complex decay chains built out of any number of $1 \to 2$ decays.

Using the helicity formalism therefore reduces the calculation of the angular distribution to one of computing the HAs. In general, these can be complicated, non-perturbative objects, but once computed, or parametrised, they can be fed through the formalism above in a systematic way.

4.1.1 Helicity formalism for $B_{J_B} \to K_{J_K}(\to K_1K_2)\gamma_{J_\gamma}(\to \bar{\ell}_1\ell_2)$

Consider the following sequential decay:

$$B_{J_B} \to K_{J_K}(\to K_1K_2)\gamma_{J_\gamma}(\to \bar{\ell}_1\ell_2)\,, \tag{4.7}$$

where J_B, J_γ and J_K denote the spin of the particles B, γ_J and K_J. Assuming the decay to be a series of sequential $1 \to 2$ decays, the amplitude can be written in terms of a product of $1 \to 2$ HAs multiplied by the corresponding Wigner functions

$$\begin{aligned}&\mathcal{A}(\Omega_B, \Omega_\ell, \Omega_K|\lambda_B, \lambda_{K_1}, \lambda_{K_2}, \lambda_1, \lambda_2) \sim \\ &\quad\sum_{\lambda_\gamma\lambda_K} \bar{D}^{J_B}_{\lambda_B,\lambda_\gamma-\lambda_K}(\Omega_B)\,\mathcal{H}_{\lambda_\gamma\lambda_K}\bar{D}^{J_K}_{\lambda_K,\lambda_{K_2}-\lambda_{K_1}}(\Omega_K)\,\mathcal{K}_{\lambda_{K_1},\lambda_{K_2}}\bar{D}^{J_\gamma}_{\lambda_\gamma,\lambda_\ell}(\Omega_\ell)\,\mathcal{L}_{\lambda_{\ell_1}\lambda_{\ell_2}}\,,\end{aligned} \tag{4.8}$$

where the λ_i are helicity indices, and

$$\lambda_\ell \equiv \lambda_1 - \lambda_2 \tag{4.9}$$

is a convenient shorthand notation. The HAs $\mathcal{H}$, $\mathcal{K}$ and $\mathcal{L}$ correspond to the transitions $B_{J_B} \to K_{J_K}\gamma_{J_\gamma}$, $K_{J_K} \to K_1K_2$, and $\gamma_{J_\gamma} \to \bar{\ell}_1\ell_2$ respectively. The helicities of the internal particles γ_J and K_J have to be coherently summed over.

In order to ease the notation slightly, it is convenient to move straight to the case $\bar{B} \to \bar{K}_J(\to K\pi)\gamma_{J_\gamma}(\to \ell_1\bar{\ell}_2)$.[1] The relation $D^{J_B=0}_{\lambda_B=0,\lambda_\gamma-\lambda_K}(\Omega) = \delta_{0,\lambda_\gamma-\lambda_K}$ implies equality of helicities

$$\lambda \equiv \lambda_\gamma = \lambda_K \ . \tag{4.10}$$

One may therefore write $\mathcal{H}_{\lambda_\gamma\lambda_K} \to H_\lambda$, which is the quantity known as the (hadronic) HA in the $\bar{B} \to \bar{K}^*\ell^+\ell^-$-literature, and carries the non-trivial dynamic information. The HA $\mathcal{K}_{\lambda_{K_1},\lambda_{K_2}}$ reduces to a scalar constant (denoted by $g_{K_JK\pi}$), since $K_1 \to K$, $K_2 \to \pi$ are both scalar particles. The third HA $\mathcal{L}_{\lambda_1\lambda_2}$ depends on the interaction vertex of the leptons, and can be systematically computed once the interaction is known. One may rewrite the amplitude (4.8) as

$$\mathcal{A}(\bar{B} \to \bar{K}_{J_K}(\to K\pi)\gamma_{J_\gamma}(\to \ell_1\bar{\ell}_2)) \sim \sum_{\lambda=-J_K}^{J_K} D^{J_K}_{\lambda,0}\left(\Omega_K\right) D^{J_\gamma}_{\lambda,\lambda_\ell}\left(\Omega_\ell\right) \mathcal{A}^{J_\gamma}_{\lambda,\lambda_1,\lambda_2} \ , \tag{4.11}$$

where the angles, depicted in figure 4.1, are $\Omega_K = (0, \theta_K, 0)$ and $\Omega_\ell = (\phi_\ell, \theta_\ell, -\phi_\ell)$. Note that the passage from $\bar{D}$ to D-functions from (4.8) to (4.11) is related to passing from B to $\bar{B}$.

In this template, the amplitude $\mathcal{A}^{J_\gamma}_{\lambda,\lambda_1,\lambda_2} \sim H_\lambda\mathcal{L}_{\lambda_1\lambda_2}|_{J_\gamma}$ is the product of the hadronic and leptonic matrix elements. The angle ϕ_ℓ is the helicity angle, and is usually called simply ϕ. The fourfold differential decay is then given by

$$\frac{d^4\Gamma}{dq^2 d\cos\theta_\ell d\cos\theta_K d\phi} \sim \sum_{\lambda_1\lambda_2} |\mathcal{A}|^2 \sim \tag{4.12}$$

$$\sum_{\lambda_1,\lambda_2=-1/2}^{1/2} \sum_{\lambda,\lambda'=-J_\gamma}^{J_\gamma} \mathcal{A}^{J_\gamma}_{\lambda,\lambda_1,\lambda_2}\bar{\mathcal{A}}^{J_\gamma}_{\lambda',\lambda_1,\lambda_2} D^{J_{K_J}}_{\lambda,0}\left(\Omega_K\right) \bar{D}^{J_{K_J}}_{\lambda',0}\left(\Omega_K\right) D^{J_\gamma}_{\lambda,\lambda_\ell}\left(\Omega_\ell\right) \bar{D}^{J_\gamma}_{\lambda',\lambda_\ell}\left(\Omega_\ell\right) \ .$$

Although the work until now has been somewhat general, the remainder of the chapter focuses on the specific decays of interest, using $\bar{B} \to \bar{K}^*\ell\bar{\ell}$ as a reference. Throughout this section, the further assumption will be made that the decay proceeds to its final state mesons via a long-lived intermediate meson state, an assumption also known as the narrow-width approximation [78].

It is important to be clear about the conventions for angles. These have been

[1] The decay mode $\bar{B} \to \bar{K}_J\ell_1\bar{\ell}_2$ serves as the main template for the results in this chapter and the associated appendix. Such transitions are governed by the $b \to s$ Hamiltonian (2.35), which is the standard in the theory literature and is used to define the Wilson coefficients. In the more conceptual sections, the $B \to K_J\bar{\ell}_1\ell_2$ transition is used instead. The two are related by a CP transformation.

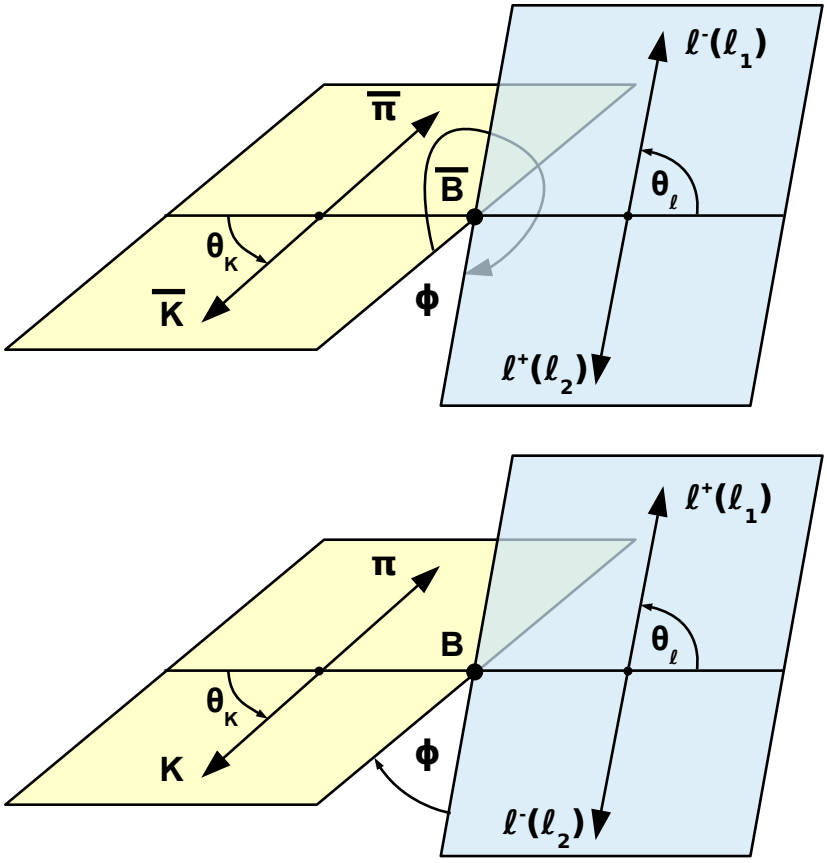

Figure 4.1 *Decay geometries for $\bar{B} \to \bar{K}^* \ell_1 \bar{\ell}_2$ (above) and $B \to K^* \bar{\ell}_1 \ell_2$ (below). In both cases $\ell_1 = \ell^-$, $\ell_2 = \ell^-$ denote the negatively charged lepton. The conventions are the same as used by the LHCb collaboration in [129] (cf. appendix A therein). Comparison to the convention used by the theory community can be found in section 4.4. It is important to remember that the angles $\theta_{\ell,K}$ are drawn in the rest frame of the lepton-pair and the K^*-meson. For decays that are not self-tagging, such as $B_s, \bar{B}_s \to \phi(\to K^+K^-)\mu^+\mu^-$ at the LHCb, the angles $(\theta_\ell, \theta_K, \phi) \to (\pi - \theta_\ell, \pi - \theta_K, 2\pi - \phi)$, and one can only measure the sum of both decay rates (see also discussion in section 4.4).*

somewhat ill-defined in the previous literature, and in particular the theoretical and experimental communities have tended to use different conventions. In this chapter, the angular conventions are the same as the LHCb collaboration ([129], appendix A), which differ from those used by the theory community. More precise statements, including a conversion diagram, can be found in section 4.4.

4.1.2 Effective theories rewritten as a coherent sum of sequential decays

The amplitude (4.11) is of a completely general form for the decay where γ_{J_γ} is an actual particle of spin J_γ. In $\bar{B} \to \bar{K}^*(\to \bar{K}\pi)\ell_1\bar{\ell}_2$ a part of the amplitude is in this form where the photon corresponds to the intermediate state ($\gamma_1 = \gamma$). In general, there are effective vertices where the intermediate particles are not present.

The effective Hamiltonian for the decays considered in this chapter was presented in (2.42). In the case where electroweak corrections are neglected, one may factorise the hadronic from the leptonic part. This is referred to as the Lepton Factorisation Approximation (LFA). Schematically, the Hamiltonian can be seen as a product of a hadronic part H and a leptonic part $\mathcal{L}$ with a certain number of Lorentz contractions between them:

$$H^{\text{eff}} \sim \sum_{a=1}^{N_0} H^a \mathcal{L}_a + \sum_{b=1}^{N_1} H^b_\mu \mathcal{L}^\mu_b + \sum_{c=1}^{N_2} H^c_{\mu_1\mu_2} \mathcal{L}^{\mu_1\mu_2}_c \ . \tag{4.13}$$

The sum over a, b and c extends over operators with 0, 1 and 2 Lorentz contractions between quark and lepton operators. In the example of the operator $O_V = C_V \bar{s}_L \gamma_\mu b \bar{\ell}\gamma^\mu \ell$, then in the notation above $H_\mu = C_V \bar{s}_L \gamma_\mu b$ and $\mathcal{L}^\mu = \bar{\ell}\gamma^\mu \ell$. On a formal level, $O_V(O_9)$ can be thought of as originating from integrating out a vector and a scalar particle, in the sense that the Lorentz contraction over index μ can be written as the sum of products of a spin-one and a (timelike) spin-0 polarisation vector. This is expressed by the well-known completeness relation (e.g. [109, 130, 131])

$$g^{\mu\nu} = \sum_{\lambda,\lambda' \in \{t,\pm,0\}} \omega^\mu(\lambda)\bar{\omega}^\nu(\lambda') G_{\lambda\lambda'} \ , \quad G_{\lambda\lambda'} = \text{diag}(1,-1,-1,-1) \ , \tag{4.14}$$

where the first entry in $G_{\lambda\lambda'}$ refers to $\lambda = \lambda' = t$, and an explicit parametrisation

is given by

$$\begin{aligned}\omega^\mu(\pm) &= \frac{1}{\sqrt{2}}(0, \pm 1, i, 0)\,, \\ \omega^\mu(0) &= \frac{1}{\sqrt{q^2}}(q_z, 0, 0, q_0)\,, \\ \omega^\mu(t) &= \frac{1}{\sqrt{q^2}}(q_0, 0, 0, q_z)\,,\end{aligned} \tag{4.15}$$

which is consistent with the parametrisation $q^\mu = (q_0, 0, 0, q_z)$.

It is worth noting that intermediate results, in particular the HAs, depend on the choice of convention for the polarisation vectors, although the final results at the level of the angular distribution do not. The conventions above are chosen to be consistent with the Jacob-Wick phase conventions [33]. These issues are discussed in more detail in appendix C.1.

The vectors ω can be associated with the Lorentz group $SO(3,1)$. In particular, in the rest frame $q_z = 0$ the timelike polarisation tensor transforms as a scalar under the restriction of $SO(3,1)$ to spatial rotations $SO(3)$. Insertion of the completeness relation (4.14) corresponds to the decomposition, or branching rule,

$$(1/2, 1/2)_{SO(3,1)}\Big|_{SO(3)} \to (\mathbf{1} + \mathbf{3})_{SO(3)}\,, \tag{4.16}$$

where $(1/2, 1/2)$ is the irreducible vector Lorentz representation. The single completeness relation (4.14) can also be written in the form

$$g_{\alpha\beta} = \sum_{J=0}^{1} \sum_{\lambda=-J}^{J} \epsilon_\alpha^{J,\lambda} \bar{\epsilon}_\beta^{J,\lambda}\,, \tag{4.17}$$

with $\epsilon_\alpha^{J,\lambda} = \delta_{J1}\omega_\alpha(\lambda) + \delta_{J0}\omega_\alpha(t)$. Written this way, it is more transparent that the completeness relation can effectively be decomposed into spin-1 and spin-0 contributions.

This can be extended in a natural way to higher-spin operators. Inserting the completeness relation twice corresponds to the tensor product $(1/2, 1/2) \otimes (1/2, 1/2)$, which decomposes as

$$\begin{aligned}&((1/2, 1/2) \otimes (1/2, 1/2))_{SO(3,1)} = ([(1,1)] \oplus [(1,0) \oplus (0,1)] \oplus (0,0))_{SO(3,1)}\Big|_{SO(3)} \to \\ &([1 \cdot \mathbf{5} \oplus 1 \cdot \mathbf{3} \oplus 1 \cdot \mathbf{1}] \oplus [2 \cdot \mathbf{3}] \oplus 1 \cdot \mathbf{1})_{SO(3)} = (1 \cdot \mathbf{5} \oplus 3 \cdot \mathbf{3} \oplus 2 \cdot \mathbf{1})_{SO(3)}\,.\end{aligned} \tag{4.18}$$

More generally, for an effective operator with n Lorentz indices, the completeness relation (4.14) can be inserted n times to obtain a HA with n helicity indices. The direct product of $SO(3,1)$ polarisation tensors decomposes into irreducible representations of $SO(3)$ polarisation tensors $\epsilon^{j,\lambda}_{\mu_1\ldots\mu_n}$ of spin $j = 0,\ldots,n$ and helicity $\lambda = -j,\ldots,j$. This allows the completeness relation to be extended to operators of arbitrarily high Lorentz index and spin decomposition. To illustrate this point, the explicit "double completeness relation" has the decomposition

$$g_{\alpha\beta}g_{\gamma\delta} = \delta_{\alpha\beta\gamma\delta} + \delta^{t}_{\alpha\beta\gamma\delta} + \delta^{tt}_{\alpha\beta\gamma\delta}\,, \tag{4.19}$$

where

$$\delta_{\alpha\beta\gamma\delta} = \sum_{J=0}^{2}\sum_{\lambda=-J}^{J}\omega^{J,\lambda}_{\alpha\gamma}\overline{\omega}^{J,\lambda}_{\beta\delta}\,, \quad \delta^{t}_{\alpha\beta\gamma\delta} = -\sum_{\lambda=-1}^{1}\omega^{t,\lambda}_{\alpha\gamma}\overline{\omega}^{t,\lambda}_{\beta\delta} - \sum_{\lambda=-1}^{1}\omega^{t,\lambda}_{\gamma\alpha}\overline{\omega}^{t,\lambda}_{\delta\beta}\,, \quad \delta^{tt}_{\alpha\beta\gamma\delta} = \omega^{tt}_{\alpha\gamma}\overline{\omega}^{tt}_{\beta\delta}\,, \tag{4.20}$$

represent the contributions to the completeness relation with zero, one, or two timelike polarisation vectors, and

$$\begin{aligned}\omega^{t,\lambda}_{\alpha\gamma} &= \omega_\alpha(t)\omega_\gamma(\lambda)\,, \quad \omega^{tt}_{\alpha\gamma} = \omega_\alpha(t)\omega_\gamma(t)\,,\\ \omega^{J,\lambda}_{\alpha\gamma} &= \sum_{\lambda_1,\lambda_2=-1}^{1} C^{J11}_{\lambda\lambda_1\lambda_2}\omega_\alpha(\lambda_1)\omega_\gamma(\lambda_2)\,,\end{aligned} \tag{4.21}$$

with $\lambda = \lambda_1 + \lambda_2$ in the first term. The minus sign in front of $\delta^{t}_{\alpha\beta\gamma\delta}$ in (4.20) arises from an odd number of timelike polarisation vectors, and this pattern would continue to higher completeness relations. The first, second, and third term in (4.19) correspond respectively to the $(1,1)$-, $[(1,0)\oplus(0,1)]$- and $(0,0)$-terms in (4.18). One may also rewrite (4.19) in a form that makes the decomposition into the different spins j explicit:

$$g_{\alpha\beta}g_{\gamma\delta} = \sum_{J=0}^{2}\sum_{\lambda=-J}^{J}\epsilon^{J,\lambda}_{\alpha\gamma}\cdot\bar{\epsilon}^{J,\lambda}_{\beta\delta}\,, \tag{4.22}$$

where the scalar product "$\cdot$" stands for

$$\epsilon^{\lambda}_{\alpha\gamma}\cdot\bar{\epsilon}^{J,\lambda'}_{\beta\delta} = \delta_{J0}\left[\omega^{0,0}_{\alpha\gamma}\overline{\omega}^{0,0}_{\beta\delta} + \omega^{tt}_{\alpha\gamma}\overline{\omega}^{tt}_{\beta\delta}\right] + \delta_{J1}\left[\omega^{1,\lambda}_{\alpha\gamma}\overline{\omega}^{1,\lambda'}_{\beta\delta} - \omega^{t,\lambda}_{\alpha\gamma}\overline{\omega}^{t,\lambda'}_{\beta\delta} - \omega^{t,\lambda}_{\gamma\alpha}\overline{\omega}^{t,\lambda'}_{\delta\beta}\right] + \delta_{J2}\left[\omega^{2,\lambda}_{\alpha\gamma}\overline{\omega}^{2,\lambda'}_{\beta\delta}\right]\,. \tag{4.23}$$

Using the expressions in equations (4.17) and (4.23), the combined HA $\mathcal{A}^{J_\gamma}_{\lambda,\lambda_1,\lambda_2}$

in (4.11) can be written as[2]

$$\mathcal{A}^{J_\gamma}_{\lambda,\lambda_1,\lambda_2} = \begin{cases} \langle H_a\rangle\langle\mathcal{L}_a\rangle + & \langle H_b^\mu\rangle\langle\mathcal{L}_b^\alpha\rangle\epsilon_\mu^{0,0}\bar{\epsilon}_\alpha^{0,0} & +\langle H_c^{\mu\nu}\rangle\langle\mathcal{L}_c^{\alpha\beta}\rangle\epsilon_{\mu\nu}^{0,0}\cdot\bar{\epsilon}_{\alpha\beta}^{0,0} & J_\gamma = 0 \\ & \langle H_b^\mu\rangle\langle\mathcal{L}_b^\alpha\rangle\epsilon_\mu^{1,\lambda}\bar{\epsilon}_\alpha^{1,\lambda_\ell} & +\langle H_c^{\mu\nu}\rangle\langle\mathcal{L}_c^{\alpha\beta}\rangle\epsilon_{\mu\nu}^{1,\lambda}\cdot\bar{\epsilon}_{\alpha\beta}^{1,\lambda_\ell} & J_\gamma = 1 \\ & & \langle H_c^{\mu\nu}\rangle\langle\mathcal{L}_c^{\alpha\beta}\rangle\epsilon_{\mu\nu}^{2,\lambda}\cdot\bar{\epsilon}_{\alpha\beta}^{2,\lambda_\ell} & J_\gamma = 2 \end{cases} \tag{4.24}$$

where summation over Lorentz indices and the number of operators in (4.13) are both implied, and

$$\langle H_a^{\mu_1\cdots\mu_n}\rangle \equiv \langle\bar{K}_J(\lambda)|H_a^{\mu_1\cdots\mu_n}|\bar{B}\rangle\ , \quad \langle\mathcal{L}_a^{\mu_1\cdots\mu_n}\rangle \equiv \langle\ell_1(\lambda_1)\bar{\ell}_2(\lambda_2)|\mathcal{L}_a^{\mu_1\cdots\mu_n}|0\rangle\ , \tag{4.25}$$

are the leptonic and hadronic matrix elements. The helicities in (4.24) are those of the outgoing particles of the HAs, with λ for $K_J(\lambda)$ in $H^{B\to K_{J_K}}$ and $\lambda_\ell = \lambda_1 - \lambda_2$ for $\ell_1(\lambda_1)\bar{\ell}_2(\lambda_2)$ in $\mathcal{L}^{\gamma_{J_\gamma}\to\ell_1\bar{\ell}_2}$. This is the main idea of the formalism: the angular dependence from the ingoing to outgoing particle is governed by the Wigner D-function, e.g. $\bar{\epsilon}^{J_{\ell,\lambda}} = \bar{D}^{J_\gamma}_{\lambda,\lambda_\ell}(\Omega_\ell)\,\bar{\epsilon}^{J_{\ell,\lambda_\ell}}$ for $\mathcal{L}^{\gamma_{J_\gamma}(\lambda)\to\ell_1(\lambda_1)\bar{\ell}_2(\lambda_2)}$, which is inherent in (4.2). The generalised HA then becomes a sum over all spin components J_γ necessary to saturate the Lorentz indices in the effective Hamiltonian

$$\mathcal{A}(\bar{B}\to\bar{K}_{J_K}(\to K\pi)\ell_1\bar{\ell}_2) = \frac{\sqrt{2J_K+1}}{4\pi}\sum_{J_\gamma=0}^{n}\sum_{\lambda=-\min(J_\gamma,J_K)}^{\min(J_\gamma,J_K)} D^{J_K}_{\lambda,0}(\Omega_K)\,D^{J_\gamma}_{\lambda,\lambda_\ell}(\Omega_\ell)\,\mathcal{A}^{J_\gamma}_{\lambda,\lambda_1,\lambda_2}\ , \tag{4.26}$$

where the overall factor follows from (4.2). A schematic representation of equation (4.26) is given in figure 4.2. The differential decay distribution (4.12) is replaced by a similar expression

$$\frac{d^4\Gamma}{dq^2 d\cos\theta_\ell d\cos\theta_K d\phi} \sim \sum_{\lambda_1\lambda_2}|\mathcal{A}|^2 = \frac{2J_K+1}{4\pi}\sum_{\lambda_1\lambda_2}\sum_{J_\gamma\lambda}\sum_{J'_\gamma\lambda'}\times$$
$$\mathcal{A}^{J_\gamma}_{\lambda,\lambda_1,\lambda_2}\bar{\mathcal{A}}^{J'_\gamma}_{\lambda',\lambda_1,\lambda_2}D^{J_K}_{\lambda,0}(\Omega_K)\,\bar{D}^{J_K}_{\lambda',0}(\Omega_K)\,D^{J_\gamma}_{\lambda,\lambda_\ell}(\Omega_\ell)\,\bar{D}^{J_\gamma}_{\lambda',\lambda_\ell}(\Omega_\ell)\ , \tag{4.27}$$

[2] In the notation used throughout the literature, $H^t = \langle H_b^\mu\rangle\epsilon_\mu^{0,0} = \langle H_b^\mu\rangle\omega_\mu(t)$ is known as the timelike HA [109, 130]. By virtue of the equation of motion, the timelike HAs can be absorbed into the scalar and pseudoscalar HAs, cf. appendix C.3.

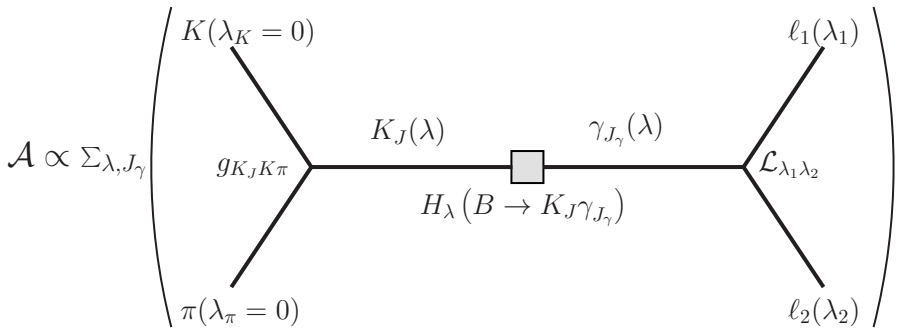

Figure 4.2 *A diagrammatic interpretation of the process described in equation* (4.26)*. The decay to two leptons is treated as being mediated by an effective particle* γ_{J_γ} *of spin* J_γ*. The factor* $g_{K_J K\pi}$ *has no dependence on helicities and depends only on the dynamics of the* K^* *decay.*

with additional coherent sums over the spins J_γ

$$\sum_{\lambda_1\lambda_2} = \sum_{\lambda_1,\lambda_2=-1/2}^{1/2}, \quad \sum_{J_\gamma\lambda} = \sum_{J_\gamma=0}^{2} \sum_{\lambda=-\min(J_\gamma, J_{K_J})}^{\min(J_\gamma, J_{K_J})} \tag{4.28}$$

and likewise for the sum over J'_γ, λ'.

Before moving on to specific applications, one further note is in order. When applying the double completeness relation to generic decay structures, it can be seen from (4.20) that, in general, one expects two distinct contributions to the amplitude from $\delta^t_{\alpha\beta\gamma\delta}$,

$$H_{\mu\nu}L^{\mu\nu} \to -\left(\mathcal{H}_{t\lambda}\mathcal{L}_{t\lambda} + \mathcal{H}_{\lambda t}\mathcal{L}_{\lambda t}\right) + \dots\,, \tag{4.29}$$

where $\mathcal{H}_{t\lambda} = H_{\mu\nu}\overline{\omega}^{\mu\nu}_{t,\lambda}$, and analogous notation for $\mathcal{H}_{\lambda t}$, $\mathcal{L}_{t\lambda}$, and $\mathcal{L}_{\lambda t}$. If, however, the objects $H_{\mu\nu}$ and $L^{\mu\nu}$ are both symmetric or antisymmetric in the Lorentz indices, then $\mathcal{H}_{\lambda t}\mathcal{L}_{\lambda t} = \mathcal{H}_{t\lambda}\mathcal{L}_{t\lambda}$ and the two contributions can therefore be combined. This simplification will be used in defining the generalised HAs for the $\bar{B} \to \bar{K}^*\ell_1\bar{\ell}_2$ (4.31) and $\bar{B} \to \bar{K}\ell_1\bar{\ell}_2$ (4.47) decays respectively, resulting in the extra factor of 2 associated with the terms $H^{T_t}_\lambda \mathcal{L}^{T_t}_{\lambda_1,\lambda_2}$ and $h^{T_t}\mathcal{L}^{T_t}_{\lambda_1,\lambda_2}$ relative to other contributions in the generalised HAs.

4.2 Angular distribution and Wigner D-functions

In this section, the method introduced previously is now applied to decays governed by the $b \to s\ell_1\bar{\ell}_2$ effective Hamiltonian (2.42); firstly, the decay $\bar{B} \to \bar{K}^* \left(\to \bar{K}\pi\right) \ell_1\bar{\ell}_2$, followed in section 4.2.4 by similar results for $\bar{B} \to \bar{K}\ell_1\bar{\ell}_2$. The related decay $\Lambda_b \to \Lambda \left(\to N\pi\right) \ell_1\bar{\ell}_2$, where $N = (p, n)$, can also be treated within this formalism, and will be briefly considered in appendix C.6.

4.2.1 $\bar{B} \to \bar{K}^* \left(\to \bar{K}\pi\right) \ell_1\bar{\ell}_2$

The use of the effective Hamiltonian (2.42) in the LFA restricts the partial waves to $J_\gamma = 0, 1$ terms in equation (4.24). The matrix element for (2.42) is then given by the sum of an S_ℓ- and P_ℓ-wave amplitude (with the subscript ℓ referring to the partial wave in the angle θ_ℓ):

$$\begin{aligned}\hat{\mathcal{M}}_{\lambda_1,\lambda_2} &= \langle \bar{K}^*(\to \bar{K}\pi)\ell_1(\lambda_1)\bar{\ell}_2(\lambda_2)|\hat{H}^{\text{eff}}|\bar{B}\rangle \\ &= \frac{\sqrt{3}}{4\pi}\left[\mathcal{A}^0_{0,\lambda_1,\lambda_2} D^1_{0,0}\left(\Omega_K\right)\delta_{\lambda_1\lambda_2} + \sum_{\lambda=\pm,0} \mathcal{A}^1_{\lambda,\lambda_1,\lambda_2} D^1_{\lambda,0}\left(\Omega_K\right) D^1_{\lambda,\lambda_\ell}\left(\Omega_\ell\right)\right] ,\end{aligned} \tag{4.30}$$

where the hat denotes the effective Hamiltonian without the c_H prefactor defined by (2.42). There is no D-wave, since the two indices in the tensor operator (2.42) are antisymmetric and therefore in a spin-1 representation[3]. The K^* has spin 1 and so is always in a P-wave in the θ_K-angle. In the scalar part of the matrix element, one can use $D^0_{0,\lambda_\ell}\left(\Omega\right) = \delta_{0\lambda_\ell}$, which leads to the presence of $\delta_{\lambda_1\lambda_2}$. The principal objects to be calculated are the amplitudes $\mathcal{A}^{J_\gamma}_{\lambda,\lambda_1,\lambda_2}$. For H^{eff} (2.42) the S_ℓ- and P_ℓ-wave amplitudes ($\mathcal{A}^0$ and $\mathcal{A}^1$ respectively) are written as

$$\begin{aligned}\mathcal{A}^0_{0,\lambda_1,\lambda_2} &= H^S\mathcal{L}^S_{\lambda_1,\lambda_2} + H^P\mathcal{L}^P_{\lambda_1,\lambda_2} , \\ \mathcal{A}^1_{\lambda,\lambda_1,\lambda_2} &= -H^V_\lambda\mathcal{L}^V_{\lambda_1,\lambda_2} - H^A_\lambda\mathcal{L}^A_{\lambda_1,\lambda_2} + H^T_\lambda\mathcal{L}^T_{\lambda_1,\lambda_2} - 2H^{T_t}_\lambda\mathcal{L}^{T_t}_{\lambda_1,\lambda_2} ,\end{aligned} \tag{4.31}$$

with the relative signs and factor of 2 emerging from the double completeness relation (4.19), and the leptonic and the hadronic HAs are

$$\mathcal{L}^X_{\lambda_1\lambda_2} \equiv \langle \ell_1(\lambda_1)\bar{\ell}_2(\lambda_2)|\bar{\ell}\Gamma^X\ell|0\rangle , \quad H^X_\lambda = \langle \bar{K}^*(\lambda)|\bar{s}\overline{\Gamma}^X b|\bar{B}\rangle , \tag{4.32}$$

[3]Consequences of breaking this restriction will be explored in the next chapter.

	$\Gamma^{S[P]}$	$\Gamma^{V[A]}$	$\Gamma^{T[T_t]}$
Γ^X	$\mathbf{1}_4[\gamma_5]$	$\gamma^\mu[\gamma_5]\omega_\mu(\lambda_X)$	$\sigma^{\mu\nu}\omega^{1,\lambda_X}_{\mu\nu}[\omega^{t,\lambda_X}_{\mu\nu}]$
$J_\gamma(X)$	0	1	1

Table 4.1 *The definitions of the Γ^X and their associated spin $J_\gamma(X)$. The contributions $J_\gamma(X) = 0, 1$ give rise to the S_ℓ- and P_ℓ-wave amplitudes respectively. The basic polarisation vector ω_μ is given in* (4.15) *and the composed ones can be found in equation* (4.21)*. The precise value of the helicity index λ_X is specified when the leptonic and hadronic HAs are defined in equations (C.15,C.18,C.29). Note that the additional structure $\Gamma^{T_5} = \sigma_{\mu\nu}\gamma_5$ can be absorbed into the other tensor structures due to the identity $\sigma^{\alpha\beta}\gamma_5 = -\frac{i}{2}\epsilon^{\alpha\beta\mu\nu}\sigma_{\mu\nu}$. Timelike contributions $\gamma^\mu[\gamma_5]\omega_\mu(t)$ can be absorbed into $\Gamma^{S,P}$ respectively, as detailed in appendix C.3.*

which arise from the expressions in (4.25) contracted with the corresponding polarisation vectors. The Lorentz structures Γ^X are defined in table 4.1. Explicit results for the HAs, as well as a more precise prescription concerning Γ^X, are given in appendices C.2 and C.3 in equations (C.15) and (C.18) respectively. Squaring the matrix element in (4.30), summing over external helicities, and averaging over final-state spins, one obtains an angular distribution

$$I_{K^*}\left(q^2, \Omega_K, \Omega_\ell\right) \equiv \frac{32\pi}{3}\frac{d^4\Gamma}{dq^2\, d\cos\theta_\ell\, d\cos\theta_K\, d\phi} = \mathcal{N}\sum_{\lambda_1,\lambda_2}\left|\hat{\mathcal{M}}_{\lambda_1,\lambda_2}\right|^2 , \tag{4.33}$$

where I_{K^*} is a shorthand, and $32\pi/3$ is a convenient normalisation factor. The factor $\mathcal{N}$,

$$\mathcal{N} \equiv |c_H|^2\kappa_{\text{kin}} , \quad \kappa_{\text{kin}} \equiv \frac{\sqrt{\lambda_B}\sqrt{\lambda_{\gamma^*}}}{2^9\pi^3 m_B^3 q^2} , \tag{4.34}$$

is the product of the prefactor resulting from the effective Hamiltonian c_H (2.42) and the kinematic phase space factor. The matrix element is defined in (4.30). Above, $\lambda_B \equiv \lambda(m_B^2, m_{K^*}^2, q^2)$ and $\lambda_{\gamma^*} \equiv \lambda(q^2, m_{\ell_1}^2, m_{\ell_2}^2)$ where $\lambda(a, b, c)$ is the Källén-function defined in (C.2).

4.2.2 Angular distribution

The squared matrix element initially contains a plethora of different products of four Wigner functions. However, these correspond to pairs of direct products

that can be reduced to single Wigner functions by the Clebsch-Gordan series

$$D^{j}_{m,n}\left(\Omega\right) D^{l}_{p,q}\left(\Omega\right) = \sum_{J=|j-l|}^{j+l} \sum_{M=-J}^{J} \sum_{N=-J}^{J} C^{Jjl}_{Mmp} C^{Jjl}_{Nnq} D^{J}_{M,N}\left(\Omega\right) \ . \tag{4.35}$$

Applied separately over the angles $\Omega_K = (0, \theta_K, 0)$ and $\Omega_\ell = (\phi, \theta_\ell, -\phi)$, along with the identity $\bar{D}^{l}_{m,m'}\left(\Omega\right) = (-1)^{m'-m} D^{l}_{-m,-m'}\left(\Omega\right)$, this allows the angular distribution to be written in the compact form

$$\begin{aligned} I^{(0)}_{K^*}\left(q^2, \Omega_K, \Omega_\ell\right) = \mathrm{Re}\Big[& G^{0,0}_0(q^2)\Omega^{0,0}_0 + G^{0,1}_0(q^2)\Omega^{0,1}_0 + G^{0,2}_0(q^2)\Omega^{0,2}_0 + \\ & G^{2,0}_0(q^2)\Omega^{2,0}_0 + G^{2,1}_0(q^2)\Omega^{2,1}_0 + G^{2,1}_1(q^2)\Omega^{2,1}_1 + \\ & G^{2,2}_0(q^2)\Omega^{2,2}_0 + G^{2,2}_1(q^2)\Omega^{2,2}_1 + G^{2,2}_2(q^2)\Omega^{2,2}_2 \quad \Big] \ , \end{aligned} \tag{4.36}$$

where the superscript (0) serves as a reminder that only S_ℓ- and P_ℓ-wave contributions have been used to describe the amplitude (4.30). The angular functions Ω are given in terms of Wigner D functions

$$\Omega^{l_K,l_\ell}_m \equiv \Omega^{l_K,l_\ell}_m\left(\Omega_K, \Omega_\ell\right) \equiv D^{l_K}_{m,0}\left(\Omega_K\right) D^{l_\ell}_{m,0}\left(\Omega_\ell\right) = D^{l_K}_{m,0}\left(\Omega'_K\right) D^{l_\ell}_{m,0}\left(\Omega'_\ell\right) \ . \tag{4.37}$$

The variables $\Omega'_K = (\phi, \theta_K, -\phi)$ and $\Omega'_\ell = (0, \theta_\ell, 0)$ form an angular reparametrisation that will prove convenient in the discussion of partial moments. The label l_K corresponds to the $(K\pi)$-system, l_ℓ to the dilepton system, and the common index m is the azimuthal component ϕ of either partial wave. The observables G^{l_K,l_ℓ}_m are functions of q^2, and the relation to the standard observables in the literature is given in section 4.2.3. The explicit Wigner D-functions used above are given by

$$\begin{aligned} & D^{0}_{0,0}\left(\Omega\right) = 1 \ , \qquad D^{2}_{0,0}\left(\Omega\right) = \frac{1}{2}\left(3\cos^2\theta - 1\right) \ , \quad D^{2}_{2,0}\left(\Omega\right) = \sqrt{\frac{3}{8}} e^{-2i\phi} \sin^2\theta \ , \\ & D^{1}_{0,0}\left(\Omega\right) = \cos\theta \ , \quad D^{1}_{1,0}\left(\Omega\right) = -\frac{1}{\sqrt{2}} e^{-i\phi} \sin\theta \ , \qquad D^{2}_{1,0}\left(\Omega\right) = -\sqrt{\frac{3}{8}} e^{-i\phi} \sin 2\theta \ , \end{aligned} \tag{4.38}$$

and can be related to spherical harmonics $Y_{lm}\left(\theta, \phi\right)$ or associated Legendre polynomials $P_{lm}(x)$ as

$$D^{l}_{m,0}\left(\phi, \theta, -\phi\right) = \sqrt{\frac{4\pi}{2l+1}} \overline{Y}_{lm}\left(\theta, \phi\right) = \sqrt{\frac{(l-m)!}{(l+m)!}} P_{lm}(\cos\theta) e^{-im\phi} \ . \tag{4.39}$$

The angular distribution above clearly has a great deal of structure. In particular, it is helpful to comment on four features of the angular distribution (4.36), all of which are encoded by the double Clebsch-Gordan series (4.35), but which can also be seen to emerge from the underlying physics:

- The second helicity index of all Wigner D-functions in the angular distribution is zero. This index is the difference of the helicities of the final-state particles, which is zero since these helicities are summed incoherently: $(\lambda_1 - \lambda_2) - (\lambda_1 - \lambda_2) = 0$.
- The first helicity index m is identical in all pairs of Wigner D-functions appearing in the angular distribution. This index contains the helicities of the internal particles, summed coherently. One can also see this as a property of the freedom of defining the reference plane for the angle ϕ.
- The range of the indices l_K and l_ℓ is fixed between the range $0, \ldots, 2\,\max[J_{K,\ell}]$. Including only $J_\gamma \leq 1$ contributions emerging from the dimension-six effective Hamiltonian (2.42) hence imposes $0 \leq l_\ell \leq 2$, and likewise $J_K = 1$ imposes $0 \leq l_K \leq 2$.
- The absence of angular structures with $l_K = 1$ is specific to this decay, due to the final state consisting of pseudoscalar mesons.

The first three features are universal to such decay chains, and apply even if some of the particles involved are fermions, such as in the decay $\Lambda_b \to \Lambda\,(\to (p, n)\pi)\,\ell_1\bar{\ell}_2$ (see appendix C.6).

Explicit results for the $G_m^{l_K,l_\ell}$ are presented in section C.4.1 for the case of identical final-state leptons $m_{\ell_1} = m_{\ell_2}$, and section C.4.2 for the more general case $m_{\ell_1} \neq m_{\ell_2}$.

4.2.3 Relation of the $G_m^{l_K,l_\ell}$ to standard literature observables

The angular distribution for $\bar{B} \to \bar{K}^*(\to \bar{K}\pi)\ell_1\bar{\ell}_2$ is usually (e.g. [113]) presented in the form

$$\frac{8\pi}{3}\frac{d^4\Gamma}{dq^2\; d\cos\theta_\ell\; d\cos\theta_K\; d\phi} = \frac{I_{K^*}^{(0)}}{4} = (g_{1s} + g_{2s}\cos 2\theta_\ell + g_{6s}\cos\theta_\ell)\sin^2\theta_K + (g_{1c} + g_{2c}\cos 2\theta_\ell + g_{6c}\cos\theta_\ell)\cos^2\theta_K +$$

$$
\begin{aligned}
&(g_3\cos 2\phi + g_9 \sin 2\phi)\sin^2\theta_K \sin^2\theta_\ell + \\
&(g_4\cos\phi + g_8\sin\phi)\sin 2\theta_K \sin 2\theta_\ell + \\
&(g_5\cos\phi + g_7\sin\phi)\sin 2\theta_K \sin\theta_\ell \ , \qquad (4.40)
\end{aligned}
$$

which can be condensed as

$$
\begin{aligned}
\frac{8\pi}{3}\frac{d^4\Gamma}{dq^2 d\cos\theta_\ell\, d\cos\theta_K\, d\phi} = \mathrm{Re}\,[\ &(g_{1s} + g_{2s}\cos 2\theta_\ell + g_{6s}\cos\theta_\ell)\sin^2\theta_K + \\
&(g_{1c} + g_{2c}\cos 2\theta_\ell + g_{6c}\cos\theta_\ell)\cos^2\theta_K + \\
&e^{-2i\phi}\mathcal{G}_3 \sin^2\theta_K \sin^2\theta_\ell + \\
&e^{-i\phi}\sin 2\theta_K\,(\mathcal{G}_4 \sin 2\theta_\ell + \mathcal{G}_5 \sin\theta_\ell)\ ] \ , \qquad (4.41)
\end{aligned}
$$

where

$$
\mathcal{G}_{3,4,5} = (g_{3,4,5} + i g_{9,8,7}) \ . \qquad (4.42)
$$

In fact, when the angular distribution is written in this basis, the angular observables are usually written J_i rather than g_i. The choice of notation g_i rather than J_i is used in order to minimise potential confusion due to the angular conventions discussed in section 4.4. This gives the same angular distribution as derived in (4.36), but in a different basis. The relationship between the $g_i(q^2)$ and the $G_m^{l_K,l_\ell}(q^2)$ is

$$
\begin{aligned}
&G_0^{0,0} = \frac{4}{9}\left(3\left(g_{1c}+2g_{1s}\right) - \left(g_{2c}+2g_{2s}\right)\right) \ , \quad G_0^{0,1} = \frac{4}{3}\left(g_{6c}+2g_{6s}\right) \ , \quad G_0^{0,2} = \frac{16}{9}\left(g_{2c}+2g_{2s}\right) \ , \\
&G_0^{2,0} = \frac{4}{9}\left(6\left(g_{1c}-g_{1s}\right) - 2\left(g_{2c}-g_{2s}\right)\right) \ , \quad G_0^{2,1} = \frac{8}{3}\left(g_{6c}-g_{6s}\right) \ , \quad G_0^{2,2} = \frac{32}{9}\left(g_{2c}-g_{2s}\right) \ , \\
&G_1^{2,1} = \frac{16}{\sqrt{3}}\underbrace{\left(g_5 + i g_7\right)}_{=\mathcal{G}_5} \ , \qquad G_1^{2,2} = \frac{32}{3}\underbrace{\left(g_4 + i g_8\right)}_{=\mathcal{G}_4} \ , \quad G_2^{2,2} = \frac{32}{3}\underbrace{\left(g_3 + i g_9\right)}_{=\mathcal{G}_3} \ . \qquad (4.43)
\end{aligned}
$$

Either the $G_m^{l_K,l_\ell}(q^2)$ or the $g_i(q^2)$ form the full basis of twelve observables for this decay, which have been rewritten in several ways in the literature. A frequently-used form is the set of observables given in [121], constructed to be insensitive to uncertainties in form factors. In the notation of LHCb [20], the observables are given in terms of $G_m^{l_K,l_\ell}$ by[4]

$$
\langle P_1\rangle_{\rm bin}\Big|_{\rm LHCb} = \frac{\left\langle \mathrm{Re}\left[G_2^{2,2}\right]\right\rangle_{\rm bin}}{\mathcal{N}_{\rm bin}} \ , \quad \langle P_2\rangle_{\rm bin}\Big|_{\rm LHCb} = \frac{\left\langle 2G_0^{0,1} - G_0^{2,1}\right\rangle_{\rm bin}}{3\mathcal{N}_{\rm bin}} \ ,
$$

[4]The extension of these relations to CP-odd and CP-even combinations, in the spirit of [78], is straightforward (see section 4 of [121]).

$$
\begin{aligned}
\langle P_3\rangle_{\text{bin}}\Big|_{\text{LHCb}} &= \frac{\left\langle \text{Im}\left[G_2^{2,2}\right]\right\rangle_{\text{bin}}}{2\mathcal{N}_{\text{bin}}}\,, \\
\langle P_4'\rangle_{\text{bin}}\Big|_{\text{LHCb}} &= \frac{\left\langle \text{Re}\left[G_1^{2,2}\right]\right\rangle_{\text{bin}}}{4\mathcal{N}'_{\text{bin}}}\,, \quad \langle P_8'\rangle_{\text{bin}}\Big|_{\text{LHCb}} = \frac{\left\langle \text{Im}\left[G_1^{2,2}\right]\right\rangle_{\text{bin}}}{4\mathcal{N}'_{\text{bin}}}\,, \\
\langle P_5'\rangle_{\text{bin}}\Big|_{\text{LHCb}} &= \frac{\left\langle \text{Re}\left[G_1^{2,1}\right]\right\rangle_{\text{bin}}}{2\sqrt{3}\mathcal{N}'_{\text{bin}}}\,, \quad \langle P_6'\rangle_{\text{bin}}\Big|_{\text{LHCb}} = \frac{\left\langle \text{Im}\left[G_1^{2,1}\right]\right\rangle_{\text{bin}}}{2\sqrt{3}\mathcal{N}'_{\text{bin}}}\,,
\end{aligned}
\tag{4.44}
$$

where

$$
\left\langle f(q^2)\right\rangle_{\text{bin}} = \int_{\text{bin}} dq^2 f(q^2)
$$

is the integral over q^2 bins of the observable of interest, and[5]

$$
\mathcal{N}_{\text{bin}} = 4\left\langle G_0^{0,2} - \frac{1}{2}G_0^{2,2}\right\rangle_{\text{bin}}\,, \quad \mathcal{N}'_{\text{bin}} = \sqrt{-\left\langle G_0^{0,2} - \frac{1}{2}G_0^{2,2}\right\rangle_{\text{bin}}\left\langle G_0^{0,2} + G_0^{2,2}\right\rangle_{\text{bin}}}\,. \tag{4.45}
$$

Three other combinations of the $G_m^{l_K,l_\ell}$ can be related to the branching fraction $\frac{d\Gamma}{dq^2}$, the forward-backward asymmetry A_{FB}, and the longitudinal polarisation fraction F_L [113]:

$$
\begin{aligned}
\left\langle \frac{d\Gamma}{dq^2}\right\rangle_{\text{bin}} &= \frac{3}{4}\left\langle G_0^{0,0}\right\rangle_{\text{bin}}\,, & \langle A_{\text{FB}}\rangle_{\text{bin}}\Big|_{\text{LHCb}} &= \frac{1}{2}\frac{\left\langle G_0^{0,1}\right\rangle_{\text{bin}}}{\left\langle G_0^{0,0}\right\rangle_{\text{bin}}}\,, \\
\langle F_L\rangle_{\text{bin}} &= \frac{\left\langle G_0^{0,0}\right\rangle_{\text{bin}} + \left\langle G_0^{2,0}\right\rangle_{\text{bin}}}{3\left\langle G_0^{0,0}\right\rangle_{\text{bin}}}\,.
\end{aligned}
\tag{4.46}
$$

The observables in equations (4.44,4.45,4.46) correspond to the twelve g_i. The definitions of the P_i' above correspond to those used by LHCb [20]; their relationship to the observables defined in [121] is presented in section 4.4.

4.2.4 $\bar{B} \to \bar{K}\ell_1\bar{\ell}_2$

The decay channel $\bar{B} \to \bar{K}\ell_1\bar{\ell}_2$ can be similarly described using the formalism presented above, and the general procedure very closely follows that of $\bar{B} \to \bar{K}^*\ell_1\bar{\ell}_2$. Analogously to equation (4.31), the S_ℓ- and P_ℓ-wave amplitudes are

$$
\begin{aligned}
\mathcal{A}^0_{0,\lambda_1,\lambda_2} &= h^S\mathcal{L}^S_{\lambda_1,\lambda_2} + h^P\mathcal{L}^P_{\lambda_1,\lambda_2}\,, \\
\mathcal{A}^1_{0,\lambda_1,\lambda_2} &= -h^V\mathcal{L}^V_{\lambda_1,\lambda_2} - h^A\mathcal{L}^A_{\lambda_1,\lambda_2} + h^T\mathcal{L}^T_{\lambda_1,\lambda_2} - 2h^{T_t}\mathcal{L}^{T_t}_{\lambda_1,\lambda_2}\,,
\end{aligned}
\tag{4.47}
$$

[5] In terms of the $g_i(q^2)$ basis, $\mathcal{N}_{\text{bin}} = \frac{64}{3}\left\langle g_{2s}\right\rangle_{\text{bin}}$ and $\mathcal{N}'_{\text{bin}} = \frac{16}{3}\sqrt{-\left\langle g_{2c}\right\rangle_{\text{bin}}\left\langle g_{2s}\right\rangle_{\text{bin}}}$.

where the $\mathcal{L}^X_{\lambda_1,\lambda_2}$ are the same as in the $\bar{B} \to \bar{K}^* \ell_1 \bar{\ell}_2$ decay, and the hadronic HAs are taken over the same set of operators, but defined instead for $\bar{B} \to \bar{K}$ transitions. All signs and factors emerge once more from the double completeness relation (4.19).

The reduced matrix element is then the sum of the S_ℓ- and P_ℓ-wave amplitudes

$$\hat{\mathcal{M}}_{\lambda_1,\lambda_2} = \frac{1}{\sqrt{4\pi}} \left(\mathcal{A}^0_{0,\lambda_1,\lambda_2} \delta_{\lambda_1\lambda_2} + \mathcal{A}^1_{0,\lambda_1,\lambda_2} D^1_{0,\lambda_\ell}(\Omega_\ell) \right) , \tag{4.48}$$

where $\Omega_\ell = (0, \theta_\ell, 0)$ in this case. The angular distribution (with $0 \le \theta_\ell \le \pi$) is given by squaring the matrix element

$$I_K(q^2, \theta_\ell) \equiv \frac{d^2\Gamma}{dq^2 \, d\cos\theta_\ell} = \mathcal{N} \sum_{\lambda_1,\lambda_2} \left| \hat{\mathcal{M}}_{\lambda_1,\lambda_2} \right|^2 . \tag{4.49}$$

Using (4.48) one obtains

$$\begin{aligned} I_K^{(0)} &= G^{(0)}(q^2) + G^{(1)}(q^2) D^1_{0,0}(\Omega_\ell) + G^{(2)}(q^2) D^2_{0,0}(\Omega_\ell) \\ &= G^{(0)}(q^2) + G^{(1)}(q^2) P_1(\cos\theta_\ell) + G^{(2)}(q^2) P_2(\cos\theta_\ell) \\ &= G^{(0)}(q^2) + G^{(1)}(q^2) \cos\theta_\ell + G^{(2)}(q^2) \frac{1}{2} \left(3\cos^2\theta_\ell - 1 \right) , \end{aligned} \tag{4.50}$$

where $P_l(\cos\theta_\ell) = D^l_{0,0}(\Omega_\ell)$ and $D^0_{0,0}(\Omega_\ell) = 1$. For convenience, these results are also given in terms of the explicit angle θ_ℓ using equation (4.38). The superscript (0) is again a reminder that the restriction to $l_\ell \le 2$ is a consequence of only including S_ℓ- and P_ℓ-waves in (4.48). The explicit functions $G^{(0,1,2)}(q^2)$ are given in appendix C.5 in terms of HAs.[6]

In [133] the angular distribution was given in the alternative form

$$\frac{1}{\Gamma} \frac{d\Gamma}{d\cos\theta_\ell} = \frac{3}{4} (1 - F_H)(1 - \cos^2\theta_\ell) + \frac{1}{2} F_H + A_{\rm FB} \cos\theta_\ell , \tag{4.51}$$

and the relation to the parametrisation (4.50) is given by

$$\Gamma = 2\langle G^{(0)} \rangle , \quad A_{\rm FB} = \sigma \frac{\langle G^{(1)} \rangle}{2\langle G^{(0)} \rangle} , \quad F_H = \frac{\langle G^{(0)} \rangle + \langle G^{(2)} \rangle}{\langle G^{(0)} \rangle} , \tag{4.52}$$

where $\langle X \rangle = \int dq^2 X$ denotes the integration or appropriate binning over q^2, and

[6] The observables $G^{(l_\ell)}$ and the angular coefficients used in [132] are related by $a(q^2) = G^{(0)} - \frac{1}{2} G^{(2)}$, $b(q^2) = G^{(1)}$ and $c(q^2) = \frac{3}{2} G^{(2)}$ where $I_K^{(0)} = a + b\cos\theta_\ell + c\cos^2\theta_\ell$.

$\sigma = \pm 1$ depending on angular conventions.[7]

4.3 Method of total and partial moments

The Method of Moments (MoM) is a powerful tool to extract the angular observables $G_m^{l_K,l_\ell}$ by the use of orthogonality relations. In B physics, for example, the method has been applied to $B \to J/\Psi(\to \bar{\ell}\ell)K^*(\to K\pi)$ type decays [134] during the first B-factory era.

In previous experiments, the angular information on $B \to K^*\ell\ell$ has been extracted through the likelihood fit method at the level of $I_{K^*}^{(0)}$ [22], and it has also been suggested that a likelihood fit analysis can be applied at the amplitude level [135]. A possible advantage of the MoM over the likelihood fit is that it is less sensitive to theoretical assumptions. More precisely, one can test each angular term independent of the rest of the distribution. The fourfold angular distribution can be expanded over the complete set of functions $\Omega_m^{l_K,l_\ell}$ (4.37)

$$I_{K^*}\left(q^2, \Omega_K, \Omega_\ell\right) = \sum_{l_K,l_\ell \geq 0} \sum_{m=0}^{\min(l_K,l_\ell)} \mathrm{Re}\left[G_m^{l_K,l_\ell}\Omega_m^{l_K,l_\ell}(\theta_K, \theta_\ell, \phi)\right] \ , \tag{4.53}$$

of which the distribution $I_{K^*}^{(0)}$ (4.36) is a subset. Note that the sum over m does not need to be continued for negative values since I_{K^*} is real-valued. By using the orthogonality properties of the Wigner D-functions (e.g. [136]) with $\Omega = (\alpha, \beta, \gamma)$

$$\int_{-1}^{1} d\cos\beta \int_0^{2\pi} \mathrm{d}\alpha \int_0^{2\pi} \mathrm{d}\gamma \ D_{m,n}^{j}\left(\Omega\right) \bar{D}_{p,q}^{l}\left(\Omega\right) = \frac{8\pi^2}{2j+1}\delta_{jl}\delta_{mp}\delta_{nq} \ , \tag{4.54}$$

the MoM allows the extraction of the observables $G_m^{l_K,l_\ell}$ from the angular distribution. In particular, one can test for the absence of all higher moments, and therefore test very specifically the assumptions made when deriving the distribution $I_{K^*}^{(0)}$ (4.36). The results of this projection onto *total* moments are given in section 4.3.1. Integrating over a subset of angles, referred to as partial moments, is discussed in section 4.3.2. In the latter case orthogonality does not hold in the generic case and different $G_m^{l_K,l_\ell}$ enter the same moment.

[7] Defining $\sigma_{\mathrm{GHZ}} = 1$ in [34], the translation to the LHCb conventions [133] are $\sigma_{\mathrm{GHZ}} = \sigma(B^{\pm})$ and $\sigma_{\mathrm{GHZ}} = -\sigma(B^0, \bar{B}^0)$. The charged and neutral decays are different because the neutral mode, being observed in K_S, is not self-tagging. Comparing with[132], one has $\sigma_{\mathrm{GHZ}} = -\sigma_{\mathrm{BHP}}$ for both charged and neutral modes.

$M_m^{l_K,l_\ell}$	$G_0^{0,0}$	$\frac{1}{3}G_0^{0,1}$	$\frac{1}{5}G_0^{0,2}$	$\frac{1}{5}G_0^{2,0}$	$\frac{1}{15}G_0^{2,1}$	$\frac{1}{25}G_0^{2,2}$	$\frac{1}{30}G_1^{2,1}$	$\frac{1}{50}G_1^{2,2}$	$\frac{1}{50}G_2^{2,2}$

Table 4.2 *Moments $M_m^{l_K,l_\ell}$ in terms of $G_m^{l_K,l_\ell}$, as defined by equation (4.56); the proportionality factors $c_m^{l_K,l_\ell}$ come from inserting the specific values of l_K, l_ℓ and m into (4.57).*

Elements of the MoM have also previously been applied to $\Lambda_b \to \Lambda\,(\to (p,n)\pi)\,\bar{\ell}_1\ell_2$ [137], and more systematically to the other channels discussed in this paper, crucially including a study of how to account for detector-resolution acceptance effects, in [138]. LHCb has now also applied the method to the $B \to K^*\ell^+\ell^-$ channels. [22, 139] However, studies such as those in [138] proceeded essentially "backwards", deriving the angular distribution (4.53) through more conventional techniques, then expanding that result in the basis of associated Legendre polynomials. This can be compared to the derivation above, where this basis was used from the start at the level of the HAs, and provides additional insight on the origin of the structure in the decay distribution (4.36), as well as what type of physics might go beyond it. This aspect will be explored further in the following chapter.

4.3.1 Method of total moments

Defining the scalar product

$$\langle f(\Omega)|g(\Omega)\rangle_{\theta_K\theta_\ell\phi} \equiv \quad \frac{1}{8\pi}\int_{-1}^{1} d\cos\theta_K \int_{-1}^{1} d\cos\theta_\ell \int_0^{2\pi} d\phi \bar{f}(\Omega)g(\Omega)\ , \quad (4.55)$$

normalised such that $\langle 1|1\rangle = 1$, it is possible to extract all observables $G_m^{l_K,l_\ell}$ separately from each other, by taking moments[8]

$$M_m^{l_K,l_\ell} \equiv \langle \Omega_m^{l_K,l_\ell}|I_{K^*}(q^2,\Omega_K,\Omega_\ell)\rangle_{\theta_K\theta_\ell\phi} = c_m^{l_K,l_\ell} G_m^{l_K,l_\ell}\ , \quad (4.56)$$

where

$$c_m^{l_K,l_\ell} = \frac{1+\delta_{m0}}{2(2l_K+1)(2l_\ell+1)}\ . \quad (4.57)$$

Using the equation above the terms in (4.36) are given in table 4.2. Furthermore,

[8]The moments $M_m^{l_K,l_\ell}$ are related to the quantities $S_{l_\ell,l_K,m}$ introduced in [138] by $8\pi G_0^{0,0} S_{l_\ell,l_K,m} = G_m^{l_K,l_\ell} = M_m^{l_K,l_\ell}/c_m^{l_K,l_\ell}$.

the orthogonality condition also implies that

$$\begin{aligned} M_m^{j,j'} &= 0 \ , \quad \forall m \text{ and } j \geq 3 \text{ or } j' \geq 3 \ , \\ M_m^{1,j'} &= 0 \ , \quad \forall j', m \ . \end{aligned} \tag{4.58}$$

Hence the higher and $l_K = 1$ moments vanish, providing a very specific test of the theoretical assumptions behind $I_{K^*}^{(0)}$.

4.3.2 Partial moments

The results given previously show how to extract the individual $G_m^{l_K,l_\ell}$. One can also consider partial moments, whereby one integrates only over a subset of angles. The distributions might be regarded as generalisations of uni- and double-angular distributions, as these in turn can be viewed as partial moments with respect to unity. The method is effectively a hybrid between the likelihood fit and the total MoM. This presents a useful compromise between the two methods of analysis of experimental studies into this decay. Such a compromise is advantageous because, whereas the MoM is well-suited to studies with a small number of events, can allow access to a wider range of observables, and is more flexible in terms of the underlying physical assumptions, it does tend to come at the expense of larger uncertainties compared with a likelihood fit. A more complete comparison of the two methods is presented in [138].

To this end, defining the further scalar products

$$\begin{aligned} \langle f(\Omega)|g(\Omega)\rangle_{\theta\phi} &\equiv \frac{1}{4\pi}\int_{-1}^{1} d\cos\theta \int_0^{2\pi} d\phi \bar{f}(\Omega)g(\Omega) \ , \\ \langle f(\Omega)|g(\Omega)\rangle_{\theta_K\theta_\ell} &\equiv \frac{1}{4}\int_{-1}^{1} d\cos\theta_K \int_{-1}^{1} d\cos\theta_\ell \bar{f}(\Omega)g(\Omega) \ , \end{aligned} \tag{4.59}$$

which are again normalised such that $\langle 1|1\rangle = 1$, the orthogonality relation (4.54) can then be rewritten as

$$\langle D_{p,0}^{l}\left(\Omega_\ell\right)|D_{m,0}^{j}\left(\Omega_\ell\right)\rangle_{\theta_\ell\phi} = \frac{1}{2l+1}\delta_{jl}\delta_{mp} \ . \tag{4.60}$$

4.3.3 Integrating over θ_ℓ, ϕ: $k_m^{l_\ell}(\theta_K)$-moments

The partial moment over θ_ℓ and ϕ is defined by

$$k_m^{l_\ell}(\theta_K) \equiv \langle D_{m,0}^{l_\ell}(\Omega_\ell)\, | I_{K^*}(q^2, \Omega_K, \Omega_\ell)\rangle_{\theta_\ell\phi} = \frac{1+\delta_{m0}}{2\,(2l_\ell+1)} \sum_{l_K \geq 0} D_{m,0}^{l_K}(\Omega_K)\, G_m^{l_K, l_\ell}\ . \tag{4.61}$$

Assuming the distribution (4.36) ($l_K = 0, 2$), there are six non-vanishing moments:

$$\begin{aligned}
k_0^0(\theta_K) &= G_0^{0,0} + G_0^{2,0} D_{0,0}^2(\Omega_K) &&= G_0^{0,0} + \frac{1}{2}\left(3\cos^2\theta_K - 1\right) G_0^{2,0}\ , \\
k_0^1(\theta_K) &= \frac{1}{3}\left(G_0^{0,1} + G_0^{2,1} D_{0,0}^2(\Omega_K)\right) &&= \frac{1}{3}\left(G_0^{0,1} + \frac{1}{2}\left(3\cos^2\theta_K - 1\right) G_0^{2,1}\right)\ , \\
k_0^2(\theta_K) &= \frac{1}{5}\left(G_0^{0,2} + G_0^{2,2} D_{0,0}^2(\Omega_K)\right) &&= \frac{1}{5}\left(G_0^{0,2} + \frac{1}{2}\left(3\cos^2\theta_K - 1\right) G_0^{2,2}\right)\ , \\
k_1^1(\theta_K) &= \frac{1}{6} G_1^{2,1} D_{1,0}^2(\Omega_K) &&= \frac{-1}{6}\sqrt{\frac{3}{8}}\sin 2\theta_K\ G_1^{2,1}\ , \\
k_1^2(\theta_K) &= \frac{1}{10} G_1^{2,2} D_{1,0}^2(\Omega_K) &&= \frac{-1}{10}\sqrt{\frac{3}{8}}\sin 2\theta_K\ G_1^{2,2}\ , \\
k_2^2(\theta_K) &= \frac{1}{10} G_2^{2,2} D_{2,0}^2(\Omega_K) &&= \frac{1}{10}\sqrt{\frac{3}{8}}\sin^2\theta_K\ G_2^{2,2}\ ,
\end{aligned} \tag{4.62}$$

where the explicit angular representation has also been provided for clarity. As was the case in the MoM, with respect to the distribution $I_{K^*}^{(0)}$ higher partial moments vanish:

$$k_m^{l_\ell}(\theta_K) = 0 \quad \forall l_\ell \geq 3, \forall m\ . \tag{4.63}$$

4.3.4 Integrating over θ_K, ϕ: $l_m^{l_\ell}(\theta_\ell)$-moments

The partial moment over θ_K and ϕ is defined in complete analogy with the previous partial moment (4.61) by

$$l_m^{l_K}(\theta_\ell) \equiv \langle D_{m,0}^{l_K}(\Omega'_K)\, | I_{K^*}(q^2, \Omega'_K, \Omega'_\ell)\rangle_{\theta_K\phi} = \frac{1+\delta_{m0}}{2\,(2l_K+1)} \sum_{l_\ell \geq 0} D_{m,0}^{l_\ell}(\Omega_K)\, G_m^{l_K, l_\ell}\ , \tag{4.64}$$

which makes use of the reparametrisation of angles given in (4.37). Again, assuming the distribution (4.36) ($l_\ell = 0, 1, 2$), there are four non-vanishing

moments:

$$
\begin{aligned}
l_0^0(\theta_\ell) &= G_0^{0,0} + G_0^{0,1} D_{0,0}^1(\Omega'_\ell) + G_0^{0,2} D_{0,0}^2(\Omega'_\ell) \\
&= G_0^{0,0} + \cos\theta_\ell G_0^{0,1} + \frac{1}{2}\left(3\cos^2\theta_\ell - 1\right) G_0^{0,2} \,, \\
l_0^2(\theta_\ell) &= \frac{1}{5}\left(G_0^{2,0} + G_0^{2,1} D_{0,0}^1(\Omega'_\ell) + G_0^{2,2} D_{0,0}^2(\Omega'_\ell)\right) \\
&= \frac{1}{5}\left(G_0^{2,0} + \cos\theta_\ell G_0^{2,1} + \frac{1}{2}\left(3\cos^2\theta_\ell - 1\right) G_0^{2,2}\right) \,, \\
l_1^2(\theta_\ell) &= \frac{1}{10}\left(G_1^{2,1} D_{1,0}^1(\Omega'_\ell) + G_1^{2,2} D_{1,0}^2(\Omega'_\ell)\right) \\
&= \frac{-1}{10\sqrt{2}}\left(\sin\theta_\ell G_1^{2,1} + \sqrt{\frac{3}{4}}\sin 2\theta_\ell G_1^{2,2}\right) \,, \\
l_2^2(\theta_\ell) &= \frac{1}{10} G_2^{2,2} D_{2,0}^2(\Omega'_\ell) = \frac{1}{10}\sqrt{\frac{3}{8}}\sin^2\theta_\ell G_2^{2,2} \,.
\end{aligned} \tag{4.65}
$$

With respect to the distribution $I_{K^*}^{(0)}$, higher partial moments vanish:

$$
l_m^{l_\ell}(\theta_\ell) = 0 \,, \quad \forall l_K \geq 3,\ \forall m \quad \text{and} \quad l_K = 1,\ \forall m \,. \tag{4.66}
$$

4.3.5 Integrating over θ_K, θ_ℓ: $p_{m,m'}^{l_K,l_\ell}(\phi)$-moments

Finally, one can project on to moments of the form $D_{m,0}^{l}(\Omega_K)\, D_{m',0}^{l'}(\Omega'_\ell)$ with respect to θ_K, θ_ℓ. In this case, the full orthogonality relation (4.54) no longer holds, but, due to (4.35), there exist selection rules as to which of the $G_m^{l_K,l_\ell}$ can contribute to the partial moments

$$
p_{m,m'}^{l_K,l_\ell}(\phi) \equiv \langle D_{m,0}^{l_K}(0,\theta_K,0)\, D_{m',0}^{l_\ell}(0,\theta_\ell,0)\, | I_{K^*}(q^2,\Omega_K,\Omega_\ell)\rangle_{\theta_K\theta_\ell} \,. \tag{4.67}
$$

Assuming $I_{K^*}^{(0)}$, a few non-vanishing moments are

$$
\begin{aligned}
p_{0,0}^{0,0}(\phi) &= \frac{1}{6}\left(6G_0^{0,0} + \mathrm{Re}[e^{-2i\phi}G_2^{2,2}]\right) \,, & p_{0,0}^{0,1}(\phi) &= \frac{1}{3}G_0^{0,1} \,, \\
p_{0,0}^{0,2}(\phi) &= \frac{1}{30}\left(6G_0^{0,2} - \mathrm{Re}[e^{-2i\phi}G_2^{2,2}]\right) \,, & p_{0,0}^{2,0}(\phi) &= \frac{1}{30}\left(6G_0^{2,0} - \mathrm{Re}[e^{-2i\phi}G_2^{2,2}]\right) \,, \\
p_{0,0}^{2,1}(\phi) &= \frac{1}{15}G_0^{2,1} \,, & p_{0,0}^{2,2}(\phi) &= \frac{1}{150}\left(6G_0^{2,2} + \mathrm{Re}[e^{-2i\phi}G_2^{2,2}]\right) \,, \\
p_{1,1}^{2,1}(\phi) &= \frac{1}{15}\mathrm{Re}[e^{-i\phi}G_1^{2,1}] \,, & p_{1,1}^{2,2}(\phi) &= \frac{1}{25}\mathrm{Re}[e^{-i\phi}G_1^{2,2}] \,.
\end{aligned} \tag{4.68}
$$

A consequence of the fact that the full orthogonality of the Wigner functions has been lost is that higher moments contain lower G-functions. As an interesting example, it is possible to show that

$$p_{2,0}^{4,1}(\phi) = \frac{1}{9\sqrt{10}}\left(G_0^{0,1} + G_0^{2,1}\right) = \frac{4}{9\sqrt{10}} g_{6c} \,. \tag{4.69}$$

This quantity is of some interest since $g_{6c} = 0$ in the SM, as it involves scalar and tensor operators at the level of the dimension-six effective Hamiltonian (2.42).

While these moments all arise ultimately from the same predictions, they provide a range of potential measurements and observations that are complementary; the particular case (4.69) may also serve as a useful null test for New Physics in its own right.

4.4 Angular conventions in the decay $\bar{B} \to \bar{K}^* \ell^+ \ell^-$

Historically, there has been some discrepancy between the experimental (in particular, the LHCb) and theory (e.g. [113]) angular conventions, which until recently had not been addressed satisfactorily. This section serves to clarify the relationships. The main result is shown in the form of a commutative diagram in figure 4.3.

The LHCb conventions [129], which are adopted in this chapter, were earlier shown in figure 4.1. The rationale behind the definition of the conjugate mode is as follows: firstly, particles are mapped into antiparticles, corresponding to a C transformation. Then the momenta of all particles are reversed, changing the angle $\phi \to 2\pi - \phi$. This leads to sign changes in $g_{7,8,9}$. Therefore, the conjugate mode corresponds to a full CP transformation

$$\frac{d^4\bar{\Gamma}}{dq^2 d\cos\theta_\ell d\cos\theta_K d\phi}\Big|_{\text{LHCb}} = \frac{d^4\Gamma}{dq^2 d\cos\theta_\ell d\cos\theta_K d\phi}\Big|_{CP} \,,$$

and the quantity

$$\frac{d^4(\Gamma \pm \bar{\Gamma})}{dq^2 d\cos\theta_\ell d\cos\theta_K d\phi}\Big|_{\text{LHCb}} \,,$$

is therefore CP-even (-odd). Above, $\Gamma = \Gamma(\bar{B} \to \bar{K}^* \ell_1 \bar{\ell}_2)$ and $\bar{\Gamma} = \Gamma(B \to K^* \bar{\ell}_1 \ell_2)$, with the (perhaps surprising) anti-relationship between barred decay rate and unbarred B meson explained by noting that theoretical papers

traditionally use $\bar{B} \to \bar{K}^* \ell_1 \bar{\ell}_2$ as the principal reference decay channel.

The theoretical community uses conventions for CP conjugates such that they facilitate the implementation of decays that are not self-tagging (eg $\bar{B}_s, B_s \to \phi(\to K^+K^-)\ell^+\ell^-$ at hadron colliders). When going between conjugate modes, the angles transform as $(\theta_\ell, \theta_K, \phi) \to (\pi - \theta_\ell, \pi - \theta_K, 2\pi - \phi)$, which leads to sign changes in $g_{5,6,8,9}$. This transformation rule corresponds to a full CP-conjugation, but with the angles θ_ℓ, θ_K associated to the same particle rather than the anti-particle.[9]

To find the transformation between the theory and LHCb conventions is not straightforward, because it is difficult to find a theory paper that resolves the four-fold ambiguity of defining the angle ϕ and/or shows a figure consistent with the definitions used in the corresponding work. Nevertheless, it is possible to check that the results in, for example, [78, 110, 113] agree with each other for common contributions, and that results in appendix C.4.1 are also in agreement with these contributions for $\bar{B} \to \bar{K}^* \ell_1 \bar{\ell}_2$ if one makes the identification $J_{4,6,7,9} = -g_{4,6,7,9}$ and $J_{1,2,3,5,8} = g_{1,2,3,5,8}$. This completes the diagram in figure 4.3. These conclusions on angular conventions and the relations between them were also reached in [141].

4.4.1 Relations between angular observables

Alongside the clarification of relationships between angular conventions, it is equally important to clarify the relation between angular $P_i^{(\prime)}$ observables as defined in [121] and their adaptation by LHCb [20]. In matching the results and creating the dictionary, one needs to pay attention to the fact that [20] and [121] define the P_i' in terms of g_i and J_i differently, as well as the different angular conventions for g_i and J_i themselves (shown in figure 4.3). Amongst the twelve observables discussed in section 4.2.3, eight of them, $P_{1,2,3}$, $P'_{4,5,6,8}$ and $A_{\rm FB}$, depend upon angles and definitions.

[9] Tagging is the identification of whether the B meson contains a b or $\bar{b}$ quark, and is an important aspect of B physics. Self-tagging decays are those where the identification of the B meson can be inferred from its final state. In the $B^0(\bar{B}^0) \to K\pi\ell_1\bar{\ell}_2$ decay, for example, the final state is $K^+\pi^-$ for a B^0 and $K^-\pi^+$ for a $\bar{B}^0$ meson, so that the initial B meson can be tagged merely from the charge of the final-state kaon. The $B_s(\bar{B}_s) \to \phi(\to K^+K^-)\ell^+\ell^-$ decay, on the other hand, cannot be so tagged, and other techniques are required. For one useful discussion of experimental aspects of tagging, see [140].

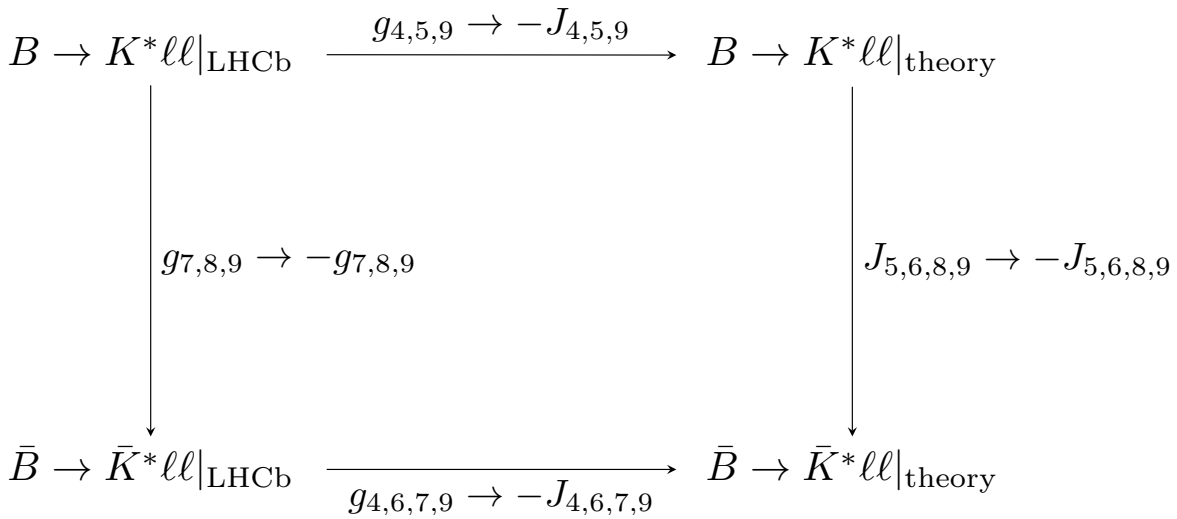

Figure 4.3 *Changes of angular functions between decay modes. For CP conjugates, the conjugation of the CP-odd (weak) phases are suppressed. Angular functions whose signs do not change are not indicated.*

The P_i' and A_{FB} are defined by LHCb [20] as

$$P'_{4,5,6,8}|_{\text{LHCb}} = \frac{S_{4,5,7,8}|_{\text{LHCb}}}{\sqrt{F_L(1-F_L)}} \,, \quad A_{\text{FB}}|_{\text{LHCb}} = \frac{3(S_{6s}|_{\text{LHCb}})}{4(\Gamma+\bar{\Gamma})} \,, \tag{4.70}$$

where S_i are CP-even quantities, defined (alongside the CP-odd quantities A_i), by

$$S_i[A_i] = \frac{g_i \pm g_i^{CP}}{\Gamma + \Gamma^{CP}} \tag{4.71}$$

and $2\mathcal{N}'_{\text{bin}} = \sqrt{F_L(1-F_L)}$ in the notation of section 4.2.3. LHCb has not defined $P_{1,2,3}$, but it is reasonable to assume the same functional form as in [121]. From the angular convention relations defined above, the relations between experimental and theory angular conventions are equivalent to

$$\begin{aligned} (g,A,S)_{1,2,3,5,8}|_{\text{LHCb}} &= +(J,A,S)_{1,2,3,5,8}|_{\text{theory}} \,, \\ (g,A,S)_{4,6,7,9}|_{\text{LHCb}} &= -(J,A,S)_{4,6,7,9}|_{\text{theory}} \,. \end{aligned} \tag{4.72}$$

In [121] the eight equivalent angular observables are defined as follows:[10]

$$P_1 = \frac{1}{2S_{2s}} S_3 \qquad = \frac{1}{2S_{2s}} (S_3|_{\text{LHCb}}) \qquad = +P_1|_{\text{LHCb}} \,,$$

[10]Note that [78, 113] define $A_{\text{FB}} = \frac{3S_{6s}}{4(\Gamma+\bar{\Gamma})}$ which results in $A_{\text{FB}}|_{[78,\,113]} = -A_{\text{FB}}|_{\text{LHCb}}$.

$$
\begin{aligned}
P_2 &= \frac{1}{8S_{2s}} S_{6s} &&= \frac{1}{8S_{2s}}(-S_{6s}|_{\text{LHCb}}) &&= -P_2|_{\text{LHCb}} \,, \\
P_3 &= \frac{-1}{4S_{2s}} S_9 &&= \frac{-1}{4S_{2s}}(-S_9|_{\text{LHCb}}) &&= -P_3|_{\text{LHCb}} \,, \\
P_4' &= \frac{1}{\mathcal{N}'_{\text{bin}}} S_4 &&= \frac{1}{\mathcal{N}'_{\text{bin}}}(-S_4|_{\text{LHCb}}) &&= -\frac{1}{2} P_4'|_{\text{LHCb}} \,, \\
P_5' &= \frac{1}{2\mathcal{N}'_{\text{bin}}} S_5 &&= \frac{1}{2\mathcal{N}'_{\text{bin}}}(S_5|_{\text{LHCb}}) &&= +P_5'|_{\text{LHCb}} \,, \\
A_{\text{FB}} &= -\frac{3S_{6s}}{4(\Gamma+\bar{\Gamma})} &&= -\frac{3(-S_{6s}|_{\text{LHCb}})}{4(\Gamma+\bar{\Gamma})} &&= +A_{\text{FB}}|_{\text{LHCb}} \,, \\
P_6' &= \frac{-1}{2\mathcal{N}'_{\text{bin}}} S_7 &&= \frac{-1}{2\mathcal{N}'_{\text{bin}}}(-S_7|_{\text{LHCb}}) &&= +P_6'|_{\text{LHCb}} \,, \\
P_8' &= \frac{-1}{\mathcal{N}'_{\text{bin}}} S_8 &&= \frac{-1}{\mathcal{N}'_{\text{bin}}}(S_8|_{\text{LHCb}}) &&= -\frac{1}{2} P_8'|_{\text{LHCb}} \,,
\end{aligned}
$$

which can be directly translated into the LHCb conventions, as shown on the right of the equations above. It seems that there is some discrepancy between the definitions above and those used by previous papers in the sign of the observables $S[A]_{7,8,9}$. For example, both $P_6' = P_6'|_{\text{LHCb}}$ and $P_8' = -\frac{1}{2}P_8'|_{\text{LHCb}}$ differ from the relations given in the caption of table 1 in [142] by the aforementioned sign. The relation $S[A]_9 = -S[A]_9|_{\text{LHCb}}$ also differs from the one given by [143] in table 1 by a sign. Nevertheless, the dictionary provided above will hopefully prove useful in standardising and harmonising the conventions and definitions used between different communities in future studies of this decay.

4.4.2 Comparison of angular distribution with the literature

An overview of the history behind the research of this decay was given at the beginning of this chapter. The most recent reference prior to the results presented in this thesis is [113], to which results given in the appendix can be compared.[11]

Taking into account the change $g_{4,6,7,9} \to -J_{4,6,7,9}$ (as shown in figure 4.3), and comparing at the level of form factors (assuming naive factorisation), the results in appendix C.4.1 are in agreement with [113] except for tensor interference terms, with full agreement established with the replacement $C_{T5} \to -C_{T5}$ in [113]. This may be related to the fact that the relations $\text{tr}[\gamma^\alpha\gamma^\beta\gamma^\gamma\gamma^\delta\gamma_5] = 4\lambda i\epsilon^{\alpha\beta\gamma\delta}$ and $\sigma^{\alpha\beta}\gamma_5 = -\lambda\frac{i}{2}\epsilon^{\alpha\beta\gamma\delta}\sigma_{\gamma\delta}$ (with $\lambda = \pm 1$ depending on conventions, $\lambda = 1$ being the

[11] At the time this research was initially performed, the latest version of [113] was (v3) as seen on the arXiv link. Since then, the authors of [113] released a revised version that restores total agreement by carrying out the change in definition of C_{T5} suggested in the following paragraph.

convention used in this thesis) are not consistent with equation C.16 [113] (v3).

A more cosmetic difference is that the authors of [113] chose not to present the tensor contribution in $J_{8,9}(g_{8,9})$, since such contributions vanish in the narrow-width approximation. There are further apparent disagreements in the definitions of the HAs between the work above and those found in [113], but these are down to conventions and such discrepancies do not carry forward to the final expression.

Finally, it is important to note that v3 of [113] states that their results agreed with those in [144] up to the sign of one scalar-tensor interference term in the observable g_7 (J_7 in [113]). The results presented in appendix C.4.1 then agree with [113] but not [144] in this respect.

4.5 Conclusions

The results presented in this chapter, and the associated explicit expressions in appendix C, provide the complete angular distribution for the most general dimension-six effective Hamiltonian applied to the $B \to K^*(\to K\pi)\ell_1\bar{\ell}_2$, and the formalism leading to this can be applied to a host of related decays. Apparent anomalies observed in such decays persist, in particular in P_5' [20] and the related $B_s \to \phi(\to KK)\ell_1\bar{\ell}_2$ decay, where the branching ratio is currently 3σ away from the SM prediction [23], and so further analyses of these decays are vital to confirm and then interpret these anomalies. Some of the methods outlined in this chapter have already been applied by the experimental community. LHCb performed a moments analysis of $B \to K_J$ decays in [139]; and with further work from the Belle II experiment expected shortly alongside Run II data from the LHC, it can be expected that the theoretical and experimental interest in this decay will only continue to grow in the near future.

This chapter has also presented, in section 4.4, the correct relations between angular conventions and observables between the theory and experimental communities. The conclusions presented in that section have since been accepted by the theory community, as can be found in, for example, [123, 141, 145, 146], facilitating future comparison between theoretical predictions and experimental results.

At the current time of writing, the anomalies in $b \to s$ decays remain at a level where they can be seen merely as a curiosity, a tantalising hint that there is more

to these decays than would be apparent from SM predictions. It may not be long before this picture changes in the light of new experimental data, but even at the $\sim 3\sigma$ level it is still reasonable to treat these anomalies as a strong motivation for further experimental studies [147]. A global analysis of all such anomalies, meanwhile, has suggested that the deviation from the SM in the light of all data is close to, or even beyond, the 5σ gold standard for a discovery. The studies in [27, 122, 145, 146, 148] point to various NP scenarios in which the data can be well-described by a simple modification in the Wilson coefficient $C_{9\mu}$, although at this stage it remains equally likely that the anomalies can be explained within the context of the SM, via charm-related anomalies [26].

In either case, the fully general angular distribution presented in this chapter may play an important part in resolving such questions; for example, the phenomenological code flavio [149] has made use of the angular observables and conventions defined above. The following chapter, meanwhile, discusses two scenarios in which the angular distribution of $B \to K_J \ell_1 \bar{\ell}_2$ decays may be modified, and how they might be distinguished from each other using the methods outlined above.

Chapter 5

Higher-spin operators and QED corrections in $b \to s$ decays

This chapter presents results pertaining to the addition of higher-spin operators to the effective Hamiltonian when computing the angular distribution of $B \to K_J(\to K\pi)\ell_1\bar{\ell}_2$ decays. Although the work is preliminary, it is sufficient to provide some hints of the effects of such operators, how to search for them, and how to distinguish them from other modifications to the theoretical assumptions that led to the angular distribution in the previous chapter. Research in this chapter was inspired by the preliminary discussions found in appendix F of [124].

Some sections of this chapter have previously appeared in [34].

5.1 Introduction

In the previous chapter, the angular distribution for the $B \to K_J(\to K\pi)\ell_1\bar{\ell}_2$ decay was presented in the context of the full dimension-six effective Hamiltonian (2.42). Along with the assumptions that there were no interactions between the final-state leptons and the hadrons in the decay (the Lepton Factorisation Approximation (LFA)), and the further restriction to a single partial wave in the $K\pi$ channel, this led to the highly compact expression for the angular distribution $I^{(0)}_{K^*}$ (4.36).

It is natural to ask what the effects are of dropping any of these assumptions.

This chapter goes some way towards answering this by discussing in particular the impact of including higher-dimensional operators in the effective Hamiltonian, as well as a partial consideration of how such effects might be distinguished from QED corrections arising from the explicit breaking of the LFA.

In one sense, at least, the answer is apparent: any new operators in the effective Hamiltonian will either induce new contributions to the observables $G_m^{l_K,l_\ell}(q^2)$, or lead to "new" observables with indices l_ℓ now allowed to be greater than 2 (as well as modifying the observables with lower values of l_ℓ). On the other hand, the number of potential angular structures that emerge grows rapidly with increasing values of l_K and l_ℓ, and it is important to make these effects explicit. To go some way towards achieving this, the new angular coefficients are presented with reference to an explicit higher-dimensional "derivative" operator, and in the context of the decay of the $K_2(1430)$ resonance, which has received some attention in the literature [130, 150, 151]; recently, it has become accessible at the LHCb [139]. Since this is a D-wave resonance that emerges from the same Hamiltonian as the usual K^* resonance, investigating this decay in the same language developed in the previous chapter might help shed further light on the origin of the reported K^* anomalies.

The remainder of this chapter is organised as follows. In section 5.2, an example of such an operator is presented, along with a preliminary estimate of the size of its associated Wilson coefficient (at the Weak scale). In section 5.3, the relevant HAs for the new operator are computed in the context of the $B \to K_2(\to K\pi)\ell_1\bar{\ell}_2$ decay, which allows access to the full range of new contributions to the angular distribution. While the full structure of the general angular distribution with higher-spin operators is exceedingly lengthy, the contributions to new observables, not accessible with the dimension-six effective Hamiltonian, are presented in section 5.4. Section 5.5 discusses in more general terms how the angular distribution can change in the light of new operators, as well as QED interactions between the leptonic and hadronic parts of the decay. Such considerations are of importance in light of the R_K anomalies [19].

5.2 Double partial wave expansion and higher-spin operators

In order to discuss the origin of generic terms in the full distribution (4.53), it is advantageous to return to the amplitude level. Symbolically, one may rewrite the amplitude (4.26), omitting the sum over J_γ, as

$$\mathcal{A}(B \to K_J(\lambda)(\to K\pi)\ell^+(\lambda_1)\ell^-(\lambda_2)) = \mathcal{A}^{J_\gamma,J_K}_{\lambda,\lambda_\ell}\, \bar{D}^{J_K}_{\lambda,0}\left(\Omega_K\right) \bar{D}^{J_\gamma}_{\lambda,\lambda_\ell}\left(\Omega_\ell\right) , \qquad (5.1)$$

with $\lambda_\ell = \lambda_1 - \lambda_2$, as defined in (4.9). The two opening angles θ_K and θ_ℓ allow for two separate partial wave expansions. The partial waves in the θ_K- and θ_ℓ-angles are denoted by $S_K, P_K, \ldots$ and $S_\ell, P_\ell, \ldots$ respectively. The decay channel with $K_J = K^*$ imposed the condition $J_K = 1$, leading to the presence of only a P_K-wave. The signal of K^* is part of the $(K\pi)$ P_K-wave. The importance of considering the S_K-wave interference through $K_0^*(800)$ (also known as $\kappa(800)$) was emphasised in [152]. The separation of the various partial waves in the $(K\pi)$-channel is a problem that can be solved experimentally e.g. [153], and see also [154] for a generic study of the lowest partial waves at high q^2. It is also possible to employ an analysis similar to the MoM but for the hadronic contributions from, for example, D-wave hadrons, such as the K_2 [151, 155]. The second partial wave expansion originates from the lepton angle θ_ℓ, which will be the main focus hereafter. By restricting to the dimension-six effective Hamiltonian (2.42), as well as the LFA, only S_ℓ- and P_ℓ-waves were allowed (cf. equation (4.30)), bounding $l_\ell \leq 2$ in (4.53).[1] This pattern is broken by the inclusion of higher spin operators and non-factorisable corrections between the lepton pair and the quarks, including the exchange of electroweak gauge bosons. It is therefore important to be able to distinguish these two effects from each other.

One natural way to introduce higher-spin operators is by the insertion of derivatives. Each extra derivative can potentially increase the spin of a natural spin-one operator by one unit. For a single derivative correction to vector or axial currents,[2] four new operators can be defined according to the symmetry

[1] This is the same approximation that is relevant for the endpoint relations [131, 156].

[2] In the discussion that follows, only derivative corrections to the vector and axial operators will be considered, although scenarios will exist where derivatives are also attached to scalar or tensor-like operators. Since this chapter is merely concerned with illustrating the consequences of such new operators, it is natural to consider only a minimal extension of the operator basis.

properties of the resulting indices:

$$\begin{aligned}\mathcal{O}_{\partial}^{S;\pm_1\pm_2} &= \bar{s}_L S_{\mu\nu}^{\pm_1} b\ \bar{\ell} S^{\pm_2;\mu\nu}(\gamma_5)\ell\,,\\ \mathcal{O}_{\partial}^{A;\pm_1\pm_2} &= \bar{s}_L A_{\mu\nu}^{\pm_1} b\ \bar{\ell} A^{\pm_2;\mu\nu}(\gamma_5)\ell\,,\end{aligned} \tag{5.2}$$

where

$$\begin{aligned}S_{\mu\nu}^{\pm} &= \overset{\leftrightarrow}{\partial}{}^{\pm}_{\{\mu}\gamma_{\nu\}}\,,\\ A_{\mu\nu}^{\pm} &= \overset{\leftrightarrow}{\partial}{}^{\pm}_{[\mu}\gamma_{\nu]}\,,\end{aligned} \tag{5.3}$$

and $\overset{\leftrightarrow}{\partial}{}^{\pm} \equiv \overset{\leftarrow}{\partial} \pm \overset{\rightarrow}{\partial}$ is the directional derivative. Brace (square) brackets denote symmetrisation (antisymmetrisation) in the Lorentz indices.[3] Such operators may arise in the presence of new spin-two particles (e.g. [157]), or as next-to-leading corrections to the effective Hamiltonian (2.42).

The derivatives in (5.2) can be rewritten in terms of momenta, using $i\partial_\mu\psi(p) = p_\mu\psi$:

$$\begin{aligned}\ell_1(S,A)^{+}_{\mu\nu}\bar{\ell}_2 &= -i(Q_\mu\ell_1\gamma_\nu\bar{\ell}_2 \pm Q_\nu\ell_1\gamma_\mu\bar{\ell}_2)\,,\\ \ell_1(S,A)^{-}_{\mu\nu}\bar{\ell}_2 &= -i(q_\mu\ell_1\gamma_\nu\bar{\ell}_2 \pm q_\nu\ell_1\gamma_\mu\bar{\ell}_2)\,,\end{aligned} \tag{5.4}$$

where q and Q are the sum and difference of the two fermion (here denoted by leptons) momenta respectively. These equations will shortly be used to compute HAs, but the relationship to momenta also leads to an estimate of the Wilson coefficients for the leading operators within the SM. To see this, consider the box diagram (figure 5.1), which at first order leads to the Wilson coefficients $C_V(C_9)$ and $C_A(C_{10})$ (and their parity-flipped equivalents $C'_{V,A}$). In Feynman gauge, it is proportional to the loop integral

$$\begin{aligned}&\int \frac{d^dk}{(2\pi)^d}\frac{(k+p_1)^\rho(k+p_1+p_2+p_3)^\tau}{(k^2-m_W^2)\left((k+p_1)^2-m_t^2\right)\left((k+p_1+p_2)^2\right)\left((k+p_1+p_2+p_3)^2-m_W^2\right)}\\ &= \int dU \int \frac{\mathrm{d}^dl}{(2\pi)^d}\frac{L_1^\rho L_2^\tau}{\left(l^2-M^2\right)^4}\end{aligned} \tag{5.5}$$

where $\int dU = \int_0^1 du_1 \int_0^{1-u_1} du_2 \int_0^{1-u_1-u_2} du_3$ and $M^2 = u_1 m_t^2 + (1-u_1-u_3)m_W^2$, while the momenta in the numerator are given by

$$L_1^\rho(l,p_i,u_i) = (l + (1-u_1-u_2-u_3)p_1 - (u_2+u_3)p_2 - u_3p_3)^\rho\,,$$

[3] In a more complete theory, the derivatives here will be promoted to covariant derivatives.

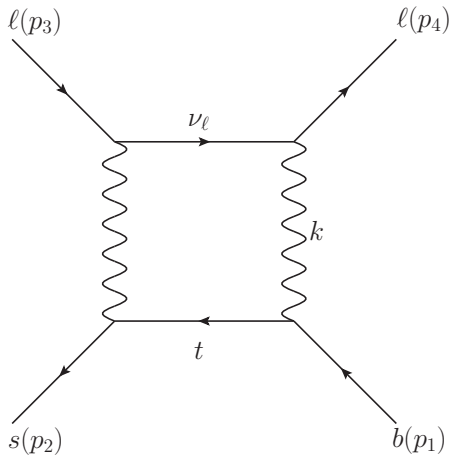

Figure 5.1 *Box diagram relevant to the computation of the Wilson coefficients $C_{V,A}$ as well as the derivative operators, presented below. The momentum assignments have been indicated.*

$$L_2^\tau(l, p_i, u_i) = (l + (1 - u_1 - u_2 - u_3)p_1 + (1 - u_2 - u_3)p_2 + (1 - u_3)p_3)^\tau \,. \quad (5.6)$$

Defining the quantities $p = p_1 + p_2$, $P = p_1 - p_2$, $q = p_3 + p_4$, $Q = p_3 - p_4$, and dropping the terms proportional to the loop momentum (which would provide the leading contribution to the box diagram), allow L_1, L_2 to be rewritten in the form

$$\begin{aligned} L_1^\rho(l, \{p, P, q, Q\}, u_i) &= \frac{1}{2}\left((1 - u_1 - 2u_2 - 2u_3)p + (1 - u_1)P - u_3(q + Q)\right)^\rho \,, \\ L_2^\tau(l, \{p, P, q, Q\}, u_i) &= \frac{1}{2}\left((2 - u_1 - 2u_2 - 2u_3)p - u_1 P + (1 - u_3)(q + Q)\right)^\tau \,. \end{aligned} \quad (5.7)$$

All of the various coefficients of the different momentum structures have well-defined integrals, but only terms that are products of p, P and q, Q are interesting, as these can be directly related to one derivative acting on each of the quark or lepton parts of the operator. Matching the relevant structures leads to Wilson coefficients

$$\begin{aligned} C_{S\pm+,L} &= \frac{1}{4m_W^2}\left(\frac{1 - 2x}{3(x-1)^3}\ln x + \frac{3x - 1}{6(x-1)^2}\right) \,, \\ C_{S\pm-,L} &= \frac{1}{4m_W^2}\left(\frac{1}{6(x-1)^2}\ln x - \frac{1}{6(x-1)}\right) \,, \end{aligned} \quad (5.8)$$

where $x = \dfrac{m_t^2}{m_W^2}$. For $m_t = 173$ GeV and $m_W = 80.2$ GeV, this leads to typical values $C_{\pm+,L} \simeq \frac{0.02}{m_W^2} \simeq 3 \times 10^{-6}$ GeV^{-2}, $C_{\pm-,L} \simeq \frac{-0.006}{m_W^2} \simeq -1 \times 10^{-6}$ GeV^{-2}. As

was stated earlier, these have been evaluated only in the Feynman gauge, and possible further corrections from penguin diagrams have been neglected, although the main feature of note is that such operators are heavily suppressed in the SM (as compared with, for example, the related Wilson coefficient $C_V \equiv C_9 \simeq 4$).

As expected, the Wilson coefficients arising from the SM weak interaction are suppressed by a factor of m_W^2, meaning that any observation of higher-spin contributions to $B \to K_J(\to K\pi)\ell_1\bar{\ell}_2$ decays could well be attributable to NP contributions.

5.3 Leptonic and hadronic HAs

It is not difficult to show that only the operator $\mathcal{O}_{S-+}$ can lead to spin-two contributions to $B \to K_J\ell_1\bar{\ell}_2$ decays. The operators that are antisymmetric in Lorentz indices certainly cannot, owing to the symmetry of the spin-two polarisation tensor in (4.24). The other condition is that the derivative acts on the fermion current to create the difference in momenta rather than the sum, as $\omega(\lambda)\cdot q = 0$ unless $\omega(\lambda)$ is the timelike polarisation, thus imposing the + structure in the leptons (5.4). Over the hadrons, as one particle is in the inital state and the other in the final state, the opposite argument applies to the sign of the derivatives, imposing the structure $\mathcal{O}_{S-+}$. This operator will simply be referred to as $\mathcal{O}_{\partial;V(A)}$ from now on, alongside its chiral-flipped partner $\mathcal{O}' = \mathcal{O}_{\bar{s}_L\to\bar{s}_R}$.

To make the results more explicit, consider the template decay $B \to K_2(\to K\pi)\ell_1\bar{\ell}_2$, where (as before) the lepton flavours need not be identical. Restricting as in the previous chapter to the LFA, the decay then proceeds from the generalised HAs

$$\begin{aligned}
\mathcal{A}^2_{\lambda,\lambda_1,\lambda_2} &= H^{\mathcal{O}_{\partial;V}}_{2,\lambda}\mathcal{L}^{\mathcal{O}_{\partial;V}}_2(\lambda_1,\lambda_2) + H^{\mathcal{O}_{\partial;A}}_{2,\lambda}\mathcal{L}^{\mathcal{O}_{\partial;A}}_2(\lambda_1,\lambda_2)\,,\\
\mathcal{A}^1_{\lambda,\lambda_1,\lambda_2} &= -H^V_\lambda\mathcal{L}^V(\lambda_1,\lambda_2) - H^A_\lambda\mathcal{L}^A(\lambda_1,\lambda_2) - 2H^{\mathcal{O}_{\partial;V}}_{t,\lambda}\mathcal{L}^{\mathcal{O}_{\partial;V}}_t(\lambda_1,\lambda_2) - 2H^{\mathcal{O}_{\partial;A}}_{t,\lambda}\mathcal{L}^{\mathcal{O}_{\partial;A}}_t(\lambda_1,\lambda_2)\,,\\
\mathcal{A}^0_{0,\lambda_1,\lambda_2} &= H^S\mathcal{L}^S(\lambda_1,\lambda_2) + H^P\mathcal{L}^P(\lambda_1,\lambda_2) + H^{\mathcal{O}_{\partial;V}}_0\mathcal{L}^{\mathcal{O}_{\partial;V}}_0(\lambda_1,\lambda_2) + H^{\mathcal{O}_{\partial;A}}_0\mathcal{L}^{\mathcal{O}_{\partial;A}}_0(\lambda_1,\lambda_2)\\
&\quad + H^{\mathcal{O}_{\partial;V}}_{tt}\mathcal{L}^{\mathcal{O}_{\partial;V}}_{tt}(\lambda_1,\lambda_2) + H^{\mathcal{O}_{\partial;A}}_{tt}\mathcal{L}^{\mathcal{O}_{\partial;A}}_{tt}(\lambda_1,\lambda_2)\,,
\end{aligned} \tag{5.9}$$

where the new operator allows for the presence of possible spin-two contributions.[4] Terms such as the spin-one contribution from the derivative operator are omitted

[4]For ease of notation, the contributions from the tensor operator are omitted, as they add no new angular structures.

as they vanish, owing to the contraction between symmetric and anti-symmetric Lorentz structures. Assuming that the $K_2 \to K\pi$ decay can be approximated in the same way as a $K^* \to K\pi$ decay (the narrow-width approximation [78]), the angular distribution is given, in complete analogy with the results in the previous chapter, by

$$I_{K_2}\left(q^2, \Omega_K, \Omega_\ell\right) \equiv \frac{32\pi}{3} \frac{d^4\Gamma}{dq^2\, d\cos\theta_\ell\, d\cos\theta_K\, d\phi} = \mathcal{N} \sum_{\lambda_1,\lambda_2} \left|\hat{\mathcal{M}}_{\lambda_1,\lambda_2}\right|^2 , \tag{5.10}$$

with the only change from the similar equation (4.33) being the normalisation factor $\mathcal{N}$, defined in (4.34), using the K_2 mass rather than the K^* mass. The remaining details are analogous to the K^* decay so it only remains to compute the new HAs for the spin-two operator over the leptonic and hadronic sectors.

5.3.1 Leptonic HAs for the spin-two operator

The calculation of the HAs is standard, and the full details of the calculation are presented more fully in appendix C.2 (see also [126]). For the spin-two projections, one needs the Clebsch-Gordan coefficients for spin two, as shown by equation (4.20), but otherwise the calculation is systematic and follows the procedure outlined in the previous chapter. The leptonic HAs for different masses for the spin-two operator $\mathcal{O}_{\partial;V(A)}$ can be written

$$\mathcal{L}_2^{\mathcal{O}_{\partial;V}} = \frac{2i\sqrt{\lambda_{\gamma^*}}}{\sqrt{q^2}} \begin{pmatrix} \sqrt{\frac{2}{3}}\left(\beta_1^+\beta_2^+ - \beta_1^-\beta_2^-\right) & -2\left(\beta_1^+\beta_2^+ + \beta_1^-\beta_2^-\right) \\ -2\left(\beta_1^+\beta_2^+ + \beta_1^-\beta_2^-\right) & \sqrt{\frac{2}{3}}\left(\beta_1^+\beta_2^+ - \beta_1^-\beta_2^-\right) \end{pmatrix} ,$$

$$\mathcal{L}_2^{\mathcal{O}_{\partial;A}} = \frac{2i\sqrt{\lambda_{\gamma^*}}}{\sqrt{q^2}} \begin{pmatrix} \sqrt{\frac{2}{3}}\left(\beta_1^+\beta_2^- - \beta_1^-\beta_2^+\right) & 2\left(\beta_1^+\beta_2^- + \beta_1^-\beta_2^+\right) \\ -2\left(\beta_1^+\beta_2^- + \beta_1^-\beta_2^+\right) & -\sqrt{\frac{2}{3}}\left(\beta_1^+\beta_2^- - \beta_1^-\beta_2^+\right) \end{pmatrix} ,$$

$$\mathcal{L}_t^{\mathcal{O}_{\partial;V}} = \frac{i}{\sqrt{q^2}} \begin{pmatrix} \sqrt{\lambda_{\gamma^*}}\left(\beta_1^+\beta_2^- - \beta_1^-\beta_2^+\right) & \sqrt{2}(E_1 - E_2)\sqrt{q^2}\left(\beta_1^+\beta_2^+ + \beta_1^-\beta_2^-\right) \\ -(E_1 - E_2)\sqrt{q^2}\left(\beta_1^+\beta_2^+ - \beta_1^-\beta_2^-\right) & \\ \sqrt{2}(E_1 - E_2)\sqrt{q^2}\left(\beta_1^+\beta_2^+ + \beta_1^-\beta_2^-\right) & \sqrt{\lambda_{\gamma^*}}\left(\beta_1^+\beta_2^- - \beta_1^-\beta_2^+\right) \\ & -(E_1 - E_2)\sqrt{q^2}\left(\beta_1^+\beta_2^+ - \beta_1^-\beta_2^-\right) \end{pmatrix} ,$$

$$\mathcal{L}_t^{\mathcal{O}_{\partial;A}} = \frac{i}{\sqrt{q^2}} \begin{pmatrix} \sqrt{\lambda_{\gamma^*}}\left(\beta_1^+\beta_2^+ - \beta_1^-\beta_2^-\right) & -\sqrt{2}(E_1-E_2)\sqrt{q^2}\left(\beta_1^+\beta_2^- + \beta_1^-\beta_2^+\right) \\ -(E_1-E_2)\sqrt{q^2}\left(\beta_1^+\beta_2^- - \beta_1^-\beta_2^+\right) & \\ \sqrt{2}(E_1-E_2)\sqrt{q^2}\left(\beta_1^+\beta_2^- + \beta_1^-\beta_2^+\right) & \sqrt{\lambda_{\gamma^*}}\left(\beta_1^-\beta_2^- - \beta_1^+\beta_2^+\right) \\ & +(E_1-E_2)\sqrt{q^2}\left(\beta_1^+\beta_2^- - \beta_1^-\beta_2^+\right) \end{pmatrix},$$

$$\mathcal{L}_0^{\mathcal{O}_{\partial;V}} = \frac{2i\sqrt{\lambda_{\gamma^*}}}{\sqrt{3}\sqrt{q^2}} \begin{pmatrix} \beta_1^-\beta_2^- - \beta_1^+\beta_2^+ & 0 \\ 0 & \beta_1^-\beta_2^- - \beta_1^+\beta_2^+ \end{pmatrix},$$

$$\mathcal{L}_0^{\mathcal{O}_{\partial;A}} = \frac{2i\sqrt{\lambda_{\gamma^*}}}{\sqrt{3}\sqrt{q^2}} \begin{pmatrix} \beta_1^-\beta_2^+ - \beta_1^+\beta_2^- & 0 \\ 0 & \beta_1^+\beta_2^- - \beta_1^-\beta_2^+ \end{pmatrix},$$

$$\mathcal{L}_{tt}^{\mathcal{O}_{\partial;V}} = 2i\,(E_1-E_2) \begin{pmatrix} \beta_1^-\beta_2^+ - \beta_1^+\beta_2^- & 0 \\ 0 & \beta_1^-\beta_2^+ - \beta_1^+\beta_2^- \end{pmatrix},$$

$$\mathcal{L}_{tt}^{\mathcal{O}_{\partial;A}} = 2i\,(E_1-E_2) \begin{pmatrix} \beta_1^-\beta_2^- - \beta_1^+\beta_2^+ & 0 \\ 0 & \beta_1^+\beta_2^+ - \beta_1^-\beta_2^- \end{pmatrix}, \tag{5.11}$$

where the spin-one contribution vanishes, as the decomposition in equation (4.20) is antisymmetric, whereas this is a symmetric operator. These HAs simplify dramatically for identical leptons:

$$\mathcal{L}_2^{\mathcal{O}_{\partial;V}} = 2iq^2\beta_\ell \begin{pmatrix} 2\sqrt{\frac{2}{3}}\frac{m_\ell}{\sqrt{q^2}} & -1 \\ -1 & 2\sqrt{\frac{2}{3}}\frac{m_\ell}{\sqrt{q^2}} \end{pmatrix},$$

$$\mathcal{L}_2^{\mathcal{O}_{\partial;A}} = 2iq^2\beta_\ell^2 \begin{pmatrix} 0 & 1 \\ -1 & 0 \end{pmatrix},$$

$$\mathcal{L}_t^{\mathcal{O}_{\partial;V}} = \begin{pmatrix} 0 & 0 \\ 0 & 0 \end{pmatrix},$$

$$\mathcal{L}_t^{\mathcal{O}_{\partial;A}} = 2i\beta_\ell m_\ell\sqrt{q^2} \begin{pmatrix} 1 & 0 \\ 0 & -1 \end{pmatrix},$$

$$
\begin{aligned}
\mathcal{L}_0^{\mathcal{O}_{\partial;V}} &= \frac{-4i\beta_\ell m_\ell \sqrt{q^2}}{\sqrt{3}} \begin{pmatrix} 1 & 0 \\ 0 & 1 \end{pmatrix} , \\
\mathcal{L}_0^{\mathcal{O}_{\partial;A}} &= \begin{pmatrix} 0 & 0 \\ 0 & 0 \end{pmatrix} , \\
\mathcal{L}_{tt}^{\mathcal{O}_{\partial;V}} &= \begin{pmatrix} 0 & 0 \\ 0 & 0 \end{pmatrix} , \\
\mathcal{L}_{tt}^{\mathcal{O}_{\partial;A}} &= \begin{pmatrix} 0 & 0 \\ 0 & 0 \end{pmatrix} ,
\end{aligned} \tag{5.12}
$$

from which it can be seen that, for this operator at least, all but the strict spin-two contributions $\mathcal{L}_2$ are $\mathcal{O}(m_\ell)$ effects.

5.3.2 Hadronic HAs for the K_2 meson

From the relation

$$
\partial_\mu(\bar{s}\gamma_\nu b) = \bar{s}\overset{\leftrightarrow}{\partial}{}^+_\mu \gamma_\nu b \,, \tag{5.13}
$$

it is clear that $\overset{\leftrightarrow}{\partial}{}^+_\mu$ represents nothing but a total derivative, and hence the momentum transfer between the quarks. Hence the form-factor parametrisation for the derivative operators in the K_2 decay becomes

$$
\begin{aligned}
\langle K_2(p,\eta_{\mu\nu})|\bar{s}_{L/R} S^+_{\mu\nu} b|B(p_B)\rangle &= -i\left(q_\mu \langle K_2|\bar{s}_{L/R}\gamma_\nu b|B\rangle + q_\nu \langle K_2|\bar{s}_{L/R}\gamma_\mu b|B\rangle\right) , \\
\langle K_2(p,\eta_{\mu\nu})|\bar{s}_{L/R} S^-_{\mu\nu} b|B(p_B)\rangle &= -i\left((p_\mu + p_{B\mu})\langle K_2|\bar{s}_{L/R}\gamma_\nu b|B\rangle \right. \\
&\qquad \left. + (p_\nu + p_{B\nu})\langle K_2|\bar{s}_{L/R}\gamma_\mu b|B\rangle\right) ,
\end{aligned} \tag{5.14}
$$

This confirms the statement earlier that only S^--type operators can access the spin-two observables, while any other operator constructed from derivatives in this way can be seen as corrections to the $\mathcal{O}_{V,A}$ operators.

For the spin-two case, the Wilson coefficents are $C^{(\prime)}_{\mathcal{O}_{\partial;V(A)}}$ for the vector and axial derivatives operators and their chiral-flipped versions. Note that $H^{\mathcal{O}_{\partial;V(A)}}_{1,\lambda} = 0$, owing to symmetry properties over the Lorentz indices. The vector and axial matrix elements can be defined in terms of the analogous form factors to those

for the $B \to K^*$ transition. The HAs are then given by

$$
\begin{aligned}
H_{2,\pm 2}^{\mathcal{O}_{\partial;V(A)}} &= 0\,, \\
H_{2,\pm 1}^{\mathcal{O}_{\partial;V(A)}} &= \frac{\mp\lambda_B^{3/2}\left(C_{\mathcal{O}_{\partial;V(A)}} + C'_{\mathcal{O}_{\partial;V(A)}}\right)V + \left(m_B^2 + m_{K_2}^2\right)\lambda_B\left(C_{\mathcal{O}_{\partial;V(A)}} - C'_{\mathcal{O}_{\partial;V(A)}}\right)A_1}{4m_B m_{K_2}\left(m_B + m_{K_2}\right)\sqrt{q^2}}\,, \\
H_{2,0}^{\mathcal{O}_{\partial;V(A)}} &= -\frac{8\lambda_B}{3q^2}\left(C_{\mathcal{O}_{\partial;V(A)}} - C'_{\mathcal{O}_{\partial;V(A)}}\right)A_{12}\,, \\
H_{t,\pm 1}^{\mathcal{O}_{\partial;V(A)}} &= \frac{\left(m_B - m_{K_2}\right)\left(\mp\lambda_B\left(C_{\mathcal{O}_{\partial;V(A)}} + C'_{\mathcal{O}_{\partial;V(A)}}\right)V\right)}{4\sqrt{2}m_B m_{K_2}\sqrt{q^2}} \\
&\quad + \frac{\left(m_B^2 + m_{K_2}^2\right)\sqrt{\lambda_B}\left(C_{\mathcal{O}_{\partial;V(A)}} - C'_{\mathcal{O}_{\partial;V(A)}}\right)A_1}{4\sqrt{2}m_B m_{K_2}\sqrt{q^2}}\,, \\
H_{t,0}^{\mathcal{O}_{\partial;V(A)}} &= -\frac{\sqrt{\lambda_B}}{2\sqrt{6}m_B m_{K_2}q^2}\left(C_{\mathcal{O}_{\partial;V(A)}} - C'_{\mathcal{O}_{\partial;V(A)}}\right)\left(8m_B m_{K_2}\left(m_B^2 - m_{K_2}^2\right)A_{12} + \lambda_B A_0\right)\,, \\
H_{0}^{\mathcal{O}_{\partial;V(A)}} &= \frac{4\sqrt{2}\lambda_B}{3q^2}\left(C_{\mathcal{O}_{\partial;V(A)}} - C'_{\mathcal{O}_{\partial;V(A)}}\right)A_{12}\,, \\
H_{tt}^{\mathcal{O}_{\partial;V(A)}} &= -\frac{\lambda_B\left(m_B^2 - m_{K_2}^2\right)}{\sqrt{6}m_B m_{K_2}q^2}\left(C_{\mathcal{O}_{\partial;V(A)}} - C'_{\mathcal{O}_{\partial;V(A)}}\right)A_0\,,
\end{aligned}
\tag{5.15}
$$

where $\lambda_B = \lambda(m_B^2, m_{K_2}^2, q^2)$ is the Källén function appropriate to this decay, defined in (C.2). The remaining HAs for the K_2 can be computed from those presented in the appendix[5] for the K^* from the general relation

$$
\eta_\mu(\lambda) \to c_\lambda \eta_\mu(\lambda)\frac{\eta(0)\cdot p_B}{m_B} = -c_\lambda\frac{\sqrt{\lambda_B}}{2m_B m_{K_2}}\eta_\mu(\lambda)\,, \tag{5.16}
$$

with the sign due to the parametrisation $\eta(0) = (-q_z, 0, 0, q_0)/m_{K_2}$, and $c_{\pm 1} = 1/\sqrt{2}$ and $c_0 = \sqrt{2/3}$ are factors emerging from the Clebsch-Gordan decomposition. Similar results can also be derived for the tensor operators, allowing one to build up the angular distribution of the $B \to K_2$-type decays in the same way as for the $B \to K^*$ decays, laid out in more detail in the previous chapter.

[5] All the HAs for vector and scalar operators also vanish at the kinematic endpoint, as they go as $\sqrt{\lambda_B} \times f(q^2, V, A_0, A_1, A_{12})$.

5.4 Angular distribution and coefficients for $m_\ell = 0$

The resulting angular distribution includes contributions up to spin-two in the lepton partial waves. Summing and squaring gives an angular distribution of the usual form

$$I_{K_2} \sim \sum_{l_K, l_\ell, m} \mathrm{Re}\left[G_m^{l_K,l_\ell} \Omega_m^{l_K,l_\ell}\right] , \tag{5.17}$$

with $0 \leq l_\ell \leq 4$, $l_K = 0, 2, 4$ and $0 \leq m \leq \min[l_K, l_\ell]$. In total there are 32 separate angular coefficients $G_m^{l_K,l_\ell}$ emerging from the operator set above, independent of lepton mass corrections or the presence of scalar/pseudoscalar operators.[6]

The angular distribution can be split into three classes of contribution:

1. Observables that would emerge without the presence of spin-two operators but are modified in their presence, of which there are nine: $G_0^{0,0}$, $G_0^{0,2}$, $G_0^{2,0}$, $G_0^{2,2}$, $G_1^{2,2}$, $G_2^{2,2}$, $G_0^{4,2}$, $G_1^{4,2}$, $G_2^{4,2}$.

2. Observables that cannot be generated due to interference terms between SM and spin-two operators, of which there are also nine, namely $G_0^{0,4}$, $G_0^{2,4}$, $G_1^{2,4}$, $G_2^{2,4}$, $G_0^{4,4}$, $G_1^{4,4}$, $G_2^{4,4}$, $G_3^{4,4}$, and $G_4^{4,4}$.

3. Observables generated strictly from the mixing of SM operators and spin-two contributions, of which there are 14. All these observables have an odd value of l_ℓ, and complete the set of observables.

The full general angular distribution in the presence of all operators considered in this chapter and the effective Hamiltonian (2.42) is exceedingly lengthy. As this is only a preliminary study, only the results for some of the new observables are presented below, focusing in particular on the higher structures that might arise. Only the terms arising from the spin-two V-type operator are presented, although the extension to A-type operators including mixing is natural. Results for the $G_m^{l_K,l_\ell} = \mathcal{N} q^4 \mathbb{G}_m^{l_K,l_\ell}$ are

$$\mathbb{G}_4^{4,4} = -\frac{192}{35} H_{2,2}^{t_1,V} \bar{H}_{2,-2}^{t_1,V} ,$$

[6] This counting is based on no further assumptions about the form of the hadronic HAs. For the explicit expressions given in (5.15) the observables in (5.18) with $m = 3, 4$ also vanish, reducing the count of angular coefficients by three.

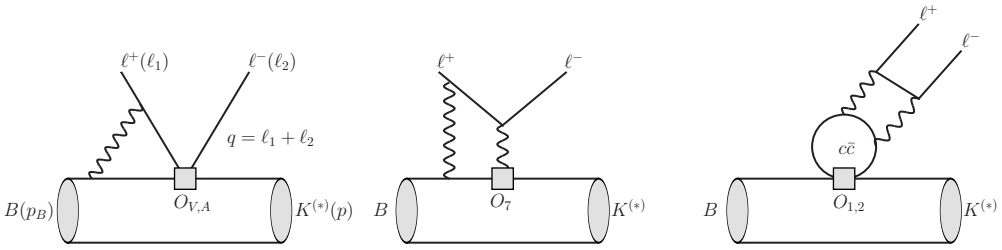

Figure 5.2 *Examples of virtual QED corrections to $B \to K\ell^+\ell^-$, where either a photon is exchanged between the decaying b-quark and a final state lepton, with effective operators $O_{V,A}$ (left) and O_7 (middle), or a second photon is emitted by the charm loop (right). Other topologies relevant for higher moments include the interaction of the leptons with the spectator as well as the B- and $K^{(*)}$-meson.*

$$
\begin{aligned}
\mathbb{G}_3^{4,4} &= -\frac{96}{35}(H_{2,1}^{t_{1,V}}\bar{H}_{2,-2}^{t_{1,V}} + H_{2,2}^{t_{1,V}}\bar{H}_{2,-1}^{t_{1,V}})\,, \\
\mathbb{G}_2^{4,4} &= -\frac{96}{245}(3H_{2,0}^{t_{1,V}}\bar{H}_{2,-2}^{t_{1,V}} + 8H_{2,1}^{t_{1,V}}\bar{H}_{2,-1}^{t_{1,V}} + 3H_{2,2}^{t_{1,V}}\bar{H}_{2,0}^{t_{1,V}})\,, \\
\mathbb{G}_1^{4,4} &= -\frac{96}{245}(H_{2,-1}^{t_{1,V}}\bar{H}_{2,-2}^{t_{1,V}} + 6H_{2,0}^{t_{1,V}}\bar{H}_{2,-1}^{t_{1,V}} + 6H_{2,1}^{t_{1,V}}\bar{H}_{2,0}^{t_{1,V}} + H_{2,2}^{t_{1,V}}\bar{H}_{2,1}^{t_{1,V}})\,, \\
\mathbb{G}_0^{4,4} &= -\frac{48}{1225}(H_{2,-2}^{t_{1,V}}\bar{H}_{2,-2}^{t_{1,V}} + 16H_{2,-1}^{t_{1,V}}\bar{H}_{2,-1}^{t_{1,V}} + 36H_{2,0}^{t_{1,V}}\bar{H}_{2,0}^{t_{1,V}} + 16H_{2,1}^{t_{1,V}}\bar{H}_{2,1}^{t_{1,V}} + H_{2,2}^{t_{1,V}}\bar{H}_{2,2}^{t_{1,V}})\,, \\
\mathbb{G}_2^{2,4} &= \frac{64}{49}\sqrt{\frac{3}{5}}(H_{2,0}^{t_{1,V}}\bar{H}_{2,-2}^{t_{1,V}} - 2H_{2,1}^{t_{1,V}}\bar{H}_{2,-1}^{t_{1,V}} + H_{2,2}^{t_{1,V}}\bar{H}_{2,0}^{t_{1,V}}))/49\,, \\
\mathbb{G}_1^{2,4} &= \frac{32}{49}\sqrt{\frac{6}{5}}(H_{2,-1}^{t_{1,V}}\bar{H}_{2,-2}^{t_{1,V}} - H_{2,0}^{t_{1,V}}\bar{H}_{2,-1}^{t_{1,V}} - H_{2,1}^{t_{1,V}}\bar{H}_{2,0}^{t_{1,V}} + H_{2,2}^{t_{1,V}}\bar{H}_{2,1}^{t_{1,V}})\,, \\
\mathbb{G}_0^{2,4} &= \frac{32}{245}(H_{2,-2}^{t_{1,V}}\bar{H}_{2,-2}^{t_{1,V}} + 2H_{2,-1}^{t_{1,V}}\bar{H}_{2,-1}^{t_{1,V}} - 6H_{2,0}^{t_{1,V}}\bar{H}_{2,0}^{t_{1,V}} + 2H_{2,1}^{t_{1,V}}\bar{H}_{2,1}^{t_{1,V}} + H_{2,2}^{t_{1,V}}\bar{H}_{2,2}^{t_{1,V}})\,, \\
\mathbb{G}_0^{0,4} &= -\frac{16}{175}(H_{2,-2}^{t_{1,V}}\bar{H}_{2,-2}^{t_{1,V}} - 4H_{2,-1}^{t_{1,V}}\bar{H}_{2,-1}^{t_{1,V}} + 6H_{2,0}^{t_{1,V}}\bar{H}_{2,0}^{t_{1,V}} - 4H_{2,1}^{t_{1,V}}\bar{H}_{2,1}^{t_{1,V}} + H_{2,2}^{t_{1,V}}\bar{H}_{2,2}^{t_{1,V}})\,.
\end{aligned}
\tag{5.18}
$$

The expressions presented above, along with the method outlined in the previous chapter to compute more general observables in these decays, should prove helpful in studying the more complete angular distribution in the full presence of mass effects and other operators.

5.5 Distinguishing higher-spin corrections from QED effects

While the inclusion of higher partial waves (from the introduction of higher spin operators or from considering higher resonances in the $(K\pi)$ channel) is one way to modify the angular distributions seen so far, both of these effects were still considered in the context of the LFA. It is worth briefly discussing the consequences of breaking the LFA, and how one might distinguish this effect from the inclusion of higher-spin contributions at the operator level.

The $B \to K\ell^+\ell^-$ channel provides a simplified set-up for this discussion, and is of particular relevance because of the recent LHCb measurement of R_K, that showed a deviation from the SM prediction of $R_K = 1$ [132, 158] at the level of 3σ [19].

In the LFA (4.49), the single opening angle θ_ℓ of the decay is restricted to $l_\ell \leq 2$ moments in $I_K^{(0)}$ (4.53). More precisely, $l_\ell \leq 2j$ with $O^{(j)}$ as in (5.2) (see also the discussion following equation (4.36)). From the viewpoint of a generic $1 \to 3$ decay, there is no reason for this restriction, as it is only the sum of the total (orbital and spin) angular momentum that is conserved. However, in the LFA, the $B \to K[\ell^+\ell^-]$ decay mimics a $1 \to 2$ process, imposing this constraint. This pattern is broken by exchanges of electroweak bosons (especially the γ), as depicted in figure 5.2 for operators relevant to the decay. The W and Z are too heavy to impact on the matrix elements, but their effect will be included in the Wilson coefficients.

Nevertheless, generic QED corrections will turn the decay into a true $1 \to 3$ process, and this necessitates a reassessment of the kinematics. By crossing, the process can be written as a $2 \to 2$ process

$$B(p_B) + \ell^-(-\ell_1) \to K(p) + \ell^-(\ell_2) \,, \tag{5.19}$$

with Mandelstam variables $s = (p + \ell_2)^2$, $t = (\ell_1 + \ell_2)^2 = q^2$ and $u = (p + \ell_1)^2$, and explicitly

$$s[u] = \frac{1}{2}\left[(m_B^2 + m_K^2 + 2m_\ell^2 - q^2) \pm \beta_\ell \sqrt{\lambda\,(m_B^2, m_K^2, q^2)}\cos\theta_\ell\right] \,, \tag{5.20}$$

obeying the Mandelstam constraint $s + t + u = m_B^2 + m_K^2 + 2m_\ell^2$. Importantly,

the kinematic variables s and u become *explicit* functions of the angle θ_ℓ. In a generic computation these variables enter (poly)logarithms that, when expanded, give contributions to any order l_ℓ in the Legendre polynomials. This statement applies at the amplitude level and therefore also to the decay distribution (4.50), which becomes a sum over all values of l_ℓ:

$$\frac{d^2\Gamma(B \to K\ell^+\ell^-)}{dq^2\ d\cos\theta_\ell} \;=\; \sum_{l_\ell \geq 0} G^{(l_\ell)} P_{l_\ell}(\cos\theta_\ell)\ . \tag{5.21}$$

The $B \to K\ell\ell$ moments are given by

$$M_{\bar{\ell}\ell}^{(l_\ell)} = \int_{-1}^{1} d\cos\theta_\ell P_{l_\ell}(\cos\theta_\ell) \frac{d^2\Gamma(B \to K\ell^+\ell^-)}{dq^2\ d\cos\theta_\ell} = \frac{1}{2l_\ell + 1} G_{\bar{\ell}\ell}^{(l_\ell)}\,, \tag{5.22}$$

where the lepton subscript has been introduced for further reference later. In the SM, the effects are dependent on the lepton mass, for example through logarithms of the form $\alpha \ln(m_\ell/m_b)$, where α is the fine structure constant. There are new qualitative features, of which it is worth highlighting the following two:

- Both vector and axial couplings $\mathcal{O}_{V(A)} = \mathcal{O}_{9(10)}$ (2.42) contribute to any moment $l_\ell \geq 0$. In the LFA, l_ℓ-odd terms (which measure forward-backward asymmetries) arise from broken parity through interference of O_V and O_A (2.42). The physical interpretation is that there is a preferred direction for charged leptons in the presence of the charged quarks of the decay. In the specific diagram, on the left of figure 5.2, the charge of the b-quark attracts or repels the charged lepton(s) with definite preference. It is possible that one can establish a higher degree of symmetry by using charge-averaged forward-backward asymmetries.

- A key question is how the moments vary in l_ℓ. Absent a full computation, a precise answer is not possible. Nevertheless, it is insightful to address the question semi-quantitatively by considering, for example, the triangle graph that would emerge from the exchange of a photon between either lepton and the b-quark (on the left of figure 5.2), along with the corresponding graph for the s-quark). Neglecting the Dirac structures and any further information, one can expect the resulting loop integral to include contributions proportional to $C_0(m_\ell^2, p_B^2, s[\cos\theta_\ell], m_\ell^2, 0, m_b^2)$.[7] Expanding this function

[7]This analysis can be refined by taking into account that the b- and s-quark only carry a fraction of the momentum of the corresponding mesons. This amounts to the substitution $p_B^2 \to (p_B - xp)^2$ and $s[u] \to (\ell_2[\ell_1] + xp)^2$, where x is the momentum fraction carried by

in partial waves $C_0 = \sum_{l_\ell \geq 0} C_0^{(l_\ell)} P_{l_\ell}(\cos\theta_\ell)$ shows that there is a fall-off of $|C_0^{(l_\ell)}|$ with increasing l_ℓ. Averaging over several configurations (cf. footnote 7), one can conclude that the $l_\ell = 2$ (D-wave) contribution is suppressed by approximately a factor of 2 with respect to $l_\ell = 0$, with a slightly steeper fall-off with increasing l_ℓ for the b-quark versus s-quark vertex correction. The graph where the photon couples to the other lepton comes with a different Dirac structure, and is not obtainable through a straightforward symmetry prescription; therefore, it is sensible to consider those graphs separately. It is important to stress that this semi-quantitative analysis does not replace a complete QED computation, which would include corrections to Wilson coefficients, all virtual corrections, and the real photon emission.

The most important consideration is the relative size of the QED corrections as compared with those arising from higher spin operators. In the SM, one expects QED effects to dominate over those due to higher spin operators, except for $j = 2$ where they could be comparable.

The discussion of $B \to K^*(\to K\pi)\ell^+\ell^-$ is similar, but involves the kinematics of a $1 \to 4$ decay. The decay distribution becomes a generic function of all three angles θ_ℓ, θ_K and ϕ. It should be added that the selection of the $K^* \to K\pi$ signal (P_K-wave) restricts $l_K = 0, 2$.

5.5.1 Diagnosing QED background to R_K

Given the predictions of the standard dimension-six effective Hamiltonian, throughout this chapter it has been stressed that probing for moments that are vanishing in the decay distributions $I_{K^*}^{(0)}$ (4.36) of $\bar{B} \to \bar{K}^*(\to K\pi)\ell\bar{\ell}$ and $I_K^{(0)}$ (4.49) of $\bar{B} \to \bar{K}\ell\bar{\ell}$ respectively is of high importance. These clean predictions of vanishing higher moments provide an important signal for NP effects, or of corrections emerging from other sources. One particular case where such observations may provide further insight is in tests for lepton universality, as explained further in what follows.

In the SM, the decays $B^+ \to K^+e^+e^-$ and $B^+ \to K^+\mu^+\mu^-$ are identical up to

the s-quark. For the vertex diagrams, one expects the Feynman mechanism (i.e. $x \simeq 0$) to dominate. This changes when spectator corrections are taken into account.

phase-space lepton mass effects and electroweak corrections. The observable

$$R_K|_{[q^2_{\rm min},q^2_{\rm max}]} \equiv \frac{\mathcal{B}(B^+ \to K^+\mu^+\mu^-)}{\mathcal{B}(B^+ \to K^+e^+e^-)}\Big|_{[q^2_{\rm min},q^2_{\rm max}]} \tag{5.23}$$

was put forward in [159] as an interesting test of lepton flavour universality. Above, $q^2_{\rm min/max}$ stands for the bin boundaries. Neglecting electroweak corrections, the SM prediction is $R_K|_{[1,6]\,\rm GeV^2} \simeq 1.00(1)$ [132, 158], which is at 2.6σ-tension with the LHCb measurement at 3fb^{-1} [19]

$$R_K = 0.745^{+0.090}_{-0.074}(\text{stat}) \pm 0.036(\text{syst}) \; . \tag{5.24}$$

Previous measurements [160, 161], with much larger uncertainties, were found to be consistent with the SM as well as (5.24). This led to investigations of physics beyond the SM with $C_9^{\bar{e}e} \neq C_9^{\bar{\mu}\mu}$ (where $O_9^{\bar{\ell}\ell} \equiv \bar{b}\gamma_\alpha s\bar{\ell}\gamma^\alpha\ell$) (eg [50, 162–170], along with [171] for further references).

As outlined above, QED corrections break the LFA, and therefore give rise to higher moments. Such corrections have a clear dependence on lepton mass through logarithmic terms $\alpha\ln(m_\ell/m_b)$. However, the QED corrections will also impact the predicted value of R_K.

In view of the lack of a full QED computation,[8] it may be insightful to diagnose the size of QED corrections, as well as their lepton dependence, by experimentally assessing higher moments, where the impact of the QED correction is more readily distinguishable from other effects.

5.6 Conclusions

This chapter has presented some preliminary studies of the impact of spin-two operators, and their origin, on the angular distributions of $B \to K_J(\to K\pi)\ell_1\bar{\ell}_2$ type decays. The number of terms in the angular distribution in the presence of spin two operators grows markedly larger, but the new structures that emerge can be naturally understood in the formalism developed in the previous chapter.

The principal results of this chapter are in the new HAs for the spin-two derivative operators $\mathcal{O}_{\partial;V(A)}$, and their contribution to the new angular observables, presented in equation (5.18). These preliminary expressions do not capture the

[8] A partial result, photon emission from the initial and final state, was reported in [172].

full complexity of the new distribution in the presence of non-zero (or non-equal) lepton masses and the full operator set. However, as within the SM it is not difficult to deduce that the size of such new operators must be small with respect to the dimension-six operators (by a factor of order $1/m_W^2$), the most important prediction is that such higher-spin operators are almost zero in the SM. The main purpose of considering higher-spin operators is that they imply that new angular observables, in the form of higher moments, can provide a new window on possible corrections to the usual theoretical predictions for the $B \to K_J(\to K\pi)\ell_1\bar{\ell}_2$ decays.

The key motivation of all such studies is the apparent discrepancy between various SM predictions of, in particular, R_K [19] and P_5' [20], which raise the possibility that there are New Physics effects in the $b \to s$ transitions. Regardless of the origin of these anomalies, it is clear that the study of related decay channels will aid in understanding their nature. Such channels would naturally include higher resonances of the Kaon, with the $K_2(1430)$ discussed above being a prime example; but it is important to emphasise that *all* related $b \to s$ decays can be understood and analysed within the formalism developed in this chapter and the preceding one.

Although this chapter has refrained from making concrete theoretical predictions, the proposal of studying higher moments of these decays is still worth stressing as a valuable new approach to the decays. Hopefully, the LHCb analysis of [139] marks only the first step in a more systematic study of the Kaon resonances and their apparent anomalies.

Chapter 6

Three-particle sum rules for vector and axial mesons

The dominant contribution to $B \to V\gamma/\ell\bar{\ell}$ decays within the SM is given by the short-distance (SD) physics of the effective Hamiltonian in (2.35). It is, however, clear that the effect of long-distance (LD) contributions needs to be properly understood, and disentangled from the SD behaviour, in order to search for any NP contributions to these processes. Understanding such LD contributions, in turn, requires a more complete understanding of the structure of mesons. It became clear over the 1980s and 1990s [173] that the leading behaviour of mesons (equivalent to the leading, twist-2, DAs) was not necessarily enough on its own to understand these processes.

The first systematic studies of the twist-3 and twist-4 DAs of vector mesons were performed at the end of the 1990s [82, 83]. It was, however, not until some time later [85, 103] that results including the corrections necessary to distinguish ρ, K^*, and ϕ mesons ($SU(3)_F$-breaking corrections) were included.

Separately, there is the question of understanding the related structure of the axial mesons. Owing to the experimental difficulties of studying axial meson decays (the decay chains typically include more hadrons in the final state, for example), these have received less attention. Currently, the most comprehensive study of axial twist-3 DAs available is in [104], and it seems that twist-4 results are still not available.

This chapter presents a fresh calculation of the twist-3 DAs for both vector and

axial mesons, including new numerical estimates of the parameters. For the first time, the contribution of the three-gluon condensate is included. While this is small for the leading parameters, it nevertheless can have some effect on higher moments in the conformal expansion. In addition, the results in this chapter explicitly show the relationships between vector and axial DAs that appear not to have been exploited in previous computations. Analytic expressions for the twist-4 DAs are presented in appendix D, although results for the tensor contributions will also be necessary to probe the full behaviour of twist-4 parameters. A separate computation, using diagonal sum rules, is presented in appendix E.

As will be shown in the following chapter, these results are also important in the computation of long-distance charm-loop contributions to $B \to (V, A)\gamma$ decays.

Material related to this chapter is to be published in [174].

6.1 Definitions of the sum rules

Throughout this analytic section, vector mesons will be denoted ρ and axial mesons $\tilde{\rho}$, while the current template will be in terms of K^* mesons. The advantage of the latter choice is that the distinction between the origins of terms proportional to quark masses and condensates will be clear. Results for the physical ρ particle then follow from the replacements $m_s \to m_q$ and $\langle \bar{s}s \rangle \to \langle \bar{q}q \rangle, \langle \bar{s}\sigma \cdot Gs \rangle \to \langle \bar{q}\sigma \cdot Gq \rangle$, and vice-versa for the physical ϕ meson.

The starting point for the non-diagonal sum rules in this chapter is the correlation function of the general form

$$(\Pi^{\chi}_{\mathcal{G}})_{\alpha\beta\alpha'\beta'} \;=\; i \int d^4y e^{-ip\cdot y} \langle 0 | \mathcal{T} \left\{ (J^{\chi}_{\mathcal{G}}(z, vz, 0))_{\alpha\beta}\, \bar{s}\, \Gamma^{\chi}_{\alpha'\beta'}\, q(y) \right\} |0\rangle \,, \quad (6.1)$$

where the currents $(J^{\chi}_{\mathcal{G}}(z, vz, 0))_{\alpha\beta} \equiv \bar{q}(z)\mathcal{G}_{\alpha\beta}(vz)\chi s(0)$ are defined in tables 3.1 and 3.2, for the ρ and $\tilde{\rho}$, respectively. The quantity $\mathcal{G}_{\alpha\beta}$ represents either the gluon field or its dual, with the choice being fixed by the current and meson of interest, according to tables 3.1 and 3.2. In this way, it is possible to compute the correlation function of all sum rules simultaneously, and choose the correct configuration of Lorentz structure χ and gluon field $\mathcal{G}$ as inputs to extract the relevant sum rule. The structures Γ are imposed by the choice of χ and the parity of the meson in question, with a more precise definition given according to the right-hand column in tables 3.1 and 3.2. Note also that the index β' is redundant

in the twist-3 V, A case.

The definition (6.1) can be used to compute twist-3 and twist-4 sum rules, but in either case the relevant structure must be projected out and the correct twist obtained. For the twist-3 sum rules, this can be achieved using the projector

$$P_3 = \frac{1}{(p\cdot z)^2(2-d)} g^{\perp}_{\alpha\alpha'} z_\beta z_\mu \,, \tag{6.2}$$

which follows from [85].

After the projections, and following the contributions below, the final relation

$$\Pi^{\chi}_{\mathcal{G}}(pz, p^2) = \int \mathcal{D}\underline{\alpha} e^{-ipz(\alpha_2 + v\alpha_3)} \pi^{\chi}_{\mathcal{G}}(\underline{\alpha}, p^2) \,, \tag{6.3}$$

defines the π, in terms of which the results will be presented. The exponential factor follows from the definition of the three-particle DAs, and it is vital to ensure that any residual exponentials in intermediate calculations are matched onto the standard form in (6.3). This will be illustrated in more detail in the calculations for the perturbative contribution. Results for the π for all DAs will be presented in 6.3.

The contributions considered for this calculation are the perturbative contribution, as well as all condensates up to dimension six. This includes, for the first time, the three-gluon condensate, which was previously neglected in non-diagonal computations [85, 103, 104]. The necessary non-local expansions for these condensates are presented in appendix A, and can also be found in [175, 176].

Using the definitions of the currents in tables 3.1 and 3.2, it is possible to calculate both the vector and axial meson sum rules separately. However, the results for vector and axial mesons are related by simple transformations. Specifically, terms proportional to m_s, $\langle \bar{s}s \rangle$, and $\langle \bar{s}\sigma \cdot Gs \rangle$, as defined below, all change sign separately – so that contributions arising from products $m_s \langle \bar{s}s \rangle$ do not change sign between vector and axial contributions. The four-quark condensates are also sensitive to this transformation, as will be made explicit by the results, but the summary is that, when transferring between the results of vector and axial mesons, the condensates $\langle V^a V^a \rangle$ and $\langle A^a A^a \rangle$ interchange, as do $\langle S^a S^a \rangle$ and $\langle P^a P^a \rangle$. This result follows from the chiral restoration limit [36, 174], but was computed explicitly for this thesis.

The following section describes how to compute the individual contributions.

Throughout this chapter, the notation $\bar{u} \equiv 1 - u$ has been used, where u stands for any parameter that ranges between the values 0 and 1.

6.2 Contributions to three-particle non-diagonal sum rules

6.2.1 Perturbative Contribution

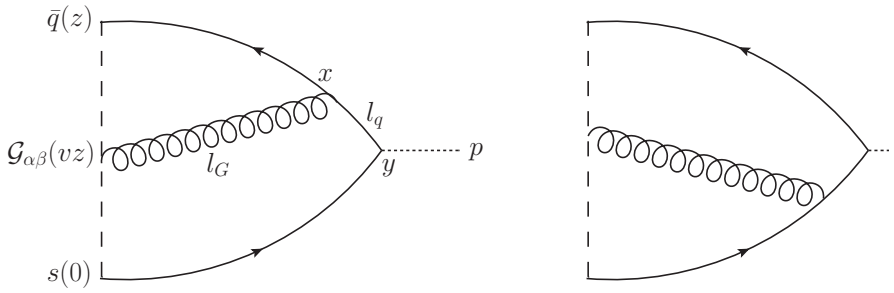

Figure 6.1 *Perturbative contributions to the non-diagonal sum rules. The left-hand diagram has also been annotated with key features to make the meaning of the diagram more transparent. In this, and all future diagrams, the s-type quark terms are along the bottom of the diagram, and the q-type quark terms along the top. The local part of the matrix element* (6.1) *is at the right, where a momentum insertion p has been indicated. At the left of the diagram is the non-local part of the matrix element* (6.1)*, which, by convention, runs from* 0 *to z. The choice of* $-z$ *to z can also be made, which serves as a useful cross-check of the calculations, as well as emphasising the symmetry of the results. The definitions of loop momenta in the perturbative diagram, and their respective propagators, have also been indicated, clarifying the result in* (6.6)*.*

The perturbative contribution arises from the diagrams in figure 6.1. Following the notation, the left-hand diagram corresponds to the expression

$$(\Pi^{\chi}_{\mathcal{G}})_{pert.} = \; i \int d^4y d^4x \, e^{-ip\cdot y} \langle 0|\mathcal{T} \left\{ \overbrace{\bar{q}(z)\mathcal{G}_{\alpha\beta}(vz)\chi \overbrace{s(0)\bar{s}}(y)\,\Gamma^{\chi}_{\alpha'\beta'}\, \overbrace{q(y)\bar{q}}(x) \not{A}(x) q(x)} \right\} |0\rangle \,, \tag{6.4}$$

where the necessary Wick contractions have been indicated. To deal with the gluon propagator, it is helpful to write $G_{\alpha\beta} = g_{\mu\alpha} g_{\nu\beta} G^{\mu\nu}$, so that both the gluon

field and its dual can be handled at once. The information about the type of gluon field in the correlation function of interest is then contained in the Lorentz structure

$$\mathcal{L}^{\mathcal{G}}_{\alpha\beta\mu\nu} = \begin{cases} g_{\mu\alpha}g_{\nu\beta}\,, & \mathcal{G}_{\alpha\beta} = G_{\alpha\beta}\,, \\ \frac{i}{2}\epsilon_{\alpha\beta\mu\nu}\,, & \mathcal{G}_{\alpha\beta} = \tilde{G}_{\alpha\beta}\,. \end{cases} \tag{6.5}$$

Performing the Wick contractions and the spatial integrals leads to the general expression

$$\begin{aligned}\Pi^{\chi}_{\Gamma} = 16\pi\alpha_s i\mathcal{L}^{\mathcal{G}}_{\alpha\beta\mu\nu}\int_{l_G,l_q}\frac{l_G^{\mu}g^{\nu\tau} - l_G^{\nu}g^{\mu\tau}}{l_G^2 + i\epsilon}\Big(e^{iz\cdot(\bar{v}l_G+l_q)}\mathrm{Tr}\left[S_q(l_q+l_G)\chi S_s(l_q+p)\Gamma S_q(l_q)\gamma_\tau\right] \\ + e^{-iz\cdot(vl_G-l_q+p)}\mathrm{Tr}\left[S_q(l_q-p)\chi S_s(l_q-l_G)\gamma_\tau S_s(l_q)\Gamma\right]\Big)\,,\end{aligned} \tag{6.6}$$

where l_G is the momentum in the gluon field and l_q the most convenient choice of momentum in the quark propagators. The first term corresponds to the diagram on the left of figure 6.1, which should clarify the notation. The fermion propagators are defined in appendix A.4.3, and for the perturbative contribution only the leading part of the propagator is required. This is a two-loop calculation, but can be factorised into two separate one-loop integrals, and the necessary general integral results are presented in appendix A.4.1. The choice of loop momentum assignments has been made to correspond to the general integrals therein.

After the loop integration, care must be paid to terms proportional to $p\cdot z$. These can be dealt with by partial integration, with the replacement rules

$$\begin{aligned}\{\bar{v},-v\}p\cdot zF(u_1,u_2) &\to -\frac{i}{\bar{u}_2}\frac{\partial}{\partial u_1}F(u_1,u_2)\,,\\ \left(\{\bar{v},-v\}p\cdot z\right)^2F(u_1,u_2) &\to \left(-\frac{i}{\bar{u}_2}\frac{\partial}{\partial u_1}\right)^2F(u_1,u_2)\,,\\ \{-(1-\bar{v}\bar{u}_1),(1-v\bar{u}_1)\}p\cdot zF(u_1,u_2) &\to -i\frac{\partial}{\partial u_2}F(u_1,u_2)\,,\\ \left(\{-(1-\bar{v}\bar{u}_1),(1-v\bar{u}_1)\}p\cdot z\right)^2F(u_1,u_2) &\to \left(-i\frac{\partial}{\partial u_2}\right)^2F(u_1,u_2)\,,\\ \{-\bar{v}(1-\bar{v}\bar{u}_1),-v(1-v\bar{u}_1)\}p\cdot z^2F(u_1,u_2) &\to -\frac{1}{\bar{u}_2}\frac{\partial}{\partial u_1}\frac{\partial}{\partial u_2}F(u_1,u_2)\,,\end{aligned} \tag{6.7}$$

where u_i are the Feynman parameters for the first and second loop integrals. The

last line can arise from mixed linear terms from the two loop integrals, and the u_2 derivative does not act on the $\frac{1}{\bar{u}_2}$ factor, which is why it has deliberately been placed outside the partial derivatives.

After all loop integrals and derivatives have been performed, the residual exponential must be matched to the "canonical form" (6.3). In this case, this is equivalent to changing variables from the Feynman parameters u_i to the DA parameters α_i. The two diagrams require a separate, but consistent, treatment. The residual exponentials from the non-local integrals in equations (A.26–A.28) are $e^{-ipz\bar{u}_2(1-\bar{v}\bar{u}_1)}$ for the diagram on the left in figure 6.1, and $e^{-ipz(1-\bar{u}_2(1-v\bar{u}_1))}$ for the diagram on the right in figure 6.1. These can be matched to the canonical form $e^{-ipz(\alpha_2+v\alpha_3)}$ by

$$\begin{aligned} e^{-ipz\bar{u}_2(1-\bar{v}\bar{u}_1)} &= \int \mathcal{D}(\alpha)\delta(\alpha_1-u_2)\delta(\alpha_2-u_1\bar{u}_2)\delta(\alpha_3-\bar{u}_1\bar{u}_2)e^{-ipz(\alpha_2+v\alpha_3)}\,, \\ e^{-ipz(1-\bar{u}_2(1-v\bar{u}_1))} &= \int \mathcal{D}(\alpha)\delta(\alpha_2-u_2)\delta(\alpha_1-u_1\bar{u}_2)\delta(\alpha_3-\bar{u}_1\bar{u}_2)e^{-ipz(\alpha_2+v\alpha_3)}\,. \end{aligned} \tag{6.8}$$

These results (which correct those presented in [70]) correspond to the choice of Feynman parameter u_2 switching from either the top or bottom quark line. The third δ function above encodes the rule $\alpha_1+\alpha_2+\alpha_3=1$. One can then perform the integrals over u_1 and u_2 using the delta functions, and the final result for the perturbative contribution is

$$\begin{aligned} &\int du_1 du_2 e^{-ipz\bar{u}_2(1-\bar{v}\bar{u}_1)}F_1(u_1,u_2) + e^{-ipz(1-\bar{u}_2(1-v\bar{u}_1))}F_2(u_1,u_2) \\ &= \int \mathcal{D}(\alpha)e^{-ipz(\alpha_2+v\alpha_3)}\left(\frac{1}{\bar{\alpha}_1}F_1(\frac{\alpha_2}{\bar{\alpha}_1},\alpha_1)+\frac{1}{\bar{\alpha}_2}F_2(\frac{\alpha_1}{\bar{\alpha}_2},\alpha_2)\right)\,, \end{aligned} \tag{6.9}$$

where F_1 and F_2 are the general structures arising from loop integrations in the diagrams on the left and right of figure 6.1 respectively.

Results for the perturbative contribution are presented in the full results section later; here, it is worth noting that the expressions presented therein do not include quark mass corrections, unlike the results in [85]. However, as will be seen in the numerical analysis, the perturbative contribution is far from the leading contribution to these sum rules, and these higher-order corrections are not significant enough to impact the results. Such corrections can, in principle, be included by considering only quark mass contributions from the numerator of the propagator, in which case the integral expressions in equations (A.26–A.28)

will be of use in including these corrections in future work.

6.2.2 Gluon Condensates

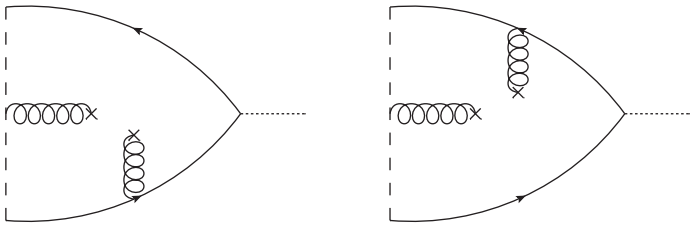

Figure 6.2 *Two-gluon condensate contribution to the non-diagonal sum rules. As before, the s-quark is at the bottom and the q-quark at the top of each diagram. The fermion propagators have been taken to second order in the background field gauge, as found in appendix A.4.3.*

From the correlation function (6.1) with the gluon field $\mathcal{G}^{\alpha\beta}$ open, it follows that

$$(\Pi^{\chi}_{\mathcal{G}})^{\alpha\beta} = i \int d^4y\, e^{-ip\cdot y} \mathrm{Tr}\left[S_q(y,z)\chi S_s(0,y)\Gamma^{\chi}\right] \mathcal{G}^{\alpha\beta}(vz) \tag{6.10}$$

where the definitions of the propagators can be found in appendix A.4.3. The two-gluon condensate then emerges from the first correction terms $S^{(2)}(x,y)$ to each propagator, whereas the three-gluon condensate emerges from terms up to and including $S^{(4)}(x,y)$, along with the second-order expansion in $\mathcal{G}^{\alpha\beta}$. Hence, the two-gluon condensate is given by

$$\begin{aligned}(\Pi^{\chi}_{\mathcal{G}})^{\alpha\beta}\big|_{G^2} = i \int d^4y\, e^{-ip\cdot y} \Big(&\mathrm{Tr}\left[S_q^{(0)}(y,z)\chi S_s^{(2)}(0,y)\Gamma^{\chi}\right] \\ &+ \mathrm{Tr}\left[S_q^{(2)}(y,z)\chi S_s^{(0)}(0,y)\Gamma^{\chi}\right]\Big) \mathcal{G}^{\alpha\beta}(vz)\,,\end{aligned} \tag{6.11}$$

where $S^{(0,2)}$ are defined in (A.33). The three-gluon condensate can be constructed similarly, but requires more terms.

The computation is facilitated by making the identification $y \to i\partial_p$, where the partial derivative acts on the propagators according to (A.33). In practice, derivatives over the external momentum p vanish, as they lead to symmetric contributions contracted with the antisymmetric gluon field. All gluon condensate contributions are proportional to $\delta(\alpha_3)$, representing the fact that the gluon emitted from the non-local operator carries no momentum, and this can be used to match to the exponential (6.3).

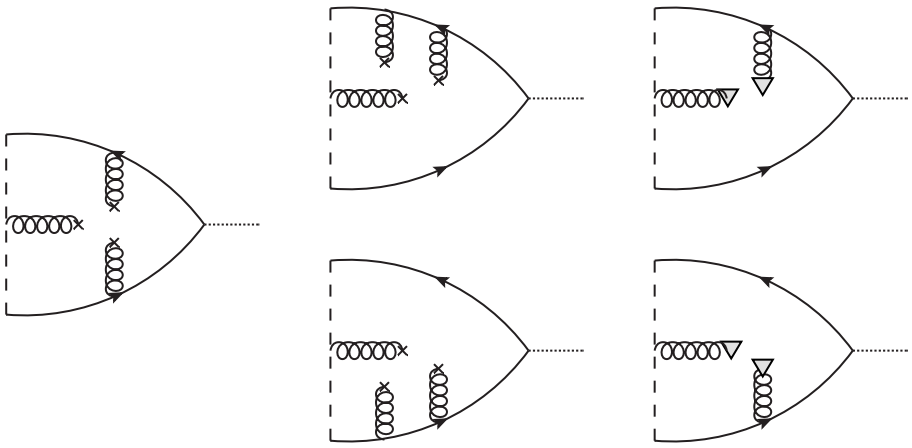

Figure 6.3 *Diagrams representing the various contributions to the three-gluon condensate in non-diagonal sum rules, arising from higher-order corrections to the fermion propagators* (A.33)*. The triangle vertex represents a field expansion, as in* (6.12)*.*

The expansion in $\mathcal{G}^{\alpha\beta}$ deserves attention. It is given by

$$\mathcal{G}^{\alpha\beta}(vz) = \mathcal{G}^{\alpha\beta}(0) + (vz)^\rho \nabla_\rho \mathcal{G}^{\alpha\beta}(0) + \frac{1}{2}(vz)^\rho (vz)^\tau \nabla_\rho \nabla_\tau \mathcal{G}^{\alpha\beta}(0) + \dots \qquad (6.12)$$

After various contractions, and using $z^2 = 0$, then the contributions from expanding $\mathcal{G}^{\alpha\beta}(vz)$ are proportional to $vp \cdot z\delta(\alpha_3)$. Noting that

$$vp \cdot z e^{-ip\cdot z(\alpha_2 + v\alpha_3)} = i\partial_{\alpha_3} e^{-ip\cdot z(\alpha_2+v\alpha_3)} \qquad (6.13)$$

means that, again, extra factors of $p\cdot z$ can be dealt with using partial integration to derive the replacement rules

$$\begin{aligned} vp \cdot z\delta(\alpha_3)\bar{\delta} e^{-ip\cdot z(\alpha_2+v\alpha_3)} &\to -i\partial_{\alpha_3}(\delta(\alpha_3)\bar{\delta}) e^{-ip\cdot z(\alpha_2+v\alpha_3)} \,, \\ p \cdot z\delta(\alpha_2)\bar{\delta} e^{-ip\cdot z(\alpha_2+v\alpha_3)} &\to -i\partial_{\alpha_2}(\delta(\alpha_2)\bar{\delta}) e^{-ip\cdot z(\alpha_2+v\alpha_3)} \,, \end{aligned} \qquad (6.14)$$

where $\bar{\delta} = \delta(1-\alpha_1-\alpha_2-\alpha_3)$. Similarly, the second-order term in (6.12) can be related to $\delta''(\alpha_3)$. However, this contribution ends up vanishing, as it picks up only the symmetric contribution to the relevant condensate (A.12), leading to a term proportional to $z^2 = 0$. Hence only the first-order expansion to $\mathcal{G}^{\alpha\beta}(vz)$ survives in the end.

The final diagrams for both two- and three-gluon condensates arise from non-local one-loop integrals, and the expression in (A.26) can be used to obtain the final expressions.

Results for the two- and three-gluon condensates are given alongside the remaining contributions in section 6.3. The two-gluon results are available for non-local twist-3 sum rules in [85]. Results for the three-gluon condensate are new, and were previously neglected as, for the leading DA parameters, they were only $\mathcal{O}(1\%)$ contributions. Numerical results show that, for higher moments in the DA, the three-gluon contribution can be more significant, and it is thus worth including.

In comparing results with previous calculations, it seems that there is a typo in [85]: in the denominator for the two-gluon condensate in equations (C.4 - C.6), α_1 and α_2 should be interchanged. The Feynman parameter for the integrals above, u, can be identified with α_2 following the same procedure as in the perturbative calculation.

6.2.3 Two-quark condensates

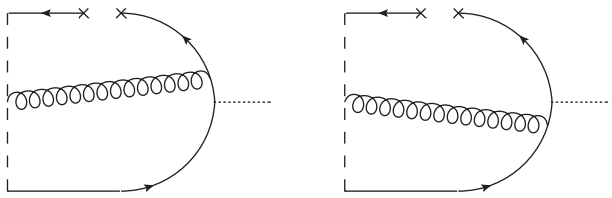

Figure 6.4 *Diagrams leading to two-quark condensate contributions.*

The two-quark contribution arises from the diagrams in figure 6.4, which are also non-local one-loop integrals. The two-quark condensate has the expansion given in the appendix in equation (A.16), and can also be found in [175]. Care must be taken to deal with the divergences correctly, as the second diagram in figure 6.4 has a subdivergence that must be subtracted. Final contributions are associated with a δ function, depending on which quark condenses. Specifically, the condensate $\langle \bar{s}s \rangle$ is associated with $\delta(\alpha_1)$ terms, and $\langle \bar{q}q \rangle$ with $\delta(\alpha_2)$.

In higher-twist computations, it is also possible for additional $p \cdot z$ factors to appear. These can be dealt with via partial integration, as was shown in the previous section, and lead to contributions proportional to derivatives acting on the moments. All such terms vanish at twist-3, but are relevant for the twist-4 results.

Results are in disagreement with those in [85], as shown in equations (C.4 - C.6)

therein. There are strong reasons to prefer the present calculation, as the results are more symmetric than those obtained in the previous calculation.

6.2.4 Four-quark and mixed condensates

The four-quark condensate contribution to the sum rules in fact emerges from two types of contribution. The first type also includes the mixed condensate, and is depicted in Fig. 6.5. This leads to the condensate $\langle \bar{q}(x_1)\mathcal{G}^{\alpha\beta}(y)q(x_2)\rangle$,

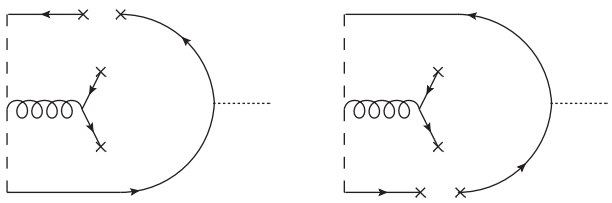

Figure 6.5 *Four quark condensates of the first kind. Such contributions are fixed in the change from vector to axial mesons, although the related mixed condensates are sensitive to the change according to the rules given for the two-quark condensates.*

or its equivalent for the s-quark, where $x_1 \to (z, y)$, $x_2 \to (y, 0)$ and $z \to vz$, respectively. The expansion for this condensate is given in equation (A.17). The y variable can be replaced with a momentum derivative via partial integration, whereas the terms proportional to z ultimately vanish under projection as they go as $z^2 = 0$. The final results are proportional to $\delta(\alpha_3)\delta(\alpha_{1,2})$ depending on which quark is in the condensate, as the only momentum transfer is through the propagating quark.

Terms proportional either to $p\cdot z$ or to $vp\cdot z$ can be traded for derivative terms by partial integration, and this will be important in results for twist-4 DAs. Initially, it seems that the two diagrams lack an $\alpha_1 \leftrightarrow \alpha_2$ exchange symmetry, but this is an artefact of choosing the asymmetric configuration $\bar{q}(z)\mathcal{G}^{\alpha\beta}(vz)s(0)$. Setting $s(0) \to s(-z)$ restores the symmetry, and serves as a useful cross-check.

The second type of contribution proceeds from the diagram in Fig. 6.6. The calculation is standard, as the diagrams are tree-level, and all non-zero contributions are proportional to $\delta(\alpha_1)\delta(\alpha_2)$. In computing these diagrams the spin sum (A.19) proves useful.

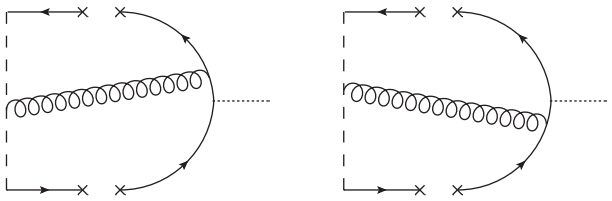

Figure 6.6 *Four-quark condensates of the second kind. Such contributions are sensitive to the change from vector to axial mesons.*

6.3 Analytic results

The final expressions for the correlation function (6.1) are formed by the sum of all contributions considered above. Recalling the definition

$$\Pi_{\mathcal{G}}^{\chi} = \int \mathcal{D}\underline{\alpha}\, e^{-ip\cdot z(\alpha_2+v\alpha_3)}\pi_{\mathcal{G}}^{\chi} \tag{6.15}$$

then the results for the $\pi_{\mathcal{G}}^{\chi}$, including quark mass corrections to the denominator for the gluon condensates, are, for twist-3 DAs,

$$\begin{aligned}
\pi_G^V &= -\frac{\alpha_s}{4\pi^3}p^2\ln\frac{-p^2}{\mu^2}\left(\alpha_1\alpha_2\alpha_3\left(\frac{1}{\bar\alpha_1}-\frac{1}{\bar\alpha_2}\right)\right)\\
&+\frac{\alpha_1\alpha_2(\alpha_1-\alpha_2)\delta(\alpha_3)}{96\pi^2\mathcal{W}}\langle G^2\rangle+\frac{\alpha_1^2\alpha_2^2\left(2(\alpha_1-\alpha_2)\delta(\alpha_3)\partial_{\alpha_3}\right)}{192\pi^2\mathcal{W}^2}\langle fG^3\rangle\\
&+\frac{1}{3p^2}\frac{\alpha_s}{\pi}\left\{\frac{1+\alpha_3\bar\alpha_3}{2}\left(m_q\langle\bar qq\rangle\delta(\alpha_2)-m_s\langle\bar ss\rangle\delta(\alpha_1)\right)\right.\\
&\left.+\alpha_3\left[1+\alpha_3\left(\ln\left(\alpha_3\bar\alpha_3\right)+\ln\frac{-p^2}{\mu^2}\right)\right]\left(m_s\langle\bar qq\rangle\delta(\alpha_2)-m_q\langle\bar ss\rangle\delta(\alpha_1)\right)\right\}\\
&+\frac{1}{12p^4}\delta(\alpha_3)\left(m_q\langle\bar q\sigma\cdot Gq\rangle\delta(\alpha_2)-m_s\langle\bar s\sigma\cdot Gs\rangle\delta(\alpha_1)\right)\\
&-\frac{2\pi\alpha_s}{3p^4}\delta(\alpha_3)\left(\left\langle V_q^aV_f^a\right\rangle\delta(\alpha_2)-\left\langle V_s^aV_f^a\right\rangle\delta(\alpha_1)\right),\\
\pi_{\tilde G}^A &= -\frac{\alpha_s}{4\pi^3}p^2\ln\frac{-p^2}{\mu^2}\left(\alpha_1\alpha_2\alpha_3\left(\frac{1}{\bar\alpha_1}+\frac{1}{\bar\alpha_2}\right)\right)\\
&+\frac{\alpha_1\alpha_2\delta(\alpha_3)}{96\pi^2\mathcal{W}}\langle G^2\rangle+\frac{\alpha_1^2\alpha_2^2\delta(\alpha_3)\left(1+2\partial_{\alpha_3}\right)}{192\pi^2\mathcal{W}^2}\langle fG^3\rangle\\
&+\frac{1}{3p^2}\frac{\alpha_s}{\pi}\left\{\frac{1-\alpha_3\bar\alpha_3}{2}\left(m_q\langle\bar qq\rangle\delta(\alpha_2)+m_s\langle\bar ss\rangle\delta(\alpha_1)\right)\right.\\
&\left.+\alpha_3\left[1-\alpha_3\left(\ln\left(\alpha_3\bar\alpha_3\right)+\ln\frac{-p^2}{\mu^2}\right)\right]\left(m_s\langle\bar qq\rangle\delta(\alpha_2)+m_q\langle\bar ss\rangle\delta(\alpha_1)\right)\right\}\\
&+\frac{1}{12p^4}\delta(\alpha_3)\left(m_q\langle\bar q\sigma\cdot Gq\rangle\delta(\alpha_2)+m_s\langle\bar s\sigma\cdot Gs\rangle\delta(\alpha_1)\right)
\end{aligned}$$

$$
\begin{aligned}
&+\frac{2\pi\alpha_s}{p^4}\langle A^aA^a\rangle\,\delta(\alpha_1)\delta(\alpha_2)-\frac{2\pi\alpha_s}{3p^4}\delta(\alpha_3)\left(\left\langle V_q^aV_f^a\right\rangle\delta(\alpha_2)+\left\langle V_s^aV_f^a\right\rangle\delta(\alpha_1)\right)\,,\\
\pi_G^T&=-\frac{\alpha_s}{2\pi^3}p^2\ln\frac{-p^2}{\mu^2}\left(\alpha_1\alpha_2\alpha_3\left(\frac{1}{\bar\alpha_1}-\frac{1}{\bar\alpha_2}\right)\right)\\
&+\frac{\alpha_1\alpha_2(\alpha_1-\alpha_2)\delta(\alpha_3)}{48\pi^2\mathcal{W}}\left\langle G^2\right\rangle+\frac{\alpha_1^2\alpha_2^2\left(2(\alpha_1-\alpha_2)\delta(\alpha_3)\partial_{\alpha_3}\right)}{96\pi^2\mathcal{W}^2}\left\langle fG^3\right\rangle\\
&+\frac{2}{3p^2}\frac{\alpha_s}{\pi}\left\{\frac{1}{2}\left(m_q\langle\bar qq\rangle\delta(\alpha_2)-m_s\langle\bar ss\rangle\delta(\alpha_1)\right)\right.\\
&\left.+\alpha_3\left[1+\alpha_3\left(\ln\left(\alpha_3\bar\alpha_3\right)+\ln\frac{-p^2}{\mu^2}\right)\right]\left(m_s\langle\bar qq\rangle\delta(\alpha_2)-m_q\langle\bar ss\rangle\delta(\alpha_1)\right)\right\}\\
&+\frac{1}{6p^4}\delta(\alpha_3)\left(m_q\langle\bar q\sigma\cdot Gq\rangle\delta(\alpha_2)-m_s\langle\bar s\sigma\cdot Gs\rangle\delta(\alpha_1)\right)\\
&-\frac{4\pi\alpha_s}{3p^4}\delta(\alpha_3)\left(\left\langle V_q^aV_f^a\right\rangle\delta(\alpha_2)-\left\langle V_s^aV_f^a\right\rangle\delta(\alpha_1)\right)\,,\\
\pi_{\tilde G}^V&=\pi_{\tilde G}^A\big|_{m_s\langle\bar qq\rangle\to-m_s\langle\bar qq\rangle,m_q\langle\bar ss\rangle\to-m_q\langle\bar ss\rangle,\langle A^aA^a\rangle\to\langle V^aV^a\rangle}\,,\\
\pi_G^A&=\pi_G^V\big|_{m_s\langle\bar qq\rangle\to-m_s\langle\bar qq\rangle,m_q\langle\bar ss\rangle\to-m_q\langle\bar ss\rangle}\,,\\
\pi_{\tilde G}^T&=\pi_G^T\big|_{m_s\langle\bar qq\rangle\to-m_s\langle\bar qq\rangle,m_q\langle\bar ss\rangle\to-m_q\langle\bar ss\rangle}\,,
\end{aligned}
\tag{6.16}
$$

where $\mathcal{W}\equiv\mathcal{W}(m_s^2,m_q^2,p^2)=\alpha_1m_s^2+\alpha_2m_q^2-\alpha_1\alpha_2p^2$ is a useful shorthand. The δ functions impose all further necessary constraints, alongside the global delta function $\delta(1-\alpha_1-\alpha_2-\alpha_3)$.

6.4 Mixing of axial mesons

Before presenting numerics, it is important to address the question of mixing, which is particularly important for the axial mesons, as the mixing behaviour is not yet completely understood.

All the mesons with the same values of J^P form $SU(3)_F$ nonets, according to the quark model of mesons. The 1^- nonet, for example, is composed of the three ρ mesons $\rho^{\pm,0}$; the four K^* mesons $K^{*,\pm,0}$ and $\bar K^{*,0}$, and the ϕ and ω mesons. The ϕ and ω are admixtures of the singlet and octet states

$$
\begin{aligned}
|\mathbf{1}\rangle&=\frac{1}{\sqrt{3}}\left(|\bar uu\rangle+|\bar dd\rangle+|\bar ss\rangle\right)\,,\\
|\mathbf{8}\rangle&=\frac{1}{\sqrt{6}}\left(|\bar uu\rangle+|\bar dd\rangle-2|\bar ss\rangle\right)\,.
\end{aligned}
\tag{6.17}
$$

The same applies to the 1^+ states, where the analogues of the ϕ and ω are the

Source	$\theta_{K_1}/^\circ$	$\theta_f/^\circ$	$\theta_h/^\circ$
Cheng, [179]	34(4)	23(6)	28(4)
Erkol et al, [180]	39(4)	30.3(53)	28.7(35)
Present thesis	37(4)	27.5(56)	30.5(34)

Table 6.1 *Mixing angles, taken from [179] and [180], and the values used in this work, where θ_K serves as an input to determine the mixing angles $\theta_{f,h}$ via the Gell-Mann–Okubo mass relation* (6.19)*. The angles $\theta_{f,h}$ were not computed in [180], but can be inferred using said relations. Since [179] was released, the mass estimates for the mesons have been updated in the PDG, in particular the $h_1(1380)$; the present thesis uses the latest values [128]. Error estimates are due to the variation in θ_K only.*

two f_1 (h_1) states. These also are mixtures of the singlet and octet states, but, unlike for the ϕ and ω, the mixing angles are not precisely determined. Likewise, the physical $K_1(1270)$ and $K_1(1400)$ are usually held to be admixtures of the pure states K_{1A} (belonging to the a_1 nonet) and K_{1B} (the b_1 nonet). This introduces a third mixing angle, θ_{K_1}, which is also yet to be precisely determined [177, 178]. The most recent studies appear to be arriving at a value of about $\theta_{K_1} \approx 35^\circ$.

Defining the mixing angles θ_f, θ_h, the physically-observed states are written [104, 179]

$$\begin{aligned}
|f_1(1285)\rangle &= \cos\theta_f\,|f_{\mathbf{1}}\rangle + \sin\theta_f\,|f_{\mathbf{8}}\rangle\ , \\
|f_1(1420)\rangle &= -\sin\theta_f\,|f_{\mathbf{1}}\rangle + \cos\theta_f\,|f_{\mathbf{8}}\rangle\ , \\
|h_1(1170)\rangle &= \cos\theta_h\,|h_{\mathbf{1}}\rangle + \sin\theta_h\,|h_{\mathbf{8}}\rangle\ , \\
|h_1(1380)\rangle &= -\sin\theta_h\,|h_{\mathbf{1}}\rangle + \cos\theta_h\,|h_{\mathbf{8}}\rangle\ .
\end{aligned} \tag{6.18}$$

Note that the angle for decoupling into pure the light quark state and the $|\bar{s}s\rangle$ state is given by the fixed angle $\theta_{dec.} = \tan^{-1}(1/\sqrt{2}) \approx 35^\circ$, and this is the angle that applies for the ϕ-ω mixing.

To determine the mixing angle for the f_1 and h_1 states is non-trivial, but use of the Gell-Mann–Okubo mass relation [104, 181, 182] provides a phenomenological method to determine the angles. Using this, it follows that ($f_1^L = f_1(1285)$, $f_1^H =$

$f_1(1420)$, and similarly for the h mesons)

$$\cos^2\theta_f = \frac{4m_{K_{1A}}^2 - m_{a_1}^2 - 3m_{f_1^L}^2}{3\left(m_{f_1^H}^2 - m_{f_1^L}^2\right)}\,,$$
$$\cos^2\theta_h = \frac{4m_{K_{1B}}^2 - m_{b_1}^2 - 3m_{h_1^L}^2}{3\left(m_{h_1^H}^2 - m_{h_1^L}^2\right)}\,, \tag{6.19}$$

where one also needs the mixing angle for the K_{1A}, K_{1B} states in terms of the physical states $K_1(1270)$, $K_1(1400)$, which is defined [177–179]

$$|K_1(1270)\rangle = \cos\theta_{K_1}\,|K_{1B}\rangle + \sin\theta_{K_1}\,|K_{1A}\rangle\ ,$$
$$|K_1(1400)\rangle = -\sin\theta_{K_1}\,|K_{1B}\rangle + \cos\theta_{K_1}\,|K_{1A}\rangle\ . \tag{6.20}$$

Table 6.1 presents the extracted values of $\theta_{f,h}$ using the input value of θ_{K_1} indicated, based on two previous determinations [179, 180], with the present calculation assuming a naive average of the two values. These values suggest that the heavier f_1 and h_1 states are not far from being pure $|\bar{s}s\rangle$ states; this assumption will therefore be made in the numerical estimates of the DA parameters.

6.5 Numerical results

To extract the DA parameters, it is necessary to consider the left-hand side of the correlation function (6.1) , which is given by

$$\Pi_{[\rho]}^{\chi}(v, pz) = \frac{m_V^2 f_V^2}{m_V^2 - p^2}\int \mathcal{D}\underline{\alpha}\, e^{-ipz(\alpha_2 + v\alpha_3)}\Phi^{\chi[\rho]}(\underline{\alpha}) + \ldots \tag{6.21}$$

where the dots stand for higher contributions from the hadronic spectrum. As seen in the case of the $B \to \pi$ sum rules, the necessary contribution can be extracted by subtracting the continuum contribution, performing a Borel transform and equating (6.21) to (6.3) in terms of a dispersion relation. The integrals over $(\alpha_1, \alpha_2, \alpha_3)$ can be performed, along with a projection onto the relevant moment, by exploiting the orthogonality relations of the basis function in (3.48).

To illustrate this procedure, the Borel-transformed sum rules for the leading

parameters for the ρ and $\tilde{\rho} \equiv a_1$ mesons are given below. The notation used below, and its relation to the previous literature [85], was established in (3.51). Defining

$$\begin{aligned}\mathcal{N}_{3,V} &= \frac{f_V^2 m_V^2}{m_{\hat{\mathcal{B}}}^2} e^{-m_V^2/m_{\hat{\mathcal{B}}}^2}\,, \\ \mathcal{N}_{3,V}^{\perp} &= \frac{f_V^{\perp 2} m_V^2}{m_{\hat{\mathcal{B}}}^2} e^{-m_V^2/m_{\hat{\mathcal{B}}}^2}\,,\end{aligned} \tag{6.22}$$

then the non-zero parameters are, for the ρ meson,

$$\begin{aligned}\mathcal{N}_{3,\rho}\mathcal{A}_{(0)\rho} &= \frac{\alpha_s}{144\pi^3}\int_0^{s_0} \frac{s}{M_{\hat{\mathcal{B}}}^2} e^{-s/M_{\hat{\mathcal{B}}}^2} ds + \frac{1}{96\pi^2}\frac{1}{M_{\hat{\mathcal{B}}}^2}\langle G^2\rangle + \frac{1}{192\pi^2}\frac{1}{M_{\hat{\mathcal{B}}}^4}\langle fG^3\rangle \\ &\quad - \frac{2\pi\alpha_s}{3}\frac{1}{M_{\hat{\mathcal{B}}}^4}\left(2\left\langle V_q^a V_f^a\right\rangle\right) + 2\pi\alpha_s \frac{1}{M_{\hat{\mathcal{B}}}^4}\left\langle A^a A^a\right\rangle\,, \\ \mathcal{N}_{3,\rho}\mathcal{A}_{(2)\rho} &= \frac{-\alpha_s}{120\pi^3}\int_0^{s_0} \frac{s}{M_{\hat{\mathcal{B}}}^2} e^{-s/M_{\hat{\mathcal{B}}}^2} ds - \frac{1}{24\pi^2}\frac{1}{M_{\hat{\mathcal{B}}}^2}\langle G^2\rangle + \frac{11}{144\pi^2}\frac{1}{M_{\hat{\mathcal{B}}}^4}\langle fG^3\rangle \\ &\quad + \frac{8\pi\alpha_s}{3}\frac{1}{M_{\hat{\mathcal{B}}}^4}\left(2\left\langle V_q^a V_f^a\right\rangle\right) + \frac{32\pi\alpha_s}{3}\frac{1}{M_{\hat{\mathcal{B}}}^4}\left\langle A^a A^a\right\rangle\,, \\ \mathcal{N}_{3,\rho}\mathcal{V}_{(1)\rho} &= \frac{7\alpha_s}{720\pi^3}\int_0^{s_0} \frac{s}{M_{\hat{\mathcal{B}}}^2} e^{-s/M_{\hat{\mathcal{B}}}^2} ds + \frac{7}{144\pi^2}\frac{1}{M_{\hat{\mathcal{B}}}^2}\langle G^2\rangle - \frac{28\pi\alpha_s}{3}\frac{1}{M_{\hat{\mathcal{B}}}^4}\left(2\left\langle V_q^a V_f^a\right\rangle\right)\,, \\ \mathcal{N}_{3,\rho}^{\perp}\mathcal{T}_{(1)\rho} &= \frac{7\alpha_s}{360\pi^3}\int_0^{s_0} \frac{s}{M_{\hat{\mathcal{B}}}^2} e^{-s/M_{\hat{\mathcal{B}}}^2} ds + \frac{7}{72\pi^2}\frac{1}{M_{\hat{\mathcal{B}}}^2}\langle G^2\rangle - \frac{56\pi\alpha_s}{3}\frac{1}{M_{\hat{\mathcal{B}}}^4}\left(2\left\langle V_q^a V_f^a\right\rangle\right)\,,\end{aligned} \tag{6.23}$$

and, for the $\tilde{\rho} \equiv a_1$,

$$\begin{aligned}\mathcal{N}_{3,\tilde{\rho}}\tilde{\mathcal{V}}_{(0)\rho} &= \frac{\alpha_s}{144\pi^3}\int_0^{s_0} \frac{s}{M_{\hat{\mathcal{B}}}^2} e^{-s/M_{\hat{\mathcal{B}}}^2} ds + \frac{1}{96\pi^2}\frac{1}{M_{\hat{\mathcal{B}}}^2}\langle G^2\rangle + \frac{1}{192\pi^2}\frac{1}{M_{\hat{\mathcal{B}}}^4}\langle fG^3\rangle \\ &\quad - \frac{2\pi\alpha_s}{3}\frac{1}{M_{\hat{\mathcal{B}}}^4}\left(2\left\langle V_q^a V_f^a\right\rangle\right) + 2\pi\alpha_s \frac{1}{M_{\hat{\mathcal{B}}}^4}\left\langle V^a V^a\right\rangle\,, \\ \mathcal{N}_{3,\tilde{\rho}}\tilde{\mathcal{V}}_{(2)\rho} &= \frac{-\alpha_s}{120\pi^3}\int_0^{s_0} \frac{s}{M_{\hat{\mathcal{B}}}^2} e^{-s/M_{\hat{\mathcal{B}}}^2} ds - \frac{1}{24\pi^2}\frac{1}{M_{\hat{\mathcal{B}}}^2}\langle G^2\rangle + \frac{11}{144\pi^2}\frac{1}{M_{\hat{\mathcal{B}}}^4}\langle fG^3\rangle \\ &\quad + \frac{8\pi\alpha_s}{3}\frac{1}{M_{\hat{\mathcal{B}}}^4}\left(2\left\langle V_q^a V_f^a\right\rangle\right) + \frac{32\pi\alpha_s}{3}\frac{1}{M_{\hat{\mathcal{B}}}^4}\left\langle V^a V^a\right\rangle\,, \\ \mathcal{N}_{3,\tilde{\rho}}\tilde{\mathcal{A}}_{(1)\rho} &= \frac{7\alpha_s}{720\pi^3}\int_0^{s_0} \frac{s}{M_{\hat{\mathcal{B}}}^2} e^{-s/M_{\hat{\mathcal{B}}}^2} ds + \frac{7}{144\pi^2}\frac{1}{M_{\hat{\mathcal{B}}}^2}\langle G^2\rangle - \frac{28\pi\alpha_s}{3}\frac{1}{M_{\hat{\mathcal{B}}}^4}\left(2\left\langle V_q^a V_f^a\right\rangle\right)\,, \\ \mathcal{N}_{3,\tilde{\rho}}^{\perp}\tilde{\mathcal{T}}_{(1)\rho} &= \frac{7\alpha_s}{360\pi^3}\int_0^{s_0} \frac{s}{M_{\hat{\mathcal{B}}}^2} e^{-s/M_{\hat{\mathcal{B}}}^2} ds + \frac{7}{72\pi^2}\frac{1}{M_{\hat{\mathcal{B}}}^2}\langle G^2\rangle - \frac{56\pi\alpha_s}{3}\frac{1}{M_{\hat{\mathcal{B}}}^4}\left(2\left\langle V_q^a V_f^a\right\rangle\right)\,.\end{aligned} \tag{6.24}$$

Expressions for the K^*- and ϕ-type mesons follow from including mass corrections, but the corresponding analytic expressions are longer, and are not given explicitly.

Numerical inputs, and errors, for the condensates are given in appendix B, along with a discussion of the competing estimates of these values. Here, it suffices to say that the numerical values for all condensate parameters align with the values in [103]. The renormalisation scale is set to $\mu = 1$ GeV. The RG evolution of the DA parameters, including mixing with twist-2 parameters, can be found in [85, 103]. Values for the quark masses are assumed to be $m_q = 0$ and $m_s(1\text{ GeV}) = 133(27)$ MeV, also used in [85, 103]. For simplicity, only linear quark mass corrections are applied, arising from the two-quark and mixed condensates, and quadratic quark mass corrections are neglected.[1]

The decay constants are taken, for vector mesons, from the results of [99], and for axial mesons, the results below are based in the observation of the Weinberg sum rules [183] that $m_\rho^2 f_\rho^2 = m_{a_1}^2 f_{a^1}^2$.[2]

The remaining question is of the Borel parameters. The continuum threshold s_0 can be determined from experimental data; threshold parameters s_0 are chosen, for the vector mesons, to coincide with those used in [85]. For the axial mesons the s_0 is taken to be slightly higher, based on the data of, for example, [184]. An alternative model that is often used in sum rules is to fix $s_0^M = (m_M + \Delta)^2$ for some parameter Δ, where m_M is the mass of the relevant meson. Here, using $s_0^\rho = 1.3\text{ GeV}^2$ implies $\Delta = 0.36$ GeV, which in turn would give $s_0^{a_1} \approx 2.55\text{ GeV}^2$, consistent with [104], but rather higher than the observed threshold in [184].

Coinciding with the values in [85], the choices for the s_0 for vector mesons are $s_0^{\mathcal{V},\mathcal{A}}(\rho,\omega,K^*) = 1.3(3)\text{ GeV}^2$, $s_0^{\mathcal{T}}(\rho,\omega,K^*) = 1.6(3)\text{ GeV}^2$, $s_0^{\mathcal{V},\mathcal{A}}(\phi) = 1.4\text{ GeV}^2$, and $s_0^{\mathcal{T}}(\phi) = 1.7(3)\text{ GeV}^2$. For axial mesons, the equivalent thresholds are chosen to be lower than in [104], but higher than the vector meson thresholds, using the results for the a_1 spectrum in $\tau \to A\nu_\tau$ decays from the ALEPH experiment [184] as a guide. This leads to all axial s_0 being 0.4 GeV^2 higher than the equivalent vector thresholds.

[1] These include corrections from propagators in the gluon condensates, although such corrections can nevertheless be obtained from the analytic expressions provided in equation (6.16).

[2] The values for the decay constants obtained in [104] are much higher than the inputs used in the present calculation, although it will also be seen that the threshold parameter used in that paper is much higher than the value implied by experimental data. The choice based on the Weinberg sum rules is more consistent with the arguments of [36].

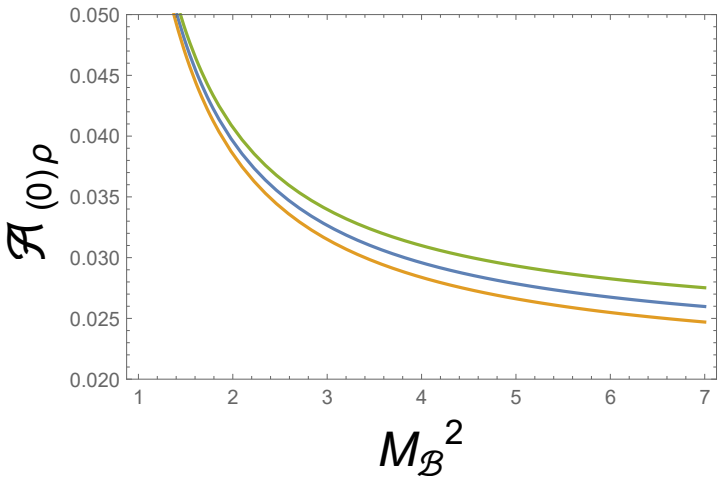

Figure 6.7 *Dependence of $\mathcal{A}_{(0)\rho}$ on the Borel mass, for central values of the condensates, at three different values of the threshold parameter (from top to bottom, $s_0 = (1.6, 1.3, 1.0)$ GeV^2). For low values of the Borel mass it can be seen that the range is too great for results to be trustworthy, whereas the relative smoothness in the chosen window is well-established.*

For the Borel mass parameter, this will be fixed by establishing the Borel window (c. 10% to c. 30% contribution of highest-dimensional condensate) for the leading DA parameter, chosen to be, by convention, $\mathcal{A}_{(0)\rho} \equiv \zeta_{3\rho}^{\parallel}$. This leads to the Borel window 2 GeV$^2 \leq M_{\hat{\mathcal{B}}}^2 \leq 5$ GeV^2, which is somewhat higher than the window quoted in [70] but is actually more consistent with the graphs provided in, for example, figure 4.10 therein. This window is then used for all the parameters, which allows to compare the changes in importance of different contributions with the same conditions, rather than arbitrary variations for each parameter. Figures 6.7, 6.8, and 6.9 illustrate the dependence on Borel mass of three of the ρ parameters, justifying the choice for the Borel window.

For the ρ meson, the numerical results for the DA parameters are

$$\begin{aligned}
\mathcal{A}_{(0)\rho} &= 0.0032|_{PT} + 0.022|_{G^2} + 0.00053|_{G^3} + 0.0032|_{\langle\bar{q}q\rangle\langle\bar{s}s\rangle} + 0.0022|_{\langle\bar{q}q\rangle^2} \\
&= 0.031(9)\,, \\
\mathcal{A}_{(2)\rho} &= -0.0038|_{PT} - 0.087|_{G^2} + 0.0077|_{G^3} + 0.017|_{\langle\bar{q}q\rangle\langle\bar{s}s\rangle} - 0.0086|_{\langle\bar{q}q\rangle^2} \\
&= -0.075(22)\,, \\
\mathcal{V}_{(1)\rho} &= 0.0044|_{PT} + 0.102|_{G^2} + 0|_{G^3} + 0|_{\langle\bar{q}q\rangle\langle\bar{s}s\rangle} + 0.030|_{\langle\bar{q}q\rangle^2} \\
&= 0.136(41)\,, \\
\mathcal{T}_{(1)\rho} &= 0.018|_{PT} + 0.360|_{G^2} + 0|_{G^3} + 0|_{\langle\bar{q}q\rangle\langle\bar{s}s\rangle} + 0.107|_{\langle\bar{q}q\rangle^2} \\
&= 0.49(15)\,,
\end{aligned} \tag{6.25}$$

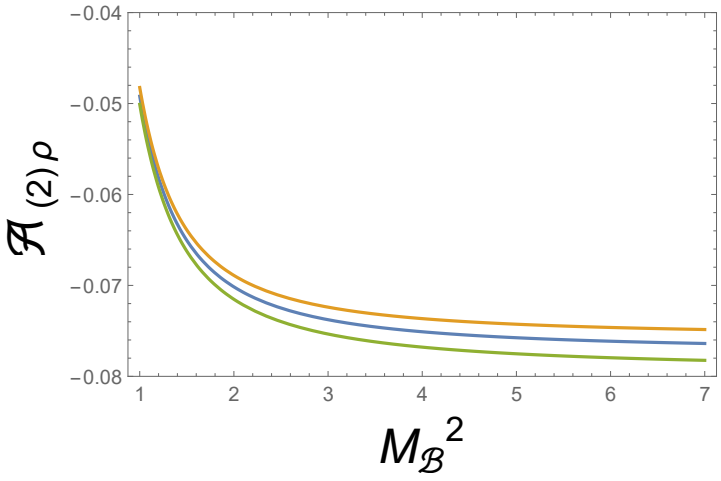

Figure 6.8 *Dependence of $\mathcal{A}_{(2)\rho}$ on the Borel mass, for central values of the condensates, at three different values of the threshold parameter (from top to bottom, $s_0 = (1.0, 1.3, 1.6)$ GeV^2). The equivalent plot (figure 4.10) in [70] shows the opposite behaviour at low values of the Borel mass. The differing behaviour can be attributed to the behaviour of the three-gluon condensate, which is dominant for small vlaues of $M_{\hat{\mathcal{B}}}^2$. Both the plot above and that in [70] converge to similar values in the region of interest.*

where the breakdown into the individual contributions has been indicated, distinguishing the two sources of the four-quark condensate contribution. The uncertainty in the overall parameter arises from uncertainties in the values of the condensates, the Borel parameters, the strange quark mass, and α_s. It has been assumed that these errors are uncorrelated. It can be seen that the two-gluon condensate provides the dominant contribution, while the three-gluon condensate is relevant to the proper evaluation of $\mathcal{A}_{(2)V}$, as it is of the same order at the four-quark condensates. For the $\tilde{\rho}$ meson, the equivalent numerical results are

$$\begin{aligned}
\tilde{\mathcal{V}}_{(0)a_1} &= 0.0065|_{PT} + 0.028|_{G^2} + 0.00068|_{G^3} - 0.0042|_{\langle\bar{q}q\rangle\langle\bar{s}s\rangle} + 0.0028|_{\langle\bar{q}q\rangle^2} \\
&= 0.0342(95)\,, \\
\tilde{\mathcal{V}}_{(2)a_1} &= -0.0078|_{PT} - 0.113|_{G^2} + 0.010|_{G^3} - 0.023|_{\langle\bar{q}q\rangle\langle\bar{s}s\rangle} - 0.0113|_{\langle\bar{q}q\rangle^2} \\
&= -0.14(5)\,, \\
\tilde{\mathcal{A}}_{(1)a_1} &= 0.0091|_{PT} + 0.132|_{G^2} + 0|_{G^3} + 0|_{\langle\bar{q}q\rangle\langle\bar{s}s\rangle} + 0.039|_{\langle\bar{q}q\rangle^2} \\
&= 0.181(67)\,, \\
\tilde{\mathcal{T}}_{(1)b_1} &= 0.020|_{PT} + 0.265|_{G^2} + 0|_{G^3} + 0|_{\langle\bar{q}q\rangle\langle\bar{s}s\rangle} + 0.079|_{\langle\bar{q}q\rangle^2} \\
&= 0.36(13)\,,
\end{aligned} \tag{6.26}$$

where the extracted DA parameter for the tensor current is for the b_1, rather than

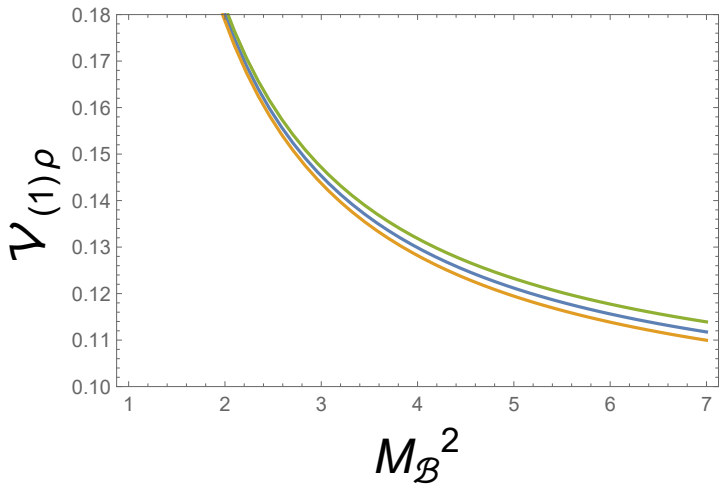

Figure 6.9 *Dependence of $\mathcal{V}_{(1)_\rho}$ on the Borel mass, for central values of the condensates, at three different values of the threshold parameter (from top to bottom, $s_0 = (1.6, 1.3, 1.0)\ GeV^2$).*

the a_1, owing to the fact that the a_1 does not couple to the tensor current.

The equivalent results for the ϕ and $f_1(1420)(h_1(1380))$ mesons, assuming that the higher-valued f_1 and h_1 are pure $|\bar{s}s\rangle$ states, also include contributions from the $\langle\bar{s}s\rangle$ and $\langle\bar{s}\sigma\cdot Gs\rangle$ condensates. For the ϕ meson, the corresponding breakdown is

$$\begin{aligned}
\mathcal{A}_{(0)\phi} &= 0.0020|_{PT} + 0.012|_{G^2} + 0.00029|_{G^3} + 0.0011|_{\langle\bar{q}q\rangle\langle\bar{s}s\rangle} + 0.0008|_{\langle\bar{q}q\rangle^2} \\
&+ 0.0060|_{\langle\bar{s}s\rangle} - 0.0013|_{\langle\bar{s}\sigma\cdot Gs\rangle} = 0.0207(79)\,, \\
\mathcal{A}_{(2)\phi} &= -0.0024|_{PT} - 0.048|_{G^2} + 0.0042|_{G^3} + 0.0061|_{\langle\bar{q}q\rangle\langle\bar{s}s\rangle} - 0.0030|_{\langle\bar{q}q\rangle^2} \\
&+ 0.014|_{\langle\bar{s}s\rangle} - 0.0053|_{\langle\bar{s}\sigma\cdot Gs\rangle} = -0.023(17)\,, \\
\mathcal{V}_{(1)\phi} &= 0.0028|_{PT} + 0.056|_{G^2} + 0|_{G^3} + 0|_{\langle\bar{q}q\rangle\langle\bar{s}s\rangle} + 0.011|_{\langle\bar{q}q\rangle^2} \\
&+ 0.016|_{\langle\bar{s}s\rangle} - 0.019|_{\langle\bar{s}\sigma\cdot Gs\rangle} = 0.066(26)\,, \\
\mathcal{T}_{(1)\phi} &= 0.011|_{PT} + 0.166|_{G^2} + 0|_{G^3} + 0|_{\langle\bar{q}q\rangle\langle\bar{s}s\rangle} + 0.032|_{\langle\bar{q}q\rangle^2} \\
&+ 0.043|_{\langle\bar{s}s\rangle} - 0.056|_{\langle\bar{s}\sigma\cdot Gs\rangle} = 0.196(75)\,,
\end{aligned} \tag{6.27}$$

and, for the $f_1(h_1)$

$$\begin{aligned}
\tilde{\mathcal{V}}_{(0)f_1(1420)} &= 0.0052|_{PT} + 0.016|_{G^2} + 0.00038|_{G^3} - 0.0015|_{\langle\bar{q}q\rangle\langle\bar{s}s\rangle} + 0.0010|_{\langle\bar{q}q\rangle^2} \\
&- 0.0036|_{\langle\bar{s}s\rangle} - 0.0018|_{\langle\bar{s}\sigma\cdot Gs\rangle} = 0.0157(50)\,, \\
\tilde{\mathcal{V}}_{(2)f_1(1420)} &= -0.0062|_{PT} - 0.064|_{G^2} + 0.0056|_{G^3} - 0.0081|_{\langle\bar{q}q\rangle\langle\bar{s}s\rangle} - 0.0041|_{\langle\bar{q}q\rangle^2} \\
&- 0.015|_{\langle\bar{s}s\rangle} + 0.007|_{\langle\bar{s}\sigma\cdot Gs\rangle} = -0.085(35)\,,
\end{aligned}$$

DA parameter	ρ	K^*	ϕ	ω
$\mathcal{A}_{(0)V}$	0.031(9)	0.031(10)	0.0207(79)	0.035(10)
$\mathcal{A}_{(1)V}$	0	0.027(17)	0	0
$\mathcal{A}_{(2)V}$	−0.075(22)	−0.048(23)	−0.023(17)	−0.086(26)
$\mathcal{V}_{(0)V}$	0	−0.001(2)	0	0
$\mathcal{V}_{(1)V}$	0.136(41)	0.112(36)	0.066(26)	0.157(47)
$\mathcal{V}_{(2)V}$	0	−0.012(7)	0	0
$\mathcal{T}_{(0)V}$	0	−0.003(5)	0	0
$\mathcal{T}_{(1)V}$	0.49(15)	0.37(12)	0.196(75)	0.56(17)
$\mathcal{T}_{(2)V}$	0	−0.040(22)	0	0

Table 6.2 *Summary of numerical results for all DA parameters for the vector mesons, with uncertainties in the last digit(s) in brackets. All values above are at the RG scale $\mu = 1$ GeV. The notation is new to this thesis, and can be related to that of the previous literature [82, 85] using the dictionary in equation* (3.51)*. G-parity odd parameters are sensitive to the sign convention for the covariant derivative, which here is $D_\mu = \partial_\mu - iA_\mu$. The values for the ω are also given separately, for the first time.*

$$\begin{aligned}
\tilde{\mathcal{A}}_{(1)f_1(1420)} &= 0.0073|_{PT} + 0.074|_{G^2} + 0|_{G^3} + 0|_{\langle\bar{q}q\rangle\langle\bar{s}s\rangle} + 0.014|_{\langle\bar{q}q\rangle^2} \\
&\quad + 0.017|_{\langle\bar{s}s\rangle} - 0.025|_{\langle\bar{s}\sigma\cdot Gs\rangle} = 0.088(37)\,, \\
\tilde{\mathcal{T}}_{(1)h_1(1380)} &= 0.015|_{PT} + 0.145|_{G^2} + 0|_{G^3} + 0|_{\langle\bar{q}q\rangle\langle\bar{s}s\rangle} + 0.028|_{\langle\bar{q}q\rangle^2} \\
&\quad + 0.027|_{\langle\bar{s}s\rangle} - 0.049|_{\langle\bar{s}\sigma\cdot Gs\rangle} = 0.166(69)\,,
\end{aligned} \tag{6.28}$$

Table 6.2 contains a summary of the numerical results, including those for the K^* mesons, and table 6.3 contains similar results for the ${}^3P_1$ axial mesons.

6.6 Conclusions

This chapter has presented a fresh determination of the three-particle twist-3 distribution amplitudes for light vector and axial mesons. The main result of this computation is to demonstrate explicitly that the resulting sum rules are identical, up to corrections from the quark condensate and hadronic parameters, where these corrections are systematic and described in (6.16). The calculations

DA parameter	a_1	$f_1(1420)$	$f_1(1285)$
$\tilde{\mathcal{V}}_{(0)A}$	0.034(9)	0.014(5)	0.041(12)
$\tilde{\mathcal{V}}_{(1)A}$	0	0	0
$\tilde{\mathcal{V}}_{(2)A}$	$-0.14(5)$	$-0.084(35)$	$-0.173(65)$
$\tilde{\mathcal{A}}_{(0)A}$	0	0	0
$\tilde{\mathcal{A}}_{(1)A}$	0.181(67)	0.086(37)	0.215(83)
$\tilde{\mathcal{A}}_{(2)A}$	0	0	0

Table 6.3 *Summary of available numerical results for vector and axial DA parameters for the $^3P_1$ axial mesons, with uncertainties in the last digit(s) in brackets. All values above are at the RG scale $\mu = 1$ GeV. A full analysis, including the tensor DAs and $^1P_1$ results, will be provided in [174].*

also update those in [85] and [104], and will lead to fresh numerical results, preliminary values for which are given in tables 6.2 and 6.3.

Although the analysis has yet to be extended completely to the $^1P_1$ mesons, combining the analysis of vector and axial mesons in a systematic manner will render future experimental studies far less susceptible to the vulnerability of using competing calculations.

The corresponding results for the twist-4 distribution amplitudes are dependent on a proper study of the tensor current, which has so far not yet been attempted. Preliminary analytic expressions, which will enable a full moments analysis of these DAs, including the $SU(3)_F$ breaking effects, are given in appendix D.

The following chapter will show an immediate application of the twist-3 results, as they will enter into the computation of long-distance charm loop contributions to radiative $B \to (V, A)\gamma$ processes.

Chapter 7

Long-distance charm loops in $B \to V\gamma$ decays from light-cone sum rules

7.1 Introduction

The leading contribution to radiative B meson decays arises from the operator O_7 (defined in (2.38), but repeated below for convenience),

$$\mathcal{H}_{eff,7} = \frac{G_F}{\sqrt{2}}\lambda_t^D \frac{e}{4\pi^2}\left(m_b C_7\, \bar{D}_L \sigma_{\mu\nu} b F^{\mu\nu} + m_D C_7'\, \bar{D}_R \sigma_{\mu\nu} b F^{\mu\nu}\right) , \qquad (7.1)$$

where the right-handed amplitude arising from the SM contribution has also been explicitly indicated. It follows that, although right-handed currents (RHC) in $b \to D\gamma$ decays can be generated by the SM, they appear to be heavily suppressed by a factor m_D/m_b. As a result, it can be expected that the presence of significant RHC in such decays is a strong signal of NP.

This statement is, however, complicated by the presence of other operators in the effective Hamiltonian. The $\mathcal{O}_2$ operator (2.36), in particular, could also play a significant role in generating RHC contributions. This has led to some research in attempting to compute such contributions to $b \to D\gamma$ processes. An inclusive $B \to X\gamma$ computation suggested that the contribution of $\mathcal{O}_2$ to RHC could be surprisingly large compared to the m_D/m_b scaling of (7.1), on the order of 10%

[185]. However, computations of the same effect in exclusive channels [186–188] have led to a far smaller contribution of $\mathcal{O}_2$ to RHC, in line with the implication from (7.1) that RHC should be small in radiative $b \to D\gamma$ decays.

Aside from the theoretical ambiguity, there is also the question of how to measure RHC in experiment. It was shown that the time-dependent decay rates and CP asymmetries are sensitive to the interference of left- and right-handed amplitudes [189, 190], and since then the B factories have attempted to measure these effects, as well as at LHCb in 2016 [191–193]. All experimental results so far suffer from significant uncertainties, so that the next generation of B factories may be required to untangle such effects properly.

Regardless, the problem of distinguishing NP sources of RHC from the LD contamination is important to solve. In [36] it was proposed that one way to resolve this is to exploit the approximate symmetry, that applies exactly in the chiral restoration limit, between vector mesons and their parity-doubled axial meson partners. Then, by combining the analysis of $B \to V\gamma$ decays with the respective $B \to A\gamma$ decay under parity doubling, it is possible to separate the measurement of LD effects from genuine NP effects in RHC, providing potentially significant improvements to the sensitivity of experiments to such effects.

This chapter presents a computation of the long-distance charm-loop in exclusive $b \to D = (d, s)\gamma$ decays, in the case where a gluon radiates into the final-state meson, using the LCSR approach. In [35] the same calculation was also presented, and extended to $b \to D = (d, s)\ell\bar{\ell}$ decays, but results in that thesis were confined, at least explicitly, to the leading contribution from the necessary three-particle DA. Furthermore, in light of the updates to the three-particle DA parameters, as provided in the previous chapter, an update of the preliminary results of [35] is desirable. Although numerical results are restricted to $q^2 = 0$, the presentation through the analytic section will allow for a future extension to $q^2 \neq 0$, which allows the results below to be applied to the $b \to D = (d, s)\ell\bar{\ell}$ case.

Parts of this chapter have been published in [36], with the remaining material to be published in [194].

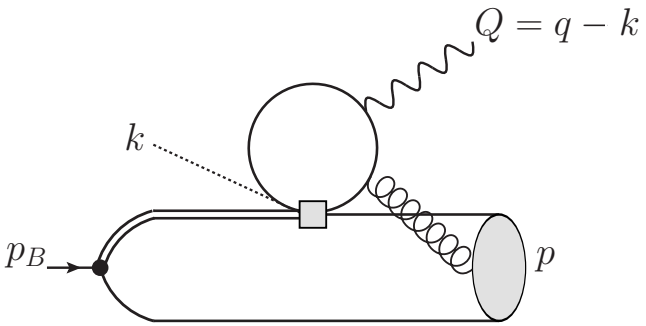

Figure 7.1 *The contribution of interest, where the charm loop radiates a gluon into the final-state meson, while the B meson is replaced by an interpolating current, following the usual LCSR procedure. Other contributions, where the gluon attaches either to the B meson or to any of the quark lines, are not indicated. The spurious momentum k, inserted at the vertex, deals with parasitic cuts, to be made clear in figure 7.2.*

7.2 Charm loop matrix element

The $B \to V\gamma$ amplitude can be expressed in terms of the two photon polarisations as

$$\mathcal{A} \equiv \langle \gamma(q,\varepsilon) V(p,\eta) | H_{\text{eff}} | \bar{B}(p_B) \rangle = \bar{\mathcal{A}}_L^{\bar{B}\to V\gamma} S_L + \bar{\mathcal{A}}_R^{\bar{B}\to V\gamma} S_R \,, \tag{7.2}$$

where

$$S_{L(R)} \equiv [\epsilon(\varepsilon^*, \eta^*, p, q) \pm i\{(\varepsilon^* \cdot \eta^*)(p \cdot q) - (\varepsilon^* \cdot p)(\eta^* \cdot q)\}] \,, \tag{7.3}$$

label the left-and right-handed contributions to the amplitude. The extension to the $q^2 \neq 0$ case can be achieved using the basis [69]

$$\begin{aligned} P_V^\mu &= 2\epsilon^\mu(\eta^*, p, q) \,, \\ P_A^\mu &= \frac{i}{\sqrt{\hat{\lambda}_V}} \left(\hat{\lambda}_V m_B^2 \eta^{*\mu} - 2\eta^* \cdot q \left((1 - \hat{m}_V^2 - \hat{q}^2) p^\mu - 2\hat{m}_V^2 q^\mu \right) \right) \,, \\ P_0^\mu &= \frac{4i\hat{m}_V}{\sqrt{2\hat{q}^2 \hat{\lambda}_V}} \eta^* \cdot q \left(2\hat{q}^2 p^\mu - (1 - \hat{m}_V^2 - \hat{q}^2) q^\mu \right) \,, \end{aligned} \tag{7.4}$$

where the hats denote normalisation to the B meson mass

$$\hat{q}^2 = \frac{q^2}{m_B^2} \,, \qquad\qquad \hat{m}_V = \frac{m_V}{m_B} \,,$$

$$\hat{\lambda}_V = \lambda(1, \hat{m}_V^2, \hat{q}^2)\,, \tag{7.5}$$

and $\lambda(a,b,c)$ is the Källén function (C.2). It is convenient to work in the $(V,A,0)$ basis as this allows to project onto the basis of DAs used in the previous chapter. Note that when $q^2 \to 0$, the invariants $S_{L(R)}$ can be expressed directly in terms of $P^\mu_{V,A}$, as $2p\cdot q = m_B^2 - m_V^2 - q^2$ and $\varepsilon^* \cdot q = 0$ in this case. More precisely, the relations are

$$S_{L(R)} = \lim_{q^2\to 0} \frac{1}{2}\varepsilon^* \cdot (P_V \pm P_A)\,, \tag{7.6}$$

with P_0^μ vanishing at $q^2 = 0$.

The matrix element of interest is

$$\sum_{i=V,A,0} L_{c,i}(q^2) P_i^\mu = \frac{4\pi^2}{m_b} i \int d^4x e^{iq\cdot x} \langle V(p)| \mathcal{T}\left(\bar{c}(x)\gamma^\mu c(x) 2\tilde{Q}_1^c(0)\right)|B(p_B)\rangle\,, \tag{7.7}$$

where

$$\tilde{Q}_1^c \equiv \frac{1}{2}\left(\mathcal{O}_2^c - \frac{1}{N_C}\mathcal{O}_1^c\right) = \bar{c}_L \lambda^a c\, \bar{s}_L \lambda^a b \tag{7.8}$$

is the colour-traceless part of the current-current operators in the effective Hamiltonian (2.35). Only the contribution arising from the charm loop has been provided above, although other quark-loop contributions arise from the natural replacement $c \to q = (u,d,s,b)$. The total contribution from such quark loops leads to the overall function

$$L_i^{D=d,s}(q^2) = -C_2 Q_u \sum_{q=u,c} \frac{\lambda_q^D}{\lambda_t^D} L_{q,i}(q^2) + C_3 Q_s L_{s,i}(q^2) + (C_4 - C_6)\sum_q Q_q L_{q,i}(q^2)\,, \tag{7.9}$$

where the final sum runs over $q = u,d,s,c,b$. Owing to the hierarchy of Wilson coefficients, the dominant contribution to the long-distance quark loops is from the C_2 term, while the CKM hierarchy leads to $|\lambda_c^D/\lambda_t^D| \sim 1$, $|\lambda_u^s/\lambda_t^s| \sim 1/50$, $|\lambda_u^d/\lambda_t^d| \sim 3/10$. Hence, the charm loops are the most significant, although $B \to \rho$ transitions are also sensitive to the up-quark contribution.

Equation (7.9) defines the full contribution due to LD charm loops, but there are several possible classes of contribution to this diagram, which can be divided according to the nature of the gluon radiated from the charm loop. The particular case of interest in this chapter is that where a soft gluon is radiated into the final-state meson, although further important contributions include those where the gluon is instead radiated into the initial-state meson or any of the quark lines.

Invariant	Quark content	Interpretation
Q^2	$\bar{c}c$	Charmonium resonances
q^2	$\bar{D}b$	B_D meson, parasitic contribution to charmonium dispersion relation
p_B^2	$\bar{q}b$	B meson
P^2	$\bar{c}c\bar{D}q$	parasitic contribution to B meson dispersion relation from multi-hadron states.

Table 7.1 *Physical interpretations of the momentum invariants and their associated cuts. In the limit $k \to 0$, the invariants q^2 and P^2 are indistinguishable from Q^2 and p_B^2, which are the physically meaningful quantities, as they are associated with the charmonium resonances and physical B meson states respectively. This justifies the introduction of the spurious momentum k, which allows the parasitic cuts to be separated, as discussed in the text.*

These have been considered previously in [35, 188] for initial-state radiation, while vertex corrections have been partially considered in [68] and, in the inclusive case, in [195]. A full exclusive calculation of these two-loop diagrams has not yet been completed. The implication from [195] is that such corrections could be sizeable compared to the leading diagram, as the resulting correction to C_7 is of order 25%, but $L^R_{c,i}(q^2)$ can also be expected not to lead to a significant right-handed amplitude. In any case, this thesis only presents the results for soft-gluon radiation into the final-state meson.

7.3 Outline of the calculation

Following the approach of [35, 71], the first step is to replace the B meson in (7.7) by an interpolating current (see also (3.22)), so that the correlation function of interest is

$$C^\mu(p,Q,k) = \frac{4\pi^2}{m_b}\frac{i^2}{f_B m_B^2}\int d^4x d^4y\, e^{i(q\cdot x - p_B\cdot y)}\langle V(p)|\mathcal{T}\left(\bar{c}(x)\gamma^\mu c(x) 2\tilde{Q}_1^c(0) J_B(y)\right)|0\rangle\,, \tag{7.10}$$

where $J_B(y) = \bar{b}(y)i\gamma_5 d(y)$ is the same interpolating current that was used in the sum rule calculation of section 3.2.

The first problem is to ensure that the dispersion relation arising from this matrix

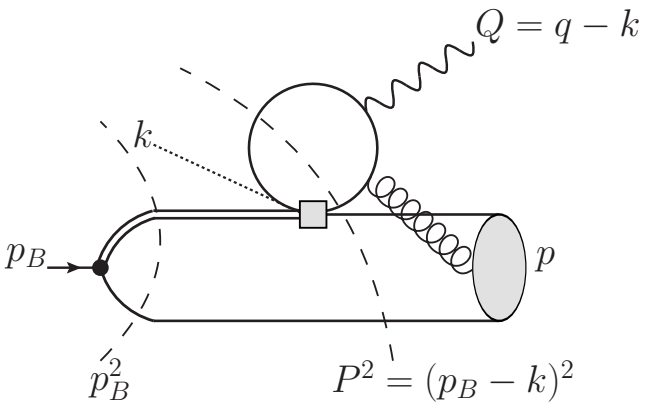

Figure 7.2 *The cut structure of the diagram in figure 7.1. Without the spurious momentum k, it would be impossible to distinguish the cuts in p_B^2 and P^2 from each other, but, as shown, the cut over P^2 does not provide the correct quantum numbers for a B meson state. A similar issue affects the dispersion relation for Q^2, also resolved by introducing the momentum k. See also table 7.1.*

element is the correct one to isolate the contribution we are interested in. This is not immediately possible, as initially there are two distinct cuts in the diagram (figure 7.2) that would appear to be related to the momentum p_B^2, but the second one also intersects with the charm loop and thus does not, in fact, have the correct quantum numbers for the B meson. The same issue impacts the q^2 behaviour, as cuts either side of the vertex would both isolate the invariant q^2, but the one passing "below" the vertex has the quantum numbers of a B meson, rather than the charmonium resonances. These are summarised in table 7.1.

The resolution of these issues was introduced, in the context of B physics, in [196], and applied to the related light quark loop calculations in [71]. It amounts to inserting a spurious momentum k at the vertex, which ensures that the two "parasitic" cuts described above do not have the correct momentum, and allows the correct cuts to be isolated. The price of this is to introduce the further momenta

$$P = p_B - k\,, \qquad Q = q - k\,, \tag{7.11}$$

with $k^2 = 0$, as its only role is to separate the correct cuts from any parasitic contributions. The new momentum Q replaces q in the exponential in (7.10). After applying the dispersion relations over p_B^2 and (for non-zero q^2) Q^2, it is then possible to restore the equalities $P = p_B$ and $Q = q$ at the end of the calculation.

One also needs the expansion of the charm propagator in a background gluon field, valid on the light-cone [35]

$$\begin{aligned} S_c(k) &= S_c^{(0)} + S_c^{(2)} + \dots \,, \\ S_c^{(0)} &= \frac{\not{k} + m_c}{k^2 - m_c^2} \,, \\ S_c^{(2)} &= -\frac{g_s}{2} \int_0^1 dv \left(v\sigma \cdot G(vx) \frac{\not{k} + m_c}{(k^2 - m_c^2)^2} + \bar{v} \frac{\not{k} + m_c}{(k^2 - m_c^2)^2} \sigma \cdot G(vx) \right) \,, \end{aligned} \tag{7.12}$$

or the equivalent expansion in equation (A.33). This leads to the expressions for the correlation function

$$\begin{aligned} \mathcal{C}_V^V &= -\frac{m_b f_V^{\parallel} m_V}{f_B m_B^2} \int d\mu_5 \frac{xv(P^2 - Q^2)}{(l^2 - m_x^2)(p_b^2 - m_b^2)} \mathcal{V}(\underline{\alpha}) \,, \\ \mathcal{C}_A^V &= -\frac{m_b f_V^{\parallel} m_V}{f_B m_B^2} \int d\mu_5 \frac{xv(P^2 - Q^2)}{(l^2 - m_x^2)(p_b^2 - m_b^2)} \mathcal{A}(\underline{\alpha}) \,, \end{aligned} \tag{7.13}$$

where the subscript on $\mathcal{C}$ relates to whether the contribution is the coefficient of the P_V or P_A Lorentz structures in (7.4), and the superscript refers to the fact that these are results for vector mesons. The five-parameter integration is defined

$$\int d\mu_5 = \int_0^1 dx \int \mathcal{D}\underline{\alpha} \int_0^1 dv \,, \tag{7.14}$$

and the mass and momentum invariants are

$$\begin{aligned} l^2 &= v\alpha_3 P^2 + (1 - v\alpha_3)Q^2 + v\alpha_3(1 - v\alpha_3)m_V^2 \,, \\ p_b^2 &= \alpha_1 q^2 + \bar{\alpha}_1 p_B^2 - \alpha_1 \bar{\alpha}_1 m_V^2 \,, \\ m_x^2 &= \frac{m_q^2}{x\bar{x}} \,. \end{aligned} \tag{7.15}$$

In the limit $m_q \to 0$, $m_x^2 \to 0$, so that the x integral drops out, recovering the light quark loop results of [71], although $m_q = m_c \neq 0$ requires that the x integral be included. The equivalent results for axial mesons can be obtained through the replacements

$$\begin{aligned} C_V^A &= C_V^V\big|_{\mathcal{V} \to \tilde{\mathcal{A}}} \,, \\ C_A^A &= C_A^V\big|_{\mathcal{A} \to \tilde{\mathcal{V}}} \,. \end{aligned} \tag{7.16}$$

To proceed further, it is useful to work in the limit $m_V^2 \to 0$, which greatly simplifies the resulting integrals, and allows some progress to be made analytically.

It is worth noting here that, if one were to include the twist-4 contributions to the correlation functions (7.13), then it would also be necessary to restore the m_V^2 contribution to the momentum invariants (7.15), as both enter at the same order in conformal twist. All four contributions above can also be performed in the same manner, so it is only necessary to present the approach for one such integral.

Following [71], the integrals over α_1, α_2 and v can be performed directly, to give

$$C_{\mathcal{F}}^{(0)} = \int_0^1 \int_0^1 \frac{dx\, d\alpha_3\, x}{(P^2-Q^2)(p_B^2-q^2)^3} \left(\left(\ln(m_b^2 - p_B^2) - \ln(m_b^2 - \alpha_3 p_B^2 - \bar{\alpha}_3 q^2) \right) P_1^{(0)} + P_2^{(0)} \right) \times \left(\left(\ln(m_x^2 - Q^2) - \ln(m_x^2 - \alpha_3 P^2 - \bar{\alpha}_3 Q^2) \right) P_3^{(0)} + P_4^{(0)} \right) P_5^{(0)}\,, \tag{7.17}$$

where the P_i are polynomial functions of the masses, momenta, and α_3, with explicit definitions in appendix F.1. Note also that this specific structure only applies to the leading DA; those for the Next-to Leading Order (NLO) contributions are similar, but, again, the explicit form is presented in appendix F.1. One can also see, from the form of the integral above, that the dispersion relations do indeed depend only on p_B^2 and Q^2, so that the spurious momentum k introduced at the vertex has had the desired effect of isolating the required cuts from parasitic cuts.

The discontinuity in p_B^2 arises solely from the logarithms, as the residue due to the pole at $p_B^2 = q^2$ vanishes, so that $P_2^{(0)}$ can be dropped, and the dispersion over p_B^2 arises from

$$C_{\mathcal{F}}^{(0)} = \int_{m_b^2}^{\infty} \frac{ds}{s-p_B^2} \int_0^1 dx\, x \int_0^{\alpha_3^*} \frac{d\alpha_3}{(P^2-Q^2)(s-q^2)^3} P_1^{(0)} P_5^{(0)} \times \left(\left(\ln(m_x^2 - Q^2) - \ln(m_x^2 - \alpha_3 P^2 - \bar{\alpha}_3 Q^2) \right) P_3^{(0)} + P_4^{(0)} \right)\,, \tag{7.18}$$

where

$$\alpha_3^* = \frac{m_b^2 - q^2}{s - q^2}\,, \tag{7.19}$$

and with this result, the final analytic integral that can be performed is the α_3 integral, leading to

$$\frac{1}{\pi}\text{Disc}.C_{\mathcal{F}}^{(0)} = \int_0^1 \frac{dx\, x}{(P^2-Q^2)^3(s-q^2)^3} \times \left(\left(\ln(m_x^2 - Q^2) - \ln(m_x^2 - \alpha_3^* P^2 - \bar{\alpha}_3^* Q^2) \right) R_1^{(0)} + R_2^{(0)} \right) R_3^{(0)}\,, \tag{7.20}$$

where the $R_i^{(j)}$ are polynomials in the masses and momenta, and are defined explicitly in appendix F.2.

The final dispersion relation is therefore

$$L^V_{c,i}(q^2,Q^2) = \int_{m_b^2}^{s_0^B} ds\, e^{(m_B^2-s)/M_B^2}\, \frac{1}{\pi}\text{Disc.}\, \mathcal{C}_i^V(q^2,Q^2,s,m_B^2+i0)\,, \tag{7.21}$$

where, as the correct cut has been made, it is possible to set $P^2 \to m_B^2 + i0$, the on-shell condition, with the $+i0$ ensuring the correct analytic continuation. Results for radiative decays follow from setting $Q^2 = q^2 = 0$.

The extension to $q^2 \neq 0$ requires further care, owing to the fact that the invariant Q^2 is sensitive to charmonium resonances. The procedure for dealing with this is presented in [35], with further details also to be given in [194]. At $q^2 = 0$, however, these subtleties do not enter the sum rule, and so setting $Q^2 = q^2 = 0$ is indeed sufficient for calculating the radiative charm loops.

The remaining two integrals are the x-integral and the s integral appearing in (7.21). For general q^2, the x integral cannot be integrated analytically,[1] so the remaining computations must be numerical. Care must be taken to avoid issues at the boundaries of the x integration. The first of these can be removed by using

$$\int_0^1 xF(x\bar{x})\,dx = \int_0^{1/2} F(x\bar{x})\,dx\,, \tag{7.22}$$

which follows from the symmetry in $x \leftrightarrow \bar{x}$, and removes the issues of numerical evaluation at $x = 1$. The numerical issues at $x = 0$ can be dealt with by imposing a cut-off

$$x_l = \frac{1}{2}\left(1 - \sqrt{\frac{4m_c^2}{m_{J/\psi}^2}}\right)\,, \tag{7.23}$$

which can also be associated with charmonium resonances leaking into the dispersion relation as $x \to 0$.

7.4 Numerical results at $q^2 = 0$

It is convenient to consider the behaviour of the integrals separately from that of the external hadronic parameters, as the structure of these integrals is universal

[1] At $q^2 = Q^2 = 0$ it is possible to obtain an analytic expression for the x-integral in terms of polylogarithms, but the resulting analytic form is far too cumbersome to be of any use.

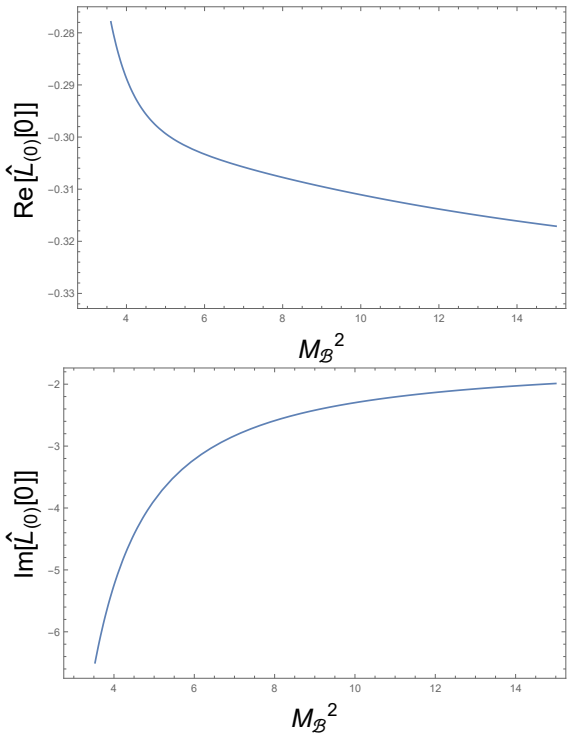

Figure 7.3 *The real (top) and imaginary (bottom) parts of the integral in equation* (7.21)*, plotted as a function of the Borel mass and for central values of the other parameters. The B meson mass still enters as an input; the plots above assume that the state is a B_q meson, where $q = u, d$. The difference due to a B_s meson state is around 10% to both real and imaginary parts. The relative stability for $M^2_{\hat{\mathcal{B}}} \sim 12\ GeV^2$ can be clearly seen, as can the strong phase, which for this term leads to a significant imaginary part.*

for all twist-3 functions of interest. With this in mind, results are presented separately for the normalised integrals $\hat{L}_{(j)}$, defined in terms of the result from (7.21) by

$$L^V_{c,i}(0) = \frac{m_b f_V m_V}{f_B m_B^2} \sum_{j=0}^{2} \varphi_i^{(j)} \hat{L}_{(j)}(0)\,, \tag{7.24}$$

so that all information about the specific state and DA parameters is separated from the integral as an overall normalisation and summed over the DA parameters.

The Borel parameter ranges are $M^2_{\hat{\mathcal{B}}} = 12 \pm 3$ GeV^2 and $s_0^B = 35 \pm 2$ GeV^2, which is consistent with the typical values used in B meson sum rules calculations in the literature [95, 186]. The quark masses are taken in the $\overline{MS}$ scheme, and, in the latest Particle Data Group (PDG) data, are given as $m_c(m_c) = 1.28 \pm 0.03$ GeV, $m_b(m_b) = 4.2 \pm 0.03$ GeV. Uncertainties are assumed to be independent and Gaussian. It can be seen from the graphs in figure 7.3 that the leading term in

the conformal expansion possesses a strong imaginary phase, while the stability for the given range of Borel masses is also apparent, justifying the values chosen above.

With these inputs, the evaluation at $q^2 = 0$ of the three integrals is, for B_q mesons,

$$\begin{aligned}
\hat{L}_{(0)}(0) &= (-0.319 \pm 0.127) - (2.110 \pm 0.197)i\,, \\
\hat{L}_{(1)}(0) &= (-0.661 \pm 0.061) - (0.197 \pm 0.073)i\,, \\
\hat{L}_{(2)}(0) &= (+0.256 \pm 0.037) - (0.159 \pm 0.049)i\,,
\end{aligned} \tag{7.25}$$

while for B_s mesons the integrals evaluate to

$$\begin{aligned}
\hat{L}_{(0)}(0) &= (-0.283 \pm 0.140) - (2.337 \pm 0.252)i\,, \\
\hat{L}_{(1)}(0) &= (-0.746 \pm 0.078) - (0.167 \pm 0.081)i\,, \\
\hat{L}_{(2)}(0) &= (+0.278 \pm 0.046) - (0.174 \pm 0.058)i\,.
\end{aligned} \tag{7.26}$$

The values above are particularly sensitive to the charm mass, and the resultant uncertainty is therefore the dominant source of error. The results above also show that, while the leading integral in the conformal expansion $\hat{L}_{(0)}$ has a large strong phase, the next term in the expansion $\hat{L}_{(1)}$ is roughly $\pi/2$ out of phase with the leading term. This can be contrasted with the results in [35], as they were presented in table 6.2, where it seems that the phase difference in the leading and next-to-leading integrals was far less dramatic. It should be noted, though, that no explicit expressions for the polynomials P_i and R_i were provided beyond the leading integral, so that a direct comparison is not possible.

Note that the absolute values of the integrals above exhibit the expected falloff for the NLO terms, so that it appears legitimate to treat the conformal expansion as perturbative and consider only the first few terms in the full DA.

The remaining input is the B meson decay constant. This can be determined in one of two ways: either from a lattice calculation or from sum rules. Lattice computations lead to the values [197]

$$f_B = 192.0(4.3)\ \text{MeV}\,, \qquad f_{B_s} = 228.4(3.7)\ \text{MeV}\,, \tag{7.27}$$

based on lattice calculations with $N_F = 2 + 1$ sea quarks. On the other hand, in LCSR calculations it is perhaps more appropriate to use a sum rules estimate for

Process	$10^3 L^V_{c;V}(0)$	$10^3 L^V_{c;A}(0)$
$B_d \to \rho$	$-9.27 - 2.76i$	$-3.43 - 4.86i$
$B_d \to K^*$	$-8.45 - 1.98i$	$-4.48 - 6.50i$
$B_s \to \phi$	$-6.31 - 1.41i$	$-1.98 - 5.53i$
$B_s \to \bar{K}^*$	$-8.51 - 1.40i$	$-4.21 - 6.33i$

Table 7.2 *Central values for the charm-loop contribution to the processes indicated at $q^2 = 0$. The errors have not been indicated, but are sizeable. Values for the DA parameters have been evolved using the RG equations (ignoring the small twist-2 corrections) from [85] to the scale $\mu = 2.2$ GeV.*

the decay constant [95]. In that case, the value $f_B m_B^2$ is given by the estimate [198]

$$\left(f_B m_B^2\right)^2 = m_b^2 \exp\left(\frac{m_B^2 - m_b^2}{M^2_{\hat{\mathcal{B}}}}\right)\left(\frac{3}{8\pi^2}\int_{m_b^2}^{s_0^B} ds \exp\left(\frac{m_b^2 - s}{M^2_{\hat{\mathcal{B}}}}\right)\frac{(s-m_b^2)^2}{s} - m_b\langle\bar{q}q\rangle - \frac{m_b}{2M^2_{\hat{\mathcal{B}}}}\left(1 - \frac{m_b^2}{2M^2_{\hat{\mathcal{B}}}}\right)\langle\bar{q}\sigma\cdot Gq\rangle\right), \tag{7.28}$$

where the appropriate value for m_b in this case is the pole mass, which is $m_b = 4.7 \pm 0.1$ GeV, while the Borel mass can be lower than for the charm loop calculation. This implies an approximate value for the combination $f_B m_B^2$ of around 3.89 ± 0.51 GeV^3 for $\bar{B}_d$, and 4.36 ± 0.54 GeV^3 for $\bar{B}_s$. The sum rules estimate for the B meson decay constants is markedly smaller than lattice computations, and the resultant error somewhat larger, dominated by the errors in m_b and s_0^B.

Following the approach of [95], the results for the charm-loop calculations will use the sum rules value for $f_B m_B^2$ instead of the lattice average values quoted above. In the final prediction for ratios of right-handed charm currents between vector and axial mesons, of course, this contribution will vanish.

When combined with the results for the twist-3 parameters in the previous chapter, the full results, at $q^2 = 0$, are given in table 7.2. The hadronic parameters are evaluated at the scale $\mu = 2.2$ GeV, with the RG evolution taken from [85] and using the value of α_s in appendix B.

7.5 Searching for right-handed currents using parity doubling

In [36], it was shown that, in the chiral symmetry restoration limit, the $B \to V\gamma$ and $B \to A\gamma$ amplitudes obey well-defined relations

$$\bar{\mathcal{A}}_\chi^{\bar{B}\to\rho\gamma}(C, C') = \bar{\mathcal{A}}_\chi^{\bar{B}\to a_1\gamma}(-C, C') \,, \quad \chi = L, R \,, \tag{7.29}$$

where the C and C' are Wilson coefficients associated with generic operators contributing to the effective Hamiltonian

$$H_{\text{eff}}^{b\to D\gamma} \sim C\, \bar{D}_L \Gamma b\, O_r + C'\, \bar{D}_R \Gamma b\, O_r' \,, \tag{7.30}$$

and $O_r^{(\prime)}$ stands for the remaining part of the effective operator. Each chirality amplitude in (7.2) can then be decomposed into contributions from O and O' operators

$$\bar{\mathcal{A}}_\chi^{\bar{B}\to V\gamma} = \bar{A}_\chi + \bar{A}_\chi' \,. \tag{7.31}$$

The relation (7.29) (with summation over $i = u, c$ implied) leads to

$\bar{\mathcal{A}}_\chi^{\bar{B}\to\rho(a_1)\gamma}$	$\bar{A}_{SD,\chi}$	$\bar{A}_{LD,\chi}$	$\bar{A}'_{SD,\chi}$	$\bar{A}'_{LD,\chi}$
$\chi = L$	± 1	$\pm\tilde{\lambda}_i \epsilon_{V,L}^i$	0	$\tilde{\lambda}_i \epsilon_{V,L}'^i$
$\chi = R$	0	$\pm\tilde{\lambda}_i \epsilon_{V,R}^i$	$\hat{m}_{d,s} + \Delta_R e^{i\phi_{\Delta_R}}$	$\tilde{\lambda}_i \epsilon_{V,R}'^i$

, (7.32)

where $\tilde{\lambda}_i = \lambda_i/\lambda_t$ is the normalised CKM factor. The SD contribution to the RHC, encoded in C_7', is parametrised by

$$\hat{C}_7' \equiv \frac{C_7'}{C_7} = \hat{m}_{d,s} + \Delta_R e^{i\phi_{\Delta_R}} \,, \tag{7.33}$$

where $\Delta_R e^{i\phi_{\Delta_R}}$ is the NP contribution to the RHC. The remaining terms in the breakdown (7.32) correspond to, for example, the LD quark loop contributions, or corrections due to the $\mathcal{O}_8$ contribution, with $\bar{A}'_{LD,L} = 0$ and $\bar{A}'_{LD,R}$ small in the normalisation above [72]. Finally, the zero entries in (7.32) follow from the algebraic relation $\sigma^{\alpha\beta}\gamma_5 = -\frac{i}{2}\epsilon^{\alpha\beta\gamma\delta}\sigma_{\gamma\delta}$, which descends to the form-factor relation $T_1(0) = T_2(0)$.

The signs in (7.32) follow from the identity

$$\gamma_5 S_{\mathcal{G}}^{(q)}(w,z) = -S_{\mathcal{G}}^{(q)}(w,z)\gamma_5 \,, \tag{7.34}$$

where $S_{\mathcal{G}}^{(q)}(w,z) = \langle w|(\not{D} + im_q)^{-1}|z\rangle$ is the quark propagator in the gluon background field. This only applies in the restoration limit

$$\{m_q, \langle\bar{q}q\rangle, \dots\} \to 0 \,, \Rightarrow SU(N_F)_V \to SU(N_F)_V \times SU(N_F)_A \times U(1)_A \,, \tag{7.35}$$

where the dots stand for other $SU(N_F)_A \times U(1)_A$-violating condensates, such as $\langle\bar{q}\sigma\cdot Gq\rangle$. In the previous chapter, this limit was seen explicitly in computations of the DA parameters, but the argument can also be made based on a path-integral approach [36].

The crucial point is that the sign relations in (7.32) survive the breaking of the chiral symmetry, even if exact equality of the contributions to (7.32) no longer holds. This will now be exploited to show that combining the time-dependent CP asymmetries of $B \to V(A)\gamma$ decays provides a powerful technique to search for RHC.

7.5.1 Time-dependent CP asymmetries

The time-dependent CP asymmetry (2.20) was used to define general observables S, C, and H, where S and C are respectively measures of indirect and direct CP violation. For the more specific case of $\bar{B} \to V\gamma$ decays, the definitions of S and H are[2]

$$\begin{aligned} S(H) &= 2\mathrm{Im(Re)}\left[\frac{q}{p}(\bar{\mathcal{A}}_L\mathcal{A}_L^* + \bar{\mathcal{A}}_R\mathcal{A}_R^*)\right]\mathcal{N}^{-1} \,, \\ C &= (|\mathcal{A}_L|^2 + |\mathcal{A}_R|^2) - (|\bar{\mathcal{A}}_L|^2 + |\bar{\mathcal{A}}_R|^2)\mathcal{N}^{-1} \,, \end{aligned} \tag{7.36}$$

where $\mathcal{N} = |\mathcal{A}_L|^2 + |\bar{\mathcal{A}}_L|^2 + |\mathcal{A}_R|^2 + |\bar{\mathcal{A}}_R|^2$ is the normalisation. It can be seen from these definitions that S and H arise from interference terms between the left- and right-handed amplitudes, whereas C is not so sensitive to RHC (on the assumption that such currents are suppressed, then the RHC contribution to C is dominated by the leading left-handed amplitude).

[2] In the PDG notation [128], $H \equiv \mathcal{A}^{\Delta\Gamma}$.

These amplitudes can be written

$$\begin{aligned}
\bar{\mathcal{A}}_L &\sim (1 \quad + \tilde{\lambda}_i\, \epsilon^i_{V,L}) \quad \Rightarrow \quad \mathcal{A}_R \sim \xi_V (1 \quad + \tilde{\lambda}^*_i\, \epsilon^i_{V,L})\,, \\
\bar{\mathcal{A}}_R &\sim (\hat{C}'_7 + \tilde{\lambda}_i\, \epsilon^i_{V,R}) \quad \Rightarrow \quad \mathcal{A}_L \sim \xi_V (\hat{C}'_7 + \tilde{\lambda}^*_i\, \epsilon^i_{V,R})\,,
\end{aligned} \tag{7.37}$$

where the result on the right follows by CP conjugation, and ξ_V is the CP eigenvalue of V. Assuming $|C'_7| \ll |C_7|$ and $\epsilon^i_{V(A)L} \ll 1$, then S and H are well-approximated by

$$\begin{aligned}
S(H)_{V(A)\gamma} = 2\xi_V \{ |\tilde{\lambda}_i| \mathrm{Re}[\epsilon^i_{V(A),R}] \begin{matrix}\sin\\ \cos\end{matrix} (\phi_t + \phi_i - \phi_{B_D}) \pm \\
(\hat{m_D} \begin{matrix}\sin\\ \cos\end{matrix} (2\phi_t - \phi_{B_D}) + \Delta_R \begin{matrix}\sin\\ \cos\end{matrix} (2\phi_t + \phi_R - \phi_{B_D}))\}\,,
\end{aligned} \tag{7.38}$$

where the sines and cosines refer to S and H, and the signs $\pm$ follow from the breakdown (7.32).

The mixing angles ϕ_{B_D} are

$$\phi_{B_d} \simeq 2\beta\,, \quad \phi_{B_d} \simeq -2\lambda^2\eta \tag{7.39}$$

and the ϕ_i $(i = u, c, t)$ in the above general expressions (7.38) are

$$\begin{aligned}
b \to d: \quad & \phi_u \simeq -\gamma\,, \quad \phi_c = \pi - A^2\eta\lambda^4 \quad \phi_t = \beta\,, \\
b \to s \ : \quad & \phi_u \simeq -\gamma\,, \quad \phi_c = O(\lambda^6) \qquad\quad \phi_t \simeq \pi - \lambda^2\eta\,,
\end{aligned} \tag{7.40}$$

where the angles above are expressed in terms of the Wolfenstein parameters, to $\mathcal{O}(\lambda^4)$, and $\beta \simeq 23^\circ$, $\gamma \simeq 70^\circ$, and $\lambda^2\eta \simeq 1^\circ$. With the approximations $m_d \approx 0$, $\lambda^2\eta \approx 0$, and $|\tilde{\lambda}^s_u| \ll 1$, explicit forms of S, H for the channels above can be written more compactly as

$$\begin{aligned}
S_{B_d \to \rho(a_1)} &= 2\left(\sin\beta \mathrm{Re}[\epsilon^c_R]|\tilde{\lambda}^d_c| \pm \Delta_R \sin\phi_R + \sin(\beta+\gamma)\mathrm{Re}[\epsilon^u_R]|\tilde{\lambda}^d_u|\right)\,, \\
S_{B_d \to K^*(K_1)} &= 2\xi\left(\mp\left(\Delta_R \sin(2\beta - \phi_R) + \frac{m_s}{m_b}\sin 2\beta\right) + \sin 2\beta \mathrm{Re}[\epsilon^c_R]|\tilde{\lambda}^s_c|\right)\,, \\
S_{B_s \to \phi(f_1)} &= 2\left(\pm\Delta_R \sin\phi_R\right)\,, \\
S_{\bar{B}_s \to K^*(K_1)} &= 2\xi\left(\frac{m_d}{m_b}\sin 2\beta + \sin(\beta)\mathrm{Re}[\epsilon^c_R]|\tilde{\lambda}^d_c| \pm \Delta_R \sin(2\beta + \phi_R)\right)\,,
\end{aligned} \tag{7.41}$$

and

$$
\begin{aligned}
H_{B_d\to\rho(a_1)} &= 2\left(\cos\beta\mathrm{Re}[\epsilon_R^c]|\tilde{\lambda}^c| \pm \Delta_R\cos\phi_R + \cos(\beta+\gamma)\mathrm{Re}[\epsilon_R^u]|\tilde{\lambda}^u|\right) ,\\
H_{B_d\to K^*(K_1)} &= 2\xi\left(\pm\left(\Delta_R\cos(2\beta-\phi_R) + \frac{m_s}{m_b}\cos 2\beta\right) + \cos 2\beta\mathrm{Re}[\epsilon_R^c]|\tilde{\lambda}^c|\right) ,\\
H_{B_s\to\phi(f_1)} &= 2\left(\pm\left(\Delta_R\cos\phi_R + \frac{m_s}{m_b}\right) - \mathrm{Re}[\epsilon_R^c]|\tilde{\lambda}^c|\right) ,\\
H_{\bar{B}_s\to K^*(K_1)} &= 2\xi\left(\pm\Delta_R\cos(2\beta+\phi_R) + \cos\beta\mathrm{Re}[\epsilon_R^c]|\tilde{\lambda}^c|\right.\\
&\qquad \left. + \cos(\beta-\gamma)\mathrm{Re}[\epsilon_R^u]|\tilde{\lambda}^u|\right) .
\end{aligned}
\tag{7.42}
$$

Of this set, H_{B_d} is in practice not measurable, as the decay width Γ_d is too small to have an observable effect, while the $\bar{B}_s \to K^*$ decays are experimentally less attractive. The remaining four observables are, however, of some interest. In particular, both S and H can be well-measured for the $B_s \to \phi(f_1)\gamma$ channels. Combining the results above, it follows that

$$
\begin{aligned}
\left(H_{\phi\gamma} \pm H_{f_1(h_1)\gamma}\right) &\simeq -2\mathrm{Re}[\epsilon_{\phi,R}^c + \epsilon_{f_1(h_1),R}^c]\\
&= -2\mathrm{Re}[\epsilon_{\phi,R}^c](1+\mathbb{R}_{f_1(h_1),\phi}^c) ,
\end{aligned}
\tag{7.43}
$$

and

$$
\Delta_R\cos(\phi_{\Delta_R}) = \frac{1}{4}(H_{\phi\gamma} \mp H_{f_1(h_1)\gamma}) + \frac{1}{2}\mathrm{Re}[\epsilon_{\phi,R}^c - \epsilon_{f_1(h_1),R}^c] - \hat{m}_s . \tag{7.44}
$$

where

$$
\mathbb{R}_{V,A}^i \equiv \frac{\mathrm{Re}[\epsilon_{V,R}^i]}{\mathrm{Re}[\epsilon_{A,R}^i]} = 1 + \mathcal{O}(m_q, \langle\bar{q}q\rangle) . \tag{7.45}
$$

In the chiral restoration limit (7.35), the ratio $\mathbb{R}_{V,A}$ approaches one, but, using the results in table 7.2, along with the estimates for axial mesons in the previous chapter, a more accurate estimate for the $B_s \to \phi(f_1(1420))\gamma$ channel is

$$
\mathbb{R}_{\phi,f_1(1420)}^c = 1.006\frac{T_{1,f_1}(0)}{T_{1,\phi}(0)} . \tag{7.46}
$$

The remaining inputs are the tensor form factors. The most recent evaluations of tensor form factors are in [99] for vector mesons, and [199] for axial mesons. As a preliminary estimate, the ratio $\left|\frac{T_{1,f_1}(0)}{T_{1,\phi}(0)}\right|$ is within 30% of 1, which is consistent with the expectations in [36]. This means that (7.44) provides a potential extraction of NP contributions to RHC with a remarkable improvement, in the region of an order of magnitude reduction in the total uncertainty from LD

contributions.

7.5.2 $B \to V\ell\bar{\ell}$ and other decay channels

Although the analysis above was restricted to $q^2 = 0$, the results in appendix F, along with the extension of (7.21) to $q^2 > 0$, allows for an estimate of the LD charm-loop contribution to $B \to V\ell\bar{\ell}$ decays, using the angular observables defined by the angular distribution in (4.40). From the explicit definitions in equation (C.25), it can be seen that $\tilde{G}_2^{2,2}$ is also sensitive to RHC. This observation was also made in [110, 200], where the same observables were referred to as $A_T^{(2)}$, or $P_{1,3}$ in the notation of [121].

A measurement of the right-handed LD contribution to $B \to (V, A), \ell\bar{\ell}$ decays, at at low q^2, could therefore also be a promising probe for NP in RHC. In this respect, $B \to K^* e^+ e^-$ is a promising channel to complement the parity-doubling approach described above. This has already been studied at the LHCb experiment [201], and Belle II is likely to study this channel as well. Exploring the potential of time-dependent angular distributions would also seem to be an interesting possibility [202].

7.6 Conclusions

This chapter has presented a preliminary analysis of the long-distance charm loop contribution to $B \to (V, A)\gamma$ decays, with an extension to $B \to (V, A)\ell\bar{\ell}$ anticipated in the related paper [194], currently in preparation. The preliminary results show that an exclusive calculation of long-distance charm loops indeed leads to only a small contribution, particularly to the right-handed currents, which is in line with the observations of [35] and [186]. The latter calculation used a different method, relying on the large m_c limit, which in particular provides no possibility of a strong phase in the contribution, but the full LCSR computation does indicate the presence of a strong phase in such loops, even at $q^2 = 0$. Both results disagree with the inclusive computations in [195], but the computation above shows that the scale of contributions to right-handed currents from the charm loop is set by the leading parameters in the three-particle distribution amplitudes, which were computed in the previous chapter and found to be small.

It appears that the charm loops do not generate large contributions to right-handed currents, but the results come with sizeable errors, so it is still important to measure the presence of right-handed currents in radiative and semileptonic $B \to V\gamma/\ell\bar{\ell}$ decays. The discussion of section 7.5, based on the expanded arguments of [36], shows that it is possible to isolate the charm-loop contribution from other, short-distance sources of right-handed currents. Moreover, the approximate symmetry between vector and axial mesons leads to results for a ratio of the right-handed currents contribution from charm loops that is very close to one, even with the breaking of this symmetry due to QCD effects. The numerical closeness to 1 is an accidental value, but as errors in the distribution amplitude parameters largely cancel in the ratio, it is reasonable to assume that the method presented in section 7.5 can offer a significant improvement in the search for right-handed currents.

Chapter 8

Conclusions

The recent experimental results at the LHCb and the first generation of B factories have provided several potential hints of New Physics in rare B meson decay processes. This thesis has provided two promising new avenues that may help to clarify the nature of these anomalies, and in the process has provided improved results for important inputs to the theoretical predictions of these decays.

The first of these approaches, presented in chapter 4, is in understanding more systematically the structure of the $B \to K_J(\to K\pi)\ell_1\bar{\ell}_2$ angular distributions. The rich structure of these distributions had already been explored, and gradually expanded to include the full dimension-six effective Hamiltonian (4.13), since the results of [108], but the results presented in this thesis complete the angular distribution for the $J = 1$ (K^*) channel, including results for non-equal lepton masses for the first time. Alongside these new results, the method detailed in chapter 4 also provides far greater clarity on the origin of the angular structure in the canonical distribution (4.36). It was seen how the restriction to the dimension-six effective Hamiltonian imposes the limitation to moments up to $l_\ell = 2$, and, as a result, plenty of null tests in the form of taking higher moments of the angular distribution at the K^* resonance can be performed in future experiments. This has already happened at LHCb [139], albeit at the $K_2(1430)$ resonance rather than the $K^*(892)$, but it is likely that the same analysis will be applied to future data sets.

The prediction that higher moments vanish, however, only applies in theoretical predictions limited to the dimension-six effective Hamiltonian (4.13) *and* with the

condition that there are no QED corrections, arising from interactions between the final-state leptons and the mesons. Understanding the full consequences of breaking this assumption will require a more complete computation in future, but chapter 5 provided a first step on the road to this. The effects of extending the effective Hamiltonian to include novel derivative operators, which may be generated in exotic NP scenarios including spin-two particles, were analysed in some detail, and it was seen how higher moments then become non-zero in the presence of such operators. An estimate of the scale of these higher moments, within the SM, was provided by a calculation of the Wilson coefficients of these operators, and it was confirmed that these terms are heavily suppressed by a factor $1/m_W^2$ in the SM. While the picture in the presence of QED corrections is more complicated, it was still shown that it is reasonable to expect that the leaking of these corrections into higher moments will fall off with increasing moments. This thesis, in conjunction with the paper [34], therefore provides a strong indication that a moments analysis will be useful in understanding the origin of the present anomalies in $b \to s$ transitions, most notably the $R_{K^{(*)}}$ and P_5' anomalies.

The second part of the thesis, in chapters 6 and 7, considered the question of searching for right-handed currents in radiative $B \to V\gamma$ decays. Based on the suggestion in [36], the key idea is to exploit the approximate symmetries, exact in the chiral restoration limit, between vector and axial mesons. These symmetries were explicitly verified in chapter 6 for the three-particle twist-3 DAs. In the process, new and updated numerical estimates and uncertainties for three-particle DAs have been provided, updating the previous results in [85, 104] by including for the first time the three-gluon condensate. There are some disagreements with the analytic results presented in the previous literature; however, the systematic relationships between the DAs for vector and axial mesons provide a powerful sign that the results in the present work are more reliable.

One application of these parameters is in the computation of long-distance loop contributions to exclusive $B \to V\gamma$ processes. Any attempt to search for NP origins of right-handed currents will necessitate a more complete understanding of such contributions, and chapter 7 presented the calculation of LD charm-loop contributions with a gluon radiated into the final-state meson. A similar calculation was also given in [35], but it appears that there are some disagreements away from the leading moment, and this thesis is the first to present explicit expressions for the next terms in the conformal expansion. When extended to

$q^2 \neq 0$, the same results will also be useful for estimating LD contributions to $B \to V\ell\bar{\ell}$ decays.

The secondary result of chapter 7 was to show that decays to vector and axial mesons are linked by the same symmetry, in the chiral restoration limit. This was exploited to show that combining the analysis of $B \to V\gamma$ and $B \to A\gamma$ decays, for example with a measure of time-dependent CP violation, can provide a much-improved measurement of NP contributions to right-handed currents. A first estimate of the ratio of LD contributions to $B_s \to \phi(f_1)\gamma$ was provided, which supports the expectation of [36] that these ratios should be close to 1, with deviations only at the order of QCD corrections and hadronic parameters.

At the time of writing, the LHC experiment has only just started to release results based on data collected in Run II, while the Belle II experiment is expected to begin collecting data this year. Both experiments are certain to provide vastly improved results concerning rare B decay processes, and it is highly likely that these new results will either confirm or rule out the anomalies so far seen in B decays. In either case, a better understanding of such processes within the SM is clearly important to complement the rapid progress in experimental precision.

Appendix A

Conventions

This appendix collects general conventions and useful general results used throughout the thesis.

A.1 Conventions

The covariant derivative has the sign convention

$$D_\mu = \partial_\mu - ieA_\mu - ig_s t^a A^a_\mu \,, \tag{A.1}$$

which is consistent with that of [38]. The relative sign of the gluon contribution to the covariant derivative is important in terms that are linear in the coupling to the strong force g_s, and terms sensitive to this (including, for example, G-parity odd parameters of DAs) change sign according to the choice of convention.

The Levi-Civita tensor $\epsilon_{\mu\nu\rho\tau}$ can also have differing sign conventions. This thesis uses the convention $\epsilon_{0123} = +1$, equivalent to the result that $\mathrm{Tr}[\gamma^\mu\gamma^\nu\gamma^\rho\gamma^\tau\gamma_5] = 4i\epsilon^{\mu\nu\rho\tau}$.

When working with FeynCalc [203, 204], it is important to ensure that the correct sign convention for the Levi-Civita tensor is employed. In older versions this would be achieved using the commands

```
SetOptions[Tr, LeviCivitaSign->1];
SetOptions[DiracTrace, LeviCivitaSign->1]; ,
```

although the most recent version of FeynCalc uses instead the global command

```
$LeviCivitaSign = 1;
```

to achieve the same effect.[1]

A.2 Fock-Schwinger gauge

The fundamental interactions in the SM possess a gauge symmetry defined by their respective gauge groups. This provides a choice of gauge-fixing condition for the fields A_μ. Many different choices can be made, each one being particularly suited for different situations. In chapter 6, heavy use was made of the Fock-Schwinger gauge condition [175, 176, 205, 206], and its properties are briefly described here.

The principal definition of the Fock-Schwinger gauge is

$$(x - x_0) \cdot A(x) = 0 \tag{A.2}$$

where x_0 is a random point in space-time that expresses the residual gauge freedom in this choice of gauge and, in practice, is usually set to zero (although preserving this freedom is useful to test whether or not particular quantities are indeed gauge-invariant). As an immediate consequence of this gauge choice, it can be seen that

$$(x - x_0) \cdot \partial \equiv (x - x_0) \cdot D \,, \tag{A.3}$$

which is to say that the partial derivatives in a Taylor expansion can always be replaced with covariant derivatives. It is possible to show that [175]

$$A_\mu(x) = \int_0^1 d\alpha \, \alpha (x - x_0)^\omega F_{\omega\mu}(\alpha x) \,, \tag{A.4}$$

and, in turn, using a Taylor expansion of $F_{\mu\nu}$ about the fixed point and exploiting (A.3), one obtains

$$A(x) = \sum_{n=0}^{\infty} \frac{1}{n!(n+2)} (x-x_0)^\omega (x-x_0)^{\omega_1} \dots (x-x_0)^{\omega_n} \left[D_{\omega_1}, [\dots [D_{\omega_n}, F_{\omega\mu}(x_0)] \dots] \right] . \tag{A.5}$$

[1] A bug related to this command was fixed after it was pointed out by the author.

The Fock-Schwinger gauge also allows the freedom to write the quark fields in terms of a Taylor expansion using the covariant derivative instead of the normal derivative:

$$q(x) = \sum_{n=0}^{\infty} \frac{1}{n!}(x - x_0)^{\omega_1} \dots (x - x_0)^{\omega_n} D_{\omega_1} \dots D_{\omega_n} q(x_0)\,, \tag{A.6}$$

and the conjugate of this for $\bar{q}(x)$. Using these relations, normal products of fields can always be expanded in terms of gauge-invariant local quantities, even if the original normal product is non-local and not itself gauge-invariant.

A.3 Vacuum condensates

The condensates used in this thesis are all those that appear up to mass dimension-six. These include the two- and three-gluon condensates, the two- and four-quark condensates, and the "mixed" condensate, made from two quark fields and one gluon field. Throughout, the shorthand notation $G_{\mu\nu} = g_s t_a G^a_{\alpha\beta}$ has been used, while the dual field $\tilde{G}$ is defined by $\tilde{G}_{\mu\nu} = \frac{i}{2}\epsilon_{\alpha\beta\mu\nu}G^{\mu\nu}$. The $t_a = \lambda_a/2$, and λ_a are the usual Gell-Mann matrices for $SU(3)$, and are used to define the structure constants f of $SU(3)$, with the algebra

$$[t_a, t_b] = i f_{abc} t_c\,. \tag{A.7}$$

The relevant gluon condensates can be found in [88, 176]. This thesis uses normalisations in which

$$\left\langle G^2 \right\rangle = \left\langle g_s^2 G^a_{\mu\nu} G^{a,\mu\nu} \right\rangle = 4\pi^2 \langle \frac{\alpha_s}{\pi} G^2 \rangle_{\text{SVZ}}\,, \tag{A.8}$$

$$\left\langle fG^3 \right\rangle = \left\langle g_s^3 f^{abc} G^a_{\mu\nu} G^{b,\nu}_{\rho} G^{c,\rho\mu} \right\rangle\,. \tag{A.9}$$

where SVZ refers to the convention in [88]. Then, in d dimensions, the two-gluon condensate is given by

$$\langle 0|G_{\alpha\beta}G_{\alpha'\beta'}|0\rangle = \frac{1}{2d(d-1)}\left(g_{\alpha\alpha'}g_{\beta\beta'} - g_{\alpha\beta'}g_{\alpha'\beta}\right)\left\langle G^2 \right\rangle, \tag{A.10}$$

while the three-gluon condensates are given by

$$\langle 0|G_{\alpha\beta}G_{\alpha'\beta'}G_{\rho\tau}|0\rangle = \frac{i}{4d(d-1)(d-2)}\left(\left(\left(g_{\alpha\alpha'}g_{\beta\rho} - g_{\alpha\rho}g_{\alpha'\beta}\right)g_{\beta'\tau} - (\alpha' \leftrightarrow \beta')\right)\right.$$

$$- (\rho \leftrightarrow \tau)) \left\langle fG^3 \right\rangle , \tag{A.11}$$

$$\langle 0|\nabla_\rho G_{\alpha\beta} \nabla_\tau G_{\alpha'\beta'}|0\rangle = \frac{-1}{2d^2(d-1)} \left(\left(\left(g_{\alpha\rho} g_{\alpha'\beta} - g_{\alpha\alpha'} g_{\beta\rho} \right) g_{\beta'\tau} - (\alpha' \leftrightarrow \beta') \right) - (\rho \leftrightarrow \tau) \right.$$
$$\left. + 2 \left(g_{\alpha\alpha'} g_{\beta\beta'} - g_{\alpha\beta'} g_{\alpha'\beta} \right) g_{\rho\tau} \right) \left\langle fG^3 \right\rangle . \tag{A.12}$$

All other gluon condensates up to dimension six either vanish or are related to those given above via partial integration.

The remaining condensates used in this thesis all include quarks, and are best-defined within the Fock-Schwinger gauge, outlined in section A.2, to make the spatial dependence explicit. The expressions below are adapted from [70, 175].

It is traditional to assume that four-quark condensates can be reduced to products of two-quark condensates by use of the Vacuum Factorisation Approximation [89, 175]. This will be used in numerical results, but it is convenient to preserve the specific origin of four-quark contributions in the analytic expressions, which make use of the following notation to represent the various condensates that arise. The first kind of four-quark condensate is written

$$\left\langle V_Q^a V_f^a \right\rangle = \left\langle \bar{Q} \gamma_\mu t^a Q \sum_f \bar{f} \gamma^\mu t^a f \right\rangle , \tag{A.13}$$

where $Q = q, s$, and the sum is over (light) quark flavours $f = u, d, s$. Condensates of the second kind are written

$$\langle \Gamma^a \Gamma^a \rangle = \langle \bar{q} \, \Gamma t^a s \bar{s} \, \Gamma^a t^a q \rangle , \tag{A.14}$$

where $\Gamma = \{S, P, V, A, T\} = \{\mathbf{1}, i\gamma_5, \gamma_\mu, \gamma_\mu\gamma_5, \sigma_{\mu\nu}\}$ are the possible Lorentz structures that arise, and summation over colour and Lorentz indices is implied.

For comparison with the previous literature, it is, however, important to apply the Vacuum Factorisation Approximation. The translations are

$$\langle \Gamma^a \Gamma^a \rangle|_{\Gamma=\{S,P,V,A,T\}} = \frac{C_F}{4N_C} \langle \bar{q}q \rangle \langle \bar{s}s \rangle \times \{-1, 1, -4, 4, -12\} ,$$
$$\left\langle V_Q^a V_f^a \right\rangle = -\frac{C_F}{N_C} \left\langle \bar{Q}Q \right\rangle^2 , \tag{A.15}$$

where $\dfrac{C_F}{N_C} = \dfrac{4}{9}$.

Using these definitions and working in Fock-Schwinger gauge, one finds

$$\left\langle \bar{q}_m^i(x_1) q_n'^j(x_2) \right\rangle = \delta_{qq'}\delta^{ij} \left[\frac{1}{12}\left(1 + \frac{i}{d} m_q \not{x}_{12}\right)_{nm} \langle \bar{q}q \rangle + \frac{\pi\alpha_s}{72}\left(\frac{i}{12} x_{12}^2 (\not{x}_{12})_{nm} \left\langle V_q^a V_f^a \right\rangle \right) + \frac{1}{192} x_{12}^2 (1 + \frac{i}{6} m_q \not{x}_{12})_{nm} \langle \bar{q}\sigma \cdot Gq \rangle \right] , \tag{A.16}$$

where $x_{12} \equiv (x_1 - x_2)$. The mixed condensate can be written, up to first order in the fields, as

$$\begin{aligned} \left\langle \bar{q}_m^i(x_1)(G^{\alpha\beta}(z) q')_n^j(x_2) \right\rangle = {} & \delta_{qq'}\delta^{ij} \frac{i\pi\alpha_s}{72} \left\langle V_q^a V_f^a \right\rangle \left(\sigma^{\alpha\beta} \not{x}_2 - \not{x}_1 \sigma^{\alpha\beta} + 2iz^{[\alpha}\gamma^{\beta]} \right)_{nm} \\ & + \delta_{qq'}\delta^{ij} \frac{1}{288} \langle \bar{q}\sigma \cdot Gq \rangle \left(2\sigma^{\alpha\beta} + m_q \left(\gamma^{[\alpha} x_{12}^{\beta]} + i\sigma^{\alpha\beta}(\not{x}_{12}) \right) \right)_{nm} , \end{aligned} \tag{A.17}$$

where the Chisholm identity

$$\gamma_\mu \gamma_\nu \gamma_\rho = g_{\mu\nu}\gamma_\rho - g_{\mu\rho}\gamma_\nu + g_{\nu\rho}\gamma_\mu - i\gamma^\tau \gamma_5 \epsilon_{\mu\nu\rho\tau} \tag{A.18}$$

has been employed to write the first line in a form symmetric in $x_1 \leftrightarrow x_2$. Note that this is different from equation (4.23) of [70], disagreeing with the factor of the $\gamma^{[\alpha} z^{\beta]}$ term in the first line and the relative sign of the two contributions in the second line.[2]

The projection of free quarks onto states of specific spin is given by

$$\begin{aligned} \bar{q}_m s_n &= \sum_i (\bar{q}\mathcal{S}_i s)(\tilde{\mathcal{S}}_i)_{nm} \\ &= (\bar{q}s)\frac{1}{4}\delta_{nm} - (\bar{q}i\gamma_5 s)\frac{1}{4}(i\gamma_5)_{nm} + (\bar{q}\gamma_\mu s)\frac{1}{4}\gamma^\mu_{nm} - (\bar{q}\gamma_\mu\gamma_5 s)\frac{1}{4}(\gamma^\mu\gamma_5)_{nm} \\ &\quad + (\bar{q}\sigma_{\mu\nu}s)\frac{1}{8}(\sigma^{\mu\nu})_{nm} , \end{aligned} \tag{A.19}$$

which is used particularly often when computing four-quark condensate contributions to DAs.

[2] The first line of (A.17) can also be written $\delta^{ij}\frac{\pi\alpha_s}{72}\left\langle V_q^a V_f^a \right\rangle \left(\sigma^{\alpha\beta}(\not{x}_1 - \not{x}_2) + 2i\gamma^{[\alpha}(z-x)^{\beta]} \right)$, which makes the gauge invariance more manifest.

A.4 Expressions for one-loop integrals

A.4.1 Massless one-loop integrals with one external momentum and up to four momenta in the numerator

In calculating the two-loop diagrams in this paper, it is useful to have a general expression for one-loop integrals with propagators to an arbitrary power. These can be found in, for example, appendix C of [175].[3] Defining structures $k^{(n)} \equiv k^{(\mu_1\mu_2\ldots\mu_n)}$ such that $k^{(n)}$ is traceless over any contraction of two indices, then

$$\begin{aligned} L^{(n)}(p;r,s) &= \mu^{2\varepsilon}\int\frac{\mathrm{d}^d k}{(2\pi)^d}\frac{k^{(n)}}{(k^2+i\epsilon)^r((k+p)^2+i\epsilon)^s} \\ &= \frac{i}{16\pi^2}\left(\frac{\mu^2}{-p^2}\right)^{\varepsilon}\frac{1}{(p^2)^{r+s-2}}p^{(n)}\frac{\Gamma(r+s-2-\varepsilon)\Gamma(n-r+2+\varepsilon)\Gamma(-s+2+\varepsilon)}{\Gamma(r)\Gamma(s)\Gamma(n-r-s+4-2\varepsilon)}\,. \end{aligned} \tag{A.20}$$

The $p^{(n)}$, up to $n=4$, are

$$p^{(0)} = 1\,, \tag{A.21}$$

$$p^{(1)} = p^\mu\,, \tag{A.22}$$

$$p^{(2)} = p^\mu p^\nu - \frac{1}{d}p^2 g^{\mu\nu}\,, \tag{A.23}$$

$$p^{(3)} = p^\mu p^\nu p^\rho - \frac{1}{d+2}p^2\left(p^\rho g^{\mu\nu}+p^\nu g^{\mu\rho}+p^\mu g^{\nu\rho}\right)\,, \tag{A.24}$$

$$\begin{aligned} p^{(4)} = {} & p^\mu p^\nu p^\rho p^\tau - \frac{p^2\left(p^\rho p^\tau g^{\mu\nu}+p^\nu p^\tau g^{\mu\rho}+p^\nu p^\rho g^{\mu\tau}+p^\mu p^\tau g^{\nu\rho}+p^\mu p^\rho g^{\nu\tau}+p^\mu p^\nu g^{\rho\tau}\right)}{d+4} \\ & + \frac{p^4\left(g^{\mu\tau}g^{\nu\rho}+g^{\mu\rho}g^{\nu\tau}+g^{\mu\nu}g^{\rho\tau}\right)}{(d+2)(d+4)}\,. \end{aligned} \tag{A.25}$$

Inverting these relations allows one to compute general one-loop integrals with up to four loop momenta in the propagator.

For the non-local sum rules one also needs the following integrals:

$$\begin{aligned} I_0[a,b,m] \quad = \quad & \int_k e^{if_k k\cdot z}\frac{(k\cdot z)^m}{(k^2-m_1^2)^a((k-p)^2-m_2^2)^b} = \frac{i}{(4\pi)^{d/2}}(-)^{a+b}\frac{\Gamma[a+b-d/2]}{\Gamma[a]\Gamma[b]} \\ \times \quad & (p\cdot z)^m\int_0^1 du\, e^{if_k\bar{u}(pz)}\,u^{a-1}\bar{u}^{b+m-1}(\Lambda^2)^{d/2-(a+b)}\,, \end{aligned} \tag{A.26}$$

[3] Note that the authors of [175] use conventions in which the dimensional regularisation scheme is performed in $d = 4+2\varepsilon$ dimensions, as opposed to $d = 4-2\varepsilon$ in the results above.

and

$$
\begin{aligned}
I_1[a,b,m,w] &= \int_k e^{if_k k\cdot z}\frac{(k\cdot z)^m(k\cdot w)}{(k^2-m_1^2)^a((k-p)^2-m_2^2)^b} = \bar{u}p\cdot w I_0[a,b,m] \\
&+ \frac{i}{(4\pi)^{d/2}}(-)^{a+b-1}\frac{\Gamma[a+b-d/2-1]}{\Gamma[a]\Gamma[b]}\frac{w\cdot z}{2}(p\cdot z)^{m-1} \\
&\times \int_0^1 du\, e^{if_k\bar{u}p\cdot z}\, u^{a-1}\bar{u}^{b+m-2}(\Lambda^2)^{1+d/2-(a+b)}\left(if_k\bar{u}p\cdot z+m\right)\ ,
\end{aligned}
\tag{A.27}
$$

$$
\begin{aligned}
I_2[a,b,m,w_1,w_2] &= \int_k e^{if_k k\cdot z}\frac{(k\cdot z)^m(k\cdot w_1)(k\cdot w_2)}{(k^2-m_1^2)^a((k-p)^2-m_2^2)^b} \\
&= (\bar{u}p\cdot w_1 I_1[a,b,m,w_2]+(w_1\leftrightarrow w_2)) - \bar{u}p\cdot w_1\bar{u}p\cdot w_2 I_0[a,b,m] \\
&+ \frac{i}{(4\pi)^{d/2}}(-)^{a+b-1}\frac{\Gamma[a+b-d/2-1]}{\Gamma[a]\Gamma[b]}\frac{w_1\cdot w_2}{2}\,(p\cdot z)^m \\
&\times \int_0^1 du\, e^{if_k\bar{u}p\cdot z}\, u^{a-1}\bar{u}^{b+m-1}(\Lambda^2)^{1+d/2-(a+b)} \\
&+ \frac{i}{(4\pi)^{d/2}}(-)^{a+b}\frac{\Gamma[a+b-d/2-2]}{\Gamma[a]\Gamma[b]}\frac{w_1\cdot z w_2\cdot z}{2}\,(p\cdot z)^{m-2} \\
&\times \int_0^1 du\, e^{if_k\bar{u}p\cdot z}\, u^{a-1}\bar{u}^{b+m-3}(\Lambda^2)^{2+d/2-(a+b)} \\
&\times \left(\frac{1}{2}(if_K\bar{u}p\cdot z)^2+mif_K\bar{u}p\cdot z+\frac{m(m-1)}{2}\right)\ ,
\end{aligned}
\tag{A.28}
$$

where $\Lambda^2 = -p^2u\bar{u}+um_1^2+\bar{u}m_2^2$, $m_1\equiv m_s$ and $m_2\equiv m_q$ in this case owing to momentum assignments, f_k is some constant factor, and w is an arbitrary four-vector. To relate to the results in chapter 6, the Feynman parameter u is further identified with α_1 or α_2, depending on the relevant diagram, by matching the exponential that results on to the canonical form $e^{-ipz(\alpha_2+v\alpha_3)}$. These results match equations (B.1,B.2) of [70], in the limit of zero masses, and with a factor of $\frac{-i}{(4\pi)^{d/2}}$ difference (which is merely a choice of normalisation). They can be derived through a series expansion, use of z^2=0, and general one-loop integrals from, for example, appendix A of [38].

A.4.2 Passarino-Veltmann functions for massless one-loop integrals

The conventions are as in FeynCalc [203, 204], while analytic results have been checked against [207] and Package-X [208, 209]. For notational convenience, the mass arguments of the function have been omitted. Dimensional regularisation with $d = 4 - 2\varepsilon$ dimensions has been used.

The general loop integral is then defined by

$$I_n(p_1^2, p_2^2, \dots) = \frac{\mu^{4-D}}{i\pi^{\frac{D}{2}}} \int \mathrm{d}^D l \frac{1}{(l^2 + i\epsilon)((l+p_1)^2 + i\epsilon)((l+p_1+p_2)^2 + i\epsilon)\dots} \tag{A.29}$$

where, eg, $I_0 = A_0$ and $I_1 = B_0$ in the usual notation of Passarino-Veltmann functions. Specific examples used in these computations, including the pole in ε, are

$$\begin{aligned} B_0(p^2) &= \frac{1}{\varepsilon} + 2 - \ln\frac{-p^2}{\mu^2}\,, \\ C_0(0, p^2, p^2) &= -\frac{1}{\varepsilon p^2} + \frac{1}{p^2}\ln\frac{-p^2}{\mu^2}\,, \\ D_0(0, p^2, 0, p^2, p^2, p^2) &= -\frac{2}{\varepsilon p^4} + \frac{2}{p^4}\left(-1 + \ln\frac{-p^2}{\mu^2}\right)\,. \end{aligned} \tag{A.30}$$

For the two-loop integral in diagonal sum rules, it is also helpful to have the unexpanded form of $B_0(p^2)$ [207], which is

$$B_0(p^2) = \left(\frac{\mu^2}{-p^2 - i\epsilon}\right)^{\varepsilon}\left(\frac{1}{\varepsilon} + 2\right)\,. \tag{A.31}$$

A.4.3 Fermion propagators in external gluon field

The fermion and gluon propagators can be expanded order-by-order in the external field. Below, the explicit expansion for the fermion propagator in a background field with Fock-Schwinger gauge $x \cdot A(x) = 0$ has been provided [210].[4] Defining

$$S(x,y) \;=\; -\,i\,\left\langle T\psi(x)\bar{\psi}(y)\right\rangle_A = S^{(0)}(x,y) + S^{(2)}(x,y) + S^{(3)}(x,y) + S^{(4)}(x,y)\,,$$

[4] For a general Fock-Schwinger gauge $(x-x_0)\cdot A(x) = 0$, one replaces $x \to x - x_0$ or $y \to y - x_0$ in the prefactors with derivatives.

then the explicit contributions $S^{(i)}$ to the fermion propagator are[5]

$$S^{(0)}(x,y) \equiv S(x-y) = \int_p e^{-ip(x-y)} S(p) \equiv \int_p e^{-ip(x-y)} \frac{\not{p}+m}{p^2-m^2} \,, \tag{A.32}$$

$$S^{(2)}(x,y) = -\frac{1}{2} G_{\alpha\beta}(0) \left\{ \begin{array}{l} (i\partial_p + x)_\alpha \\ (-i\partial_q + y)_\alpha \end{array} \right\} \int_p e^{-ip\cdot(x-y)} S(p)\gamma_\beta S(q) \,,$$

$$S^{(3)}(x,y) = -\frac{1}{3} \nabla_\alpha G_{\beta\gamma}(0) \left\{ \begin{array}{l} (i\partial_p + x)_\alpha (i\partial_p + x)_\beta \\ (-i\partial_q + y)_\alpha (-i\partial_q + y)_\beta \end{array} \right\} \int_p e^{-ip\cdot(x-y)} S(p)\gamma_\gamma S(q) \,,$$

$$\begin{aligned} S^{(4)}(x,y) = & \frac{1}{4} G_{\alpha\beta} G_{\gamma\delta} \left\{ \begin{array}{l} (+i\partial_p + x)_\alpha (+i\partial_{p+q} + x)_\gamma \\ (-i\partial_{q+k} + y)_\alpha (-i\partial_k + y)_\gamma \end{array} \right\} \int_p e^{-ip\cdot(x-y)} S(p)\gamma_\beta S(q)\gamma_\delta S(k) \\ & - \frac{1}{8} \nabla_\alpha \nabla_\beta G_{\gamma\delta} \left\{ \begin{array}{l} (i\partial_p + x)_\alpha (i\partial_p + x)_\beta (i\partial_p + x)_\gamma \\ (y - i\partial_q)_\alpha (y - i\partial_q)_\beta (y - i\partial_q)_\gamma \end{array} \right\} \int_p e^{-ip\cdot(x-y)} S(p)\gamma_\delta S(q) \,, \end{aligned}$$

where two possible representations are given, either of which can be chosen, with the choice dictated by whichever is most convenient for the specific calculation. The derivatives act on the propagator according to

$$\partial_p^\mu S(p) = -S(p)\gamma^\mu S(p) \,. \tag{A.33}$$

A.5 Borel transformations

The Borel transform is defined as

$$f_{\hat{\mathcal{B}}}(M^2_{\hat{\mathcal{B}}}) = \hat{\mathcal{B}} f(Q^2) = \lim_{Q^2\to\infty, n\to\infty} \frac{(Q^2)^{n+2}}{n!} \left(-\frac{d}{dQ^2}\right)^{n+1} f(Q^2) \,, \tag{A.34}$$

where $Q^2 = -q^2$ is a Euclidean momentum, and $Q^2/n = M^2_{\hat{\mathcal{B}}}$ defines the *Borel mass*.[6]

[5] This also includes the $S^{(3)}$-contribution , which can be inferred from Eq. 2.7 of [211].

[6] Note that the Borel transformation can also be defined as

$$f_{\hat{\mathcal{B}}}(M^2_{\hat{\mathcal{B}}}) = \hat{\mathcal{B}} f(Q^2) = \lim_{Q^2\to\infty, n\to\infty} \frac{(Q^2)^{n+1}}{n!} \left(-\frac{d}{dQ^2}\right)^{n+1} f(Q^2) \,,$$

Here is a selection of useful results.

$$\begin{aligned}
\hat{\mathcal{B}}(Q^2+m^2)^a &= 0\,,\\
\hat{\mathcal{B}}\frac{1}{(Q^2+m^2)^a} &= \frac{1}{\Gamma(a)(M_{\hat{\mathcal{B}}}^2)^{a-1}}e^{-m^2/M_{\hat{\mathcal{B}}}^2}\,,\\
\hat{\mathcal{B}}(Q^2+m^2)^a\ln\frac{Q^2+m^2}{\mu^2} &= (-1)^{a+1}\Gamma(a+1)(M_{\hat{\mathcal{B}}}^2)^{a+1}e^{-m^2/M_{\hat{\mathcal{B}}}^2}\,,\\
\hat{\mathcal{B}}\frac{1}{(Q^2+m^2)^a}\ln\frac{Q^2+m^2}{\mu^2} &= \left(\frac{\Gamma'(a)}{\Gamma(a)}+\ln\frac{M_{\hat{\mathcal{B}}}^2}{\mu^2}\right)\frac{1}{\Gamma(a)(M_{\hat{\mathcal{B}}}^2)^{a-1}}e^{-m^2/M_{\hat{\mathcal{B}}}^2}\,.
\end{aligned}\tag{A.35}$$

In practice, one also needs to perform the Borel transform with a continuum subtraction, defined by the general form

$$\begin{aligned}
\hat{\mathcal{B}}_{sub.}f(Q^2) &= \int_0^{s_0} ds\, e^{-s/M_{\hat{\mathcal{B}}}^2}\frac{1}{\pi}\mathrm{Im}_s f(s)\\
&= f_{\hat{\mathcal{B}}}(M_{\hat{\mathcal{B}}}^2) - \int_{s_0}^{\infty} ds\, e^{-s/M_{\hat{\mathcal{B}}}^2}\frac{1}{\pi}\mathrm{Im}_s f(s)\,,
\end{aligned}\tag{A.36}$$

where the two definitions above are equivalent, but one may be practically easier than the other in numerical applications. In this context the results above can be expressed as

$$\begin{aligned}
\hat{\mathcal{B}}_{sub.}(Q^2+m^2)^a &= 0\,,\\
\hat{\mathcal{B}}_{sub.}\frac{1}{(Q^2+m^2)^a} &= \frac{1}{\Gamma(a)(M_{\hat{\mathcal{B}}}^2)^{a-1}}e^{-m^2/M_{\hat{\mathcal{B}}}^2}\,,\\
\hat{\mathcal{B}}_{sub.}(Q^2+m^2)^a\ln\frac{Q^2+m^2}{\mu^2} &= (-1)^{a+1}\int_0^{s_0} ds\, e^{-s/M_{\hat{\mathcal{B}}}^2}(s-m^2)^a\Theta(s-m^2)\,,\\
\hat{\mathcal{B}}_{sub.}\frac{1}{(Q^2+m^2)^a}\ln\frac{Q^2+m^2}{\mu^2} &= \left(\frac{\Gamma'(a)}{\Gamma(a)}+\ln\frac{M_{\hat{\mathcal{B}}}^2}{\mu^2}\right)\frac{e^{-m^2/M_{\hat{\mathcal{B}}}^2}}{\Gamma(a)(M_{\hat{\mathcal{B}}}^2)^{a-1}} - \int_{s_0}^{\infty} ds\, e^{-s/M_{\hat{\mathcal{B}}}^2}\frac{1}{(s-m^2)^a}\,.
\end{aligned}\tag{A.37}$$

It is also useful to note that the vanishing of polynomial terms under a Borel transformation allows for replacements such as $\frac{(p^2)^n}{m^2-p^2}\to\frac{(m^2)^n}{m^2-p^2}$.

which preserves the dimensionality, but the convention used above is standard in sum rules literature (e.g. appendix B of [70]), and leads to the same results.

Appendix B

Numerical inputs

This appendix briefly presents numerical inputs used in the thesis.

B.1 Meson parameters

The latest meson mass parameters have been taken from the 2016 edition of the PDG [128]. For most of the mesons under consideration, these values have not changed significantly from the 2006 edition [212], except for the f and h particles, where there have been small corrections. These values are presented in tables B.1 and B.2.

B.2 CKM matrix

The CKM matrix was defined, within the Wolfenstein parametrisation, in (2.5). This is useful for phenomenology, but the PDG [128] uses a parametrisation in terms of the three angles θ_{12}, θ_{13}, and θ_{23}, along with the CP-violating phase δ_{13}. These have the physical interpretation of representing probabilities of transitioning between the three quark generations, and in these terms the

Meson	mass/ MeV	Γ/ MeV	$f^{\parallel}$ / GeV	$f^{\perp}(1\text{ GeV})$/ GeV
ρ	775.26(25)	147.8(9)	0.213(5)	0.160(7)
K^*	895.55(20)	50.3(8)	0.204(7)	0.159(6)
ϕ	1019.46(2)	4.247(16)	0.233(4)	0.191(4)
ω	782.65(12)	8.49(8)	0.197(8)	0.148(13)

Table B.1 *Central values and error estimates for the masses and widths Γ, taken from [128], and the decay constants, from [99], for the neutral $J^P = 1^-$ mesons. $f^{\perp}$ is RG-dependent, and the value above is taken at the scale $\mu_f = 1$ GeV.*

CKM matrix is expressed

$$V = \begin{pmatrix} 1 & 0 & 0 \\ 0 & c_{23} & s_{23} \\ 0 & -s_{23} & c_{23} \end{pmatrix} \begin{pmatrix} c_{13} & 0 & s_{13}e^{-i\delta_{13}} \\ 0 & 1 & 0 \\ -s_{13}e^{i\delta_{13}} & 0 & c_{13} \end{pmatrix} \begin{pmatrix} c_{12} & s_{12} & 0 \\ -s_{12} & c_{12} & 0 \\ 0 & 0 & 1 \end{pmatrix}$$
$$= \begin{pmatrix} c_{12}c_{13} & s_{12}c_{13} & s_{13}e^{-i\delta_{13}} \\ -s_{12}c_{23} - c_{12}s_{23}s_{13}e^{i\delta_{13}} & c_{12}c_{23} - s_{12}s_{23}s_{13}e^{i\delta_{13}} & s_{23}c_{13} \\ s_{12}s_{23} - c_{12}c_{23}s_{13}e^{i\delta_{13}} & -c_{12}s_{23} - s_{12}c_{23}s_{13}e^{i\delta_{73}} & c_{23}c_{13} \end{pmatrix}, \quad \text{(B.1)}$$

where $c_{ij} = \cos\theta_{ij}$ and $s_{ij} = \sin\theta_{ij}$.

The Wolfenstein parametrisation [45, 46] can be derived from this by using the redefinitions

$$\begin{aligned} s_{12} &= \lambda\,, \\ s_{23} &= A\lambda^2\,, \\ s_{13}e^{-i\delta_{13}} &= A\lambda^3(\rho - i\eta)\,, \end{aligned} \quad \text{(B.2)}$$

where these relationships apply to all orders in the expansion parameter λ. The series expansion can then be derived from, for example, replacing $c_{12} = \sqrt{1-\lambda^2}$.

Meson	mass / MeV	Γ/ MeV	$f^{\parallel}$ / GeV	$f^{\perp}(1\text{ GeV})$/ GeV
$a_1(1260)$	1230(40)	250-600	0.134	0.134
$b_1(1235)$	1229.5(32)	142(9)	0.134	0.134
$K_1(1270)$	1272(7)	90(20)	0.204	0.159
$K_1(1400)$	1403(7)	174(13)	0.204	0.159
$f_1(1285)$	1281.9(5)	22.7(1)	0.120	0.120
$f_1(1420)$	1426.4(9)	54.9(26)	0.166	0.166
$h_1(1170)$	1170(20)	360(40)	0.132	0.132
$h_1(1380)$	1407(12)	89(23)	0.169	0.169

Table B.2 *Central values for the masses and widths for the axial mesons [128]. The decay constants are computed from the Weinberg sum rules relation $m_V^2 f_V^2 = m_A^2 f_A^2$ [183], while $f^{\parallel} = f^{\perp}$ is assumed. These inputs will be updated based on sum rules determinations in the future [174]. For the f_1 and h_1 sector, the light and heavy mesons are taken to be exactly analogous to the ϕ-ω sector, although a future determination will more properly account for the mixing, as discussed in section 6.4.*

To fourth order in λ, the CKM matrix is

$$V = \begin{pmatrix} 1 - \frac{1}{2}\lambda^2 - \frac{1}{8}\lambda^4 & \lambda & A\lambda^3(\rho - i\eta) \\ -\lambda & 1 - \frac{1}{2}\lambda^2 - \frac{1}{8}(1+4A^2)\lambda^4 & A\lambda^2 \\ A\lambda^3(1 - \rho - i\eta) & -A\lambda^2 + A\lambda^4\left(\frac{1}{2} - \rho - i\eta\right) & 1 - \frac{1}{2}A^2\lambda^4 \end{pmatrix} + \mathcal{O}(\lambda^5), \tag{B.3}$$

where the modifications from the expansion in (2.5) are relatively slight, and in fact a third-order expansion is on its own reasonably accurate. Nevertheless, the elements V_{cd} and V_{cs} acquire non-zero phases at $\mathcal{O}(\lambda^5)$ and $\mathcal{O}(\lambda^6)$ respectively, and this does have an impact on the expressions for observables S, H, defined in equation (7.38).

The latest values for the parameters are [128]

$$\begin{aligned} \lambda &= 0.22506(50), & A &= 0.811(26)\,, \\ \rho &= 0.124(18), & \eta &= 0.356(11)\,, \end{aligned} \tag{B.4}$$

with the uncertainties in the last two digits given in brackets. These can be used to determine the full CKM matrix.

B.3 α_s running

Quite an important input is the value of α_s. As the energy scale decreases, α_s increases, and approaching the QCD scale $\Lambda \sim 200$ MeV is no longer perturbative. Meanwhile, coefficients in the β-function of QCD (2.23) have only been computed up to five-loop accuracy, so the full RG dependence is not yet known. Nevertheless, α_s running is far from the dominant uncertainty in sum rules calculations, and three-loop running is sufficient.

The typical procedure is to extract the value of α_s at the Z-mass scale, and the extracted value of $\alpha_s(m_Z)$ has changed slightly in the iterations of PDG. The 2006 PDG average was $\alpha_s(m_Z) = 0.1176$ [212], whereas in 2014 the average was $\alpha_s(m_Z) = 0.1184$ [213]. Most recently [128], the average has converged between the two, but for α_s running the 2014 average will be the preferred value.

As the RG equations are evolved down to lower mass scales, the number of active quark flavours also changes. This has to be taken into account by matching the value of α_s across the quark mass thresholds, which in this thesis are taken to be at $m_c = 1.29$ GeV and $m_b = 4.2$ GeV (i.e. the $\overline{MS}$ masses according to the 2014 PDG averages):

$$\alpha_s(m_c, N_f = 3) = \alpha_s(m_c, N_f = 4) \tag{B.5}$$

and similarly for m_b.

The necessary definitions of β-function coefficients can be found in the PDG, but the results below have been computed for the purposes of this thesis. They include independent definitions of the QCD scale for 3, 4 and 5 active flavours, for both two- and three-loop running. To check the method against the previous sum rules literature, the 2006 PDG values have also been used, and the running is also performed for both two- and three-loop definitions.

At two loops, the RG behaviour of α_s is given by

$$\alpha_s(\mu) = \frac{4\pi}{\beta_0 \ln \frac{\mu^2}{\Lambda^2(N_f)}} \left(1 - \frac{\beta_1}{\beta_0^2} \frac{\ln\left(\ln \frac{\mu^2}{\Lambda^2(N_f)}\right)}{\ln \frac{\mu^2}{\Lambda^2(N_f)}} \right) , \tag{B.6}$$

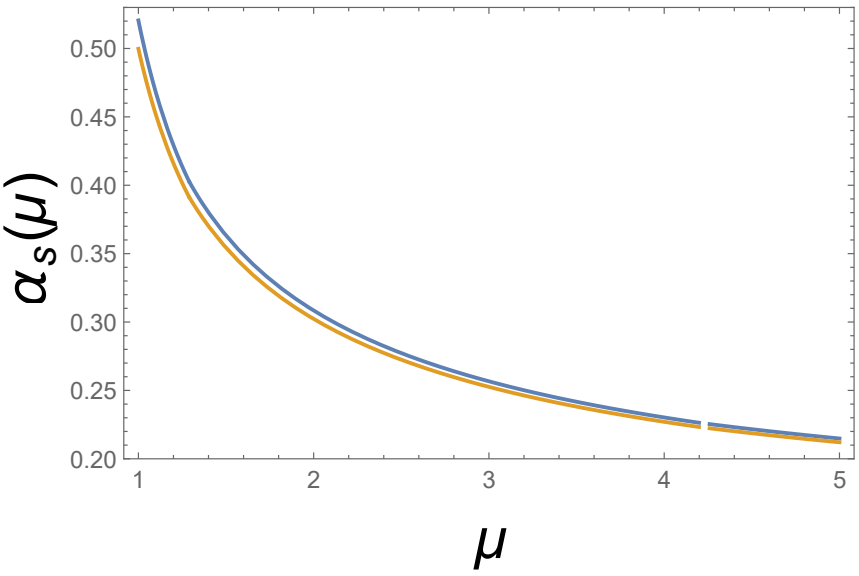

Figure B.1 *Two-loop running of α_s, based on the procedure described in the text, for $\alpha_s(m_Z) = 0.1184$ (top line) and $\alpha_s(m_Z) = 0.1176$ (bottom line). The gap at m_b is an unfortunate relic of the matching procedure as implemented in Mathematica, but it can nevertheless be seen that the values are consistent with the matching condition over this boundary. Matching at the charm threshold is visible as a slight "kink" around $\mu = m_c = 1.29$. The lower line is the most consistent with the determination of [85], confirming the independent code written for this thesis.*

where

$$\begin{aligned}
\beta_0 &= 11 - \frac{2}{3}N_f\,, \\
\beta_1 &= \frac{2}{3}(153 - 19N_f)\,, \\
\beta_2 &= \frac{1}{2}\left(2857 - \frac{5033}{9}N_f + \frac{325}{27}N_f^2\right)\,,
\end{aligned} \tag{B.7}$$

and N_f is the number of active quark flavours. The expressions above can also be generalised to arbitrary gauge groups $SU(N)$, but for simplicity these expressions are given for $N_C = 3$. The equivalent three-loop expression is too lengthy to be included here, but is presented in [128]; nevertheless, the necessary coefficient β_2 is given above. It is a scheme-dependent quantity, although the expression above is for the most commonly-used $\overline{MS}$ scheme.

The matching requirement imposes different values $\Lambda(N_f)$ depending on the initial value and number of loops. For example, for two-loop running with $\alpha_s(m_Z) = 0.1184$, the extracted values of $\Lambda(N_f)$ are $\Lambda(3) = 376.1$ MeV, $\Lambda(4) = 330$ MeV,

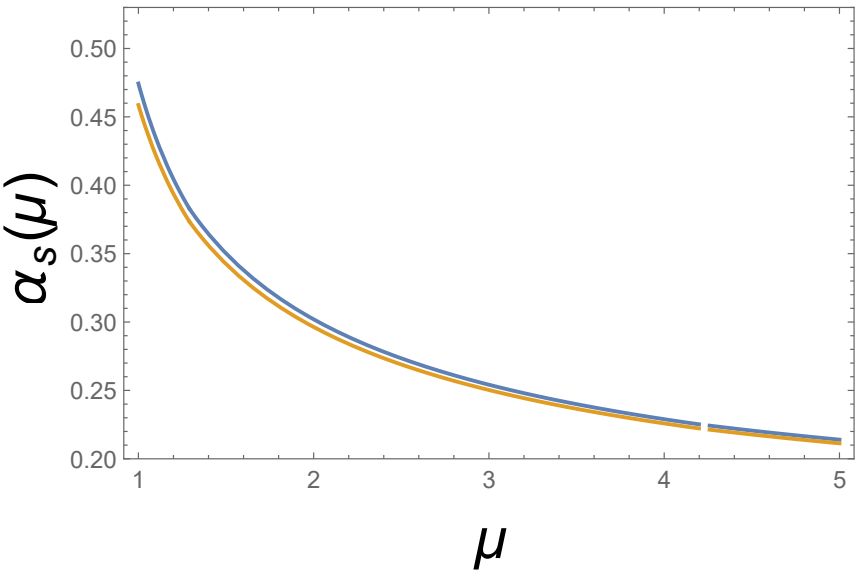

Figure B.2 *Three-loop running of α_s, based on the procedure described in the text, for $\alpha_s(m_Z) = 0.1184$ (top line) and $\alpha_s(m_Z) = 0.1176$ (bottom line). As with the two-loop graph, the gap at m_b is an unfortunate relic of the matching procedure as implemented in Mathematica, but it can nevertheless be seen that the values are consistent with the matching condition over this boundary. Matching at the charm threshold is visible as a slight "kink" around $\mu = m_c = 1.29$. Three-loop running produces somewhat lower values for $\alpha_s(1\ GeV)$, but are still close enough to the two-loop values that a perturbative description of α_s can be said to apply in this region.*

and $\Lambda(5) = 231.4$ MeV. The equivalent values in three-loop runnings will be somewhat lower, but these values can be determined by matching by hand, and are specific to the code used for this thesis.

The resulting values of $\alpha_s(1\text{ GeV})$ are presented, for central values, in table B.3, and graphs showing the RG behaviour are in figures B.1 and B.2 for two-loop and three-loop running respectively. It is safe to assume, based on these results, that [85, 103] made use of two-loop running only.

The final value for $\alpha_s(1\ \text{GeV})$ is taken to be the average of these four determinations, with a naive estimate of the error following from the range:

$$\alpha_s(1\text{ GeV}) = 0.488 \pm 0.030\,, \tag{B.8}$$

while the ratio $\dfrac{\alpha_s(2.2\text{ GeV})}{\alpha_s(1\text{ GeV})}$, which enters the RG evolution of the DA parameters, is found to be

$$\frac{\alpha_s(2.2\text{ GeV})}{\alpha_s(1\text{ GeV})} = 0.592 \pm 0.027\,. \tag{B.9}$$

running	$\alpha_s(m_Z) = 0.1184$	$\alpha_s(m_Z) = 0.1176$
two-loop	0.5205	0.4998
three-loop	0.4744	0.4586

Table B.3 *Values of $\alpha_s(1\ GeV)$ based on two- or three-loop running with the initial value $\alpha_s(m_Z)$ set by either the 2006 or the 2014 PDG averages. In numerical estimates for the DA parameters, the average of these determinations will be used, with the range providing an error estimate for the value. As α_s is not the dominant uncertainty in the three-particle sum rules, this method of estimating $\alpha_s(1\ GeV)$ and its error is sufficiently accurate to give reliable numerical values.*

B.4 Vacuum condensates

The values used in this thesis for the two- and three-gluon condensates are given in (B.13), but it is worth considering these more carefully, in particular for the two-gluon condensate, in the light of some disagreement in the literature over their correct values.

Sum rules papers, as exemplified by [85, 103, 214], all use a central value $\left\langle \frac{\alpha_s}{\pi} G^2 \right\rangle = 0.012$ GeV^4. However, this appears to be based on an old estimate from the original SVZ sum rules [88, 89]. Recent papers have attempted to compute the condensate using various other methods, and have arrived at a range of values. These are summarised in [215], which gives a higher value, based on experimental, over twice as large as the SVZ value: $\left\langle \frac{\alpha_s}{\pi} G^2 \right\rangle = 0.037$ GeV^4. A recent lattice computation [216] gives an intermediate value: $\left\langle \frac{\alpha_s}{\pi} G^2 \right\rangle = 0.028$ GeV^4. Since, in many sum rules in this thesis, the two-gluon condensate is dominant or at least significant, this tension over the value can have a major impact on the extracted values of DA parameters.

For the three-gluon condensate, the opposite problem occurs. In earlier work on two-point sum rules, it was found that the three-gluon condensate does not contribute [176]. As a result, it seems that the numerical determination of the three-gluon condensate has received comparatively little attention, and the only source for its value appears to be [217], as cited in [103]. With the possible exception of [218], it appears that the three-gluon condensate has not received any fresh attention since the early 1990s; although this time the competing results are in broad agreement with each other.

For the single-quark condensate, the papers [85, 103, 214] all cite $\langle\bar{q}q\rangle = (-0.24 \pm 0.01)^3$ GeV^3, while [219] gives $\langle\bar{q}q\rangle = (-0.229 \pm 0.009)^3$ GeV^3. Here there is much less uncertainty, owing to the Gell-Mann-Oakes-Renner relation [93]. As these values are consistent with each other, again, the values from [85, 103, 214] will be used in numerical outputs.

The mixed and strange condensates $\langle\bar{q}\sigma\cdot Gq\rangle$, $\langle\bar{s}s\rangle$ can be related to the light condensates through the relationships

$$\begin{aligned}\langle\bar{q}\sigma\cdot Gq\rangle &= m_0^2\langle\bar{q}q\rangle\,,\\ \langle\bar{s}s\rangle &= (1-\delta_3)\,\langle\bar{q}q\rangle\,,\\ \langle\bar{s}\sigma\cdot Gs\rangle &= (1-\delta_5)\,\langle\bar{q}\sigma\cdot Gq\rangle\,,\end{aligned} \tag{B.10}$$

where [219] provides the first line, and gives the value of $m_0^2 = 0.8 \pm 0.1$ GeV^2. The definitions of $\delta_{3,5}$ are as in [85], but these values are not well-determined. One more recent estimate [220] gives the ratio

$$\frac{\langle\bar{s}s\rangle}{\langle\bar{q}q\rangle} = 0.6 \pm 0.1\,, \tag{B.11}$$

from which $\delta_3 = 0.4 \pm 0.1$, while a Lattice calculation in 2012 [221] found that, at the scale $\mu = 2$ GeV, the same ratio equals 1.08 ± 0.17. It is safe to say, then, that there is no fixed determination of these inputs or ratios, and that these issues are not yet resolved. It is beyond the purview of this thesis to determine which values are the most reliable. Priority is given to the values used in [85, 103, 214], with the intent of maintaining as much consistency as possible with those results, to enable an easier comparison with previous determinations of the DA parameters.

Consequently, the input central values and uncertainties for the condensates are

$$\left\langle G^2\right\rangle = 4\pi^2\left\langle\frac{\alpha_s}{\pi}G^2\right\rangle = 4\pi^2(0.012 \pm 0.006)\text{ GeV}^4 = 0.474 \pm 0.237\text{ GeV}^4\,, \tag{B.12}$$

and

$$\begin{aligned}\left\langle fG^3\right\rangle &= (0.08 \pm 0.02)\text{ GeV}^6\,,\\ \langle\bar{q}q\rangle &= (-0.24 \pm 0.01)^3\text{ GeV}^3\,,\end{aligned} \tag{B.13}$$

which values are valid at scale $\mu = 1$ GeV only. The parameters $\delta_{3,5}$ are both taken as 0.2 ± 0.2, which encompass the values in both [220] and [221], while being taken directly from [85].

Appendix C

Additional material for the $\bar{B} \to \bar{K}^*(\to K\pi)\ell_1\bar{\ell}_2$ decay

This appendix presents explicit results relevant to the work presented in chapters 4 and 5.

C.1 Details on kinematics for decay modes

In this section, the specific kinematics of the decay

$$\bar{B} \to \bar{K}^*\big(\to \bar{K}(p_K)\pi(p_\pi)\big)\,\ell_1(\ell_1)\bar{\ell}_2(\ell_2)\,, \tag{C.1}$$

with ($\ell_1 = \ell^-$ and $\bar{\ell}_2 = \ell^+$ in the equal-mass case), are parametrised. Within the helicity formalism described in this thesis, it is not essential to consider the full kinematics, as the evaluation of the hadronic and leptonic helicity amplitudes (HAs) can be performed within their respective rest frames. However, calculating the angular distribution using the Dirac trace technology approach [108, 109] serves to provide a useful cross-check of the results. The Källén function $\lambda(a, b, c)$ is defined as

$$\lambda(a, b, c) \equiv a^2 + b^2 + c^2 - 2(ab + ac + bc)\,. \tag{C.2}$$

and, for a decay $A \to B + C$, in the rest-frame of A, is related to the absolute value of the spatial momentum of the B and C particles as

$$|\vec{p}_B| = |\vec{p}_C| = \frac{\sqrt{\lambda\left(m_A^2, m_B^2, m_C^2\right)}}{2m_A} \,. \tag{C.3}$$

C.1.1 Basis-dependent kinematics for $\bar{B} \to \bar{K}^* \ell_1 \bar{\ell}_2$

It is simplest to first obtain the momenta $\ell_{1,2}$ and $p_{\pi,K}$ in the rest frame of the lepton pair and the $\bar{K}^*$-meson respectively:

$$\begin{aligned} &\ell_{1,2}\text{-rest frame}: \qquad \ell_1^\mu = (E_1, |\vec{p}_\ell|\ \hat{\ell}) \,, \qquad \ell_2^\mu = (E_2, -|\vec{p}_\ell|\ \hat{\ell}) \,, \\ &p_{\pi,K}\text{-rest frame}: \qquad p_K^\mu = (E_K, |\vec{p}_K|\ \hat{k}) \,, \quad p_\pi^\mu = (E_\pi, -|\vec{p}_K|\ \hat{k}) \,, \end{aligned} \tag{C.4}$$

with the definitions

$$\begin{aligned} \hat{\ell} &= (\cos\phi \sin\theta_\ell, -\sin\phi \sin\theta_\ell, \cos\theta_\ell) \,, \quad & |\vec{p}_\ell| &= \frac{\sqrt{\lambda_{\gamma^*}}}{2\sqrt{q^2}} \,, \\ \hat{k} &= (-\sin\theta_K, 0, -\cos\theta_K) \,, & |\vec{p}_K| &= \frac{\sqrt{\lambda_{K^*}}}{2m_{K^*}} \,, \end{aligned} \tag{C.5}$$

where

$$\lambda_{\gamma^*} \equiv \lambda(q^2, m_1^2, m_2^2) \,, \quad \lambda_{K^*} \equiv \lambda(m_{K^*}^2, m_K^2, m_\pi^2) \,, \quad \lambda_B \equiv \lambda(m_B^2, m_{K^*}^2, q^2) \,, \tag{C.6}$$

are the explicit Källén functions. The lepton and hadron energies are then given by $E_{1,2} = \sqrt{m_{\ell_{1,2}}^2 + |\vec{p}_\ell|^2}$ and $E_{\pi,K} = \sqrt{m_{\pi,K}^2 + |\vec{p}_K|^2}$, and obey $E_1 + E_2 = \sqrt{q^2}$ and $E_\pi + E_K = m_{K^*}$.

The polarisation vectors $\eta^\mu(\lambda)$ of the $\bar{K}^*$-meson in its rest frame, using the conventions in [131], are[1]

$$\eta^\mu(0) = (0, 0, 0, 1) \,, \quad \eta^\mu(\pm) = (0, \mp 1, i, 0)/\sqrt{2} \,. \tag{C.7}$$

[1]The polarisation vector η corresponds to γ in [131] (c.f. appendix A therein). The exact correspondence between the convention used in [34, 131] and the Jacob-Wick convention [33, 126] is $\eta(\pm)_\mu|_{[131]} = -\eta(\pm)_\mu|_{[33]}$, $\eta(0)_\mu|_{[131]} = \eta(0)_\mu|_{[33]}$. The final distributions remain the same, but the off-diagonal elements of the leptonic HAs (or matrices) change sign (C.16). Note in particular that the hadronic HAs (C.19) remain unchanged.

In the $\bar{B}$-rest frame, $p_B = (m_B, 0, 0, 0)$, the momenta take the form

$$\begin{aligned}
(\ell_1)^\mu &= (f_\ell(E_1, q_0, q_z), |\vec{p}_\ell| \sin\theta_\ell \cos\phi, -|\vec{p}_\ell| \sin\theta_\ell \sin\phi, f_\ell(E_1, q_z, q_0)) \,, \\
(\ell_2)^\mu &= (f_\ell(E_2, q_0, -q_z), -|\vec{p}_\ell| \sin\theta_\ell \cos\phi, +|\vec{p}_\ell| \sin\theta_\ell \sin\phi, f_\ell(E_2, q_z, -q_0)) \,, \\
(p_K)^\mu &= (f_{K^*}(E_K, p_0, q_z), -|\vec{p}_K| \sin\theta_K, 0, -f_{K^*}(E_K, q_z, p_0)) \,, \\
(p_\pi)^\mu &= (f_{K^*}(E_\pi, p_0, -q_z), |\vec{p}_K| \sin\theta_K, 0, -f_{K^*}(E_\pi, q_z, -p_0)) \,,
\end{aligned} \tag{C.8}$$

with $f_\ell(a, b, c) = (ab + c\,|\vec{p}_\ell| \cos\theta_\ell)/\sqrt{q^2}$ and $f_{K^*}(a, b, c) = (ab + c\,|\vec{p}_K| \cos\theta_K)/m_K^*$, and it can be verified that

$$q^\mu = (\ell_1 + \ell_2)^\mu = (q_0, 0, 0, q_z) \,, \quad p^\mu = (p_K + p_\pi)^\mu = (p_0, 0, 0, -q_z) \,, \tag{C.9}$$

(where $p_0 = E_{K^*}$ is the energy of the K^*). The polarisation vectors of the $\bar{K}^*$ in the $\bar{B}$-rest frame are

$$\eta^\mu(0) = (-q_z, 0, 0, p_0)/m_{K^*} \,, \quad \eta^\mu(\pm) = (0, \mp 1, i, 0)/\sqrt{2} \,, \tag{C.10}$$

where $p_0 + q_0 = m_B$, and $q_z = \sqrt{\lambda_B}/(2m_B)$, in accordance with (C.3), is the three-momentum of the lepton pair.

For the CP conjugate decay, $B \to K^* \bar{\ell}_1(\ell_1)\ell_2(\ell_2)$, the replacement rule $\hat{\ell} \to \hat{\ell}_{\phi\to-\phi} = (\cos\phi \sin\theta_\ell, +\sin\phi \sin\theta_\ell, \cos\theta_\ell)$ applies, while the kinematics for identical lepton masses can be recovered by the replacements

$$E_{1,2} \to \sqrt{q^2}/2 \,, \quad \sqrt{\lambda_{\gamma^*}} \to (q^2)\beta_\ell \,, \tag{C.11}$$

where $\beta_\ell = \sqrt{1 - \frac{4m_\ell^2}{q^2}}$. The kinematics for the decay $B \to K\ell_1\bar{\ell}_2$ can be obtained by setting $\theta_K = \phi = 0$, equivalent to the simplifying case of no subsequent decay $K^* \to K\pi$.

C.1.2 Basis-independent kinematics for $\bar{B} \to \bar{K}^*\ell_1\bar{\ell}_2$

Defining the momentum differences

$$Q^\mu = (\ell_1 - \ell_2)^\mu \,, \quad P^\mu = (p_K - p_\pi)^\mu \,, \tag{C.12}$$

in addition to (C.9), the invariants that can be formed out of p, P, q, and Q are given by

$$
\begin{aligned}
q\cdot Q \;&= m_{\ell_1}^2 - m_{\ell_2}^2\,, \quad Q^2 = 2\left(m_{\ell_1}^2 + m_{\ell_2}^2\right) - q^2\,, \quad q\cdot p = \frac{1}{2}\left(m_B^2 - m_{K^*}^2 - q^2\right)\,,\\
p\cdot P \;&= m_K^2 - m_\pi^2\,, \quad P^2 = 2\left(m_K^2 + m_\pi^2\right) - m_{K^*}^2\,, \quad q\cdot P = \frac{2p\cdot P\, q\cdot p + \cos\theta_K\sqrt{\lambda_B\lambda_{K^*}}}{2m_{K^*}^2}\,,\\
Q\cdot P \;&= \frac{p\cdot P\sqrt{\lambda_B\lambda_{\gamma^*}}\cos\theta_\ell + 2q\cdot p\sqrt{\lambda_{K^*}\lambda_{\gamma^*}}\cos\theta_K\cos\theta_\ell}{2m_{K^*}^2 q^2} + \frac{\sqrt{\lambda_{K^*}\lambda_{\gamma^*}}\sin\theta_K\sin\theta_\ell\cos\phi}{m_{K^*}\sqrt{q^2}}\\
&\quad + \frac{q\cdot Q\, q\cdot P}{q^2}\,,\\
Q\cdot p \;&= \frac{2q\cdot Q\, q\cdot p + \cos\theta_\ell\sqrt{\lambda_B\lambda_{\gamma^*}}}{2q^2}\,,\\
\epsilon\left(P,p,Q,q\right) &= -\frac{\sin\theta_K\sin\theta_\ell\sin\phi\sqrt{\lambda_B\lambda_{K^*}\lambda_{\gamma^*}}}{2m_{K^*}\sqrt{q^2}}
\end{aligned}
\tag{C.13}
$$

with $p^2 = m_{K^*}^2$, $\epsilon\left(P,p,Q,q\right) = \epsilon_{\alpha\beta\gamma\delta}P^\alpha p^\beta Q^\gamma q^\delta$, and using the $\epsilon_{0123} = +1$ convention for the Levi-Civita tensor. The kinematic invariants for $B \to K^*\bar{\ell}_1(\ell_1)\ell_2(\ell_2)$ are the same up to $\epsilon\left(P,p,Q,q\right) \to -\epsilon\left(P,p,Q,q\right)$, which originates from the change in angles $\phi \to -\phi$.

C.2 Leptonic HAs

The calculation of the leptonic HAs is an important part of the generalised helicity formalism described in this thesis, and the method for their calculation is outlined in [126]. Within the Lepton Factorisation Approximation (LFA), the leptonic HAs are universal to all relevant decays. The expressions for different lepton masses $m_{\ell_1} \neq m_{\ell_2}$ can be applied to studies of lepton flavour-violating processes, or to decays involving an $l\bar{\nu}$ in the final state e.g. $B \to D^*\ell\bar{\nu}$.

In the Dirac basis of the Clifford algebra, with σ^i as the usual 2×2 Pauli matrices,

$$
\gamma^0 = \begin{pmatrix} 1 & 0 \\ 0 & -1 \end{pmatrix}\,, \qquad \gamma^i = \begin{pmatrix} 0 & \sigma^i \\ -\sigma^i & 0 \end{pmatrix}\,, \qquad \gamma_5 = \begin{pmatrix} 0 & 1 \\ 1 & 0 \end{pmatrix}\,, \tag{C.14}
$$

the particle and anti-particle spinors u, v are given by

$$
u\left(\frac{1}{2}\right) \;= \left(\sqrt{E_1 + m_{\ell_1}}, 0, \sqrt{E_1 - m_{\ell_1}}, 0\right)^T \;= \left(\beta_1^+, 0, \beta_1^-, 0\right)^T\,,
$$

$$
\begin{aligned}
u\left(-\frac{1}{2}\right) &= \left(0, \sqrt{E_1+m_{\ell_1}}, 0, -\sqrt{E_1-m_{\ell_1}}, \right)^T = \left(0, \beta_1^+, 0, -\beta_1^-\right)^T \ , \\
v\left(\frac{1}{2}\right) &= \left(\sqrt{E_2-m_{\ell_2}}, 0, -\sqrt{E_2+m_{\ell_2}}, 0\right)^T = \left(\beta_2^-, 0, -\beta_2^+, 0\right)^T \ , \\
v\left(-\frac{1}{2}\right) &= \left(0, \sqrt{E_2-m_{\ell_2}}, 0, \sqrt{E_2+m_{\ell_2}}\right)^T = \left(0, \beta_2^-, 0, \beta_2^+\right)^T \ ,
\end{aligned}
$$

with implicit definition of $\beta_i^\pm \equiv \sqrt{E_i \pm m_{\ell_i}}$. The spinors are normalised as $\bar{u}(\lambda_1)u(\lambda_2) = \delta_{\lambda_1\lambda_2} 2m_{\ell_1}$ and $\bar{v}(\lambda_1)v(\lambda_2) = -\delta_{\lambda_1\lambda_2} 2m_{\ell_2}$. The leptonic matrix elements (4.25) contracted with polarisation vectors give rise to the HAs $\mathcal{L}_{\lambda_1\lambda_2}$,

$$
\mathcal{L}^X_{\lambda_1\lambda_2} \equiv \langle \ell_1(\lambda_1)\bar{\ell}_2(\lambda_2)|\bar{\ell}\,\Gamma^X \ell|0\rangle = \bar{u}(\lambda_1)\Gamma^X v(\lambda_2) \ , \tag{C.15}
$$

where the $\Gamma^X|_{\lambda_X\to\lambda_\ell}$ ($\lambda_\ell = \lambda_1 - \lambda_2$) are defined in table 4.1. Using the definitions above, the evaluation of the leptonic HAs is then straightforward, and the results are presented below. The first row (column) corresponds to $\lambda_1(\lambda_2) = -\frac{1}{2}$, and the second row (column) to $\lambda_1(\lambda_2) = +\frac{1}{2}$. For the $\bar{B} \to \bar{K}^*\ell_1\bar{\ell}_2$ decay mode, i.e. $\ell_1 = \ell^-$, the leptonic HAs are given by

$$
\begin{aligned}
\mathcal{L}^V(\lambda_1,\lambda_2) &= \begin{pmatrix} \beta_1^+\beta_2^+ - \beta_1^-\beta_2^- & -\sqrt{2}\left(\beta_1^+\beta_2^+ + \beta_1^-\beta_2^-\right) \\ -\sqrt{2}\left(\beta_1^+\beta_2^+ + \beta_1^-\beta_2^-\right) & \beta_1^+\beta_2^+ - \beta_1^-\beta_2^- \end{pmatrix} \ , \\
\mathcal{L}^A(\lambda_1,\lambda_2) &= \begin{pmatrix} \beta_1^+\beta_2^- - \beta_1^-\beta_2^+ & \sqrt{2}\left(\beta_1^+\beta_2^- + \beta_1^-\beta_2^+\right) \\ -\sqrt{2}\left(\beta_1^+\beta_2^- + \beta_1^-\beta_2^+\right) & \beta_1^-\beta_2^+ - \beta_1^+\beta_2^- \end{pmatrix} \ , \\
\mathcal{L}^S(\lambda_1,\lambda_2) &= \begin{pmatrix} \beta_1^+\beta_2^- + \beta_1^-\beta_2^+ & 0 \\ 0 & \beta_1^+\beta_2^- + \beta_1^-\beta_2^+ \end{pmatrix} \ , \\
\mathcal{L}^P(\lambda_1,\lambda_2) &= \begin{pmatrix} \beta_1^+\beta_2^+ + \beta_1^-\beta_2^- & 0 \\ 0 & -\beta_1^+\beta_2^+ - \beta_1^-\beta_2^- \end{pmatrix} \ , \\
\mathcal{L}^T(\lambda_1,\lambda_2) &= \begin{pmatrix} -i\sqrt{2}\left(\beta_1^+\beta_2^- + \beta_1^-\beta_2^+\right) & -2i\left(\beta_1^+\beta_2^- - \beta_1^-\beta_2^+\right) \\ 2i\left(\beta_1^+\beta_2^- - \beta_1^-\beta_2^+\right) & i\sqrt{2}\left(\beta_1^+\beta_2^- + \beta_1^-\beta_2^+\right) \end{pmatrix} \ , \\
\mathcal{L}^{T_t}(\lambda_1,\lambda_2) &= \begin{pmatrix} i\left(\beta_1^+\beta_2^+ + \beta_1^-\beta_2^-\right) & -i\sqrt{2}\left(\beta_1^+\beta_2^+ - \beta_1^-\beta_2^-\right) \\ -i\sqrt{2}\left(\beta_1^+\beta_2^+ - \beta_1^-\beta_2^-\right) & i\left(\beta_1^+\beta_2^+ + \beta_1^-\beta_2^-\right) \end{pmatrix} \ ,
\end{aligned} \tag{C.16}
$$

where $\beta^{\pm}_{1,2} = \sqrt{E_{1,2} \pm m_{\ell_{1,2}}}$ as before. Note that the scalar transitions S and P are necessarily diagonal, since $\lambda_\ell = \lambda_1 - \lambda_2 = 0$. Timelike vector and axial leptonic HAs are integrated into the hadronic HAs (C.19).

In the case where the lepton masses are equal, the leptonic HAs simplify to

$$\begin{aligned}
\mathcal{L}^V(\lambda_1,\lambda_2) &= \begin{pmatrix} 2m_\ell & -\sqrt{2q^2} \\ -\sqrt{2q^2} & 2m_\ell \end{pmatrix} , \\
\mathcal{L}^A(\lambda_1,\lambda_2) &= \begin{pmatrix} 0 & \sqrt{2q^2}\beta_\ell \\ -\sqrt{2q^2}\beta_\ell & 0 \end{pmatrix} , \\
\mathcal{L}^S(\lambda_1,\lambda_2) &= \begin{pmatrix} \sqrt{q^2}\beta_\ell & 0 \\ 0 & \sqrt{q^2}\beta_\ell \end{pmatrix} , \\
\mathcal{L}^P(\lambda_1,\lambda_2) &= \begin{pmatrix} \sqrt{q^2} & 0 \\ 0 & -\sqrt{q^2} \end{pmatrix} , \\
\mathcal{L}^T(\lambda_1,\lambda_2) &= \begin{pmatrix} -i\sqrt{2q^2}\beta_\ell & 0 \\ 0 & i\sqrt{2q^2}\beta_\ell \end{pmatrix} , \\
\mathcal{L}^{T_t}(\lambda_1,\lambda_2) &= \begin{pmatrix} i\sqrt{q^2} & -2i\sqrt{2}m_\ell \\ -2i\sqrt{2}m_\ell & i\sqrt{q^2} \end{pmatrix} ,
\end{aligned} \tag{C.17}$$

where $\beta_\ell = \sqrt{1 - \frac{4m_\ell^2}{q^2}}$.

C.3 Explicit hadronic HAs in terms of form factors

Provided below are the definitions of the hadronic HAs in terms of the standard matrix elements and form factors (e.g. [99]), in terms of which the results are expressed. The hadronic HA is defined by

$$H^X_\lambda = \langle \bar{K}^*(\lambda)|\bar{s}\overline{\Gamma}^X b|\bar{B}\rangle \, , \tag{C.18}$$

with $\overline{\Gamma}^X|_{\lambda_X\to\lambda}$ as defined in table 4.1, and the further replacement $\omega \to \bar{\omega}$ from (4.15).

Explicit results for the $\bar{B} \to \bar{K}^*(\ell_1\bar{\ell}_2)$-mode are given by

$$
\begin{aligned}
H_0^V &= \frac{4im_Bm_{K^*}\left[(C_V - C_V')\,(m_B + m_{K^*})\,A_{12} + m_b(C_7 - C_7')T_{23}\right]}{\sqrt{q^2}\,(m_B + m_{K^*})}\,,\\
H_0^A &= \frac{4im_Bm_{K^*}}{\sqrt{q^2}}(C_A - C_A')A_{12}\,,\\
H_\pm^V &= \frac{i}{2\,(m_B + m_{K^*})}\left(\pm(C_V + C_V')\sqrt{\lambda_B}\,V - (m_B + m_{K^*})^2\,(C_V - C_V')A_1\right)\\
&\quad + \frac{im_b}{q^2}\left(\pm(C_7 + C_7')\sqrt{\lambda_B}\,T_1 - (C_7 - C_7')\left(m_B^2 - m_{K^*}^2\right)T_2\right)\,,\\
H_\pm^A &= \frac{i}{2\,(m_B + m_{K^*})}\left(\pm(C_A + C_A')\sqrt{\lambda_B}\,V - (m_B + m_{K^*})^2\,(C_A - C_A')A_1\right)\,,\\
H^P &= \frac{i\sqrt{\lambda_B}}{2}\left(\frac{C_P - C_P'}{m_b + m_s} + \frac{m_{\ell_1} + m_{\ell_2}}{q^2}(C_A - C_A')\right)A_0\,,\\
H^S &= \frac{i\sqrt{\lambda_B}}{2}\left(\frac{C_S - C_S'}{m_b + m_s} + \frac{m_{\ell_1} - m_{\ell_2}}{q^2}(C_V - C_V')\right)A_0\,,\\
H_0^T &= \frac{2\sqrt{2}m_Bm_{K^*}}{m_B + m_{K^*}}\,(C_{\mathcal{T}} + C_{\mathcal{T}}')\,T_{23}\,,\\
H_0^{T_t} &= \frac{2m_Bm_{K^*}}{m_B + m_{K^*}}\,(C_{\mathcal{T}} - C_{\mathcal{T}}')\,T_{23}\,,\\
H_\pm^T &= \frac{1}{\sqrt{2q^2}}\left(\pm\,(C_{\mathcal{T}} - C_{\mathcal{T}}')\,\sqrt{\lambda_B}T_1 - (C_{\mathcal{T}} + C_{\mathcal{T}}')\left(m_B^2 - m_{K^*}^2\right)T_2\right)\,,\\
H_\pm^{T_t} &= \frac{1}{2\sqrt{q^2}}\left(\pm\,(C_{\mathcal{T}} + C_{\mathcal{T}}')\,\sqrt{\lambda_B}T_1 - (C_{\mathcal{T}} - C_{\mathcal{T}}')\left(m_B^2 - m_{K^*}^2\right)T_2\right)\,,
\end{aligned}
\tag{C.19}
$$

where $C_{V(A)} = C_{9(10)}$ in the standard notation used in the literature, and the q^2-dependence of the form factors is suppressed. The zero-helicity form factor combinations are defined by [99, 222]

$$
A_{12} = \frac{(m_B + m_{K^*})^2\,(m_B^2 - m_{K^*}^2 - q^2)\,A_1 - \lambda_B A_2}{16m_Bm_{K^*}^2\,(m_B + m_{K^*})}\,, \tag{C.20}
$$

$$
T_{23} = \frac{(m_B^2 - m_{K^*}^2)\,(m_B^2 + 3m_{K^*}^2 - q^2)\,T_2 - \lambda_B T_3}{8m_Bm_{K^*}^2\,(m_B - m_{K^*})}\,. \tag{C.21}
$$

The "timelike" HAs, often denoted by H_t in the literature [113], have been absorbed into H^S and H^P. This is exceptional and follows from the vector and axial Ward identities $q^\mu\bar{u}(\ell_1)\gamma_\mu[\gamma_5]v(\ell_2) = (m_{\ell_1} \mp m_{\ell_2})\bar{u}(\ell_1)[\gamma_5]v(\ell_2)$. A similar simplification procedure could be repeated by use of the equation of motion

$i\partial^\nu(\bar{s}i\sigma_{\mu\nu}b) = -(m_s+m_b)\bar{s}\gamma_\mu b + i\partial_\mu(\bar{s}b) - 2\bar{s}i\overleftarrow{D}_\mu\, b$ [223] for $H_\lambda^{T_t}$, if all of the operators present in the equation were used in the effective Hamiltonian. Since the higher derivative operators are not present in the effective Hamiltonian used in this thesis (2.42), such a simplification does not occur.

C.4 $G_m^{l_k,l_\ell}$ for $\bar{B}\to\bar{K}^*\ell_1\bar{\ell}_2$ in terms of HAs

C.4.1 $m_{\ell_i}\equiv m_\ell$

When the masses of the leptons are identical, the results for $G_m^{l_K,l_\ell} = \mathcal{N}q^2\mathbb{G}_m^{l_K,l_\ell}$ (with $\mathcal{N}$ defined in (4.34)) are

$$\begin{aligned}
\mathbb{G}_0^{0,0} &= \frac{4}{9}\left(1-\hat{m_\ell}^2\right)\left(\left|H_+^V\right|^2+\left|H_-^V\right|^2+\left|H_0^V\right|^2+(V\to A)\right)\\
&+\frac{4\hat{m_\ell}^2}{3}\left(\left|H_+^V\right|^2+\left|H_-^V\right|^2+\left|H_0^V\right|^2-(V\to A)\right)+\frac{2}{3}\beta_\ell^2\left|H^S\right|^2+\frac{2}{3}\left|H^P\right|^2\\
&+\frac{8}{9}\left(1+8\hat{m_\ell}^2\right)\left(\left|H_+^{T_t}\right|^2+\left|H_-^{T_t}\right|^2+\left|H_0^{T_t}\right|^2\right)+\frac{4}{9}\beta_\ell^2\left(\left|H_+^T\right|^2+\left|H_-^T\right|^2+\left|H_0^T\right|^2\right)\\
&+\frac{16}{3}\hat{m_\ell}\,\mathrm{Im}\left[H_+^V\bar{H}_+^{T_t}+H_-^V\bar{H}_-^{T_t}+H_0^V\bar{H}_0^{T_t}\right]\ ,\\
\mathbb{G}_0^{0,1} &= \frac{4\beta_\ell}{3}\Big(\mathrm{Re}\left[H_+^V\bar{H}_+^A-H_-^V\bar{H}_-^A\right]+\mathrm{Im}\left[\sqrt{2}H_0^T\bar{H}^P+2H_0^{T_t}\bar{H}^S\right]\\
&\qquad -2\hat{m_\ell}\mathrm{Re}\left[H_0^V\bar{H}^S\right]+4\hat{m_\ell}\mathrm{Im}\left[H_+^A\bar{H}_+^{T_t}-H_-^A\bar{H}_-^{T_t}\right]\Big)\ ,\\
\mathbb{G}_0^{0,2} &= -\frac{2}{9}\beta_\ell^2\left(2\left|H_0^V\right|^2-\left|H_+^V\right|^2-\left|H_-^V\right|^2+(V\to A)-2\left(2\left|H_0^T\right|^2-\left|H_+^T\right|^2-\left|H_-^T\right|^2\right)\right.\\
&\qquad \left.-4\left(2\left|H_0^{T_t}\right|^2-\left|H_+^{T_t}\right|^2-\left|H_-^{T_t}\right|^2\right)\right)\ ,\\
\mathbb{G}_0^{2,0} &= -\frac{4}{9}\left(1-\hat{m_\ell}^2\right)\left(\left|H_+^V\right|^2+\left|H_-^V\right|^2-2\left|H_0^V\right|^2+(V\to A)\right)\\
&-\frac{4\hat{m_\ell}^2}{3}\left(\left|H_+^V\right|^2+\left|H_-^V\right|^2-2\left|H_0^V\right|^2-(V\to A)\right)+\frac{4}{3}\beta_\ell^2\left|H^S\right|^2+\frac{4}{3}\left|H^P\right|^2\\
&-\frac{8}{9}\left(1+8\hat{m_\ell}^2\right)\left(\left|H_+^{T_t}\right|^2+\left|H_-^{T_t}\right|^2-2\left|H_0^{T_t}\right|^2\right)-\frac{4}{9}\beta_\ell^2\left(\left|H_+^T\right|^2+\left|H_-^T\right|^2-2\left|H_0^T\right|^2\right)\\
&-\frac{16}{3}\hat{m_\ell}\,\mathrm{Im}\left[H_+^V\bar{H}_+^{T_t}+H_-^V\bar{H}_-^{T_t}-2H_0^V\bar{H}_0^{T_t}\right]\ ,\\
\mathbb{G}_0^{2,1} &= -\frac{4\beta_\ell}{3}\Big(\mathrm{Re}\left[H_+^V\bar{H}_+^A-H_-^V\bar{H}_-^A\right]-2\,\mathrm{Im}\left[\sqrt{2}H_0^T\bar{H}^P+2H_0^{T_t}\bar{H}^S\right]
\end{aligned}$$

$$+ 4\hat{m}_\ell \left(\mathrm{Re}\left[H_0^V \bar{H}^S \right] + \mathrm{Im}\left[H_+^A \bar{H}_+^{T_t} - H_-^A \bar{H}_-^{T_t} \right] \right) \Big) \,,$$

$$\mathbb{G}_0^{2,2} = -\frac{2}{9}\beta_\ell^2 \Big(4\left|H_0^V\right|^2 + \left|H_+^V\right|^2 + \left|H_-^V\right|^2 + (V \to A) - 2\left(4\left|H_0^T\right|^2 + \left|H_+^T\right|^2 + \left|H_-^T\right|^2 \right)$$
$$-4\left(4\left|H_0^{T_t}\right|^2 + \left|H_+^{T_t}\right|^2 + \left|H_-^{T_t}\right|^2 \right) \Big) \,,$$

$$\mathbb{G}_1^{2,1} = \frac{4\beta_\ell}{\sqrt{3}} \Big(H_+^V \bar{H}_0^A + H_+^A \bar{H}_0^V - H_0^V \bar{H}_-^A - H_0^A \bar{H}_-^V + 2\hat{m}_\ell \left(H_+^V \bar{H}^S + H^S \bar{H}_-^V \right)$$
$$- \sqrt{2} i \left(H^P \bar{H}_-^T - H_+^T \bar{H}^P + \sqrt{2}\left(H^S \bar{H}_-^{T_t} - H_+^{T_t} \bar{H}^S \right) \right)$$
$$- 4i\hat{m}_\ell \left(H_+^A \bar{H}_0^{T_t} + H_0^{T_t} \bar{H}_-^A - H_+^{T_t} \bar{H}_0^A - H_0^A \bar{H}_-^{T_t} \right) \Big) \,,$$

$$\mathbb{G}_1^{2,2} = \frac{4}{3}\beta_\ell^2 \left(H_+^V \bar{H}_0^V + H_0^V \bar{H}_-^V + (V \to A) - 2\left(H_+^T \bar{H}_0^T + H_0^T \bar{H}_-^T + 2\left(H_+^{T_t} \bar{H}_0^{T_t} + H_0^{T_t} \bar{H}_-^{T_t} \right) \right) \right) \,,$$

$$\mathbb{G}_2^{2,2} = -\frac{8}{3}\beta_\ell^2 \left(H_+^V \bar{H}_-^V + H_+^A \bar{H}_-^A - 2\left(H_+^T \bar{H}_-^T + 2 H_+^{T_t} \bar{H}_-^{T_t} \right) \right) \,, \tag{C.22}$$

where $\hat{m}_\ell = m_\ell / \sqrt{q^2}$ and $\beta_\ell = \sqrt{1 - 4\hat{m}_\ell^2}$. The index m in $G_m^{l_k, l_\ell}$ corresponds to the units of positive helicities (where, for example, H_+^V and $\bar{H}_-^V$ both carry one unit of positive helicity). The common factor of q^2 in all observables as compared with standard literature results is a consequence of the choice of normalisation, whereby all global factors are placed outside the HAs. The factors of i where they appear (explicitly and implicitly) in $\mathbb{G}_1^{2,1}$, $\mathbb{G}_1^{2,2}$ and $\mathbb{G}_2^{2,2}$ are not accidental, as the results given above are complex, and one must take the real and imaginary parts of these results to recover the observables $g_{3,4,5,7,8,9}$.

It is sometimes convenient to express results in terms of the transversity amplitudes, which possess a definite parity. The relations to the HAs used above are

$$\begin{aligned}
H_{\parallel(\perp)}^{L/R} &\equiv \frac{1}{\sqrt{2}}(H_+^{L/R} \pm H_-^{L/R}) \,, \\
H_S \quad &\equiv H^S \,, & H_t \quad &\equiv H^t \,, \\
H_{\parallel(\perp)}^{\mathcal{T}_t} &\equiv \frac{1}{\sqrt{2}}(H_+^{T_t} \pm H_-^{T_t}) \,, & H_0^{\mathcal{T}_t} \quad &\equiv H_0^{T_t} \,, \\
H_{\parallel(\perp)}^{\mathcal{T}} &\equiv \frac{1}{\sqrt{2}}(H_+^{T} \pm H_-^{T}) \,, & H_{\parallel\perp}^{\mathcal{T}} \quad &\equiv H_0^{T} \,.
\end{aligned} \tag{C.23}$$

In [113], the notation A_{ij}, with $i, j = \parallel, \perp, 0$, is used for the transversity

amplitudes. Note that, when comparing to the results above, the difference in the convention of the polarisation vectors has to be taken into account.

C.4.2 $m_{\ell_1} \neq m_{\ell_2}$

Using the leptonic HAs (C.16) allows a simple extension to the case $m_{\ell_1} \neq m_{\ell_2}$, so that the results presented in (C.22) can be adapted to test for possible lepton-flavour violating processes. Using the simplification

$$\beta_1^+ \beta_1^- \beta_2^+ \beta_2^- = \frac{\lambda_{\gamma^*}}{4q^2} \,, \tag{C.24}$$

(λ_{γ^*} given in (C.6) and $\beta_{1,2}^{\pm} \equiv \sqrt{E_{1,2} \pm m_{\ell_{1,2}}}$), the results for $G_m^{l_K,l_\ell} = \mathcal{N}\tilde{G}_m^{l_K,l_\ell}$ (with $\mathcal{N}$ defined in (4.34)) are

$$\begin{aligned}
\tilde{G}_0^{0,0} = {} & \frac{4}{9}\left(3E_1E_2 + \frac{\lambda_{\gamma^*}}{4q^2}\right)\left(\left|H_+^V\right|^2 + \left|H_-^V\right|^2 + \left|H_0^V\right|^2 + (V \to A)\right) \\
& + \frac{4m_{\ell_1}m_{\ell_2}}{3}\left(\left|H_+^V\right|^2 + \left|H_-^V\right|^2 + \left|H_0^V\right|^2 - (V \to A)\right) \\
& + \frac{4}{3}\left(E_1E_2 - m_{\ell_1}m_{\ell_2} + \frac{\lambda_{\gamma^*}}{4q^2}\right)\left|H^S\right|^2 + \frac{4}{3}\left(E_1E_2 + m_{\ell_1}m_{\ell_2} + \frac{\lambda_{\gamma^*}}{4q^2}\right)\left|H^P\right|^2 \\
& + \frac{16}{9}\left(3\left(E_1E_2 + m_{\ell_1}m_{\ell_2}\right) - \frac{\lambda_{\gamma^*}}{4q^2}\right)\left(\left|H_+^{T_t}\right|^2 + \left|H_-^{T_t}\right|^2 + \left|H_0^{T_t}\right|^2\right) \\
& + \frac{8}{9}\left(3\left(E_1E_2 - m_{\ell_1}m_{\ell_2}\right) - \frac{\lambda_{\gamma^*}}{4q^2}\right)\left(\left|H_+^{T}\right|^2 + \left|H_-^{T}\right|^2 + \left|H_0^{T}\right|^2\right) \\
& + \frac{16}{3}\left(m_{\ell_1}E_2 + m_{\ell_2}E_1\right)\mathrm{Im}\left[H_+^V\bar{H}_+^{T_t} + H_-^V\bar{H}_-^{T_t} + H_0^V\bar{H}_0^{T_t}\right] \\
& + \frac{8\sqrt{2}}{3}\left(m_{\ell_1}E_2 - m_{\ell_2}E_1\right)\mathrm{Im}\left[H_+^A\bar{H}_+^{T} + H_-^A\bar{H}_-^{T} + H_0^A\bar{H}_0^{T}\right] \,, \\
\tilde{G}_0^{0,1} = {} & \frac{4\sqrt{\lambda_{\gamma^*}}}{3}\left(\mathrm{Re}\left[H_+^V\bar{H}_+^A - H_-^V\bar{H}_-^A\right] + 2\sqrt{2}\frac{m_{\ell_1}^2 - m_{\ell_2}^2}{q^2}\mathrm{Re}\left[H_+^T\bar{H}_+^{T_t} - H_-^T\bar{H}_-^{T_t}\right]\right. \\
& + 2\frac{m_{\ell_1} + m_{\ell_2}}{\sqrt{q^2}}\mathrm{Im}\left[H_+^A\bar{H}_+^{T_t} - H_-^A\bar{H}_-^{T_t}\right] + \sqrt{2}\frac{m_{\ell_1} - m_{\ell_2}}{\sqrt{q^2}}\mathrm{Im}\left[H_+^V\bar{H}_+^{T} - H_-^V\bar{H}_-^{T}\right] \\
& \left. - \frac{m_{\ell_1} - m_{\ell_2}}{\sqrt{q^2}}\mathrm{Re}\left[H_0^A\bar{H}^P\right] - \frac{m_{\ell_1} + m_{\ell_2}}{\sqrt{q^2}}\mathrm{Re}\left[H_0^V\bar{H}^S\right] + \mathrm{Im}\left[\sqrt{2}H_0^T\bar{H}^P + 2H_0^{T_t}\bar{H}^S\right]\right) \,, \\
\tilde{G}_0^{0,2} = {} & -\frac{2}{9}\frac{\lambda_{\gamma^*}}{q^2}\left(2\left|H_0^V\right|^2 - \left|H_+^V\right|^2 - \left|H_-^V\right|^2 + (V \to A) - 2\left(2\left|H_0^T\right|^2 - \left|H_+^T\right|^2 - \left|H_-^T\right|^2\right)\right. \\
& \left. -4\left(2\left|H_0^{T_t}\right|^2 - \left|H_+^{T_t}\right|^2 - \left|H_-^{T_t}\right|^2\right)\right) \,,
\end{aligned}$$

$$
\begin{aligned}
\tilde{G}_0^{2,0} = & -\frac{4}{9}\left(3E_1E_2+\frac{\lambda_{\gamma^*}}{4q^2}\right)\left(\left|H_+^V\right|^2+\left|H_-^V\right|^2-2\left|H_0^V\right|^2+(V\to A)\right)\\
& -\frac{4m_{\ell_1}m_{\ell_2}}{3}\left(\left|H_+^V\right|^2+\left|H_-^V\right|^2-2\left|H_0^V\right|^2-(V\to A)\right)\\
& +\frac{8}{3}\left(E_1E_2-m_{\ell_1}m_{\ell_2}+\frac{\lambda_{\gamma^*}}{4q^2}\right)\left|H^S\right|^2+\frac{8}{3}\left(E_1E_2+m_{\ell_1}m_{\ell_2}+\frac{\lambda_{\gamma^*}}{4q^2}\right)\left|H^P\right|^2\\
& -\frac{16}{9}\left(3\left(E_1E_2+m_{\ell_1}m_{\ell_2}\right)-\frac{\lambda_{\gamma^*}}{4q^2}\right)\left(\left|H_+^{T_t}\right|^2+\left|H_-^{T_t}\right|^2-2\left|H_0^{T_t}\right|^2\right)\\
& -\frac{8}{9}\left(3\left(E_1E_2-m_{\ell_1}m_{\ell_2}\right)-\frac{\lambda_{\gamma^*}}{4q^2}\right)\left(\left|H_+^{T}\right|^2+\left|H_-^{T}\right|^2-2\left|H_0^{T}\right|^2\right)\\
& -\frac{16}{3}\left(m_{\ell_1}E_2+m_{\ell_2}E_1\right)\mathrm{Im}\left[H_+^V\bar{H}_+^{T_t}+H_-^V\bar{H}_-^{T_t}-2H_0^V\bar{H}_0^{T_t}\right]\\
& -\frac{8\sqrt{2}}{3}\left(m_{\ell_1}E_2-m_{\ell_2}E_1\right)\mathrm{Im}\left[H_+^A\bar{H}_+^{T}+H_-^A\bar{H}_-^{T}-2H_0^A\bar{H}_0^{T}\right]\ ,
\end{aligned}
$$

$$
\begin{aligned}
\tilde{G}_0^{2,1} = & -\frac{4\sqrt{\lambda_{\gamma^*}}}{3}\left(\mathrm{Re}\left[H_+^V\bar{H}_+^A-H_-^V\bar{H}_-^A\right]+2\sqrt{2}\frac{m_{\ell_1}^2-m_{\ell_2}^2}{q^2}\mathrm{Re}\left[H_+^T\bar{H}_+^{T_t}-H_-^T\bar{H}_-^{T_t}\right]\right.\\
& +\frac{2\left(m_{\ell_1}+m_{\ell_2}\right)}{\sqrt{q^2}}\mathrm{Im}\left[H_+^A\bar{H}_+^{T_t}-H_-^A\bar{H}_-^{T_t}\right]+\frac{\sqrt{2}\left(m_{\ell_1}-m_{\ell_2}\right)}{\sqrt{q^2}}\mathrm{Im}\left[H_+^V\bar{H}_+^{T}-H_-^V\bar{H}_-^{T}\right]\\
& \left.+2\frac{m_{\ell_1}-m_{\ell_2}}{\sqrt{q^2}}\mathrm{Re}\left[H_0^A\bar{H}^P\right]+2\frac{m_{\ell_1}+m_{\ell_2}}{\sqrt{q^2}}\mathrm{Re}\left[H_0^V\bar{H}^S\right]-2\,\mathrm{Im}\left[\sqrt{2}H_0^T\bar{H}^P+2H_0^{T_t}\bar{H}^S\right]\right)\ ,
\end{aligned}
$$

$$
\begin{aligned}
\tilde{G}_0^{2,2} = & -\frac{2}{9}\frac{\lambda_{\gamma^*}}{q^2}\left(4\left|H_0^V\right|^2+\left|H_+^V\right|^2+\left|H_-^V\right|^2+(V\to A)-2\left(4\left|H_0^T\right|^2+\left|H_+^T\right|^2+\left|H_-^T\right|^2\right)\right.\\
& \left.-4\left(4\left|H_0^{T_t}\right|^2+\left|H_+^{T_t}\right|^2+\left|H_-^{T_t}\right|^2\right)\right)\ ,
\end{aligned}
$$

$$
\begin{aligned}
\tilde{G}_1^{2,1} = & \frac{4\sqrt{\lambda_{\gamma^*}}}{\sqrt{3}}\left(\left(H_+^V\bar{H}_0^A+H_+^A\bar{H}_0^V-H_0^V\bar{H}_-^A-H_0^A\bar{H}_-^V\right)+\frac{m_{\ell_1}+m_{\ell_2}}{\sqrt{q^2}}\left(H_+^V\bar{H}^S+H^S\bar{H}_-^V\right)\right.\\
& -\sqrt{2}i\left(H^P\bar{H}_-^T-H_+^T\bar{H}^P+\sqrt{2}\left(H^S\bar{H}_-^{T_t}-H_+^{T_t}\bar{H}^S\right)\right)\\
& +\frac{m_{\ell_1}-m_{\ell_2}}{\sqrt{q^2}}\left(H_+^A\bar{H}^P+H^P\bar{H}_-^A\right)\\
& -2i\frac{m_{\ell_1}+m_{\ell_2}}{\sqrt{q^2}}\left(H_+^A\bar{H}_0^{T_t}+H_0^{T_t}\bar{H}_-^A-H_+^{T_t}\bar{H}_0^A-H_0^A\bar{H}_-^{T_t}\right)\\
& -\sqrt{2}i\frac{m_{\ell_1}-m_{\ell_2}}{\sqrt{q^2}}\left(H_+^V\bar{H}_0^T+H_0^T\bar{H}_-^V-H_+^T\bar{H}_0^V-H_0^V\bar{H}_-^T\right)\\
& \left.+2\sqrt{2}\frac{m_{\ell_1}^2-m_{\ell_2}^2}{q^2}\left(H_+^T\bar{H}_0^{T_t}+H_+^{T_t}\bar{H}_0^T-H_0^T\bar{H}_-^{T_t}-H_0^{T_t}\bar{H}_-^T\right)\right)\ ,
\end{aligned}
$$

$$\tilde{G}_1^{2,2} = \frac{4}{3}\frac{\lambda_{\gamma^*}}{q^2}\left(H_+^V\bar{H}_0^V + H_0^V\bar{H}_-^V + (V\to A) - 2\left(H_+^T\bar{H}_0^T + H_0^T\bar{H}_-^T + 2\left(H_+^{T_t}\bar{H}_0^{T_t} + H_0^{T_t}\bar{H}_-^{T_t}\right)\right)\right) ,$$

$$\tilde{G}_2^{2,2} = -\frac{8}{3}\frac{\lambda_{\gamma^*}}{q^2}\left(H_+^V\bar{H}_-^V + H_+^A\bar{H}_-^A - 2\left(H_+^T\bar{H}_-^T + 2H_+^{T_t}\bar{H}_-^{T_t}\right)\right) . \tag{C.25}$$

C.5 Specific results for $\bar{B}\to\bar{K}\ell_1\bar{\ell}_2$

The angular distribution for this decay is

$$\frac{d^2\Gamma}{dq^2\, d\cos\theta_\ell} = G^{(0)}D^0_{0,0}(\Omega_\ell) + G^{(1)}D^1_{0,0}(\Omega_\ell) + G^{(2)}D^2_{0,0}(\Omega_\ell) ,$$

where, using the general leptonic HAs in appendix C.2 and taking $m_{\ell_1}\neq m_{\ell_2}$, the functions $G^{(l_\ell)} = \mathcal{N}\tilde{G}^{(l_\ell)}$ (with $\mathcal{N}$ defined in (4.34)) are given in terms of $\bar{B}\to\bar{K}$ HAs by

$$\begin{aligned}
\tilde{G}^{(0)} = {} & \left(4\left(E_1E_2 + m_{\ell_1}m_{\ell_2}\right) + \frac{\lambda_{\gamma^*}}{3q^2}\right)\left|h^V\right|^2 + \left(4\left(E_1E_2 - m_{\ell_1}m_{\ell_2}\right) + \frac{\lambda_{\gamma^*}}{3q^2}\right)\left|h^A\right|^2 \\
& + \left(4\left(E_1E_2 - m_{\ell_1}m_{\ell_2}\right) + \frac{\lambda_{\gamma^*}}{q^2}\right)\left|h^S\right|^2 + \left(4\left(E_1E_2 + m_{\ell_1}m_{\ell_2}\right) + \frac{\lambda_{\gamma^*}}{q^2}\right)\left|h^P\right|^2 \\
& + 16\left(E_1E_2 + m_{\ell_1}m_{\ell_2} - \frac{\lambda_{\gamma^*}}{12q^2}\right)\left|h^{T_t}\right|^2 + 8\left(E_1E_2 - m_{\ell_1}m_{\ell_2} - \frac{\lambda_{\gamma^*}}{12q^2}\right)\left|h^T\right|^2 \\
& + 16\left(m_{\ell_1}E_2 + m_{\ell_2}E_1\right)\mathrm{Im}\left[h^V\bar{h}^{T_t}\right] + 8\sqrt{2}\left(m_{\ell_1}E_2 - m_{\ell_2}E_1\right)\mathrm{Im}\left[h^A\bar{h}^T\right] ,
\end{aligned}$$

$$\begin{aligned}
\tilde{G}^{(1)} = {} & -4\sqrt{\lambda_{\gamma^*}}\left(\mathrm{Re}\left[\frac{m_{\ell_1}+m_{\ell_2}}{\sqrt{q^2}}h^V\bar{h}^S + \frac{m_{\ell_1}-m_{\ell_2}}{\sqrt{q^2}}h^A\bar{h}^P\right]\right. \\
& \left. - \mathrm{Im}\left[2h^{T_t}\bar{h}^S + \sqrt{2}h^T\bar{h}^P\right]\right) ,
\end{aligned}$$

$$\tilde{G}^{(2)} = -\frac{4\lambda_{\gamma^*}}{3q^2}\left(\left|h^V\right|^2 + \left|h^A\right|^2 - 2\left|h^T\right|^2 - 4\left|h^{T_t}\right|^2\right) . \tag{C.26}$$

The equivalent expressions for equal lepton masses are, using the notation $G^{(l_\ell)} = \mathcal{N}q^2\mathbb{G}^{(l_\ell)}$,

$$\begin{aligned}
\mathbb{G}^{(0)} = {} & \frac{4}{3}\left(1+2\hat{m}_\ell{}^2\right)\left|h^V\right|^2 + \frac{4}{3}\beta_\ell^2\left|h^A\right|^2 + 2\beta_\ell^2\left|h^S\right|^2 + 2\left|h^P\right|^2 \\
& + \frac{8}{3}\left(1+8\hat{m}_\ell{}^2\right)\left|h^{T_t}\right|^2 + \frac{4}{3}\beta_\ell^2\left|h^T\right|^2 + 16\hat{m}_\ell\,\mathrm{Im}\left[h^V\bar{h}^{T_t}\right] ,
\end{aligned}$$

$$\mathbb{G}^{(1)} = -4\beta_\ell\left(2\hat{m}_\ell\,\mathrm{Re}\left[h^V\bar{h}^S\right] - \mathrm{Im}\left[2h^{T_t}\bar{h}^S + \sqrt{2}h^T\bar{h}^P\right]\right) ,$$

$$\mathbb{G}^{(2)} = -\frac{4\beta_\ell^2}{3}\left(\left|h^V\right|^2 + \left|h^A\right|^2 - 2\left|h^T\right|^2 - 4\left|h^{T_t}\right|^2\right) , \tag{C.27}$$

where $\hat{m}_\ell \equiv m_\ell/\sqrt{q^2}$ and $\beta_\ell = \sqrt{1-4\hat{m}_\ell^2}$.

C.5.1 Explicit $\bar{B} \to \bar{K}$ HAs in terms of form factors

As for $\bar{B} \to \bar{K}^*\ell_1\bar{\ell}_2$, the hadronic HAs are given below for form factor contributions only, which allows for comparison with the literature. The form factor matrix elements relevant to $\bar{B} \to \bar{K}$ transition, in standard parametrisation, are

$$\begin{aligned}
\langle \bar{K}(p)|\bar{s}\gamma_\mu b|\bar{B}(p_B)\rangle &= (p_B+p)_\mu f_+(q^2) + \frac{m_B^2-m_K^2}{q^2}q_\mu\left(f_0(q^2)-f_+(q^2)\right) , \\
\langle \bar{K}(p)|\bar{s}\sigma_{\mu\nu} b|\bar{B}(p_B)\rangle &= i\left[(p_B+p)_\mu q_\nu - (p_B+p)_\nu q_\mu\right]\frac{f_T(q^2)}{m_B+m_K} , \\
\langle \bar{K}(p)|\bar{s}b|\bar{B}(p_B)\rangle &= \frac{m_B^2-m_K^2}{m_b-m_s}f_0(q^2) ,
\end{aligned} \tag{C.28}$$

with $\langle \bar{K}(p)|\bar{s}\gamma_\mu\gamma_5 b|\bar{B}(p_B)\rangle = \langle \bar{K}(p)|\bar{s}\gamma_5 b|\bar{B}(p_B)\rangle = 0$ in QCD. The hadronic HA is defined by

$$h^X = \langle \bar{K}|\bar{s}\overline{\Gamma}^X b|\bar{B}\rangle , \tag{C.29}$$

where $\overline{\Gamma}^X|_{\lambda_X\to 0}$ as in table 4.1 and $\omega \to \bar{\omega}$ from (4.15), containing the full set of dimension-six operators in the effective Hamiltonian (2.42). The HAs are

$$\begin{aligned}
h^V &= \frac{\sqrt{\lambda_{BK}}}{2\sqrt{q^2}}\left(\frac{2m_b}{m_B+m_K}(C_7+C_7')f_T + (C_V+C_V')f_+\right) , \\
h^A &= \frac{\sqrt{\lambda_{BK}}}{2\sqrt{q^2}}(C_A+C_A')f_+ , \\
h^S &= \frac{m_B^2-m_K^2}{2}\left(\frac{(C_S+C_S')}{m_b-m_s} + \frac{m_{\ell_1}-m_{\ell_2}}{q^2}(C_V+C_V')\right)f_0 , \\
h^P &= \frac{m_B^2-m_K^2}{2}\left(\frac{(C_P+C_P')}{m_b-m_s} + \frac{m_{\ell_1}+m_{\ell_2}}{q^2}(C_A+C_A')\right)f_0 , \\
h^T &= -i\frac{\sqrt{\lambda_{BK}}}{\sqrt{2}\,(m_B+m_K)}\,(C_\mathcal{T}-C_\mathcal{T}')\,f_T , \\
h^{T_t} &= -i\frac{\sqrt{\lambda_{BK}}}{2\,(m_B+m_K)}\,(C_\mathcal{T}+C_\mathcal{T}')\,f_T ,
\end{aligned} \tag{C.30}$$

where the Källén function (C.2) $\lambda_{BK} \equiv \lambda(m_B^2, m_K^2, q^2)$ replaces $\lambda_B \equiv \lambda(m_B^2, m_{K^*}^2, q^2)$, and $C_{V(A)} = C_{9(10)}$ in the standard notation used in the literature. These

results are consistent with previous work [132], so long as the angular redefinition $\theta_\ell \to \pi - \theta_\ell$ is taken into account.

C.6 $\Lambda_b \to \Lambda\,(\to (p,n)\pi)\,\ell_1\bar{\ell}_2$ angular distribution

The decay $\Lambda_b \to \Lambda\,(\to (p,n)\pi)\,\ell_1\bar{\ell}_2$ with a final-state proton or neutron, recently measured by the LHCb Collaboration [224], can also be considered within the generalised helicity formalism, and is particularly relevant because this decay can also be described using the effective Hamiltonian defined in (2.42). In this case, equation (4.8) becomes, in the rest frame of the Λ_b,

$$\begin{aligned}\mathcal{A}(\Omega_{\Lambda_b},\Omega_\ell,\Omega_\Lambda|\lambda_{\Lambda_b},\lambda_N,\lambda_1,\lambda_2) \sim \\ \sum_{\lambda_\gamma,\lambda_\Lambda,J_\gamma} \delta_{\lambda_{\Lambda_b},\lambda_\gamma-\lambda_\Lambda}\mathcal{H}_{\lambda_\gamma\lambda_\Lambda} D^{\frac{1}{2}}_{\lambda_\Lambda,\lambda_N}(\Omega_\Lambda)\,\mathcal{N}_{\lambda_N} D^{J_\gamma}_{\lambda_\gamma,\lambda_\ell}(\Omega_\ell)\,\ell_{\lambda_1\lambda_2} \\ = \sum_{\lambda_\gamma,J_\gamma} \mathcal{H}_{\lambda_\gamma,\lambda_\gamma-\lambda_{\Lambda_b}} D^{\frac{1}{2}}_{\lambda_\gamma-\lambda_{\Lambda_b},\lambda_N}(\Omega_\Lambda)\,\mathcal{N}_{\lambda_N} D^{J_\gamma}_{\lambda_\gamma,\lambda_\ell}(\Omega_\ell)\,\ell_{\lambda_1\lambda_2}\ ,\end{aligned} \tag{C.31}$$

where the leptonic HAs are the same as before, and $\mathcal{N}_{\lambda_N}$ is the HA for the decay $\Lambda \to N\pi$ analogous to the $g_{K^*K\pi}$ factor in the $B \to K^*$ decay, this time carrying non-trivial dependence on helicities, owing to the final state particle N having spin-$\frac{1}{2}$. The terms $\mathcal{H}_{\lambda_\gamma\lambda_\Lambda}$ are the HAs for the $\Lambda_b \to \Lambda$ decay, and can be expressed in the form

$$\mathcal{H}_{\lambda_\gamma\lambda_\Lambda} = \langle \Lambda(\lambda_\Lambda)|\bar{s}\overline{\Gamma}^X b|\Lambda_b(\lambda_{\Lambda_b})\rangle\ , \tag{C.32}$$

with the $\overline{\Gamma}^X$ the same as defined in table 4.1. The resulting angular distribution is then

$$\begin{aligned}K(q^2,\Omega_\Lambda,\Omega_\ell) \sim \mathrm{Re}\big[&\mathcal{K}_0^{0,0}\Omega_0^{0,0}(\Omega_\Lambda,\Omega_\ell) + \mathcal{K}_0^{0,1}\Omega_0^{0,1}(\Omega_\Lambda,\Omega_\ell) + \mathcal{K}_0^{0,2}\Omega_0^{0,2}(\Omega_\Lambda,\Omega_\ell) \\ &+ \mathcal{K}_0^{1,0}\Omega_0^{1,0}(\Omega_\Lambda,\Omega_\ell) + \mathcal{K}_0^{1,1}\Omega_0^{1,1}(\Omega_\Lambda,\Omega_\ell) + \mathcal{K}_0^{1,2}\Omega_0^{1,2}(\Omega_\Lambda,\Omega_\ell) \\ &+ \mathcal{K}_1^{1,1}\Omega_1^{1,1}(\Omega_\Lambda,\Omega_\ell) + \mathcal{K}_1^{1,2}\Omega_1^{1,2}(\Omega_\Lambda,\Omega_\ell)\big]\ ,\end{aligned} \tag{C.33}$$

where $\Omega_\Lambda = (0,\theta_\Lambda,0)$ and $\Omega_\ell = (\phi,\theta_\ell,-\phi)$. A theoretical angular analysis of this decay has been performed in [137, 225], and more recently in [226, 227]. In terms of the functions defined in [137], the $\mathcal{K}_m^{l_\Lambda,l_\ell}$ above are

$$\mathcal{K}_0^{0,0} = \frac{1}{3}\left(K_{1cc} + 2K_{1ss}\right)\ ,\quad \mathcal{K}_0^{0,1} = K_{1c}\ ,\quad \mathcal{K}_0^{0,2} = \frac{2}{3}\left(K_{1cc} - K_{1ss}\right)\ ,$$

$$\mathcal{K}_0^{1,0} = \frac{1}{3}\left(K_{2cc} + 2K_{2ss}\right) \ , \quad \mathcal{K}_0^{1,1} = K_{2c} \ , \quad \mathcal{K}_0^{1,2} = \frac{2}{3}\left(K_{2cc} - K_{2ss}\right) \ ,$$
$$\mathcal{K}_1^{1,1} = K_{3s} + iK_{4s} \ , \qquad \mathcal{K}_1^{1,2} = \frac{1}{\sqrt{3}}\left(K_{3sc} + iK_{4sc}\right) \ . \quad \text{(C.34)}$$

These results can also be compared with those found in [138]. It follows that the MoM will be equally useful in future angular analyses of this decay.

Appendix D

Results for twist-four non-diagonal distribution amplitudes

This appendix presents the analytic expressions for non-local twist-4 DAs. The details of the computation for individual contributions are given in chapter 6. Many of the complicated aspects of the computation first enter at twist-4, in particular when computing the perturbative contribution.

The leading non-diagonal sum rules for twist-4 DAs were first presented in [103]. Comments on the comparison to these results will be given at the end of this appendix.

For the scalar and pseudoscalar currents, the correlation function can be written more explicitly as

$$\begin{aligned}(\Pi^{S(P)}_{[\rho]})_{\alpha\beta\alpha'\beta'} &= i\int d^4y e^{-ip\cdot y}\langle 0|\mathcal{T}\left\{(J^{S(P)[\rho]}(z,vz,0))_{\alpha\beta}\bar{s}\sigma_{\alpha'\beta'}(\gamma_5)q(y)\right\}|0\rangle\,,\\ &= X_{\alpha\beta\alpha'\beta'}\Pi^{\chi}_{[\rho]}(p^2)+\tilde{X}_{\alpha\beta\alpha'\beta'}\Pi^{\chi}_{[\tilde{\rho}]}(p^2)+\mathcal{O}(z)\,,\end{aligned} \tag{D.1}$$

where the Lorentz structures X, $\tilde{X}$ are given by

$$\begin{aligned}X_{\alpha\beta\alpha'\beta'} &= \frac{1}{p^2}\left(p_\alpha p_{\alpha'}(-P_{\beta\beta'})+\text{antisym}\right)\\ \tilde{X}_{\alpha\beta\alpha'\beta'} &= \frac{1}{4}\epsilon_{\alpha\beta\bar{\alpha}\bar{\beta}}\epsilon_{\alpha'\beta'\bar{\alpha}'\bar{\beta}'}X^{\bar{\alpha}\bar{\alpha}'\bar{\beta}\bar{\beta}'}=X^{\alpha\alpha'\beta\beta'}+\left(g^{\alpha\alpha'}g^{\beta\beta'}-g^{\alpha\beta'}g^{\alpha'\beta}\right)\,,\end{aligned} \tag{D.2}$$

where $P_{\alpha\beta} = (g_{\alpha\beta} - p_\alpha p_\beta/p^2) = -\sum_\lambda \eta^*_\alpha\eta_\beta$ follows from the sum over

polarisations. Defining the structures

$$\begin{aligned}\mathcal{P}_1^{\alpha\alpha'\beta\beta'} &= \frac{p^2}{(2-d)(p\cdot z)^2} z^\alpha z^{\alpha'} g_\perp^{\beta\beta'} \,, \\ \mathcal{P}_2^{\alpha\alpha'\beta\beta'} &= \frac{1}{(d-2)} g_\perp^{\alpha\alpha'} g_\perp^{\beta\beta'} \,, \end{aligned} \tag{D.3}$$

then the projectors

$$\begin{aligned}\mathcal{P}^{[\rho]} &= \frac{1}{3-d}\left((1-d)\mathcal{P}_1 + \mathcal{P}_2\right) \,, \\ \tilde{\mathcal{P}}^{[\rho]} &= \frac{1}{3-d}\left(2\mathcal{P}_1 - \mathcal{P}_2\right) \,, \end{aligned} \tag{D.4}$$

satisfy $\mathcal{P}^{[\rho]}\cdot X = \tilde{\mathcal{P}}^{[\rho]}\cdot \tilde{X} = 1$ and $\mathcal{P}^{[\rho]}\cdot \tilde{X} = \tilde{\mathcal{P}}^{[\rho]}\cdot X = 0$, and are thus sufficient to extract both of the possible scalar correlation functions in (D.1).

In the results below, the derivatives are understood to act on the projection functions that will be used to extract the parameters of the distribution amplitude. For the gluon condensate, it is convenient to include dependence on the dimensional-regularisation parameter ϵ, as the divergence only appears following integration over the DA parameters ($\underline{\alpha}$).

$$\begin{aligned}
\pi_G^S &= \frac{\alpha_s}{16\pi^3} p^4 \ln\frac{-p^2}{\mu^2}\left(\frac{\alpha_3}{\bar\alpha_1^2}\left(\alpha_2(1-2\bar\alpha_1)+\alpha_1\bar\alpha_1(6\bar\alpha_1-1)\right)+\alpha_1\leftrightarrow\alpha_2\right) \\
&- \frac{1}{192\pi^2}\delta(\alpha_3)(\alpha_1-\alpha_2)^2(\alpha_1+\alpha_2)\frac{p^2}{\mathcal{W}^{1+\epsilon}}\langle G^2\rangle - \frac{\alpha_1\alpha_2}{192\pi^2\mathcal{W}}\delta(\alpha_3)\partial_{\alpha_3}\langle fG^3\rangle \\
&- \frac{1}{3\pi}\alpha_s\left(1-2\alpha_3+(1-2\alpha_3\bar\alpha_3)\ln\frac{-p^2\alpha_3\bar\alpha_3}{\mu^2}\right)\left(m_s\langle\bar qq\rangle\delta(\alpha_2)+m_q\langle\bar ss\rangle\delta(\alpha_1)\right) \\
&+ \frac{1}{6\pi}\alpha_s\left(1+2\bar\alpha_3+\bar\alpha_3^2\ln\frac{-p^2\alpha_3\bar\alpha_3}{\mu^2}\right)\left(m_q\langle\bar qq\rangle\delta(\alpha_2)+m_s\langle\bar ss\rangle\delta(\alpha_1)\right) \\
&- \frac{\bar\alpha_3}{12\pi}\alpha_s\left(4\alpha_3-1-(1-3\alpha_3)\ln\frac{-p^2\alpha_3\bar\alpha_3}{\mu^2}\right)\left(m_q\langle\bar qq\rangle\delta(\alpha_2)\partial_{\alpha_2}+m_s\langle\bar ss\rangle\delta(\alpha_1)\partial_{\alpha_1}\right) \\
&+ \frac{1}{24p^2}\delta(\alpha_3)\left(\delta(\alpha_2)\langle\bar q\sigma\cdot Gq\rangle\left(2m_q-2m_s+m_q\partial_{\alpha_2}\right)\right. \\
&\qquad\left. +\,\delta(\alpha_1)\langle\bar s\sigma\cdot Gs\rangle\left(2m_s-2m_q+m_s\partial_{\alpha_1}\right)\right) \\
&- \frac{\pi\alpha_s}{6p^2}\delta(\alpha_3)\left(\left\langle V_q^aV_f^a\right\rangle\delta(\alpha_2)(2+\partial_{\alpha_2})+\left\langle V_s^aV_f^a\right\rangle\delta(\alpha_1)(2+\partial_{\alpha_1})\right) \\
&+ \frac{8\pi\alpha_s}{p^2}\left\langle S^aS^a\right\rangle\delta(\alpha_1)\delta(\alpha_2)\,, \\
\pi_{\tilde G}^P &= \frac{\alpha_s}{16\pi^3} p^4 \ln\frac{-p^2}{\mu^2}\left(\frac{1}{\bar\alpha_1^2}\left(\alpha_2^2(1-2\alpha_1)+2\alpha_1\bar\alpha_1\alpha_3(1-3\bar\alpha_1)\right)+\alpha_1\leftrightarrow\alpha_2\right)
\end{aligned}$$

$$
\begin{aligned}
&- \frac{1}{96\pi^2}\delta(\alpha_3)\frac{\Gamma(\epsilon)\mathcal{W}+2\alpha_1\alpha_2(\alpha_1+\alpha_2)p^2}{\mathcal{W}^{1+\epsilon}}\langle G^2\rangle - \frac{\alpha_1\alpha_2}{576\pi^2\mathcal{W}}\delta(\alpha_3)\partial_{\alpha_3}\langle fG^3\rangle \\
&- \frac{1}{3\pi}\alpha_s\left(1-2\alpha_3-2\alpha_3\bar{\alpha}_3\ln\frac{-p^2\alpha_3\bar{\alpha}_3}{\mu^2}\right)(m_s\langle\bar{q}q\rangle\delta(\alpha_2)+m_q\langle\bar{s}s\rangle\delta(\alpha_1)) \\
&- \frac{1}{6\pi}\alpha_s\frac{\bar{\alpha}_3}{\alpha_3}\left(1-2\bar{\alpha}_3+\alpha_3(1+\alpha_3)\ln\frac{-p^2\alpha_3\bar{\alpha}_3}{\mu^2}\right)(m_q\langle\bar{q}q\rangle\delta(\alpha_2)+m_s\langle\bar{s}s\rangle\delta(\alpha_1)) \\
&- \frac{\bar{\alpha}_3}{12\pi}\alpha_s\left(1-4\alpha_3-(1+\alpha_3)\ln\frac{-p^2\alpha_3\bar{\alpha}_3}{\mu^2}\right)(m_q\langle\bar{q}q\rangle\delta(\alpha_2)\partial_{\alpha_2}+m_s\langle\bar{s}s\rangle\delta(\alpha_1)\partial_{\alpha_1}) \\
&+ \frac{1}{12p^2}\delta(\alpha_3)\left(m_s\langle\bar{q}\sigma\cdot Gq\rangle\delta(\alpha_2)+m_q\langle\bar{s}\sigma\cdot Gs\rangle\delta(\alpha_1)\right) \\
&- \frac{\pi\alpha_s}{6p^2}\delta(\alpha_3)\left(\left\langle V_q^aV_f^a\right\rangle\delta(\alpha_2)\left(2-\partial_{\alpha_2}+2\partial_{\alpha_3}\right)+\left\langle V_s^aV_f^a\right\rangle\delta(\alpha_1)\left(2-\partial_{\alpha_1}+2\partial_{\alpha_3}\right)\right), \\
\tilde{\pi}_G^S =& \frac{\alpha_s}{16\pi^3}p^4\ln\frac{-p^2}{\mu^2}\left(\frac{\alpha_3(1-2\alpha_1)(\alpha_2-\alpha_1\bar{\alpha}_1)}{\bar{\alpha}_1^2}+\alpha_1\leftrightarrow\alpha_2\right) \\
&+ \frac{1}{192\pi^2}\delta(\alpha_3)(1-2\alpha_1\alpha_2)(\alpha_1+\alpha_2)\frac{p^2}{\mathcal{W}^{1+\epsilon}}\langle G^2\rangle - \frac{\alpha_1\alpha_2}{192\pi^2\mathcal{W}}\delta(\alpha_3)\langle fG^3\rangle \\
&+ \frac{\bar{\alpha}_3}{3\pi}\alpha_s\left(1+\bar{\alpha}_3\ln\frac{-p^2\alpha_3\bar{\alpha}_3}{\mu^2}\right)(m_s\langle\bar{q}q\rangle\delta(\alpha_2)+m_q\langle\bar{s}s\rangle\delta(\alpha_1)) \\
&- \frac{\bar{\alpha}_3}{6\pi}\alpha_s\left(1+\bar{\alpha}_3\ln\frac{-p^2\alpha_3\bar{\alpha}_3}{\mu^2}\right)(m_q\langle\bar{q}q\rangle\delta(\alpha_2)+m_s\langle\bar{s}s\rangle\delta(\alpha_1)) \\
&- \frac{\bar{\alpha}_3}{12\pi}\alpha_s\left(1-2\alpha_3+(1-3\alpha_3)\ln\frac{-p^2\alpha_3\bar{\alpha}_3}{\mu^2}\right)(m_q\langle\bar{q}q\rangle\delta(\alpha_2)\partial_{\alpha_2}+m_s\langle\bar{s}s\rangle\delta(\alpha_1)\partial_{\alpha_1}) \\
&+ \frac{1}{24p^2}\delta(\alpha_3)\left(\delta(\alpha_2)\langle\bar{q}\sigma\cdot Gq\rangle\left(2m_s-m_q\partial_{\alpha_2}\right)+\left(\delta(\alpha_1)\langle\bar{s}\sigma\cdot Gs\rangle\left(2m_q-m_s\partial_{\alpha_1}\right)\right)\right) \\
&+ \frac{\pi\alpha_s}{6p^2}\delta(\alpha_3)\left(\left\langle V_q^aV_f^a\right\rangle\delta(\alpha_2)(2+\partial_{\alpha_2})+\left\langle V_s^aV_f^a\right\rangle\delta(\alpha_1)(2+\partial_{\alpha_1})\right), \\
\tilde{\pi}_{\tilde{G}}^P =& -\frac{\alpha_s}{16\pi^3}p^4\ln\frac{-p^2}{\mu^2}\left(\frac{1}{\bar{\alpha}_1^2}\left(\alpha_2^2(1-2\alpha_1)+2\alpha_1^2\bar{\alpha}_1\alpha_3\right)+\alpha_1\leftrightarrow\alpha_2\right) \\
&+ \frac{1}{96\pi^2}\delta(\alpha_3)\frac{\Gamma(\epsilon)\mathcal{W}+\alpha_1\alpha_2(\alpha_1+\alpha_2)p^2}{\mathcal{W}^{1+\epsilon}}\langle G^2\rangle + \frac{\alpha_1\alpha_2}{576\pi^2\mathcal{W}}\delta(\alpha_3)(3+4\partial_{\alpha_3})\langle fG^3\rangle \\
&+ \frac{1}{3\pi}\alpha_s\left(\bar{\alpha}_3-\alpha_3(1+\bar{\alpha}_3)\ln\frac{-p^2\alpha_3\bar{\alpha}_3}{\mu^2}\right)(m_s\langle\bar{q}q\rangle\delta(\alpha_2)+m_q\langle\bar{s}s\rangle\delta(\alpha_1)) \\
&- \frac{1}{6\pi}\alpha_s\frac{1}{\alpha_3}\left(1-\alpha_3\bar{\alpha}_3-\alpha_3\bar{\alpha}_3(1+\alpha_3)\ln\frac{-p^2\alpha_3\bar{\alpha}_3}{\mu^2}\right)(m_q\langle\bar{q}q\rangle\delta(\alpha_2)+m_s\langle\bar{s}s\rangle\delta(\alpha_1)) \\
&+ \frac{\bar{\alpha}_3}{12\pi}\alpha_s\left(1-2\alpha_3-(1+\alpha_3)\ln\frac{-p^2\alpha_3\bar{\alpha}_3}{\mu^2}\right)(m_q\langle\bar{q}q\rangle\delta(\alpha_2)\partial_{\alpha_2}+m_s\langle\bar{s}s\rangle\delta(\alpha_1)\partial_{\alpha_1}) \\
&- \frac{m_q+m_s}{12p^2}\delta(\alpha_3)\left(\langle\bar{s}\sigma\cdot Gs\rangle\delta(\alpha_1)+\langle\bar{q}\sigma\cdot Gq\rangle\delta(\alpha_2)\right) \\
&+ \frac{\pi\alpha_s}{6p^2}\delta(\alpha_3)\left(\left\langle V_q^aV_f^a\right\rangle\delta(\alpha_2)\left(2-\partial_{\alpha_2}+2\partial_{\alpha_3}\right)+\left\langle V_s^aV_f^a\right\rangle\delta(\alpha_1)\left(2-\partial_{\alpha_1}+2\partial_{\alpha_3}\right)\right) \\
&- \frac{8\pi\alpha_s}{p^2}\left\langle P^aP^a\right\rangle\delta(\alpha_1)\delta(\alpha_2), \\
\pi_{\tilde{G}}^S =& -\pi_{\tilde{G}}^P|_{m_s\langle\bar{q}q\rangle\to-m_s\langle\bar{q}q\rangle,m_q\langle\bar{s}s\rangle\to-m_q\langle\bar{s}s\rangle},
\end{aligned}
$$

$$\pi_G^P = -\pi_G^S|_{m_s\langle\bar{q}q\rangle\to-m_s\langle\bar{q}q\rangle, m_q\langle\bar{s}s\rangle\to-m_q\langle\bar{s}s\rangle, \langle S^aS^a\rangle\to\langle P^aP^a\rangle} ,$$
$$\tilde{\pi}_{\tilde{G}}^S = -\tilde{\pi}_{\tilde{G}}^P|_{m_s\langle\bar{q}q\rangle\to-m_s\langle\bar{q}q\rangle, m_q\langle\bar{s}s\rangle\to-m_q\langle\bar{s}s\rangle, \langle P^aP^a\rangle\to\langle S^aS^a\rangle} ,$$
$$\tilde{\pi}_G^P = -\tilde{\pi}_G^S|_{m_s\langle\bar{q}q\rangle\to-m_s\langle\bar{q}q\rangle, m_q\langle\bar{s}s\rangle\to-m_q\langle\bar{s}s\rangle} . \tag{D.5}$$

To relate the results above to those in [103], the following equations hold:

$$\Pi_V^{\pm}\big|_{[103]} = \int \mathcal{D}\underline{\alpha}\left(\pi_G^S \pm \pi_{\tilde{G}}^P\right) , \tag{D.6}$$

$$\Pi_A^{\pm}\big|_{[103]} = \int \mathcal{D}\underline{\alpha}\left(\tilde{\pi}_G^S \pm \tilde{\pi}_{\tilde{G}}^P\right) . \tag{D.7}$$

The results above are found to be in agreement with [103], apart from the following:

- The gluon contributions match the logarithmic terms in equation (C.6) of [103], but not the constant terms;
- The sign of the mixed condensate cross-terms, $m_q\langle\bar{s}\sigma\cdot Gs\rangle, m_s\langle\bar{q}\sigma\cdot Gq\rangle$, is opposite to that given in the functions $\Pi_{V,A}^-$ of [103];
- Results for the non-logarithmic terms for the two-quark condensates are also in disagreement.

Constant terms will vanish under a Borel transformation, so these disagreements should not be relevant to numerical results.

Appendix E

Three-particle diagonal sum rules

This appendix presents computations related to the diagonal sum rules for twist-3 and twist-4 DAs. As will shortly become clear, the diagonal sum rules are not well-suited to computing three-particle DAs, and even without this handicap the results presented below are confined to local sum rules, meaning that the results presented below merely serve as alternative computations for the leading parameters in the three-particle DAs.

Nevertheless, the computation for the twist-3 case of the diagonal sum rules is new, and still instructive precisely because of these limitations. Results for diagonal twist-4 sum rules were first considered in [103].

E.1 Definition of diagonal sum rules

As opposed to the interpolating currents in the right-hand column of table 3.1, the second possible choice for an interpolating current of the vector meson is to replace it again by the current of interest, leading to the general correlation function

$$\begin{aligned}(\Delta^{\chi\bar{\chi}}_{\mathcal{G}\bar{\mathcal{G}}})^{\alpha\beta\alpha'\beta'} &= i\int d^4y e^{ip\cdot y}\langle 0|\mathcal{T}\left\{(J^{\chi}_{\mathcal{G}}(y))^{\alpha\beta}((J^{\dagger})^{\bar{\chi}}_{\bar{\mathcal{G}}}(0))^{\alpha'\beta'}\right\}|0\rangle\,, \\ &= \left(X^{\alpha\alpha'\beta\beta'}\Delta^{\chi\bar{\chi}}_{\mathcal{G}\bar{\mathcal{G}}}(p^2)+\tilde{X}^{\alpha\alpha'\beta\beta'}\tilde{\Delta}^{\chi\bar{\chi}}_{\mathcal{G}\bar{\mathcal{G}}}(p^2)\right)\,, \end{aligned} \tag{E.1}$$

where $J^{\chi}(y)=\bar{q}(y)\mathcal{G}(y)\chi s(y)$, and the χ, $\bar{\chi}$ are defined in table 3.1. In principle, one could also consider cases where the χ and $\bar{\chi}$ are different structures, but in

all cases of interest, such cross-terms do not contribute, and so to ease notation correlation functions will be denoted $\Delta^{\chi}_{\mathcal{G}}$ in future. The Lorentz structures $X^{\alpha\alpha'\beta\beta'}$ are identical to those defined in equation (D.2). To eliminate potential spin-two contributions in the V, A currents, the relevant correlation functions are further contracted with $p^\mu p^\nu/p^2$. In the local case, the projectors

$$\mathcal{P}^{\alpha\alpha'\beta\beta'} = \frac{-1}{3p^2} p^\alpha p^{\alpha'} g^{\beta\beta'} \,, \qquad \tilde{\mathcal{P}}^{\alpha\alpha'\beta\beta'} = \mathcal{P}^{\alpha\alpha'\beta\beta'} + \frac{1}{6} g^{\alpha\alpha'} g^{\beta\beta'} \tag{E.2}$$

suffice to extract the two structures cleanly. In fact, one only needs to compute the $\Delta^{\chi\bar{\chi}}_{\mathcal{G}\bar{\mathcal{G}}}$ explicitly. The $\tilde{\Delta}$-functions can be obtained through the relations

$$\Delta^{\chi\bar{\chi}}_{\mathcal{G}\bar{\mathcal{G}}} = \tilde{\Delta}^{\chi\bar{\chi}}_{*\mathcal{G}*\bar{\mathcal{G}}} \,, \tag{E.3}$$

where the $*$ denotes the Hodge dual.

The twist-4 diagonal sum rules were considered in appendix C of [103]; the relationship between the sum rules defined above and those in that paper is

$$\Pi_V^{\pm_1\pm_2}|_{[103]} = \left(\Delta^{SS} \pm_1 \Delta^{PS} \pm_2 \Delta^{SP} + (\pm_1\pm_2)\Delta^{PP}\right) \,, \tag{E.4}$$

where potential non-zero cross-terms Δ^{PS} have been included, but in fact these identically vanish. As noted above, there has not been a previous computation of the diagonal sum rules for twist-3 matrix elements.

It is worth noting that the three-particle diagonal sum rules have a higher mass dimension, owing to the presence of an extra $\mathcal{G}$ field, and for this reason it would formally be important, in a complete calculation, to include higher-dimensional condensates. In [103], this was partially achieved by including the dimension-eight condensate $\langle\bar{q}q\rangle\langle\bar{q}\sigma\cdot Gq\rangle$, a step not performed here. Dimension-eight corrections are on the order of 10-20%, depending on the Borel parameters, so restricting to dimension-six contributions is unlikely to be sufficient to provide a reasonably accurate value for the DA parameters.

Moreover, as will be seen in the explicit results, the prediction for the DA parameter $\mathcal{V}_{(0)\rho}$ is non-zero, whereas G-parity imposes $\mathcal{V}_{(0)\rho} \equiv \kappa^{\parallel}_{3\rho} = 0$. This arises because the diagonal sum rules cannot separate states of different parity, so the ρ and a_1 sum rules can mix into each other.

The remainder of this appendix presents the individual contributions considered in the three-particle diagonal sum rules, with analytic results in E.2.

E.1.1 Perturbative contribution

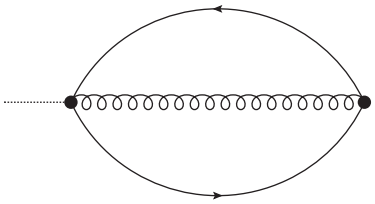

Figure E.1 *Perturbative contribution to the diagonal sum rules. In this diagram, and subsequent diagrams in this appendix, the q-quark line is on the top and the s-quark line is on the bottom, as was the case with the non-diagonal sum rules diagrams in chapter 6. Momentum insertion is indicated by the dotted line to the left.*

The perturbative contribution emerges from the diagram in figure E.1, with the general expression

$$(\Delta^{\chi\bar{\chi}})^{\alpha\beta\alpha'\beta'}\Big|_{pert.} = i\int d^4y\, e^{ip\cdot y}\,\mathrm{Tr}\left[S_q(0,y)\chi S_s(y,0)\bar{\chi}\right]\overbrace{\mathcal{G}^{\alpha\beta}(y)\bar{\mathcal{G}}^{\alpha'\beta'}}(0) \tag{E.5}$$

where the contraction over the general gluon fields leads to the propagator

$$\begin{aligned}
\overbrace{G^{\alpha\beta}(y)G}^{\alpha'\beta'}(0) &= \int \frac{\mathrm{d}^d k}{(2\pi)^d}\frac{-i}{k^2+i\epsilon}e^{-ik\cdot y}\left(k^\alpha k^{\alpha'}g^{\beta\beta'} - k^\beta k^{\alpha'}g^{\alpha\beta'} - k^\alpha k^{\beta'}g^{\beta\alpha'} + k^\beta k^{\beta'}g^{\alpha\alpha'}\right),\\
\overbrace{\tilde{G}^{\alpha\beta}(y)\tilde{G}}^{\alpha'\beta'}(0) &= \overbrace{G^{\alpha\beta}(y)G}^{\alpha'\beta'}(0) + \int \frac{\mathrm{d}^d k}{(2\pi)^d}\frac{-i}{k^2+i\epsilon}e^{-ik\cdot y}k^2\left(g^{\alpha\beta'}g^{\beta\alpha'} - g^{\alpha\alpha'}g^{\beta\beta'}\right).
\end{aligned} \tag{E.6}$$

This is a two-loop integral, but can be performed as two one-loop integrals, using the results in A.4.1 and the unexpanded form of the Passarino-Veltmann function $B_0((k+p)^2)$ (A.31).

E.1.2 Gluon condensates

The second contributions considered are those from the two- and three-gluon condensates. The two-gluon condensate arises from the diagram at the top-left of figure E.2, with general expression

$$(\Delta^{\chi\bar{\chi}})^{\alpha\beta\alpha'\beta'}\Big|_{G^2} = i\int d^4y\, e^{ip\cdot y}\,\mathrm{Tr}\left[S_q(0,y)\chi S_s(y,0)\bar{\chi}\right]\left\langle \mathcal{G}^{\alpha\beta}\bar{\mathcal{G}}^{\alpha'\beta'}\right\rangle \tag{E.7}$$

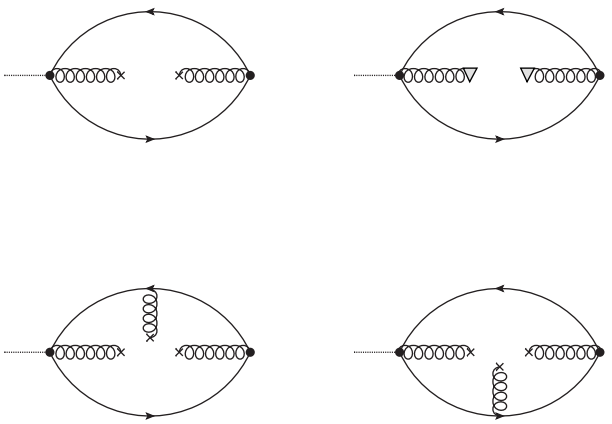

Figure E.2 *Gluon condensate contributions to the diagonal sum rules. Top left: Two-gluon condensate contribution. Top right: three-gluon condensate contribution from expansion of the background fields* (E.8)*. Bottom: three-gluon condensate contributions from expansion of the fermion propagators. As discussed in the text, these contributions vanish upon contraction with the projectors* (E.2)*.*

where the general condensate $\left\langle \mathcal{G}^{\alpha\beta}\bar{\mathcal{G}}^{\alpha'\beta'}\right\rangle$ can be related to the definition of the two-gluon condensate given in (A.10).

The three-gluon condensate emerges, in principle, from two types of contribution: corrections to the propagators in the two-gluon result, and the expansion of the gluon fields $\mathcal{G}^{\alpha\beta}$. The first type of contribution, however (shown at the bottom of figure E.2), always vanishes, independent of the structure $\chi, \tilde{\chi}$, as the projection (E.2) acting on the three-gluon condensate (A.11) is zero. The three-gluon contribution instead comes from expanding the gluon fields. The double expansion reads

$$\begin{aligned}\mathcal{G}^{\alpha\beta}(y)\bar{\mathcal{G}}^{\alpha'\beta'}(z) =& \mathcal{G}^{\alpha\beta}\bar{\mathcal{G}}^{\alpha'\beta'} + \frac{1}{2}y^\rho y^\tau \nabla_\rho\nabla_\tau \mathcal{G}^{\alpha\beta}\bar{\mathcal{G}}^{\alpha'\beta'} + \frac{1}{2}\mathcal{G}^{\alpha\beta} z^\rho z^\tau \nabla_\rho\nabla_\tau \bar{\mathcal{G}}^{\alpha'\beta'} \\ &+ y^\rho \nabla_\rho \mathcal{G}^{\alpha\beta} z^\tau \nabla_\tau \bar{\mathcal{G}}^{\alpha'\beta'} + (\text{linear terms}) + h.o. \end{aligned} \tag{E.8}$$

where linear terms contributing to the mixed condensate $\langle \bar{q}\sigma \cdot Gq\rangle$, are neglected, as they are quark mass corrections at dimension six. For the terms of interest, making the identifications $y \to -i\partial_p$ and $z \to -i\left(\partial_p - \partial_{\Delta k}\right)$, where $\Delta k = k_s - k_q$, then, after partial integration, the three-gluon contribution becomes

$$\begin{aligned}\left(\Delta^{\chi\bar{\chi}}\right)^{\alpha\beta\alpha'\beta'}\Big|_{G^3} = \frac{-i}{2}\int_{y,\,k_s,\,k_q} & e^{-iy(k_s-k_q-p)}e^{-iz(k_q-k_s)}\left\langle \nabla_\rho \mathcal{G}^{\alpha\beta}\nabla_\tau\bar{\mathcal{G}}^{\alpha'\beta'}\right\rangle \\ & \times\left(\partial^\rho_{\Delta k}\partial^\tau_{\Delta k} + \partial^\rho_p\partial^\tau_{\Delta k} - \partial^\rho_{\Delta k}\partial^\tau_p\right) Tr\left[S(k_q)\chi S(k_s)\bar{\chi}\right]\,. \end{aligned} \tag{E.9}$$

The antisymmetric term vanishes, leaving the trace

$$\begin{aligned}\partial^{\rho}_{\Delta k}\partial^{\tau}_{\Delta k}\mathrm{Tr}\left[S(k_q)\chi S(k_s)\bar{\chi}\right] &= \mathrm{Tr}\left[S_q\gamma^{\rho}S_q\gamma^{\tau}S_q\chi S_s\bar{\chi} + S_q\gamma^{\tau}S_q\gamma^{\rho}S_q\chi S_s\bar{\chi}\right] \\ &- \mathrm{Tr}\left[S_q\gamma^{\tau}S_q\chi S_s\gamma^{\rho}S_s\bar{\chi} + S_q\gamma^{\rho}S_q\chi S_s\gamma^{\tau}S_s\bar{\chi}\right] \\ &+ \mathrm{Tr}\left[S_q\chi S_s\gamma^{\rho}S_s\gamma^{\tau}S_s\bar{\chi} + S_q\chi S_s\gamma^{\tau}S_s\gamma^{\rho}S_s\bar{\chi}\right] \\ &\equiv \mathrm{Tr}_{\nabla G\nabla G}(\chi,\bar{\chi})\end{aligned} \tag{E.10}$$

The resulting integral is again a one-loop diagram, and final expressions can be obtained using the results given in appendix A.4.2. Note that the diagrams are divergent in $d = 4$ dimensions, and care therefore needs to be taken in implementing d-dimensional traces.

E.1.3 Four-quark condensate

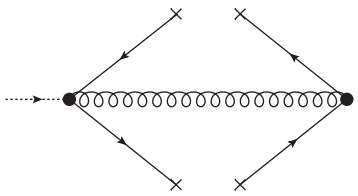

Figure E.3 *Four-quark condensate contribution to the diagonal sum rules.*

The final contribution to the diagonal sum rules relevant at dimension six is the four-quark condensate, which arises from figure E.3, and has the general expression

$$(\Delta^{\chi\bar{\chi}})^{\alpha\beta\alpha'\beta'}\Big|_{\text{Four-quark}} = i\int \mathrm{d}^4y\, e^{ip\cdot y}\,\langle\bar{q}(y)\chi s(y)\bar{s}(0)\tilde{\chi}q(0)\rangle\,\overbrace{\mathcal{G}^{\alpha\beta}(y)\bar{\mathcal{G}}^{\alpha'\beta'}}(0)\,, \tag{E.11}$$

where the contraction over gluon fields is given as before in equation (E.6). There is no loop momentum to integrate over, so this reduces to

$$(\Delta^{\chi}_{G})|_{\text{Four-quark}} = -4\pi\alpha_s\,\langle\bar{q}(y)\chi t^a s(y)\bar{s}(0)\tilde{\chi}t^a q(0)\rangle\ , \tag{E.12}$$

$$(\Delta^{\chi}_{\tilde{G}})\Big|_{\text{Four-quark}} = 0\,, \tag{E.13}$$

and similarly for $\tilde{\Delta}^{\chi}_{\mathcal{G}}$, where instead $\Delta^{\tilde{\chi}}_{G}\Big|_{\text{Four-quark}} = 0$.

E.2 Results

The resulting sum rules have the following form, with other combinations being zero:

$$\begin{aligned}
\Delta_G^S &= -\frac{\alpha_s}{960\pi^3}p^6\ln\frac{-p^2}{\mu^2} + \frac{1}{192\pi^2}p^2\ln\frac{-p^2}{\mu^2}\langle G^2\rangle + \frac{1}{24\pi^2}\ln\frac{-p^2}{\mu^2}\langle fG^3\rangle - 4\pi\alpha_s\langle S^aS^a\rangle\,,\\
\Delta_{\tilde{G}}^P &= -\frac{\alpha_s}{960\pi^3}p^6\ln\frac{-p^2}{\mu^2} - \frac{1}{192\pi^2}p^2\ln\frac{-p^2}{\mu^2}\langle G^2\rangle - \frac{1}{24\pi^2}\ln\frac{-p^2}{\mu^2}\langle fG^3\rangle\,,\\
\Delta_G^P &= -\frac{\alpha_s}{960\pi^3}p^6\ln\frac{-p^2}{\mu^2} + \frac{1}{192\pi^2}p^2\ln\frac{-p^2}{\mu^2}\langle G^2\rangle + \frac{1}{24\pi^2}\ln\frac{-p^2}{\mu^2}\langle fG^3\rangle - 4\pi\alpha_s\langle P^aP^a\rangle\,,\\
\Delta_{\tilde{G}}^S &= -\frac{\alpha_s}{960\pi^3}p^6\ln\frac{-p^2}{\mu^2} - \frac{1}{192\pi^2}p^2\ln\frac{-p^2}{\mu^2}\langle G^2\rangle - \frac{1}{24\pi^2}\ln\frac{-p^2}{\mu^2}\langle fG^3\rangle\,,\\
\Delta_G^V &= -\frac{\alpha_s}{1728\pi^3}p^6\ln\frac{-p^2}{\mu^2} + (0+\mathcal{O}(\alpha_s))\langle G^2\rangle - \frac{1}{48\pi^2}\ln\frac{-p^2}{\mu^2}\langle fG^3\rangle - 4\pi\alpha_s\langle V^aV^a\rangle\,,\\
\Delta_{\tilde{G}}^A &= -\frac{\alpha_s}{1728\pi^3}p^6\ln\frac{-p^2}{\mu^2} + (0+\mathcal{O}(\alpha_s))\langle G^2\rangle + \frac{1}{48\pi^2}\ln\frac{-p^2}{\mu^2}\langle fG^3\rangle\,,\\
\Delta_G^A &= -\frac{\alpha_s}{1728\pi^3}p^6\ln\frac{-p^2}{\mu^2} + (0+\mathcal{O}(\alpha_s))\langle G^2\rangle - \frac{1}{48\pi^2}\ln\frac{-p^2}{\mu^2}\langle fG^3\rangle - 4\pi\alpha_s\langle A^aA^a\rangle\,,\\
\Delta_{\tilde{G}}^V &= -\frac{\alpha_s}{1728\pi^3}p^6\ln\frac{-p^2}{\mu^2} + (0+\mathcal{O}(\alpha_s))\langle G^2\rangle + \frac{1}{48\pi^2}\ln\frac{-p^2}{\mu^2}\langle fG^3\rangle\,,
\end{aligned} \tag{E.14}$$

where any constants arising from the loop integrals are dropped, as they either vanish under the Borel transformation or are scheme-dependent terms that must ultimately cancel from any combination.

As noted before, the twist-4 results can be related to a previous computation, presented in appendix C of [103]. The results above, however, are not consistent with those expressions. In particular, in the three-gluon contribution, the equivalent expression for Δ_G^S is

$$\Delta_G^S\big|_{G^3,BBL} = -\frac{1}{48\pi^2p^2}\log\frac{-p^2}{\mu^2}\,, \tag{E.15}$$

which differs from the result in this thesis by a factor of $-1/2$. It is possible that this discrepancy arises from an error in the definition of the three-gluon condensate used by [103].

Results for the twist-3 diagonal sum rules are new. Again, it is clear that the prediction for Δ_G^V, which can be related to the leading parameter in the vector DAs, is non-zero in general, which strongly indicates that these sum rules are

unreliable or, at the very least, require careful study in order to extract useful information about the parameters of interest.

As a result, the non-diagonal sum rules, presented in greater detail in chapter 6, should be preferred for numerical evaluation of the three-particle sum rules.

Appendix F

Further material for the long-distance charm loop calculation

Here the polynomials P_i and R_i, defined in the main text but whose explicit forms were not given in chapter 7, are provided in full.

It is helpful to note that, owing to the structure of the three-particle DAs (3.48), each result can be expanded in the form

$$C_{\mathcal{F}} = C_{\mathcal{F}}^{(0)}\varphi^{(0)} + C_{\mathcal{F}}^{(1)}\varphi^{(1)} + C_{\mathcal{F}}^{(2)}\varphi^{(2)}\,, \tag{F.1}$$

where the $\varphi^{(j)}$ stand for generic DA parameters, as specified by the defintions in section 3.4. Hence, only three integrals need be calculated, and the input parameters that distinguish one DA from another can be separated from the properties of the integral.

The leading results were first provided in [35], and are consistent with the expressions below. The remainder are given for the first time.

F.1 Explicit expressions for the $P_i^{(j)}$

The P_i are defined in terms of the integrals

$$\begin{aligned}
C_{\mathcal{F}}^{(0)} &= \int_0^1\int_0^1 \frac{dx\,d\alpha_3\,x}{(P^2-Q^2)(p_B^2-q^2)^3}\left(\left(\ln(m_b^2-p_B^2)-\ln(m_b^2-\alpha_3 p_B^2-\bar\alpha_3 q^2)\right)P_1^{(0)}+P_2^{(0)}\right)\\
&\quad\times\left(\left(\ln(m_x^2-Q^2)-\ln(m_x^2-\alpha_3 P^2-\bar\alpha_3 Q^2)\right)P_3^{(0)}+P_4^{(0)}\right)P_5^{(0)}\,,\\
C_{\mathcal{F}}^{(1)} &= \int_0^1\int_0^1 \frac{dx\,d\alpha_3\,x}{(P^2-Q^2)(p_B^2-q^2)^4}\left(\left(\ln(m_b^2-p_B^2)-\ln(m_b^2-\alpha_3 p_B^2-\bar\alpha_3 q^2)\right)P_1^{(1)}+P_2^{(1)}\right)\\
&\quad\times\left(\left(\ln(m_x^2-Q^2)-\ln(m_x^2-\alpha_3 P^2-\bar\alpha_3 Q^2)\right)P_3^{(1)}+P_4^{(1)}\right)P_5^{(1)}\,,\\
C_{\mathcal{F}}^{(2)} &= \int_0^1\int_0^1 \frac{dx\,d\alpha_3\,x}{(P^2-Q^2)(p_B^2-q^2)^3}\left(\left(\ln(m_b^2-p_B^2)-\ln(m_b^2-\alpha_3 p_B^2-\bar\alpha_3 q^2)\right)P_1^{(2)}+P_2^{(2)}\right)\\
&\quad\times\left(\left(\ln(m_x^2-Q^2)-\ln(m_x^2-\alpha_3 P^2-\bar\alpha_3 Q^2)\right)P_3^{(2)}+P_4^{(2)}\right)P_5^{(2)}\,, \qquad \text{(F.2)}
\end{aligned}$$

where there is an extra factor of $(p_B^2-q^2)^{-1}$ for the $C_{\mathcal{F}}^{(1)}$-type integral, owing to the different functional dependence on $\alpha_{1,2}$, but otherwise the structures for all DAs are universal.

The explicit forms of the P_i are then given below. For $i=1,\ldots,4$, they are

$$\begin{aligned}
P_1^{(0)} &= 2(m_b^2-p_B^2)(m_b^2-\alpha_3 p_B^2-\bar\alpha_3 q^2)\,,\\
P_2^{(0)} &= \bar\alpha_3(p_B^2-q^2)\left((m_b^2-p_B^2)+(m_b^2-\alpha_3 p_B^2-\bar\alpha_3 q^2)\right)\,,\\
P_3^{(0)} &= Q^2-m_x^2\,,\\
P_4^{(0)} &= \alpha_3(P^2-Q^2)\,,\\
P_1^{(1)} &= 6(m_b^2-p_B^2)(m_b^2-\alpha_3 p_B^2-\bar\alpha_3 q^2)\left((m_b^2-p_B^2)+(m_b^2-\alpha_3 p_B^2-\bar\alpha_3 q^2)\right)\,,\\
P_2^{(1)} &= \bar\alpha_3(p_B^2-q^2)\big[\left((m_b^2-p_B^2)+(m_b^2-\alpha_3 p_B^2-\bar\alpha_3 q^2)\right)^2\\
&\qquad +8(m_b^2-p_B^2)(m_b^2-\alpha_3 p_B^2-\bar\alpha_3 q^2)\big]\,,\\
P_3^{(1)} &= Q^2-m_x^2\,,\\
P_4^{(1)} &= \alpha_3(P^2-Q^2)\,,\\
P_i^{(2)} &= P_i^{(0)}\,, \qquad i=1,\ldots,4\,. \qquad \text{(F.3)}
\end{aligned}$$

The overall normalisations are contained in P_5, and are

$$\begin{aligned}
P_5^{(0)} &= \frac{1}{2}\frac{m_b m_V f_V}{f_B m_B^2}360\,,\\
P_5^{(1)} &= \frac{-1}{6}\frac{m_b m_V f_V}{f_B m_B^2}360\,,
\end{aligned}$$

$$P_5^{(2)} = \frac{1}{4}\frac{m_b m_V f_V}{f_B m_B^2} 360(7\alpha_3 - 3)\,. \tag{F.4}$$

F.2 Explicit expressions for the $R_i^{(j)}$

The polynomials R_i are defined in terms of the integrals

$$\begin{aligned}
\frac{1}{\pi}\text{Disc.}C_{\mathcal{F}}^{(0)} &= \int_0^1 \frac{dx\,x}{(P^2-Q^2)^3(s-q^2)^3}\times \\
&\quad \Big(\big(\ln(m_x^2-Q^2) - \ln(m_x^2 - \alpha_3^* P^2 - \bar{\alpha}_3^* Q^2)\big)\,R_1^{(0)} + R_2^{(0)}\Big)\,R_3^{(0)}\,, \\
\frac{1}{\pi}\text{Disc.}C_{\mathcal{F}}^{(1)} &= \int_0^1 \frac{dx\,x}{(P^2-Q^2)^4(s-q^2)^4}\times \\
&\quad \Big(\big(\ln(m_x^2-Q^2) - \ln(m_x^2 - \alpha_3^* P^2 - \bar{\alpha}_3^* Q^2)\big)\,R_1^{(1)} + R_2^{(1)}\Big)\,R_3^{(1)}\,, \\
\frac{1}{\pi}\text{Disc.}C_{\mathcal{F}}^{(2)} &= \int_0^1 \frac{dx\,x}{(P^2-Q^2)^4(s-q^2)^3}\times \\
&\quad \Big(\big(\ln(m_x^2-Q^2) - \ln(m_x^2 - \alpha_3^* P^2 - \bar{\alpha}_3^* Q^2)\big)\,R_1^{(2)} + R_2^{(2)}\Big)\,R_3^{(2)}\,,
\end{aligned} \tag{F.5}$$

where, again, away from the leading DA one can pick up extra poles in $s-q^2$ and P^2-Q^2, but otherwise the structure is identical to that outlined in chapter 7. The polynomials are also universal up to the specific values for DA parameters.

The $R_3^{(j)}$ contain all dependence on hadronic parameters, and are given by

$$\begin{aligned}
R_3^{(0)} &= \frac{1}{12}\frac{m_b f_V m_V}{f_B m_B^2} 360(s-m_b^2)\,, \\
R_3^{(1)} &= \frac{1}{36}\frac{m_b f_V m_V}{f_B m_B^2} 360(s-m_b^2)\,, \\
R_3^{(2)} &= \frac{1}{72}\frac{m_b f_V m_V}{f_B m_B^2} 360(s-m_b^2)\,.
\end{aligned} \tag{F.6}$$

Specific forms for the remaining R_i are given below. α_3^* is as defined in (7.19), and $m_x^2 = m_c^2/(x\bar{x})$.

$$\begin{aligned}
R_1^{(0)} &= 6(m_x^2-Q^2)\left(m_x^2 - \alpha_3^* P^2 - \bar{\alpha}_3^* Q^2)(P^2 q^2(\alpha_3^*-2) + 2m_b^2(P^2-Q^2)\right. \\
&\qquad \left. + \bar{\alpha}_3^* q^2 Q^2 - \alpha_3^* P^2 s + (1+\alpha_3^*)Q^2 s + (q^2-s)m_x^2\right)\,, \\
R_1^{(1)} &= 6(m_x^2-Q^2)\left((Q^2-P^2)\alpha_3^* + m_x^2 - Q^2\right)\left(-(P^2-Q^2)(q^2-s)\alpha_3^*\left(9m_b^2(Q^2-P^2)\right.\right. \\
&\quad \left. +2m_x^2(s-q^2) + 6P^2q^2 + 3P^2 s - 4q^2Q^2 - 5Q^2 s\right) + 2(P^2-Q^2)^2(q^2-s)^2(\alpha_3^*)^2 \\
&\quad - 3m_b^2(P^2-Q^2)(3m_x^2(s-q^2) + 6P^2q^2 + 2P^2 s - 3q^2Q^2 - 5Q^2 s)
\end{aligned}$$

$$
\begin{aligned}
&+12m_b^4(P^2-Q^2)^2+m_x^2(q^2-s)(2m_x^2(q^2-s)-6P^2q^2-3P^2s+2q^2Q^2+7Q^2s)\\
&+6P^4q^2(q^2+s)-3P^2Q^2(2q^4+5q^2s+s^2)+Q^4(2q^4+5q^2s+5s^2)\big)\,,\\
R_1^{(2)}=&-6(m_x^2-Q^2)\left((Q^2-P^2)\alpha_3^*+m_x^2-Q^2\right)\left((P^2-Q^2)\alpha_3^*\left(21m_b^2(Q^2-P^2)\right.\right.\\
&+14m_x^2(s-q^2)+30P^2q^2-9P^2s-16q^2Q^2-5Q^2s\big)\\
&-14(P^2-Q^2)^2(q^2-s)(\alpha_3^*)^2+3m_b^2(P^2-Q^2)(-7m_x^2+6P^2+Q^2)\\
&-m_x^2(14m_x^2(q^2-s)-30P^2q^2+9P^2s+2q^2Q^2+19Q^2s)\\
&\left.-2q^2(9P^4-3P^2Q^2+Q^4)+Q^2s(9P^2+5Q^2)\right)\,,\\
R_2^{(0)}=&-(P^2-Q^2)\alpha_3^*\left(3\alpha_3^*(P^2-Q^2)\left(2m_b^2(Q^2-P^2)+m_x^2(q^2-s)+2P^2q^2-3q^2Q^2+Q^2s\right)\right.\\
&-4(P^2-Q^2)^2(q^2-s)(\alpha_3^*)^2-6(Q^2-m_x^2)\left(2m_b^2(P^2-Q^2)+m_x^2(q^2-s)\right.\\
&\left.\left.-2P^2q^2+Q^2(q^2+s)\right)\right)\,,\\
R_2^{(1)}=&-(P^2-Q^2)^3(\alpha_3^*)^2\left(4\alpha_3^*(s-q^2)\left(9m_b^2(Q^2-P^2)+m_x^2(q^2-s)+6P^2q^2+3P^2s\right.\right.\\
&\left.-7q^2Q^2-2Q^2s\right)+9(P^2-Q^2)(q^2-s)^2(\alpha_3^*)^2+18(P^2-Q^2)(q^2-m_b^2)\\
&\left.(-2m_b^2+q^2+s)\right)+3(P^2-Q^2)^2(q^2-s)(Q^2-m_x^2)(\alpha_3^*)^2(9m_b^2(Q^2-P^2)\\
&+2m_x^2(s-q^2)+6P^2q^2+3P^2s-4q^2Q^2-5Q^2s)-6\alpha_3^*(P^2-Q^2)(Q^2-m_x^2)\\
&(-3m_b^2(P^2-Q^2)(3m_x^2(s-q^2)+6P^2q^2+2P^2s-3q^2Q^2-5Q^2s)+12m_b^4(P^2-Q^2)^2\\
&+m_x^2(q^2-s)(2m_x^2(q^2-s)-6P^2q^2-3P^2s+2q^2Q^2+7Q^2s)+6P^4q^2(q^2+s)\\
&-3P^2Q^2(2q^4+5q^2s+s^2)+Q^4(2q^4+5q^2s+5s^2))\,,\\
R_2^{(2)}=&\alpha_3^*(P^2-Q^2)(-3(P^2-Q^2)\alpha_3^*(-3m_b^2(P^2-Q^2)(7m_x^2+6P^2-13Q^2)-m_x^2(14m_x^2(q^2-s)\\
&-30P^2q^2+9P^2s+2q^2Q^2+19Q^2s)+2q^2(9P^4-33P^2Q^2+17Q^4)\\
&+Q^2s(9P^2+5Q^2))+4(P^2-Q^2)^2(\alpha_3^*)^2(21m_b^2(Q^2-P^2)+7m_x^2(q^2-s)\\
&+30P^2q^2-9P^2s-37q^2Q^2+16Q^2s)-63(P^2-Q^2)^3(q^2-s)(\alpha_3^*)^3\\
&-6(Q^2-m_x^2)(-3m_b^2(P^2-Q^2)(-7m_x^2+6P^2+Q^2)+m_x^2(14m_x^2(q^2-s)\\
&-30P^2q^2+9P^2s+2q^2Q^2+19Q^2s)+2q^2(9P^4-3P^2Q^2+Q^4)-Q^2s(9P^2+5Q^2)))\,.
\end{aligned}
\tag{F.7}
$$

These results are for general q^2, although the method for evaluating the sum rules beyond $q^2=0$ is non-trivial, owing to the issue of dealing with charmonium resonances. The resolution is described in [35, 194]. Away from $q^2=0$, one also needs the longitudinal contributions, which can be calculated in like manner to the transverse results derived above, but the polynomials involved are far lengthier, and are not given here.

List of Acronyms

CKM Cabibbo-Kobayashi-Maskawa

DA distribution amplitude

FCNC flavour-changing neutral current

GIM Glashow-Iliopolous-Maiani

HA helicity amplitude

IR infrared

LCSR Light-Cone Sum Rules

LD long-distance

LFA Lepton Factorisation Approximation

LHC Large Hadron Collider

MoM Method of Moments

NLO Next-to Leading Order

NP New Physics

OPE Operator Product Expansion

PDG Particle Data Group

PMNS Pontecorvo-Maki-Nakagawa-Sakata

QCD Quantum Chromodynamics

QED Quantum Electrodynamics

QFT Quantum Field Theory

RG Renormalisation Group

RHC right-handed currents

SD short-distance

SM Standard Model

UV ultraviolet

Bibliography

[1] **ATLAS** Collaboration, G. Aad *et al.*, "Observation of a new particle in the search for the Standard Model Higgs boson with the ATLAS detector at the LHC," *Phys. Lett.* **B716** (2012) 1–29, arXiv:1207.7214 [hep-ex].

[2] **CMS** Collaboration, S. Chatrchyan *et al.*, "Observation of a new boson at a mass of 125 GeV with the CMS experiment at the LHC," *Phys. Lett.* **B716** (2012) 30–61, arXiv:1207.7235 [hep-ex].

[3] S. L. Glashow, "Partial Symmetries of Weak Interactions," *Nucl. Phys.* **22** (1961) 579–588.

[4] A. Salam, "Weak and Electromagnetic Interactions," *Conf. Proc.* **C680519** (1968) 367–377.

[5] S. Weinberg, "A Model of Leptons," *Phys. Rev. Lett.* **19** (1967) 1264–1266.

[6] M. Gell-Mann, "A Schematic Model of Baryons and Mesons," *Phys. Lett.* **8** (1964) 214–215.

[7] F. Englert and R. Brout, "Broken Symmetry and the Mass of Gauge Vector Mesons," *Phys. Rev. Lett.* **13** (1964) 321–323.

[8] P. W. Higgs, "Broken symmetries, massless particles and gauge fields," *Phys. Lett.* **12** (1964) 132–133.

[9] P. W. Higgs, "Broken Symmetries and the Masses of Gauge Bosons," *Phys. Rev. Lett.* **13** (1964) 508–509.

[10] G. S. Guralnik, C. R. Hagen, and T. W. B. Kibble, "Global Conservation Laws and Massless Particles," *Phys. Rev. Lett.* **13** (1964) 585–587.

[11] P. A. M. Dirac, "The quantum theory of the electron," *Proc. Roy. Soc. Lond.* **A117** (1928) 610–624.

[12] P. A. M. Dirac, "A Theory of Electrons and Protons," *Proc. Roy. Soc. Lond.* **A126** (1930) 360.

[13] C. D. Anderson, "The positive electron," *Phys. Rev.* **43** (Mar, 1933) 491–494. https://link.aps.org/doi/10.1103/PhysRev.43.491.

[14] A. D. Sakharov, "Violation of CP Invariance, C Asymmetry, and Baryon Asymmetry of the Universe," *Pisma Zh. Eksp. Teor. Fiz.* **5** (1967) 32–35. [Usp. Fiz. Nauk161,61(1991)].

[15] B. Gripaios, "Lectures on Physics Beyond the Standard Model," arXiv:1503.02636 [hep-ph].

[16] **LHCb** Collaboration, R. Aaij *et al.*, "Observation of $J/\psi p$ Resonances Consistent with Pentaquark States in $\Lambda_b^0 \to J/\psi K^- p$ Decays," *Phys. Rev. Lett.* **115** (2015) 072001, arXiv:1507.03414 [hep-ex].

[17] Y. Grossman, "Introduction to flavor physics," in *Flavianet School on Flavour Physics Karlsruhe, Germany, September 7-18, 2009*, pp. 111–144. 2014. arXiv:1006.3534 [hep-ph]. https://inspirehep.net/record/858514/files/arXiv:1006.3534.pdf. [,73(2014)].

[18] M. Neubert, "Introduction to B physics," in *Proceedings, Summer School in Particle Physics: Trieste, Italy, June 21-July 9, 1999*, pp. 244–295. 2000. arXiv:hep-ph/0001334 [hep-ph].

[19] **LHCb** Collaboration, R. Aaij *et al.*, "Test of lepton universality using $B^+ \to K^+ \ell^+ \ell^-$ decays," *Phys.Rev.Lett.* **113** (2014) 151601, arXiv:1406.6482 [hep-ex].

[20] **LHCb** Collaboration, R. Aaij *et al.*, "Measurement of Form-Factor-Independent Observables in the Decay $B^0 \to K^{*0} \mu^+ \mu^-$," *Phys.Rev.Lett.* **111** (2013) 191801, arXiv:1308.1707 [hep-ex].

[21] **LHCb** Collaboration, R. Aaij *et al.*, "Measurement of the ratio of branching fractions $\mathcal{B}(\overline{B}^0 \to D^{*+} \tau^- \overline{\nu}_\tau)/\mathcal{B}(\overline{B}^0 \to D^{*+} \mu^- \overline{\nu}_\mu)$," *Phys. Rev. Lett.* **115** no. 11, (2015) 111803, arXiv:1506.08614 [hep-ex].

[22] **LHCb** Collaboration, R. Aaij *et al.*, "Angular analysis of the $B^0 \to K^{*0} \mu^+ \mu^-$ decay using 3 fb^{-1} of integrated luminosity," *JHEP* **02** (2016) 104, arXiv:1512.04442 [hep-ex].

[23] **LHCb** Collaboration, R. Aaij *et al.*, "Angular analysis and differential branching fraction of the decay $B_s^0 \to \phi \mu^+ \mu^-$," *JHEP* **09** (2015) 179, arXiv:1506.08777 [hep-ex].

[24] **BaBar** Collaboration, J. P. Lees *et al.*, "Measurement of angular asymmetries in the decays $B \to K^* \ell^+ \ell^-$," *Phys. Rev.* **D93** no. 5, (2016) 052015, arXiv:1508.07960 [hep-ex].

[25] **Belle** Collaboration, A. Abdesselam *et al.*, "Angular analysis of $B^0 \to K^*(892)^0 \ell^+ \ell^-$," in *Proceedings, LHCSki 2016 - A First Discussion of 13 TeV Results: Obergurgl, Austria, April 10-15.* 2016. arXiv:1604.04042 [hep-ex].

[26] J. Lyon and R. Zwicky, "Resonances gone topsy turvy – the charm of QCD or new physics in $b \to s\ell^+\ell^-$?," arXiv:1406.0566 [hep-ph].

[27] B. Capdevila, A. Crivellin, S. Descotes-Genon, J. Matias, and J. Virto, "Patterns of New Physics in $b \to s\ell^+\ell^-$ transitions in the light of recent data," *JHEP* **01** (2018) 093, arXiv:1704.05340 [hep-ph].

[28] T. Blake, G. Lanfranchi, and D. M. Straub, "Rare B Decays as Tests of the Standard Model," *Prog. Part. Nucl. Phys.* **92** (2017) 50–91, arXiv:1606.00916 [hep-ph].

[29] **BaBar** Collaboration, J. P. Lees *et al.*, "Evidence for an excess of $\bar{B} \to D^{(*)}\tau^-\bar{\nu}_\tau$ decays," *Phys. Rev. Lett.* **109** (2012) 101802, arXiv:1205.5442 [hep-ex].

[30] **Belle** Collaboration, M. Huschle *et al.*, "Measurement of the branching ratio of $\bar{B} \to D^{(*)}\tau^-\bar{\nu}_\tau$ relative to $\bar{B} \to D^{(*)}\ell^-\bar{\nu}_\ell$ decays with hadronic tagging at Belle," *Phys. Rev.* **D92** no. 7, (2015) 072014, arXiv:1507.03233 [hep-ex].

[31] **LHCb** Collaboration, R. Aaij *et al.*, "Measurement of the ratio of branching fractions $\mathcal{B}(\bar{B}^0 \to D^{*+}\tau^-\bar{\nu}_\tau)/\mathcal{B}(\bar{B}^0 \to D^{*+}\mu^-\bar{\nu}_\mu)$," *Phys. Rev. Lett.* **115** no. 11, (2015) 111803, arXiv:1506.08614 [hep-ex]. [Erratum: Phys. Rev. Lett. 115, no. 15, 159901 (2015)].

[32] D. Bardhan, P. Byakti, and D. Ghosh, "A closer look at the R_D and R_{D^*} anomalies," *JHEP* **01** (2017) 125, arXiv:1610.03038 [hep-ph].

[33] M. Jacob and G. Wick, "On the general theory of collisions for particles with spin," *Annals Phys.* **7** (1959) 404–428.

[34] J. Gratrex, M. Hopfer, and R. Zwicky, "Generalised helicity formalism, higher moments and the $B \to K_{J_K}(\to K\pi)\bar{\ell}_1\ell_2$ angular distributions," *Phys. Rev.* **D93** no. 5, (2016) 054008, arXiv:1506.03970 [hep-ph].

[35] J. Lyon, *Rare semi-leptonic B meson decays*. PhD thesis, Edinburgh U., 2014-06-28. http://hdl.handle.net/1842/8904.

[36] J. Gratrex and R. Zwicky, "Parity Doubling as a Tool for Right-handed Current Searches," *JHEP* **08** (2018) 178, arXiv:1804.09006 [hep-ph].

[37] J. Gratrex and R. Zwicky, "Right-handed Currents Searches and Parity Doubling," in *53rd Rencontres de Moriond on QCD and High Energy Interactions (Moriond QCD 2018) La Thuile, Italy, March 17-24*. 2018. arXiv:1807.01643 [hep-ph].

[38] M. E. Peskin and D. V. Schroeder, *An Introduction to quantum field theory*. Addison-Wesley, Reading, USA, 1995.

[39] G. Buchalla, A. J. Buras, and M. E. Lautenbacher, "Weak decays beyond leading logarithms," *Rev. Mod. Phys.* **68** (1996) 1125–1144, arXiv:hep-ph/9512380 [hep-ph].

[40] C. P. Burgess and G. D. Moore, *The Standard Model: A primer*. Cambridge University Press, 2006.

[41] G. Altarelli, "Collider Physics within the Standard Model: a Primer," arXiv:1303.2842 [hep-ph].

[42] N. Cabibbo, "Unitary Symmetry and Leptonic Decays," *Phys. Rev. Lett.* **10** (1963) 531–533. [,648(1963)].

[43] M. Kobayashi and T. Maskawa, "CP Violation in the Renormalizable Theory of Weak Interaction," *Prog. Theor. Phys.* **49** (1973) 652–657.

[44] L.-L. Chau and W.-Y. Keung, "Comments on the Parametrization of the Kobayashi-Maskawa Matrix," *Phys. Rev. Lett.* **53** (1984) 1802.

[45] L. Wolfenstein, "Parametrization of the Kobayashi-Maskawa Matrix," *Phys. Rev. Lett.* **51** (1983) 1945.

[46] A. J. Buras, M. E. Lautenbacher, and G. Ostermaier, "Waiting for the top quark mass, $K^+ \to \pi\nu\bar{\nu}$, $B^0_{(s)} - \overline{B^0_{(s)}}$ mixing and CP asymmetries in B decays," *Phys. Rev.* **D50** (1994) 3433–3446, arXiv:hep-ph/9403384 [hep-ph].

[47] H. Fritzsch and Z.-z. Xing, "Mass and flavor mixing schemes of quarks and leptons," *Prog. Part. Nucl. Phys.* **45** (2000) 1–81, arXiv:hep-ph/9912358 [hep-ph].

[48] W. Bernreuther, "CP violation and baryogenesis," *Lect. Notes Phys.* **591** (2002) 237–293, arXiv:hep-ph/0205279 [hep-ph].

[49] S. L. Glashow, J. Iliopoulos, and L. Maiani, "Weak Interactions with Lepton-Hadron Symmetry," *Phys. Rev.* **D2** (1970) 1285–1292.

[50] D. Bečirević, S. Fajfer, and N. Kosnik, "Lepton flavor non-universality in $b \to s\ell^+\ell^-$ processes," *Phys. Rev.* **D92** no. 1, (2015) 014016, arXiv:1503.09024 [hep-ph].

[51] **Super-Kamiokande** Collaboration, Y. Fukuda *et al.*, "Evidence for oscillation of atmospheric neutrinos," *Phys. Rev. Lett.* **81** (1998) 1562–1567, arXiv:hep-ex/9807003 [hep-ex].

[52] **SNO** Collaboration, Q. R. Ahmad *et al.*, "Direct evidence for neutrino flavor transformation from neutral current interactions in the Sudbury Neutrino Observatory," *Phys. Rev. Lett.* **89** (2002) 011301, arXiv:nucl-ex/0204008 [nucl-ex].

[53] B. Pontecorvo, "Inverse beta processes and nonconservation of lepton charge," *Sov. Phys. JETP* **7** (1958) 172–173. [Zh. Eksp. Teor. Fiz.34,247(1957)].

[54] Z. Maki, M. Nakagawa, and S. Sakata, "Remarks on the unified model of elementary particles," *Prog. Theor. Phys.* **28** (1962) 870–880.

[55] S. Weinberg, "Baryon and Lepton Nonconserving Processes," *Phys. Rev. Lett.* **43** (1979) 1566–1570.

[56] S. Davidson, M. Gorbahn, and M. Leak, "Majorana Neutrino Masses in the RGEs for Lepton Flavour Violation," `arXiv:1807.04283 [hep-ph]`.

[57] S. F. King, "Models of Neutrino Mass, Mixing and CP Violation," *J. Phys.* **G42** (2015) 123001, `arXiv:1510.02091 [hep-ph]`.

[58] I. I. Bigi, *CP violation*. Cambridge University Press, 2009.

[59] J. Schwinger, "The theory of quantized fields," *Phys. Rev.* **82** (Jun, 1951) 914–927. `https://link.aps.org/doi/10.1103/PhysRev.82.914`.

[60] S. Benson, *Searching for CP violation in the $B_s^0 \to \phi\phi$ decay at LHCb*. PhD thesis, Edinburgh U., 2014-01-20. `http://inspirehep.net/record/1339887/files/CERN-THESIS-2014-087.pdf`.

[61] N. N. Bogoliubov and O. S. Parasiuk, "On the Multiplication of the causal function in the quantum theory of fields," *Acta Math.* **97** (1957) 227–266.

[62] K. Hepp, "Proof of the Bogolyubov-Parasiuk theorem on renormalization," *Commun. Math. Phys.* **2** (1966) 301–326.

[63] G. 't Hooft and M. J. G. Veltman, "Regularization and Renormalization of Gauge Fields," *Nucl. Phys.* **B44** (1972) 189–213.

[64] D. J. Gross and F. Wilczek, "Ultraviolet Behavior of Nonabelian Gauge Theories," *Phys. Rev. Lett.* **30** (1973) 1343–1346. [,271(1973)].

[65] H. D. Politzer, "Reliable Perturbative Results for Strong Interactions?," *Phys. Rev. Lett.* **30** (1973) 1346–1349. [,274(1973)].

[66] P. A. Baikov, K. G. Chetyrkin, and J. H. Kühn, "Five-Loop Running of the QCD coupling constant," *Phys. Rev. Lett.* **118** no. 8, (2017) 082002, `arXiv:1606.08659 [hep-ph]`.

[67] S. A. Larin and J. A. M. Vermaseren, "The Three loop QCD Beta function and anomalous dimensions," *Phys. Lett.* **B303** (1993) 334–336, `arXiv:hep-ph/9302208 [hep-ph]`.

[68] M. Beneke, T. Feldmann, and D. Seidel, "Systematic approach to exclusive $B \to V l^+ l^-, V\gamma$ decays," *Nucl.Phys.* **B612** (2001) 25–58, `arXiv:hep-ph/0106067 [hep-ph]`.

[69] J. Lyon and R. Zwicky, "Isospin asymmetries in $B \to (K^*, \rho) l^+ l^-$ and $B \to K l^+ l^-$ in and beyond the standard model," *Phys.Rev.* **D88** no. 9, (2013) 094004, arXiv:1305.4797 [hep-ph].

[70] G. W. Jones, *Meson distribution amplitudes - applications to weak radiative B decays and B transition form factors*. PhD thesis, Durham U., 2007. arXiv:0710.4479 [hep-ph].

[71] P. Ball, G. W. Jones, and R. Zwicky, "$B \to V\gamma$ beyond QCD factorisation," *Phys.Rev.* **D75** (2007) 054004, arXiv:hep-ph/0612081 [hep-ph].

[72] M. Dimou, J. Lyon, and R. Zwicky, "Exclusive Chromomagnetism in heavy-to-light FCNCs," *Phys.Rev.* **D87** no. 7, (2013) 074008, arXiv:1212.2242 [hep-ph].

[73] S. W. Bosch, *Exclusive radiative decays of B mesons in QCD factorization*. PhD thesis, Munich, Max Planck Inst., 2002. arXiv:hep-ph/0208203 [hep-ph].

[74] K. G. Chetyrkin, M. Misiak, and M. Munz, "Weak radiative B meson decay beyond leading logarithms," *Phys. Lett.* **B400** (1997) 206–219, arXiv:hep-ph/9612313 [hep-ph]. [Erratum: Phys. Lett. B425, 414 (1998)].

[75] M. Misiak and M. Steinhauser, "Three loop matching of the dipole operators for $b \to s\gamma$ and $b \to sg$," *Nucl. Phys.* **B683** (2004) 277–305, arXiv:hep-ph/0401041 [hep-ph].

[76] M. Czakon, U. Haisch, and M. Misiak, "Four-Loop Anomalous Dimensions for Radiative Flavour-Changing Decays," *JHEP* **03** (2007) 008, arXiv:hep-ph/0612329 [hep-ph].

[77] C. Bobeth, M. Misiak, and J. Urban, "Photonic penguins at two loops and m_t dependence of $BR[B \to X_s l^+ l^-]$," *Nucl. Phys.* **B574** (2000) 291–330, arXiv:hep-ph/9910220 [hep-ph].

[78] W. Altmannshofer, P. Ball, A. Bharucha, A. J. Buras, D. M. Straub, and M. Wick, "Symmetries and Asymmetries of $B \to K^* \mu^+ \mu^-$ Decays in the Standard Model and Beyond," *JHEP* **0901** (2009) 019, arXiv:0811.1214 [hep-ph].

[79] D. Bečirević and O. Sumensari, "A leptoquark model to accommodate $R_K^{\rm exp} < R_K^{\rm SM}$ and $R_{K^*}^{\rm exp} < R_{K^*}^{\rm SM}$," *JHEP* **08** (2017) 104, arXiv:1704.05835 [hep-ph].

[80] D. Bardhan, P. Byakti, and D. Ghosh, "Role of Tensor operators in R_K and R_{K^*}," *Phys. Lett.* **B773** (2017) 505–512, arXiv:1705.09305 [hep-ph].

[81] V. M. Braun, G. P. Korchemsky, and D. Mueller, "The Uses of Conformal Symmetry in *QCD*," *Prog. Part. Nucl. Phys.* **51** (2003) 311–398, arXiv:hep-ph/0306057 [hep-ph].

[82] P. Ball, V. M. Braun, Y. Koike, and K. Tanaka, "Higher twist distribution amplitudes of vector mesons in QCD: Formalism and twist-three distributions," *Nucl. Phys.* **B529** (1998) 323–382, arXiv:hep-ph/9802299 [hep-ph].

[83] P. Ball and V. M. Braun, "Higher twist distribution amplitudes of vector mesons in QCD: Twist-4 distributions and meson mass corrections," *Nucl. Phys.* **B543** (1999) 201–238, arXiv:hep-ph/9810475 [hep-ph].

[84] H. Bateman and A. Erdélyi, *Higher transcendental functions*. Calif. Inst. Technol. Bateman Manuscr. Project. McGraw-Hill, New York, NY, 1955. https://cds.cern.ch/record/100233.

[85] P. Ball and G. W. Jones, "Twist-3 distribution amplitudes of K^* and ϕ mesons," *JHEP* **03** (2007) 069, arXiv:hep-ph/0702100 [HEP-PH].

[86] K. G. Wilson, "Confinement of Quarks," *Phys. Rev.* **D10** (1974) 2445–2459. [,319(1974)].

[87] R. Gupta, "Introduction to lattice QCD: Course," in *Probing the standard model of particle interactions. Proceedings, Summer School in Theoretical Physics, NATO Advanced Study Institute, 68th session, Les Houches, France, July 28-September 5, 1997. Pt. 1, 2*, pp. 83–219. 1997. arXiv:hep-lat/9807028 [hep-lat].

[88] M. A. Shifman, A. I. Vainshtein, and V. I. Zakharov, "QCD and Resonance Physics. Theoretical Foundations," *Nucl. Phys.* **B147** (1979) 385–447.

[89] M. A. Shifman, A. I. Vainshtein, and V. I. Zakharov, "QCD and Resonance Physics: Applications," *Nucl. Phys.* **B147** (1979) 448–518.

[90] I. I. Balitsky, V. M. Braun, and A. V. Kolesnichenko, "Radiative Decay $\Sigma^+ \to p\gamma$ in Quantum Chromodynamics," *Nucl. Phys.* **B312** (1989) 509–550.

[91] V. M. Braun and I. E. Filyanov, "Conformal Invariance and Pion Wave Functions of Nonleading Twist," *Z. Phys.* **C48** (1990) 239–248. [Yad. Fiz.52,199(1990)].

[92] K. G. Wilson, "Nonlagrangian models of current algebra," *Phys. Rev.* **179** (1969) 1499–1512.

[93] M. Gell-Mann, R. J. Oakes, and B. Renner, "Behavior of current divergences under $SU(3) \times SU(3)$," *Phys. Rev.* **175** (1968) 2195–2199.

[94] S. Weinberg, *The quantum theory of fields. Vol. 2: Modern applications.* Cambridge University Press, 2013.

[95] E. Bagan, P. Ball, and V. M. Braun, "Radiative corrections to the decay $B \to \pi e \nu$ and the heavy quark limit," *Phys. Lett.* **B417** (1998) 154–162, arXiv:hep-ph/9709243 [hep-ph].

[96] V. M. Braun, "Light cone sum rules," in *Progress in heavy quark physics. Proceedings, 4th International Workshop, Rostock, Germany, September 20-22, 1997*, pp. 105–118. 1997. arXiv:hep-ph/9801222 [hep-ph].

[97] V. M. Belyaev, V. M. Braun, A. Khodjamirian, and R. Ruckl, "$D^*D\pi$ and $B^*B\pi$ couplings in QCD," *Phys. Rev.* **D51** (1995) 6177–6195, arXiv:hep-ph/9410280 [hep-ph].

[98] P. Ball, V. M. Braun, and A. Lenz, "Higher-twist distribution amplitudes of the K meson in QCD," *JHEP* **05** (2006) 004, arXiv:hep-ph/0603063 [hep-ph].

[99] A. Bharucha, D. M. Straub, and R. Zwicky, "$B \to V \ell^+ \ell^-$ in the Standard Model from Light-Cone Sum Rules," *JHEP* **08** (2016) 098, arXiv:1503.05534 [hep-ph].

[100] M. A. Shifman, "Theory of preasymptotic effects in weak inclusive decays," in *Workshop on Continuous Advances in QCD Minneapolis, Minnesota, February 18-20, 1994*, pp. 249–286. 1994. arXiv:hep-ph/9405246 [hep-ph].

[101] M. A. Shifman, "Snapshots of hadrons or the story of how the vacuum medium determines the properties of the classical mesons which are produced, live and die in the QCD vacuum," *Prog. Theor. Phys. Suppl.* **131** (1998) 1–71, arXiv:hep-ph/9802214 [hep-ph]. [,111(1998)].

[102] P. Ball and R. Zwicky, "New results on $B \to \pi$, K, η decay formfactors from light-cone sum rules," *Phys.Rev.* **D71** (2005) 014015, arXiv:hep-ph/0406232 [hep-ph].

[103] P. Ball, V. M. Braun, and A. Lenz, "Twist-4 distribution amplitudes of the K^* and ϕ mesons in QCD," *JHEP* **08** (2007) 090, arXiv:0707.1201 [hep-ph].

[104] K.-C. Yang, "Light-cone distribution amplitudes of axial-vector mesons," *Nucl. Phys.* **B776** (2007) 187–257, arXiv:0705.0692 [hep-ph].

[105] N. G. Deshpande and J. Trampetic, "Improved Estimates for Processes $b \to s e^+ e^-$, $B \to K e^+ e^-$ and $B \to K^* e^+ e^-$," *Phys. Rev. Lett.* **60** (1988) 2583.

[106] W. Jaus and D. Wyler, "The Rare Decays of $B \to K l \bar{l}$ and $B \to K^* l \bar{l}$," *Phys. Rev.* **D41** (1990) 3405.

[107] F. Kruger and L. M. Sehgal, "CP violation in the exclusive decays $B \to \pi e^+ e^-$ and $B \to \rho e^+ e^-$," *Phys. Rev.* **D56** (1997) 5452–5465, arXiv:hep-ph/9706247 [hep-ph]. [Erratum: Phys. Rev. D60, 099905 (1999)].

[108] F. Kruger, L. M. Sehgal, N. Sinha, and R. Sinha, "Angular distribution and CP asymmetries in the decays $\bar{B} \to K^- \pi^+ e^- e^+$ and $\bar{B} \to \pi^- \pi^+ e^- e^+$," *Phys.Rev.* **D61** (2000) 114028, arXiv:hep-ph/9907386 [hep-ph].

[109] A. Faessler, T. Gutsche, M. Ivanov, J. Korner, and V. E. Lyubovitskij, "The Exclusive rare decays $B \to$ K(K*) $\bar{\ell}\ell$ and $B_c \to$ D(D*) $\bar{\ell}\ell$ in a relativistic quark model," *Eur.Phys.J.direct* **C4** (2002) 18, arXiv:hep-ph/0205287 [hep-ph].

[110] F. Kruger and J. Matias, "Probing new physics via the transverse amplitudes of $B_0 \to K^{*,0}(K \to \pi^+)\ell^+\ell^-$ at large recoil," *Phys.Rev.* **D71** (2005) 094009, arXiv:hep-ph/0502060 [hep-ph].

[111] C. Kim and T. Yoshikawa, "Systematic analysis of $B \to K\pi\ell^+\ell^-$ decay through angular decomposition," arXiv:0711.3880 [hep-ph].

[112] A. K. Alok, A. Dighe, D. Ghosh, D. London, J. Matias, *et al.*, "New-physics contributions to the forward-backward asymmetry in $B \to K^* \mu^+ \mu^-$," *JHEP* **1002** (2010) 053, arXiv:0912.1382 [hep-ph].

[113] C. Bobeth, G. Hiller, and D. van Dyk, "General analysis of $\bar{B} \to \bar{K}^{(*)}\ell^+\ell^-$ decays at low recoil," *Phys.Rev.* **D87** no. 3, (2013) 034016, arXiv:1212.2321 [hep-ph].

[114] **Belle** Collaboration, A. Ishikawa *et al.*, "Observation of $B \to K^*\ell^+\ell^-$," *Phys. Rev. Lett.* **91** (2003) 261601, arXiv:hep-ex/0308044 [hep-ex].

[115] **BaBar** Collaboration, B. Aubert *et al.*, "Evidence for the rare decay $B \to K^*\ell^+\ell^-$ and measurement of the $B \to K\ell^+\ell^-$ branching fraction," *Phys. Rev. Lett.* **91** (2003) 221802, arXiv:hep-ex/0308042 [hep-ex].

[116] **Belle** Collaboration, A. Ishikawa *et al.*, "Measurement of Forward-Backward Asymmetry and Wilson Coefficients in $B \to K^*\ell^+\ell^-$," *Phys. Rev. Lett.* **96** (2006) 251801, arXiv:hep-ex/0603018 [hep-ex].

[117] **BaBar** Collaboration, J. P. Lees *et al.*, "Search for lepton-number violating $B \to X^-\ell^+\ell'^+$ decays," *Phys. Rev.* **D89** no. 1, (2014) 011102, arXiv:1310.8238 [hep-ex].

[118] **Belle** Collaboration, S. Wehle *et al.*, "Lepton-Flavor-Dependent Angular Analysis of $B \to K^*\ell^+\ell^-$," *Phys. Rev. Lett.* **118** no. 11, (2017) 111801, arXiv:1612.05014 [hep-ex].

[119] **ATLAS** Collaboration, M. Aaboud *et al.*, "Angular analysis of $B^0_d \to K^* \mu^+ \mu^-$ decays in pp collisions at $\sqrt{s} = 8$ TeV with the ATLAS detector," arXiv:1805.04000 [hep-ex].

[120] **CMS** Collaboration, A. M. Sirunyan *et al.*, "Measurement of angular parameters from the decay $B^0 \to K^{*0}\mu^+\mu^-$ in proton-proton collisions at $\sqrt{s} = 8$ TeV," *Phys. Lett.* **B781** (2018) 517–541, arXiv:1710.02846 [hep-ex].

[121] S. Descotes-Genon, T. Hurth, J. Matias, and J. Virto, "Optimizing the basis of $B \to K^*\ell^+\ell^-$ observables in the full kinematic range," *JHEP* **1305** (2013) 137, arXiv:1303.5794 [hep-ph].

[122] W. Altmannshofer, C. Niehoff, P. Stangl, and D. M. Straub, "Status of the $B \to K^*\mu^+\mu^-$ anomaly after Moriond 2017," *Eur. Phys. J.* **C77** no. 6, (2017) 377, arXiv:1703.09189 [hep-ph].

[123] J. Albrecht, S. Reichert, and D. van Dyk, "Status of rare exclusive B meson decays in 2018," *Int. J. Mod. Phys.* **A33** no. 18n19, (2018) 1830016, arXiv:1806.05010 [hep-ex].

[124] M. Hopfer, *Gauge theories: QCD & beyond*. PhD thesis, Graz U., 2014. http://unipub.uni-graz.at/obvugrhs/content/titleinfo/269085.

[125] R. Kutschke, "An Angular Distribution Cookbook." unpublished, 1996.

[126] H. E. Haber, "Spin formalism and applications to new physics searches," arXiv:hep-ph/9405376 [hep-ph].

[127] J. D. Richman, "An Experimenter's Guide to the Helicity Formalism,".

[128] **Particle Data Group** Collaboration, C. Patrignani *et al.*, "Review of Particle Physics," *Chin. Phys.* **C40** no. 10, (2016) 100001.

[129] **LHCb** Collaboration, R. Aaij *et al.*, "Differential branching fraction and angular analysis of the decay $B^0 \to K^{*0}\mu^+\mu^-$," *JHEP* **1308** (2013) 131, arXiv:1304.6325.

[130] C.-D. Lu and W. Wang, "Analysis of $B \to K_J^*(\to K\pi)\mu^+\mu^-$ in the higher kaon resonance region," *Phys.Rev.* **D85** (2012) 034014, arXiv:1111.1513 [hep-ph].

[131] G. Hiller and R. Zwicky, "(A)symmetries of weak decays at and near the kinematic endpoint," *JHEP* **1403** (2014) 042, arXiv:1312.1923 [hep-ph].

[132] C. Bobeth, G. Hiller, and G. Piranishvili, "Angular distributions of $\bar{B} \to \bar{K}\bar{\ell}\ell$ decays," *JHEP* **0712** (2007) 040, arXiv:0709.4174 [hep-ph].

[133] **LHCb** Collaboration, R. Aaij *et al.*, "Angular analysis of charged and neutral $B \to K\mu^+\mu^-$ decays," *JHEP* **1405** (2014) 082, arXiv:1403.8045 [hep-ex].

[134] A. S. Dighe, I. Dunietz, and R. Fleischer, "Extracting CKM phases and $B_s - \bar{B}_s$ mixing parameters from angular distributions of nonleptonic B decays," *Eur.Phys.J.* **C6** (1999) 647–662, arXiv:hep-ph/9804253 [hep-ph].

[135] U. Egede, M. Patel, and K. A. Petridis, "Method for an unbinned measurement of the q^2 dependent decay amplitudes of $\bar{B}^0 \to \bar{K}^{*0}\mu^+\mu^-$ decays," arXiv:1504.00574 [hep-ph].

[136] K. Hecht, *Quantum Mechanics*. Springer, 2000.

[137] P. Boer, T. Feldmann, and D. van Dyk, "Angular Analysis of the Decay $\Lambda_b \to \Lambda(\to N\pi)\ell^+\ell^-$," *JHEP* **1501** (2015) 155, arXiv:1410.2115 [hep-ph].

[138] F. Beaujean, M. Chrzaszcz, N. Serra, and D. van Dyk, "Extracting Angular Observables without a Likelihood and Applications to Rare Decays," *Phys. Rev.* **D91** no. 11, (2015) 114012, arXiv:1503.04100 [hep-ex].

[139] **LHCb** Collaboration, R. Aaij *et al.*, "Differential branching fraction and angular moments analysis of the decay $B^0 \to K^+\pi^-\mu^+\mu^-$ in the $K^*_{0,2}(1430)^0$ region," *JHEP* **12** (2016) 065, arXiv:1609.04736 [hep-ex].

[140] **LHCb** Collaboration, R. Aaij *et al.*, "Opposite-side flavour tagging of B mesons at the LHCb experiment," *Eur. Phys. J.* **C72** (2012) 2022, arXiv:1202.4979 [hep-ex].

[141] D. Bečirević, O. Sumensari, and R. Zukanovich Funchal, "Lepton flavor violation in exclusive $b \to s$ decays," *Eur. Phys. J.* **C76** no. 3, (2016) 134, arXiv:1602.00881 [hep-ph].

[142] S. Descotes-Genon, J. Matias, and J. Virto, "Understanding the $B \to K^*\mu^+\mu^-$ Anomaly," *Phys.Rev.* **D88** (2013) 074002, arXiv:1307.5683 [hep-ph].

[143] W. Altmannshofer and D. M. Straub, "New physics in $B \to K^*\mu\mu$?," *Eur.Phys.J.* **C73** (2013) 2646, arXiv:1308.1501 [hep-ph].

[144] A. K. Alok, A. Datta, A. Dighe, M. Duraisamy, D. Ghosh, *et al.*, "New Physics in $b \to \mu^+\mu^-$: CP-Conserving Observables," *JHEP* **1111** (2011) 121, arXiv:1008.2367 [hep-ph].

[145] A. Arbey, T. Hurth, F. Mahmoudi, and S. Neshatpour, "Hadronic and New Physics Contributions to $B \to K^*\ell^+\ell^-$," arXiv:1806.02791 [hep-ph].

[146] S. Descotes-Genon, L. Hofer, J. Matias, and J. Virto, "Global analysis of $b \to s\ell\ell$ anomalies," *JHEP* **06** (2016) 092, arXiv:1510.04239 [hep-ph].

[147] B. C. Allanach, B. Gripaios, and T. You, "The Case for Future Hadron Colliders From $B \to K^{(*)}\mu^+\mu^-$ Decays," *JHEP* **03** (2018) 021, arXiv:1710.06363 [hep-ph].

[148] M. Ciuchini, A. M. Coutinho, M. Fedele, E. Franco, A. Paul, L. Silvestrini, and M. Valli, "On Flavourful Easter eggs for New Physics hunger and Lepton Flavour Universality violation," *Eur. Phys. J.* **C77** no. 10, (2017) 688, arXiv:1704.05447 [hep-ph].

[149] D. Straub *et al.*, "Flavio v0.23," Sept., 2017. https://doi.org/10.5281/zenodo.897989.

[150] H. Hatanaka and K.-C. Yang, "Radiative and Semileptonic B Decays Involving the Tensor Meson $K_2^*(1430)$ in the Standard Model and Beyond," *Phys. Rev.* **D79** (2009) 114008, arXiv:0903.1917 [hep-ph].

[151] B. Dey, "Angular analyses of exclusive $\overline{B} \to X_J \ell_1 \ell_2$ decays for spin $J \leq 4$," *Phys. Rev.* **D95** no. 3, (2017) 033004, arXiv:1609.06115 [hep-ph].

[152] D. Bečirević and A. Tayduganov, "Impact of $B \to K_0^* \ell^+ \ell^-$ on the New Physics search in $B \to K^* \ell^+ \ell^-$ decay," *Nucl.Phys.* **B868** (2013) 368–382, arXiv:1207.4004 [hep-ph].

[153] T. Blake, U. Egede, and A. Shires, "The effect of S-wave interference on the $B^0 \to K^{*0} \ell^+ \ell^-$ angular observables," *JHEP* **1303** (2013) 027, arXiv:1210.5279 [hep-ph].

[154] D. Das, G. Hiller, M. Jung, and A. Shires, "The $\overline{B} \to \overline{K} \pi \ell\ell$ and $\overline{B}_s \to \overline{K} K \ell\ell$ distributions at low hadronic recoil," *JHEP* **1409** (2014) 109, arXiv:1406.6681 [hep-ph].

[155] B. Dey, "Angular analyses of exclusive $\bar{B} \to X \ell_1 \ell_2$ with complex helicity amplitudes," *Phys. Rev.* **D92** (2015) 033013, arXiv:1505.02873 [hep-ex].

[156] R. Zwicky, "Endpoint symmetries of helicity amplitudes," arXiv:1309.7802 [hep-ph].

[157] S. Fajfer, B. Melic, and M. Patra, "Testing Spin-2 Mediator in $b \to s \mu^+ \mu^-$," *Phys. Rev.* **D97** no. 9, (2018) 095036, arXiv:1801.07115 [hep-ph].

[158] M. Bordone, G. Isidori, and A. Pattori, "On the Standard Model predictions for R_K and R_{K^*}," *Eur. Phys. J.* **C76** no. 8, (2016) 440, arXiv:1605.07633 [hep-ph].

[159] G. Hiller and F. Kruger, "More model independent analysis of $b \to s$ processes," *Phys.Rev.* **D69** (2004) 074020, arXiv:hep-ph/0310219 [hep-ph].

[160] **Belle** Collaboration, J.-T. Wei *et al.*, "Measurement of the Differential Branching Fraction and Forward-Backward Asymmetry for $B \to K^{(*)}\ell^+\ell^-$," *Phys.Rev.Lett.* **103** (2009) 171801, arXiv:0904.0770 [hep-ex].

[161] **BaBar** Collaboration, J. Lees *et al.*, "Measurement of Branching Fractions and Rate Asymmetries in the Rare Decays $B \to K^{(*)}l^+l^-$," *Phys.Rev.* **D86** (2012) 032012, arXiv:1204.3933 [hep-ex].

[162] B. Gripaios, M. Nardecchia, and S. Renner, "Composite leptoquarks and anomalies in B-meson decays," *JHEP* **1505** (2015) 006, arXiv:1412.1791 [hep-ph].

[163] C. Niehoff, P. Stangl, and D. M. Straub, "Violation of lepton flavour universality in composite Higgs models," *Phys.Lett.* **B747** (2015) 182–186, arXiv:1503.03865 [hep-ph].

[164] A. Crivellin, L. Hofer, J. Matias, U. Nierste, S. Pokorski, *et al.*, "Lepton-flavour violating B decays in generic Z' models," *Phys. Rev.* **D92** no. 5, (2015) 054013, arXiv:1504.07928 [hep-ph].

[165] A. Greljo, G. Isidori, and D. Marzocca, "On the breaking of Lepton Flavor Universality in B decays," *JHEP* **07** (2015) 142, arXiv:1506.01705 [hep-ph].

[166] R. Alonso, B. Grinstein, and J. M. Camalich, "Lepton universality violation and lepton flavor conservation in B-meson decays," *JHEP* **10** (2015) 184, arXiv:1505.05164 [hep-ph].

[167] I. de Medeiros Varzielas and G. Hiller, "Clues for flavor from rare lepton and quark decays," *JHEP* **06** (2015) 072, arXiv:1503.01084 [hep-ph].

[168] A. Crivellin, G. D'Ambrosio, and J. Heeck, "Addressing the LHC flavor anomalies with horizontal gauge symmetries," *Phys.Rev.* **D91** no. 7, (2015) 075006, arXiv:1503.03477 [hep-ph].

[169] L. Calibbi, A. Crivellin, and T. Ota, "Effective field theory approach to $b \to s\ell\ell^{(\prime)}$, $B \to K^{(*)}\nu\bar{\nu}$ and $B \to D^{(*)}\tau\nu$ with third generation couplings," *Phys. Rev. Lett.* **115** (2015) 181801, arXiv:1506.02661 [hep-ph].

[170] A. Crivellin, G. D'Ambrosio, and J. Heeck, "Explaining $h \to \mu^\pm\tau^\mp$, $B \to K^*\mu^+\mu^-$ and $B \to K\mu^+\mu^-/B \to Ke^+e^-$ in a two-Higgs-doublet model with gauged $L_\mu - L_\tau$," *Phys.Rev.Lett.* **114** (2015) 151801, arXiv:1501.00993 [hep-ph].

[171] T. Blake, T. Gershon, and G. Hiller, "Rare b hadron decays at the LHC," *Ann. Rev. Nucl. Part. Sci.* **65** (2015) 113–143, arXiv:1501.03309 [hep-ex].

[172] A. Guevara, G. L. Castro, P. Roig, and S. Tostado, "One-photon exchange contribution to $B^{\pm} \to (\pi^{\pm}, K^{\pm})\ell^{+}\ell^{-}$ decays," arXiv:1503.06890 [hep-ph].

[173] V. L. Chernyak and A. R. Zhitnitsky, "Asymptotic Behavior of Exclusive Processes in QCD," *Phys. Rept.* **112** (1984) 173.

[174] J. Gratrex and R. Zwicky, "Axial and vector meson distribution amplitudes and their symmetries." In preparation.

[175] P. Pascual and R. Tarrach, "QCD: Renormalization for the practitioner," *Lect. Notes Phys.* **194** (1984) 1–277.

[176] W. Hubschmid and S. Mallik, "Operator Expansion at short distance in QCD," *Nucl. Phys.* **B207** (1982) 29–42.

[177] L. Burakovsky and J. T. Goldman, "Towards resolution of the enigmas of P wave meson spectroscopy," *Phys. Rev.* **D57** (1998) 2879–2888, arXiv:hep-ph/9703271 [hep-ph].

[178] M. Suzuki, "Strange axial-vector mesons," *Phys. Rev. D* **47** (Feb, 1993) 1252–1255. https://link.aps.org/doi/10.1103/PhysRevD.47.1252.

[179] H.-Y. Cheng, "Revisiting Axial-Vector Meson Mixing," *Phys. Lett.* **B707** (2012) 116–120, arXiv:1110.2249 [hep-ph].

[180] H. Dag, A. Ozpineci, A. Cagil, and G. Erkol, "Theoretical determination of $K_1(1270, 1400)$ mixing angle in QCD," *J. Phys. Conf. Ser.* **348** (2012) 012012.

[181] M. Gell-Mann, "The Eightfold Way: A Theory of strong interaction symmetry." CTSL-20 (1961), unpublished.

[182] S. Okubo, "Note on unitary symmetry in strong interactions," *Prog. Theor. Phys.* **27** (1962) 949–966.

[183] S. Weinberg, "Precise relations between the spectra of vector and axial vector mesons," *Phys. Rev. Lett.* **18** (1967) 507–509.

[184] **ALEPH** Collaboration, S. Schael *et al.*, "Branching ratios and spectral functions of tau decays: Final ALEPH measurements and physics implications," *Phys. Rept.* **421** (2005) 191–284, arXiv:hep-ex/0506072 [hep-ex].

[185] B. Grinstein, Y. Grossman, Z. Ligeti, and D. Pirjol, "The Photon polarization in $B \to X\gamma$ in the standard model," *Phys. Rev.* **D71** (2005) 011504, arXiv:hep-ph/0412019 [hep-ph].

[186] P. Ball and R. Zwicky, "Time-dependent CP Asymmetry in $B \to K^{*}\gamma$ as a (Quasi) Null Test of the Standard Model," *Phys. Lett.* **B642** (2006) 478–486, arXiv:hep-ph/0609037 [hep-ph].

[187] A. Khodjamirian, R. Ruckl, G. Stoll, and D. Wyler, "QCD estimate of the long distance effect in $B \to K^* \gamma$," *Phys. Lett.* **B402** (1997) 167–177, arXiv:hep-ph/9702318 [hep-ph].

[188] A. Khodjamirian, T. Mannel, A. Pivovarov, and Y.-M. Wang, "Charm-loop effect in $B \to K^{(*)} \ell^+ \ell^-$ and $B \to K^* \gamma$," *JHEP* **1009** (2010) 089, arXiv:1006.4945 [hep-ph].

[189] D. Atwood, M. Gronau, and A. Soni, "Mixing induced CP asymmetries in radiative B decays in and beyond the standard model," *Phys. Rev. Lett.* **79** (1997) 185–188, arXiv:hep-ph/9704272 [hep-ph].

[190] F. Muheim, Y. Xie, and R. Zwicky, "Exploiting the width difference in $B_s \to \phi \gamma$," *Phys.Lett.* **B664** (2008) 174–179, arXiv:0802.0876 [hep-ph].

[191] **Belle** Collaboration, Y. Ushiroda *et al.*, "Time-Dependent CP Asymmetries in $B^0 \to K^0_S \pi^0 \gamma$ transitions," *Phys. Rev.* **D74** (2006) 111104, arXiv:hep-ex/0608017 [hep-ex].

[192] **BaBar** Collaboration, B. Aubert *et al.*, "Measurement of Time-Dependent CP Asymmetry in $B^0 \to K^0_S \pi^0 \gamma$ Decays," *Phys. Rev.* **D78** (2008) 071102, arXiv:0807.3103 [hep-ex].

[193] **LHCb** Collaboration, R. Aaij *et al.*, "First experimental study of photon polarization in radiative B^0_s decays," *Phys. Rev. Lett.* **118** no. 2, (2017) 021801, arXiv:1609.02032 [hep-ex]. [Addendum: Phys. Rev. Lett.118,no.10,109901(2017)].

[194] J. Gratrex and R. Zwicky, "Long-distance charm loops in $B \to (V, A) \ell \bar{\ell}$ decays from light-cone sum rules." In preparation.

[195] H. Asatryan, H. Asatrian, C. Greub, and M. Walker, "Calculation of two loop virtual corrections to $b \to s \ell^+ \ell^-$ in the Standard Model," *Phys.Rev.* **D65** (2002) 074004, arXiv:hep-ph/0109140 [hep-ph].

[196] A. Khodjamirian, "$B \to \pi\pi$ decay in QCD," *Nucl. Phys.* **B605** (2001) 558–578, arXiv:hep-ph/0012271 [hep-ph].

[197] S. Aoki *et al.*, "Review of lattice results concerning low-energy particle physics," *Eur. Phys. J.* **C77** no. 2, (2017) 112, arXiv:1607.00299 [hep-lat].

[198] T. M. Aliev and V. L. Eletsky, "On Leptonic Decay Constants of Pseudoscalar D and B Mesons," *Sov. J. Nucl. Phys.* **38** (1983) 936. [Yad. Fiz.38,1537(1983)].

[199] R.-H. Li, C.-D. Lu, and W. Wang, "Transition form factors of B decays into p-wave axial-vector mesons in the perturbative QCD approach," *Phys. Rev.* **D79** (2009) 034014, arXiv:0901.0307 [hep-ph].

[200] D. Bečirević and E. Schneider, "On transverse asymmetries in $B \to K^* l^+ l^-$," *Nucl. Phys.* **B854** (2012) 321–339, arXiv:1106.3283 [hep-ph].

[201] **LHCb** Collaboration, R. Aaij *et al.*, "Angular analysis of the $B^0 \to K^{*0} e^+ e^-$ decay in the low-q^2 region," *JHEP* **1504** (2015) 064, arXiv:1501.03038 [hep-ex].

[202] S. Descotes-Genon and J. Virto, "Time dependence in $B \to V\ell\ell$ decays," *JHEP* **1504** (2015) 045, arXiv:1502.05509 [hep-ph].

[203] R. Mertig, M. Bohm, and A. Denner, "FEYN CALC: Computer algebraic calculation of Feynman amplitudes," *Comput. Phys. Commun.* **64** (1991) 345–359.

[204] V. Shtabovenko, R. Mertig, and F. Orellana, "New Developments in FeynCalc 9.0," *Comput. Phys. Commun.* **207** (2016) 432–444, arXiv:1601.01167 [hep-ph].

[205] C. Cronstrom, "A Simple and Complete Lorentz Covariant Gauge Condition," *Phys. Lett.* **90B** (1980) 267–269.

[206] J. Schwinger, "Particles, sources, and fields. Volume 1,".

[207] R. K. Ellis and G. Zanderighi, "Scalar one-loop integrals for QCD," *JHEP* **02** (2008) 002, arXiv:0712.1851 [hep-ph].

[208] H. H. Patel, "Package-X: A Mathematica package for the analytic calculation of one-loop integrals," *Comput. Phys. Commun.* **197** (2015) 276–290, arXiv:1503.01469 [hep-ph].

[209] H. H. Patel, "Package-X 2.0: A Mathematica package for the analytic calculation of one-loop integrals," *Comput. Phys. Commun.* **218** (2017) 66–70, arXiv:1612.00009 [hep-ph].

[210] I. I. Bigi, N. Uraltsev, and R. Zwicky, "On the nonperturbative charm effects in inclusive $B \to X(c)l\nu$ decays," *Eur. Phys. J.* **C50** (2007) 539–556, arXiv:hep-ph/0511158 [hep-ph].

[211] V. A. Novikov, M. A. Shifman, A. I. Vainshtein, and V. I. Zakharov, "Calculations in External Fields in Quantum Chromodynamics. Technical Review," *Fortsch. Phys.* **32** (1984) 585.

[212] **Particle Data Group** Collaboration, W.-M. Yao *et al.*, "Review of Particle Physics," *Journal of Physics G* **33** (2006) .

[213] **Particle Data Group** Collaboration, K. Olive *et al.*, "Review of Particle Physics," *Chin.Phys.* **C38** (2014) 090001.

[214] P. Ball and M. Boglione, "$SU(3)$ breaking in K and K^* distribution amplitudes," *Phys. Rev.* **D68** (2003) 094006, arXiv:hep-ph/0307337 [hep-ph].

[215] C. A. Dominguez, L. A. Hernandez, and K. Schilcher, "Determination of the gluon condensate from data in the charm-quark region," *JHEP* **07** (2015) 110, arXiv:1411.4500 [hep-ph].

[216] R. Horsley, G. Hotzel, E. M. Ilgenfritz, R. Millo, H. Perlt, P. E. L. Rakow, Y. Nakamura, G. Schierholz, and A. Schiller, "Wilson loops to 20th order numerical stochastic perturbation theory," *Phys. Rev.* **D86** (2012) 054502, arXiv:1205.1659 [hep-lat].

[217] A. R. Zhitnitsky, "Method of Calculating many-component Vacuum Expectation Values ($\langle\bar{Q}Q\rangle^2$, $\langle G^3\rangle$, $\langle G^4\rangle$) in QCD," *Sov. J. Nucl. Phys.* **41** (1985) 846. [Yad. Fiz. 41, 1331 (1985)].

[218] J.-P. Liu and P.-X. Yang, "Temperature dependence of two- and three-gluon condensates in the instanton vacuum," *Communications in Theoretical Physics* **27** no. 2, (1997) 229. http://stacks.iop.org/0253-6102/27/i=2/a=229.

[219] H. G. Dosch and S. Narison, "Direct extraction of the chiral quark condensate and bounds on the light quark masses," *Phys. Lett.* **B417** (1998) 173–176, arXiv:hep-ph/9709215 [hep-ph].

[220] C. A. Dominguez, N. F. Nasrallah, and K. Schilcher, "Strange quark condensate from QCD sum rules to five loops," *JHEP* **02** (2008) 072, arXiv:0711.3962 [hep-ph].

[221] C. McNeile, A. Bazavov, C. T. H. Davies, R. J. Dowdall, K. Hornbostel, G. P. Lepage, and H. D. Trottier, "Direct determination of the strange and light quark condensates from full lattice QCD," *Phys. Rev.* **D87** no. 3, (2013) 034503, arXiv:1211.6577 [hep-lat].

[222] R. R. Horgan, Z. Liu, S. Meinel, and M. Wingate, "Lattice QCD calculation of form factors describing the rare decays $B \to K^* \ell^+ \ell^-$ and $B_s \to \phi \ell^+ \ell^-$," *Phys.Rev.* **D89** (2014) 094501, arXiv:1310.3722 [hep-lat].

[223] C. Hambrock, G. Hiller, S. Schacht, and R. Zwicky, "$B \to K^\star$ form factors from flavor data to QCD and back," *Phys. Rev.* **D89** no. 7, (2014) 074014, arXiv:1308.4379 [hep-ph].

[224] **LHCb** Collaboration, R. Aaij *et al.*, "Differential branching fraction and angular analysis of $\Lambda_b^0 \to \Lambda^0 \mu^+ \mu^-$ decays," *JHEP* **06** (2015) 115, arXiv:1503.07138 [hep-ex].

[225] T. Gutsche, M. A. Ivanov, J. G. Korner, V. E. Lyubovitskij, and P. Santorelli, "Rare baryon decays $\Lambda_b \to \Lambda l^+ l^- (l = e, \mu, \tau)$ and $\Lambda_b \to \Lambda \gamma$: differential and total rates, lepton- and hadron-side forward-backward asymmetries," *Phys.Rev.* **D87** (2013) 074031, arXiv:1301.3737 [hep-ph].

[226] S. Roy, R. Sain, and R. Sinha, "Lepton mass effects and angular observables in $\Lambda_b \to \Lambda(\to p\pi)\ell^+\ell^-$," *Phys. Rev.* **D96** no. 11, (2017) 116005, arXiv:1710.01335 [hep-ph].

[227] D. Das, "Model independent New Physics analysis in $\Lambda_b \to \Lambda\mu^+\mu^-$ decay," *Eur. Phys. J.* **C78** no. 3, (2018) 230, arXiv:1802.09404 [hep-ph].